Technical Report
TR-17-06
December 2017

Buffer design and installation method

Installation report

David Luterkort
Lars-Erik Johannesson
Peter Eriksson

SVENSK KÄRNBRÄNSLEHANTERING AB

SWEDISH NUCLEAR FUEL
AND WASTE MANAGEMENT CO

Box 3091, SE-169 03 Solna
Phone +46 8 459 84 00
skb.se

SVENSK KÄRNBRÄNSLEHANTERING

ISSN 1404-0344
SKB TR-17-06
ID 1528690
December 2017

Buffer design and installation method

Installation report

David Luterkort, Lars-Erik Johannesson, Peter Eriksson
Svensk Kärnbränslehantering AB

Keywords: Bentonite, Buffer installation, THM processes, Water inflow to deposition holes, Buffer design, KBP1012.

Abstract

This report addresses recent development concerning the buffer installation method and buffer design. The requirements on the buffer have been updated (Posiva SKB 2017) and the buffer design has been adapted. The design work and the resulting buffer design are presented in this report.

The result of earlier SKB technology development (Johannesson et al. 2014) was that SKB's previous reference method for installation of the buffer did not provide a sufficiently robust installation due to redistribution of water causing unacceptable cracking of the buffer blocks. The cracks are not problematic by themselves but may result in to lower-than desired final buffer density and pose practical installation problems. In order to achieve a robust installation two installation procedures, one for relatively dry deposition holes and one for wetter deposition holes, have been developed and tested. Two full scale tests examining buffer installation, one for dry conditions and one for wet, were completed.

In the test examining behaviour in dry conditions the pellets were installed directly after the installation of the blocks. The test was undertaken such that it simulated the time from the installation of the buffer and the canister until the tunnel is backfilled and thereby confines the buffer. This time-period was estimated to be at maximum 90 days. The installation was made using full size buffer blocks and a simulated canister in a full scale deposition hole with a natural water inflow of 8E−4 l/min (0.048 l/h). Most of the water inflow was related to a zone close to the tunnel floor. The canister was equipped with a heater generating 1 700 W to simulate the power from the waste in a real canister. During dismantling of the test, samples of the buffer were taken and water content and density were determined. The total axial expansion of the buffer in the deposition borehole was 4 cm which is considered to be acceptable. The test evolved as predicted and the installation method was deemed to work well for the tested water inflow conditions. The model of the early THM (Thermal Hydraulic and Mechanical) evolution was updated based on results from the first full scale installation test.

The purpose of the test done under wet conditions was to test the installation method for relatively large water inflow. Using the model and earlier experiences from buffer protection development, different designs for the buffer protection were evaluated. From this, a design where the buffer protection only extended down to the top of the canister, showed the most promising results when modelled and was selected for the wet test.

The wet condition test was installed as intended but it did not develop as predicted as unexpected fracturing of the upper bentonite rings occurred. The fracturing could be explained when open pathways (joints between buffer blocks) between the inner and outer slot were introduced into the numerical model. The new numerical simulation showed that for some fracture widths hot air would flow from the hotter inner slot to the outer slot. The temperature of the air decreased enough to cause condensation of water at the outer parts of the bentonite blocks. The condensed water then caused swelling and cracking of the bentonite rings. The magnitude of cracking was such that parts of the blocks fell into the outer slot, a situation that is not considered to be acceptable since it obstructs pellet installation and results in lower installed buffer density.

The results from the tests for wet conditions in combination with the increased understanding of the early THM processes made it evident that the developed buffer protection does not result in a robust installation process.

Based on the predicted water inflow to the deposition holes (Joyce at al. 2013) and the results from Test 1, this installation method will give a robust installation for about 6 000 of the 6 916 deposition holes in the planned repository in Forsmark. If the installation sequence is modified so that the deposition holes with water inflow > 8E−4 m/s are installed in conjunction with the backfilling of the tunnel the majority of the remaining deposition holes can also be used for deposition. The recommended installation method is therefore simultaneous installation of blocks and pellets without any buffer protection.

Sammanfattning

Denna rapport beskriver den senaste utvecklingen när det gäller installation och utformning av bufferten. Kraven på bufferten har uppdaterats sedan ansökan (Posiva SKB 2017) och buffertens utformning har uppdaterats baserat på dessa nya krav. Konstruktionsarbetet och den resulterande buffertutformningen samt rekommendation för installationsmetod presenteras i denna rapport.

Resultaten från tidigare teknikutveckling (Johannesson et al. 2014) visade att SKB:s tidigare metod för installation av bufferten inte var robust. Anledningen är att den termiska gradienten leder till omfördelning av vatten i buffertblocken vilket resulterar i att buffertblocken spricker. Sprickorna är inte problematisk i sig själva men kan resultera i låg slutlig buffertdensitet och praktiska installationsproblem. I syfte att uppnå en robust installation har två installationsprocedurer, en för relativt torra deponeringshål och en för våtare deponeringshål, utvecklats och testats. Två fullskaletester av buffertinstallation, en för torra förhållanden och en för våta, har genomförts.

I testet av metod för torra förhållanden installeras pelletsfyllningen direkt efter blocken. Testet simulerade tiden från installationen av bufferten och kapseln tills tunneln ovan deponeringshålet återfyllts. Denna tidsperiod uppskattades vara maximalt 90 dagar. Installationen gjordes i ett fullskaligt deponeringshål med ett naturligt vatteninflöde på 8E−4 l/min. Det mesta av vatteninflödet var relaterat till en zon nära tunnelgolvet. Kapseln var utrustad med en värmare som genererade 1 700 W vilket motsvarar den planerade effekten från det använda kärnbränslet i en kapsel.

Under demontering av testet togs prover av bufferten och vattenkvot och densitet bestämdes. Den totala axiella expansionen var 4 cm vilket anses godtagbart. Testet utvecklades som förväntat och bedömningen är att installationsmetoden fungerar bra för det testade vatteninflödet.

Syftet med testet för våta förhållanden var att simulera förhållandena vid installationen av buffert vid relativt stora vatteninflöden till deponeringshålet. Tidigare erfarenheter och modellering användes för att vidareutveckla buffertskyddet. Det testade buffertskyddet sträcker sig från toppen på bufferten ner till toppen av kapseln.

Testet för våta förhållanden installerades som planerat men tidigt kunde det konstateras att det inte utvecklades som förväntat. De översta buffertringarna och blocken sprack betydligt mer än förväntat. Detta kunde förklaras när öppna sprickor mellan den inre och den yttre spalten introducerades i den numeriska modellen. Modelleringen visade att luft strömmar från den varmare inre slitsen till den yttre slitsen. För vissa sprickbredder minskar temperaturen hos luften tillräckligt för att orsaka kondensation av vatten vid de yttre delarna av bentonitblocken. Det kondenserade vattnet orsakar därefter sprickor i bentonitringarna. Magnituden av sprickbildning där delar av blocken föll i den yttre slitsen anses inte vara acceptabel, eftersom den kan hindra installationen av pelletar och därmed ger en lägre installerad buffertdensitet.

Resultaten från buffertinstallationstestet för våta deponeringshål i kombination med den ökade förståelsen av de tidiga THM-processerna gjorde det uppenbart att det utvecklade buffertskyddet inte resulterar i en robust installationsprocess. Baserat på det modellerade vatteninflödet till deponeringshålen (Joyce et al. 2013) och resultaten från det fullskaliga installationstestet för torra deponeringshål, kan det uppskattas att denna installationsmetod kommer att ge en robust installation för ca 6 000 deponeringshål av de 6 916 möjliga positionerna i det planerade slutförvaret i Forsmark. Om installationssekvensen dessutom modifieras så att deponeringshålen med vatteninflöde 8 > 1E−4 installeras sist, i samband med återfyllningen av tunnlarna, kommer en stor andel av de kvarvarande deponeringshålen också att kunna användas för deponering.

Contents

1 Introduction

1.1 Background

The results of earlier technology development (Johannesson et al. 2014) was that SKB's reference method for the installation of the buffer does not provide a robust installation. The thermal gradient resulted in a redistribution of water in the blocks. Convection in the gap between the buffer protection and buffer blocks accelerated drying of the buffer. Water condensed on the inside of the buffer protection and cumulated at the bottom of the buffer protection where it came in contact with buffer blocks that swelled. Desiccation cracks also occurred in the buffer blocks, causing concern that cracking of the buffer blocks could result in blocks falling into the gap and preventing the retrieval of the buffer protection. Swelling of the bottom block while the protection sheeting was in place also results in a lower density in this volume and poses a risk of jamming the buffer protection in the borehole. It was therefore concluded that this installation approach does not provide a robust buffer installation method.

The recommendation was to move forward with two installation procedures, a method for use in relatively dry deposition holes and a method for wetter deposition holes. For the relatively dry holes, simultaneous installation of buffer blocks and pellets were recommended. For the wet deposition holes it was recommended to use 1) controlled atmosphere or 2) coating of the buffer block with a material that delays hydration or 3) further development of buffer protection methodologies. Approaches 1) and 2) have been investigated prior to the work presented here (Eriksson 2017). The conclusions was that 1) and 2) are not recommended for further investigation (Eriksson 2017).

1.2 Objective

The objective of the work described in this report is 1) to improve the buffer installation method and 2) to update buffer design based on reformulated technical design requirements. To achieve 2) it was necessary to improve the understanding the early THM processes in the buffer. The improved understanding was also used for designing the buffer and backfill so that the requirements related to long-term safety are met while a rational and robust installation is achieved. This includes describing the resulting thermal conductivity of the buffer and its components.

1.3 Report overview

In *Chapter 1, Introduction,* the background and prerequisites are given. In *Chapter 2, Iterative development for understanding Thermal-Mechanical (THM) processes,* the way the work was structured, i.e. how modelling, laboratory and full scale tests were combined to build knowledge and come to the conclusions, is described. In *Chapter 3, Laboratory tests*, the laboratory tests and the related modelling is described. In this chapter the general background and basic model used is also described. In *Chapter 4, Full scale test 1…,* the test performed to simulate the early THM evolution in a relatively dry deposition hole is described. The chapter also includes pre-modelling and how the results were used for designing the test. In *Chapter 5, Full scale installation test 2…,* the test performed to test the installation method for higher water inflows is described together with input from pre-modelling. In *Chapter 6, Post modelling and analysis,* the improvements made to the model based on the lessons learned from the tests is described. In *Chapter 7, Buffer design and installation method,* the requirements set on the buffer, the method for buffer design and the TH evolution of the recommended buffer design is presented. In *Chapter 8* the conclusions and recommendations considering buffer design and installation method are given.

1.4 Prerequisites

1.4.1 Installation sequence

When the work in this report was initiated, the installation sequence assumed was according to that described in the application: First buffer and canisters are installed in all deposition holes and thereafter the deposition tunnel is backfilled. This meant that the buffer in a deposition hole might not get support/restraint by the backfill for up to three months. The knowledge gained in the work presented in this report resulted in a recommendation to change the deposition sequence. This is described in Chapter 7.

1.4.2 Anticipated water inflow

The inflow to the deposition holes in Forsmark have been modelled by Joyce et al. (2013, Section 3.1) and the results are shown in Figure 1-1.

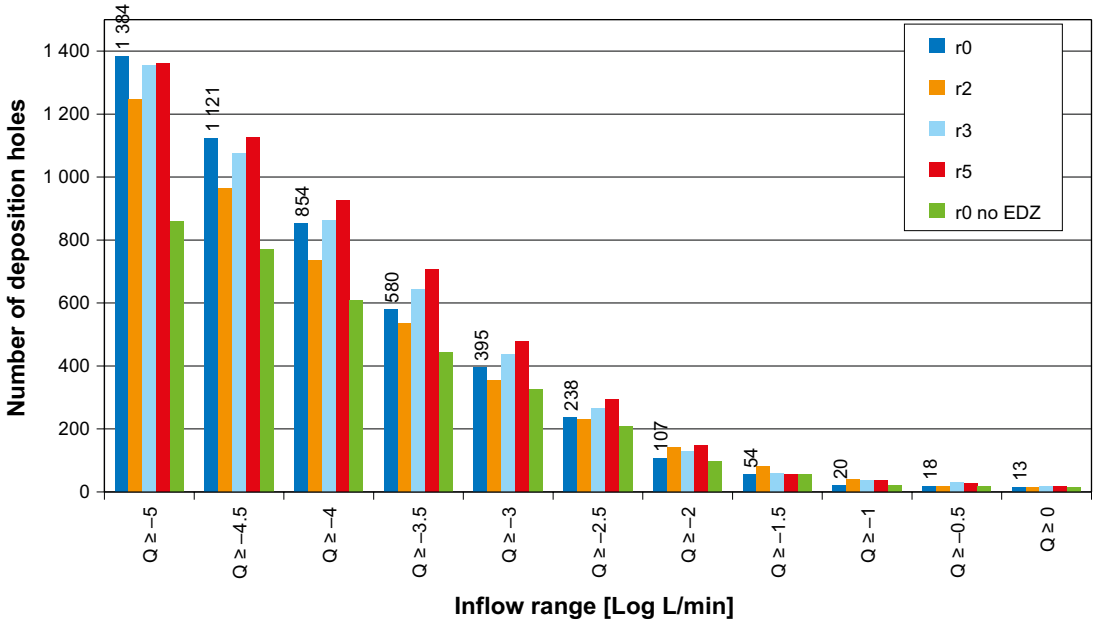

Figure 1-1. *Cumulative distributions of the total inflow to the individual deposition holes. The different columns represent different realisations of the fracture network in the bedrock based on the available statistics from the site investigation. (Joyce et al. 2013, Section 3.1). The model is based on a total of 6916 deposition holes. For realisation r0 a total of 854 deposition holes have an inflow higher of equal to E−4 l/min, i.e. 6062 deposition holes have an inflow lower than E−4 l/min. This means that 88 % of the deposition holes have an inflow lower than E−4 l/min.*

2 Iterative development for understanding Thermal-Hydraulic-Mechanical (THM) processes

2.1 Problem description and hypotheses

Before the start of the development work described in this report, the current conceptual understanding of the early THM processes were described. Hypotheses for the THM processes and for the function of buffer protection system were formulated. Risks for the proposed installation methods that needed further investigations to evaluate were also identified. The hypotheses were used for setting up the tests and modelling described in Chapter 3, 4, 5 and 6 in this report. The results from the performed work was used for developing, evaluating the hypotheses and for making conclusions. The key hypotheses examined include those that assume that:

a) Simultaneous installation of buffer and pellet materials works in most of the deposition holes but may result in unacceptable upward heaving if the water inflow is too high. There is a risk that the axial swelling heaving will be greater than what is acceptable even for relatively low water inflows. The consequence would be that the number of deposition holes where this method can be used will be low.

b) The risks associated with the installation method with a developed buffer protection are that the drawbacks of the original buffer protection remain. Water in the buffer blocks is redistributed so that the buffer blocks crack. If the cracks are too extensive, this would result in pieces of buffer blocks falling into the gap when the buffer cover is removed. This would in turn result in an uneven density distribution in the deposition hole. Block pieces can also lock the buffer protection so that it cannot be dismantled. How the buffer stack expands radially and axially as a result of heating, redistribution of water, cracking and swelling have to be investigated as it affects the installed density.

c) The thermal conductivity of the buffer after redistribution of water, drying and cracking are adequately described. The thermal conductivity of the buffer has a considerable impact on the thermal dimensioning of the repository. The processes described in (b) were not considered fully in the most recently completed assessment of the canister spacing in Forsmark (Hökmark et al. 2009). To understand, describe and quantify processes and risks described above requires a combination of modelling, testing in laboratory scale and full-scale tests. SKB has in earlier development work built up the ability to model THM processes in the bentonite including convection in the slots. The latter turned out to have great impact on the redistribution of water for the traditional buffer protection (the reference design of the application). A major challenge handled in this report is to understand, describe and model cracking the buffer blocks. Results from earlier experiments indicate that the blocks crack in a systematically predictable manner at a certain change of the water ratio. The link between the cracking of the blocks and the upward expansion is more challenging to describe since it probably also depends on the geometry of the blocks and tensions of external loads (overlying blocks, etc.). When the blocks crack this opens new channels for convection allowing dehydration and faster redistribution of water. The array of laboratory tests, full scale tests and modelling was developed to increase the understanding of the described processes.

d) One hypothesis is that the resistance to air flow in the slots depends on the type of pellets, the amount of fines and the water content of the pellets filling. Convection in the pellet filled gap can also play a role in the large-scale redistribution of water in the system and thus the resulting thermal conductivity. The heating of the air in the gap results in moist air being transported upwards. When the air cools, the water condenses increasing the water content in the pellet filling. This is evaluated through experiments and numerical and conceptual modelling presented in this report.

2.2 Strategy for the work

The approach for the successive development of understanding the THM processes in the buffer and the interaction with development of design and installation was developed during the planning that preceded the lab and full scale tests is provided in Figure 2-1. The 8-step process is also listed below.

1. **Design laboratory tests**

   Laboratory experiments were carried out to develop a general understanding of the early THM processes associated with the buffer. The experiments were designed to address the parameter input needs of the models.

2. **Evaluation of the laboratory tests**

   The results from the tests of water flow resistance were used to describe the relationship between pellet type, water ratio and proportion of fines. The laboratory experiments with heating of 30 cm rings were evaluated by measuring the water redistribution and by describing how the blocks cracked and by measuring the axial deformations.

3. **Updating models**

   The numerical models were updated based on the results from the laboratory tests.

4. **Design of full scale tests**

   After comparison with the tests in 30 cm scale and input from the tests of flow resistance, the models were used for simulating the THM evolution of the large-scale tests. This knowledge was used to design the buffer protection system. It was also used to position sensors in the full scale tests in locations where they provide the most information. The model was for example used to predict where water condenses and adapting the instrumentation.

5. **Evaluation of full scale tests**

   The full scale tests gave information on heaving, redistribution of water, evolution of temperature and how and to what extent the blocks crack. This was compared to predictions from the modelling results.

6. **Updating of models**

   The model was updated based on the lessons learnt from the full scale tests.

7. **Recommendation for buffer design and installation method**

   After the model update, the model is used to check and update the buffer design and installation method.

8. **Choice of installation method**

   Following completion of updating of buffer design and installation method recommendations, the reference installation method was revised.

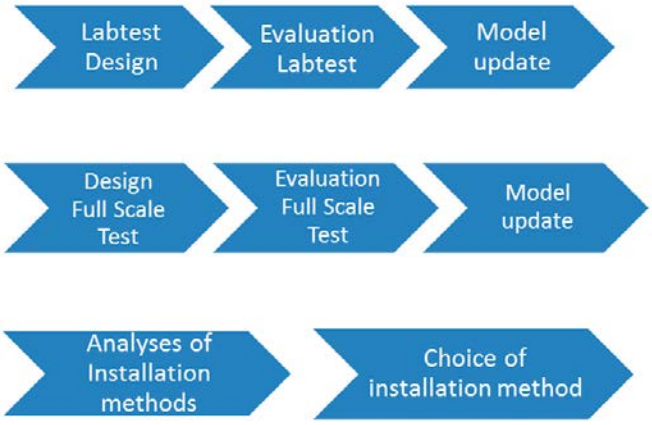

Figure 2-1. *Strategy for iterative development of design, understanding and modelling capability for early THM processes. The different steps in the process are described in the preceding text.*

3 Laboratory tests

3.1 Objective and scope

The objectives of the laboratory tests are to further develop the understanding of the processes involved in the redistribution of the water in the buffer components, buffer blocks and pellets. This includes at the time of installation and the period when the buffer together with the warm canister are standing in a deposition hole before the backfill is put in place in the tunnel above the buffer. The results from the laboratory tests are used for developing models for early THM evolution of the buffer.

An important part of this work is to further develop the models describing how humid air flows through a pellet filled gap and how the pellets take up the water from the air. Several tests where a pellets filled gap was given access to air with a specified relative humidity and air flow were performed and evaluated using numerical models. The outcomes from these tests were later used for the updating the THM model.

A test in small scale with buffer blocks and pellets filled outer gap and a heater simulating a real deposition hole was also performed. It is recognized that the scale of the experiment affects the results obtained and thus the outcome from this test cannot be used directly to describe the behaviour of the buffer in a full scale deposition hole. The small scale test is used for calibrating the numerical models used for evaluating the large scale experiments.

3.2 Air flow test through a pellets filling

3.2.1 Test set-up

In this test air with a specified relative humidity was passed through a filling of bentonite pellets at a constant air flow. The test examined water uptake of the pellets was studied as a function of the relative humidity of the air, the air flow and the duration of the test were varied. Furthermore, the increase of the flow resistance for the air to pass through a pellet filling i.e. the air pressure gradient caused by the water uptake by the pellets and the air flow was also measured.

The test set-up consisted of several tubes of acrylic, see also Figure 3-1.

1. *A mixing tube*, where dry air and humid air was mixed to a mixture with a specific relative humidity and pressurized with a constant pressure. This tube had a length of 50 cm with an inner diameter of 10 cm. A differential pressure sensor for measuring the air pressure and a sensor for measuring the relative humidity of the air was placed in this tube.
2. Underneath the *mixing tube* there was a small tube, the *bottom tube*, where possible water condensation was collected.
3. A *sample holder* was placed on top of the *mixing tube*. The tube had a total length of 50 cm and a diameter of 10 cm. This tube was filled with pellets during the tests.
4. A plate with several drilled holes (ø 8 mm) was placed between the *mixing tube* and the *sample holder.* The pellets were placed on this plate. The plate with its holes was assumed not to affect the flow rate and the air pressure gradient over the sample of pellets during the tests. The plate had an open area of 70 %.
5. A fourth tube was placed on top of the *sample holder*, the *top tube.* Inside this tube another relative humidity sensor was placed. This arrangement made it possible to measure the relative humidity of the air passing through the pellet filling with good accuracy.

The first step in the preparation was to adjust the total airflow rate to a specific value. Then the mixing of dry air and humid air was adjusted to get a specific relative humidity of the air used for the test. The next step was to prepare the sample of pellets. The bulk supply of pellets might contain undesirable fines from damaged and crushed pellets. These fines were removed by dry sieving before the sample holder was filled with pellets. The pellets used in the test was roller compacted pellets of MX-80 with an initial water content of 14.7 %.

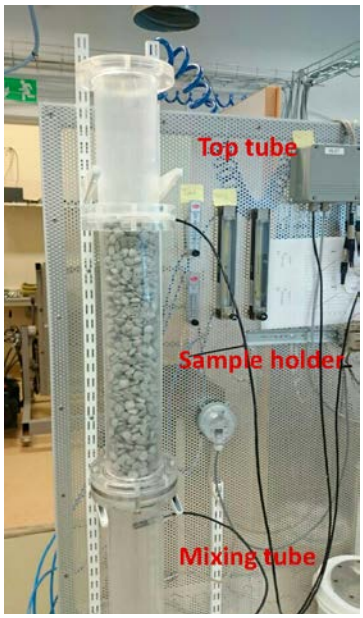

Figure 3-1. *A picture of the test set up.*

The test was then started by passing the humid air through the pellet fill for a specified time period. The airflow rate, the air pressure in the mixing tube, the relative humidity of the air entering the pellet fill and the relative humidity of the air coming out from the pellets filling was measured continuously during testing.

After the test, the gravimetric water content of the pellets filling was determined at three locations, at the bottom (0 cm), at mid height (25 cm) and at the top (50 cm) of the sample holder.

3.2.2 Test results

The tests results from a total of 10 laboratory tests are summarised in Table 3-1 and Figure 3-2. The data in these tables indicate that the largest changes in the water content of the pellets was found, as expected, close to the bottom of the sample holder i.e. at the point of inflow of the air. No significant changes in the water content of the filling was observed at the top of the sample holder, except for the test that was run for 24 h rather than 6 hours.

The measurements of the water content of the pellets are shown in Figure 3-2 and show that the change in water content increased with increasing relative humidity in the air. There was also a tendency for an increase in water content with increasing air flow, although this trend was not very strong. Figure 3-2 also shows, as expected, that the increase in water content was highest close to the air inlet.

Table 3-1. A summary of the performed test with airflow through a pellet filling.

Dry density (kg/m^3)	Duration (h)	Air flow (l/minutes)	Rel. hum. (%)	Pressure drop (Pa)	Change in water content (%)		
					Bottom	Mid height	Top
1 057	6	10	80	0.0	0.9	−0.1	0.0
1064	6	10	95	0.0	4.2	0.4	0.2
1 060	6	20	80	5.3	1.7	0.0	−0.1
1 069	6	20	90	5.6	4.0	0.3	0.0
1 063	6	20	95	5.0	6.2	0.9	0.3
1 112	6	30	80	11.0	2.9	0.4	0.3
1 067	6	40	60	17.0	−0.2	−0.1	−0.1
1 045	6	40	82	27.0	2.9	0.0	−0.3
1 056	6	40	96	7.0	5.0	0.5	0.3
1 070	24	20	95	5.0	17.1	2.0	1.0

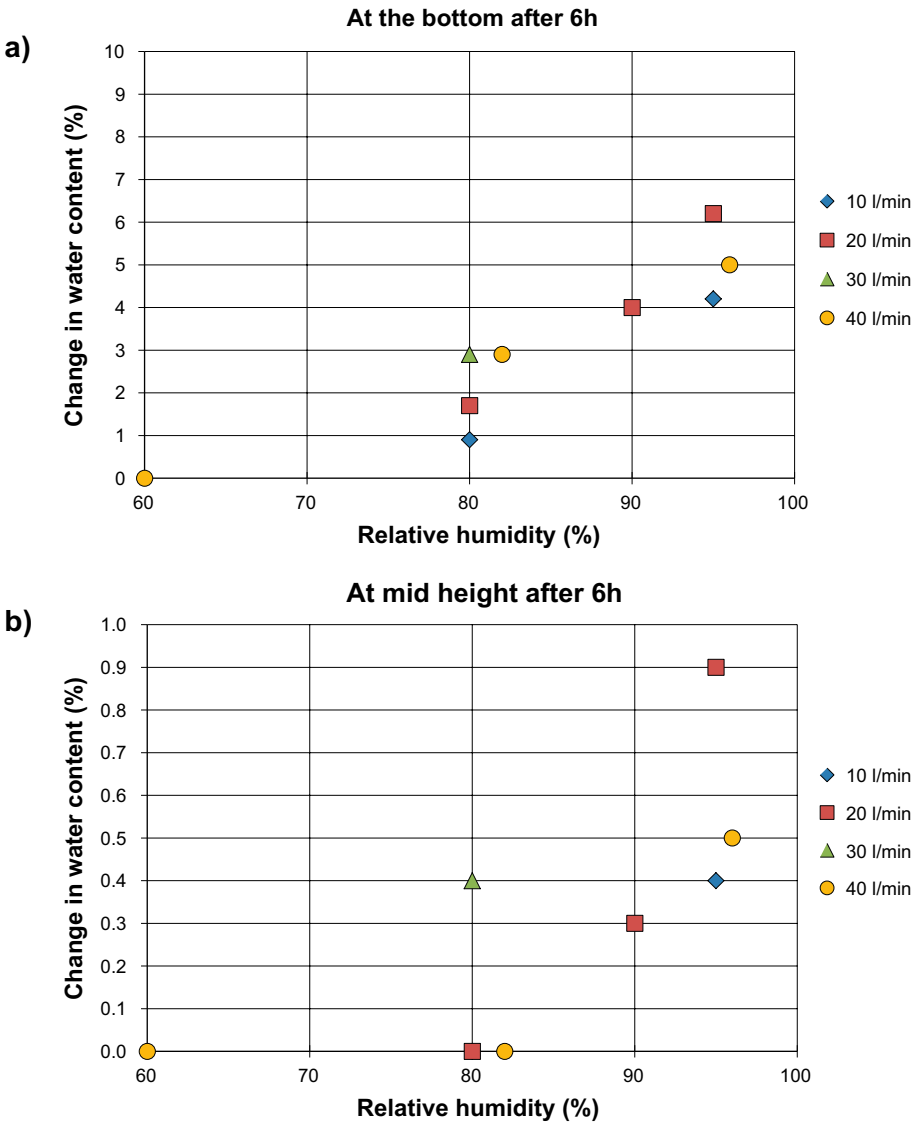

Figure 3-2. *The measured change in water content as function of both the relative humidity and the air flow at two positions in the sample holder a) at the bottom (air inflow location) and b) at mid height.*

Two examples of the evolution of the pressure drop are shown in Figure 3-3. The trend in the two examples is that the pressure drop over the pellets sample was increasing flow resistance was increasing with time (increasing flow resistance with time).

No visible impact on the pellets was observed at the dismantling of the 6 h tests. For the single test that was run for 24 h, a clogging of the pellets due to wetting close to the air inlet was observed, see Figure 3-4.

Two tests examined how the pressure drop over the pellet filling was affected by the air flow rate and the density of the filling. These tests were made with dry air i.e. no water was added. The pressure drop was measured for two installed densities of pellets and at 7 different air flow rates. The results from the tests are summarised in Figure 3-5. The figure shows that the pressure drop (resistance to flow), increased with increasing air flow rate. An increase in the filling density was also increasing the pressure drop.

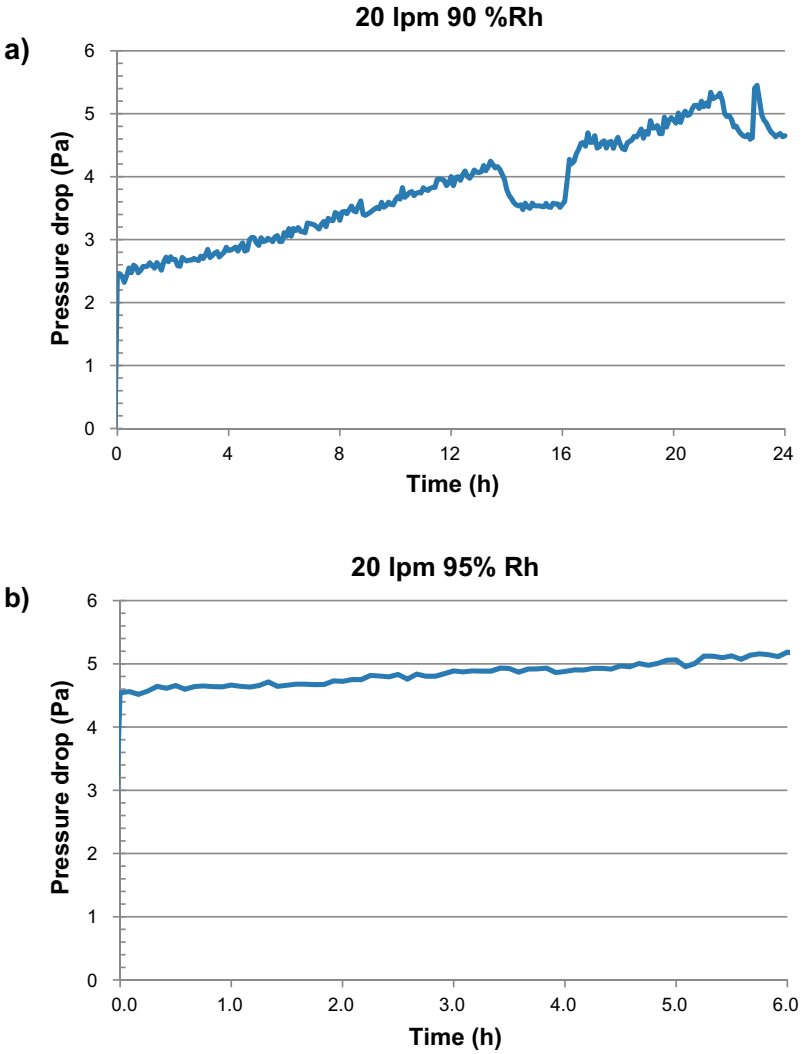

Figure 3-3. *The evolution of the pressure drop for a) a test with a running time of 24 h and b) a test with a running time of 6h. The flow in both tests was 20 litres per minute.*

Figure 3-4. *The pellets close to the air inlet at the dismantling of the 24 h test.*

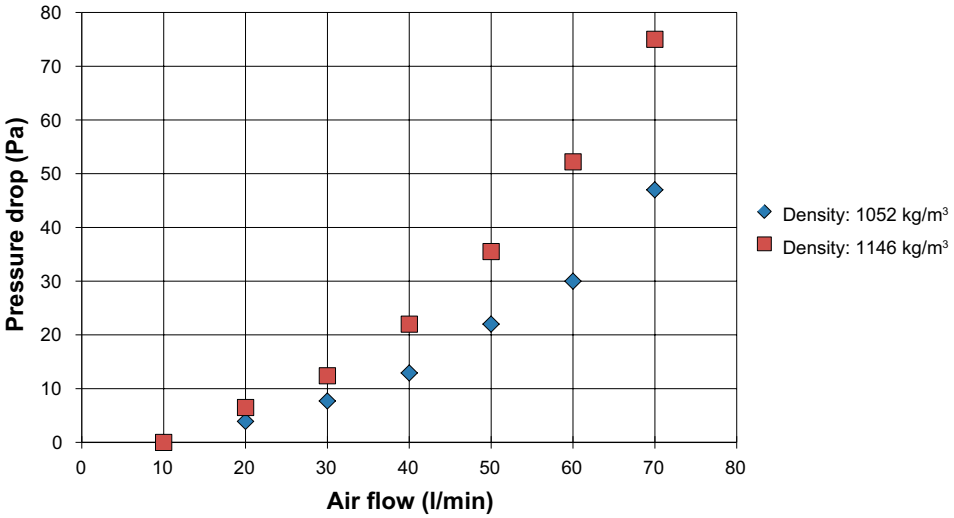

Figure 3-5. *The pressure drop over the pellet filling as function of the air flow rate. The tests were made with two different filling densities.*

3.3 Test description laboratory test with thermal gradient

3.3.1 Buffer components and heater

The test setup and dimensions are shown schematically in Figure 3-6 and in the photos provided in Appendix 1 consisted of:

- A base cylinder of bentonite (C1) on which the heater was placed.
- Four ring shaped blocks of bentonite were placed around a heater (R1–R4).
- Three solid blocks of bentonite were placed on top of the heater (C2–C4).

All the blocks had a height of 100 mm while the height of the heater was 408 mm. A groove with a diameter of about 110 mm was made in the bottom block (C4). The depth of the groove was adjusted so the gap between the top of the heater and block C2 was about 1 mm.

The power to the heater was applied by circulating hot water through pipes lead through block C1. The package of heater and bentonite blocks was placed on a plate of PVC and a pipe made of Polyethene (PE) was threaded over the bentonite blocks. The pipe consisted of two parts, one upper and one lower part with a sealing between the two parts, in order to facilitate the installation and the dismantling of the test, see Figure 3-6. The outer gap between the PE pip and the bentonite blocks was filled with pellets of bentonite. Finally, a rubber mat was placed on the top of block C4. The purpose with the mat is to minimise the desiccation of the buffer from the upper surface of block C4

The initial water content of the buffer blocks was 17.0 % and the dry density for the ring shaped blocks was 1 743 kg/m^3 while the solid blocks had a dry density of 1 695 kg/m^3. The pellets, manufactured by roller compaction, had an initial water content of 14.6 %. The bentonite, both in the blocks and in the pellets was of type MX-80.

3.3.2 Instrumentation

A total of 12 thermocouples and 4 relative humidity sensors supplied by AITEMIN were installed in the tests. The relative humidity sensors also measured the temperature. The positons of the sensors are shown in the sketches provided in Figure 3-7 and photographs provided in Appendix 1. The sensors installed consisted of:

- ThermocouplesT1 and T4 measured the temperature on the surface of the heater while the thermocouples T2 and T3 measured the temperature on the inner surface of bentonite blocks. These sensors were installed from below. Two thermocouples, T6 and T7, measured the temperature at the PE tube.

- The thermocouples T5, T8 and T10 were installed from below through the PVC plate in order to measure the temperature on the outer surface of the bentonite blocks while the sensor T11, also used to measure the temperature on the outer surface of the blocks was installed from above.
- Thermocouple T12 and relative humidity sensor RH4 measured the conditions present in the room where the test was placed.
- Relative humidity sensors RH1–RH3 measured the relative humidity in the pellet-filled outer slot. These sensors were installed from outside of the PE tube. Only the outer tip of the sensors was put into the pellets filling.
- The power to the heater was adjusted by measuring the temperature of the water circulated inside the heating device.

In addition to the measurement of relative humidity and the temperature, the displacement of the upper block was monitored continuously during the test. No sensors were installed in the upper part of the buffer, see Figure 3-7.

3.3.3 Installation

All the installed blocks were weighed and their dimensions were measured before their installation. Block C1, R1 and R2 were first installed and then the thermocouples were installed. The straightness of the stack of blocks was checked. The heater was then installed and the hole in the centre of block C1, through which the pipes from the heating system and the thermocouples were led, was filled with insulation. Block R3 was then mounted and the first part of the PE-pipe was put on place and the outer slot was filled with pellets. The rest of the blocks were then installed, the second part of the PE-pipe was put on place after which the rest of the outer slot was filled with pellets. A rubber mat was placed on the top of block C4 and finally steel plate was placed in the central void and this was used to determine the vertical displacement of the bentonite. The sequencing of the assembly is shown photographically in Appendix 1.

The logging of the temperature and the deformation was tested over a weekend before the test started.

The initial dry density of the pellet fill was calculated to be 900 kg/m^3.

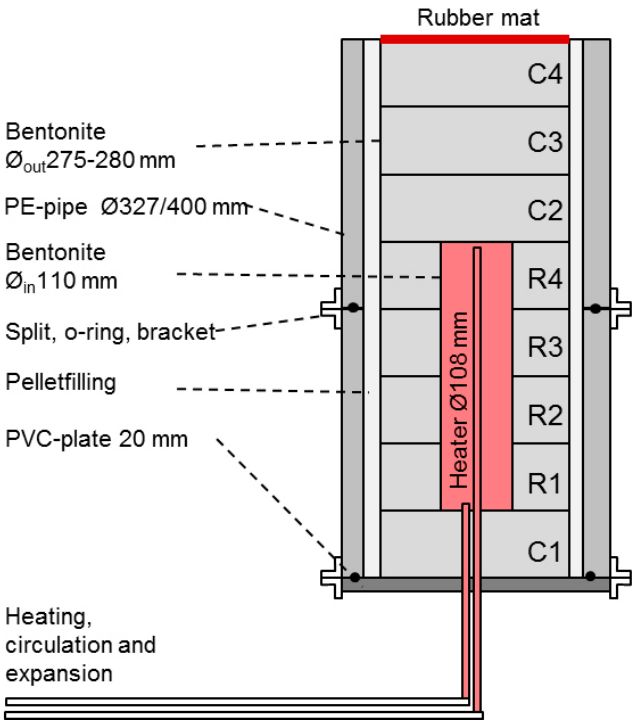

Figure 3-6. *A schematic drawing of the laboratory test set up.*

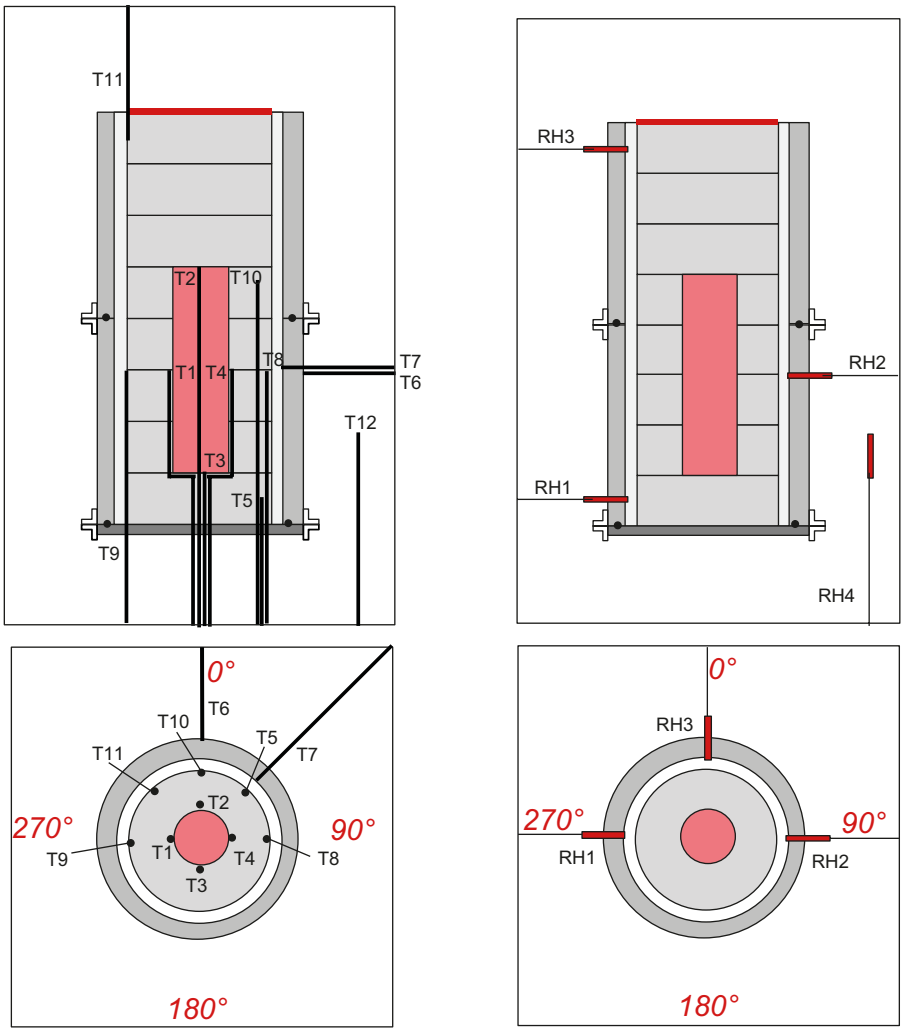

Figure 3-7. *The position of the thermocouples and RH-sensors installed in the laboratory test.*

3.3.4 Results

Running of the test

The test started by setting the temperature on the circulated water to 40 °C and the circulation pump was started. Once the temperature was stabilized, it was stepwise increased in 10 °C increments every hour until 60 °C was reached in the circulated water (Figure 3-8). When the measured temperature close to the heater was about 50 °C, the temperature of the circulated water was adjusted to 67 °C in order to reach 60 °C on the surface of the heater. After about 24 h, all the temperature measurements seem to have essentially stabilized ash shown in Figure 3-8. A continuing, very slow increase of the temperature was observed between 12 and 24 hours and so no further adjustment of the power to the heater was made. Only minor changes of the temperature were observed after 24 hours and the temperatures measured at the surface of the heater ranged between 58 and 62 °C after this time, see Figure 3-9.

The measured displacement of the upper surface of the test is shown in Figure 3-10b. The deformation was limited to about 1 mm.

After 336 hour, about 2 weeks, the power to the heater was switched off and the tubes for the water were emptied. The test was cooled down during 11 hours and after that the dismantling started.

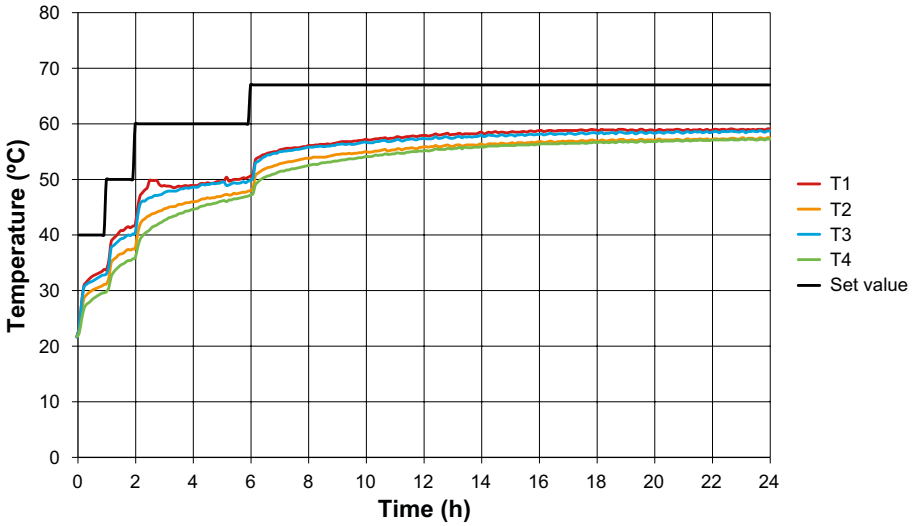

Figure 3-8. *Readings during the first day of the test from thermocouples installed on the heater.*

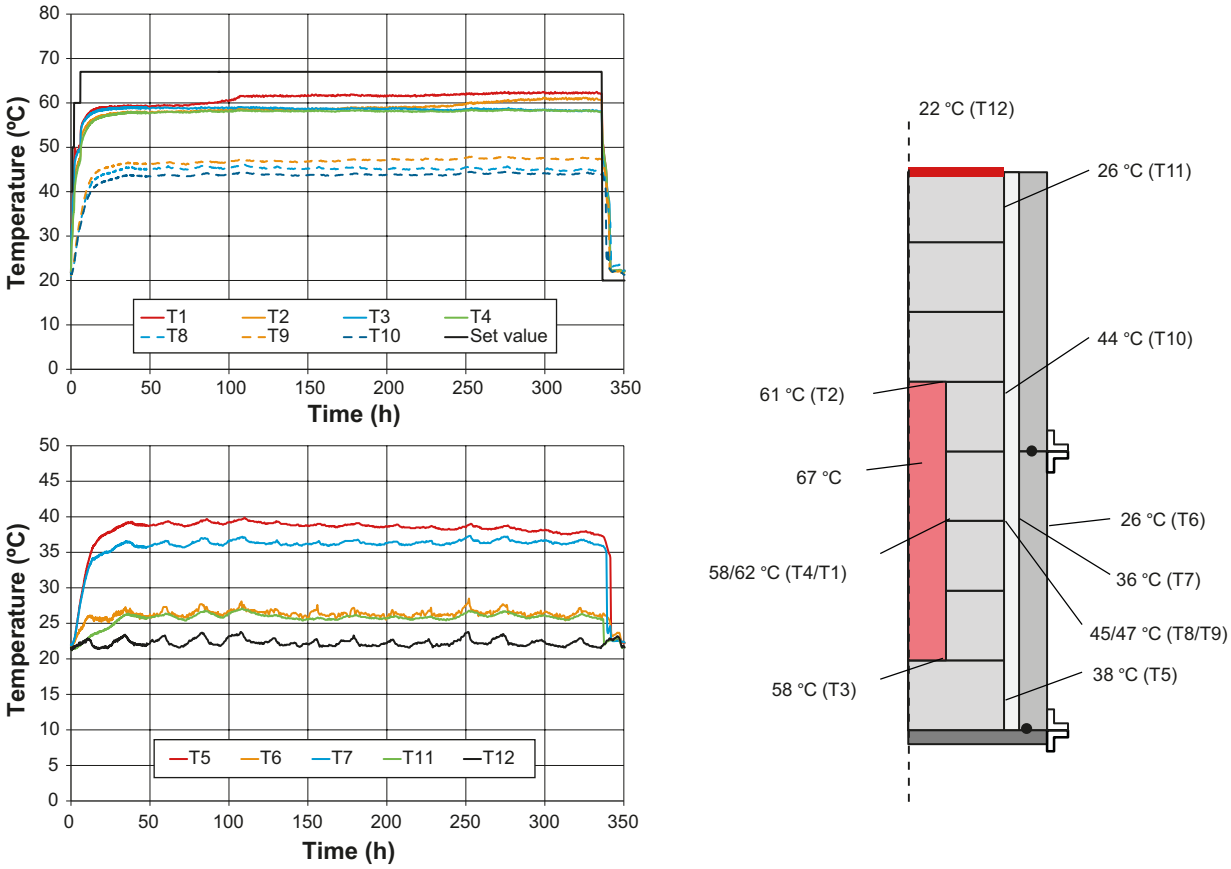

Figure 3-9. *The temperature evolution in the test over the whole test period (left). The measured temperatures at the last day before the dismantling (right).*

The relative humidity measured in the tests is shown in Figure 3-10. Note that sensor No RH4 was measuring the relative humidity in the room were the test was placed. Sensor RH2 indicated 100 % relative humidity after about one day until it was dried out during the dismantling of the test, see Figure 3-10. The reason for this was probably that a condensation of water occurred on the sensor since the temperature was lower at that point compared to the rest of the outer tube due to high thermal conductivity of the sensor.

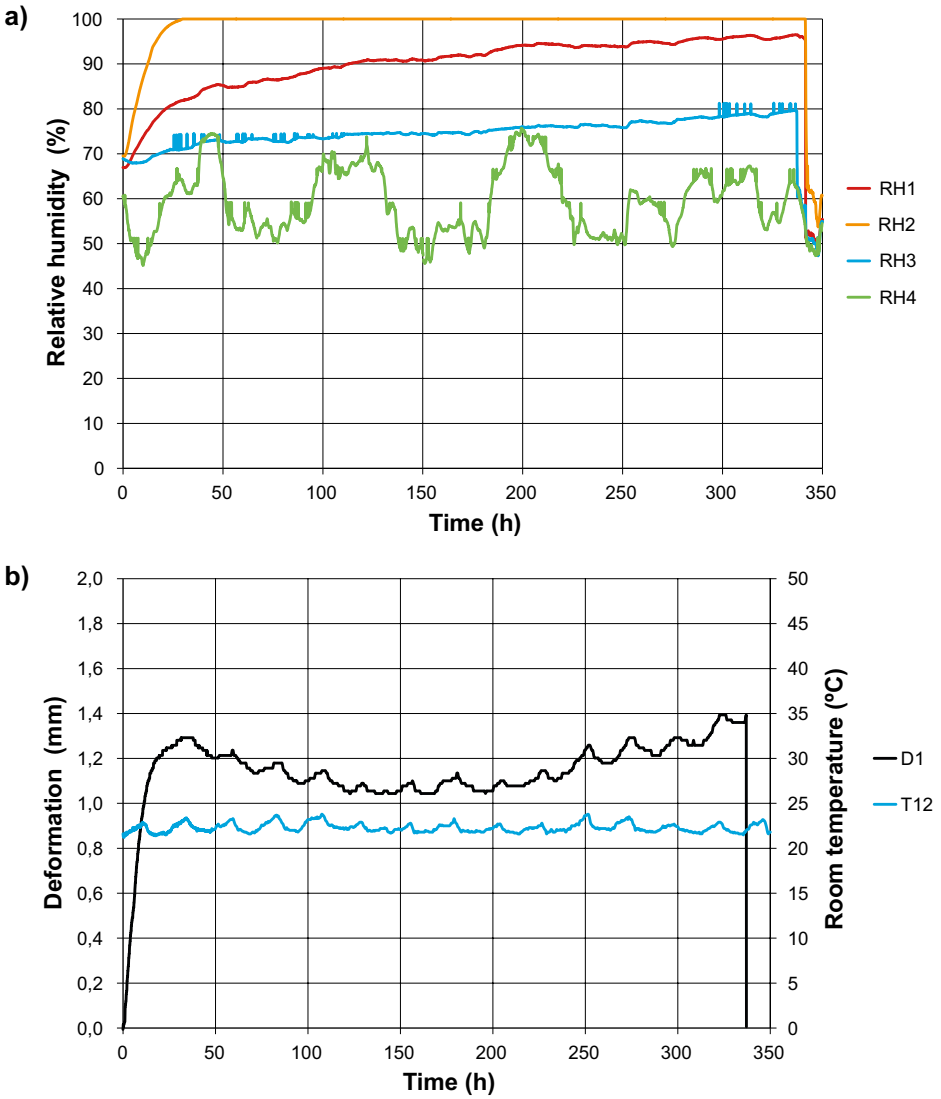

Figure 3-10. *Evolution of a) relative humidity and b) the displacement of the upper surface of the stack over the test period.*

The measured displacement of the upper surface of the test is shown in Figure 3-10b. The deformation was limited to about 1 mm.

After 336 hour, about 2 weeks, the power to the heater was switched off and the tubes for the water were emptied The test was cooled down, by passive air cooling, during 11 hours and after that the dismantling started.

Dismantling of the test

After the deformation sensor on the top of the test was removed the dismantling and sampling of the bentonite started. Appendix 1 provides photos showing the appearance of the various sections of the test at the time of dismantling. The dismantling was done as follows:

- A photo was taken of the block before it was removed.
- Samples of the pellets were taken in direction 0° and 180°.
- The rest of the pellets surrounding the block were removed. The pellets were weighed to allow for mass and water content determinations.
- Installed sensors were removed.
- The block was removed.

Each block was weighed and its dimensions were measured at the same positions as at the installation. of the thermocouples. None of the blocks had fallen into pieces during the test but some of them were damaged during the dismantling of the test.

The outer tube, consisting of two parts, was removed as soon it was possible. The outer pipe, consisting of two parts, was removed as soon it was possible i.e. the upper part of the pipe after the sampling of block R4 while the lower part was removed before the sampling of block C1. The heater was lifted up and out of the test assembly just after block R1 was removed

It was noted that pellets were stuck on the inside of the PE pipe. The pellets covered almost the whole inner surface of the lower pipe while only parts of the upper pipe were covered with pellets (direction 0–150°).

A compilation of the weights of the blocks and pellets before and after the test is shown in Table 3-2. The data in the table shows that the blocks have lost water, about 0.76 kg while the pellets filling in the outer slot have taken up water, about 0.51 kg and thus the bentonite as a whole has lost about 0.25 kg water by vapour transport through the outer slot From the data in the table it is also possible calculate the final water content, as an average for each separate section of the test, see the left column of the table. These values are in accordance with the measured water contents, see section below.

Table 3-2. Initial and final weight of the installed blocks and calculated final water content of them.

Block No	Initial weight (kg)	Final weight (kg)	Difference in weight (kg)	Water content*) (%)
C4	11.961	11.934	−0.027	16.7
C3	12.035	12.047	0.012	17.1
C2	11.981	11.978	−0.003	17.0
R4	10.361	10.280	−0.081	16.1
R3	10.432	10.326	−0.106	15.8
R2	10.396	10.243	−0.153	15.3
R1	10.390	10.173	−0.217	14.6
C1	11.632	11.444	−0.188	15.1
Pellets	19.385	19.898	0.513	17.6

*) Calculated from the initial water content of the blocks (17 %) and pellets (14.6 %).

Determination of the water content

The water content was determined on samples taken in several positions in each block.

For the ring shaped blocks, block R1–R4, in total 16 samples were taken from each block. The samples were taken at the centre of the blocks in axial direction. Eight of the samples were taken in direction 0° where most of the sensors were installed and the rest of the samples were taken in direction 180°, which is at the centre of the part of the test with no sensors. For block R1 an addition set of samples were taken in direction 90°.

In the bottom block, block C1, through which tubes were led, a total of 16 samples were taken in two directions 0° and 180° respectively.

In block C2 placed just above the heater, 25 samples were taken. These samples were taken close to the bottom of the block, i.e. close to the heater also in the two directions 0° and 180°.

A total of 25 samples were taken in each of blocks C3 and C4. These samples were taken at the centre of the blocks in axial direction.

The determinations of the water content in each block are shown in Figure 3-11. Note that also the water content of the pellets in the outer slot at radial distance of 150 mm is plotted in the same plots.

Pictures of the buffer at the dismantling of the test are shown in Appendix 1.

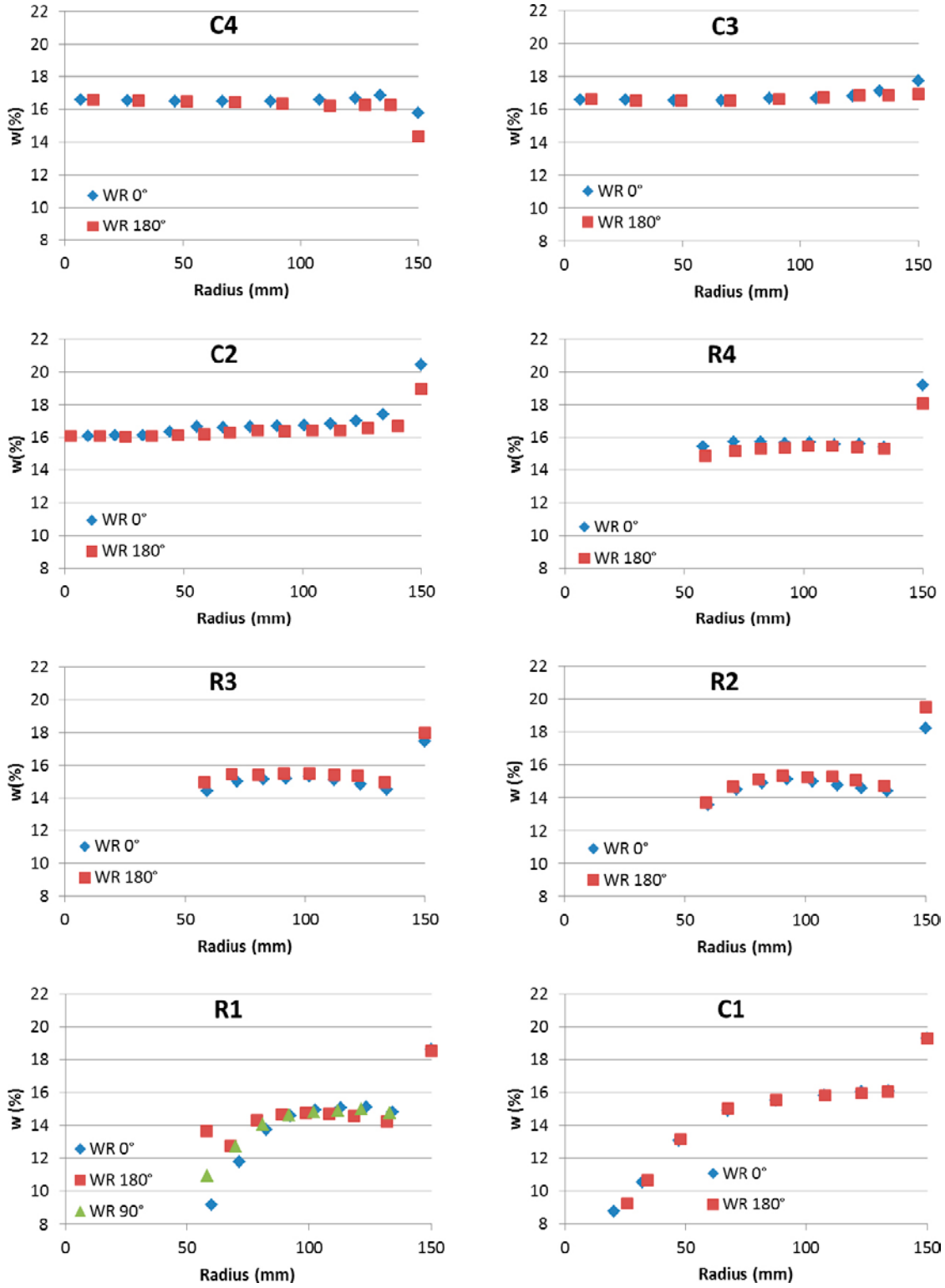

Figure 3-11. *The determined water contents of the blocks and pellets at the time of dismantling the test as a function of the distance from the centre. Note that the water content for the pellets is plotted at the radial distance 150 mm.*

Analysis of the experiment

The temperature was measured with thermocouples at four points (T1…T4) on the surfaces of the heater see Figure 3-6. Three of the senses gave similar values while one sensor (T1) showing a 3 °C higher temperature after about 100 hours, see Figure 3-9. The temperature is set by water circulating inside the heater and the determinations which should give an axisymmetric temperature on the heater surface. Furthermore, the water content after the test are indicating an axisymmetric distribution, see Figure 3-11.

The temperature drop over the buffer was determined in two directions, see Figure 3-7, direction 270° by the sensors T1 and T9 which show a temperature drop over the buffer after 300 hours of about 14.7 °C and in direction (90°) by the sensors T4 and T8 with a temperature drop of 13.3 °C.

The temperature measurements are indicating that the temperature in the test was not axisymmetric. One explanation for this might be that the heater was not placed exactly in the centre of the ring shaped blocks and thus the gap between the heater and the inner surface of the block was not the same in all directions. The nominal gap was 1 mm. The same reasoning can be made for the outer gap filled with pellets with a nominal value of about 25 mm.

3.4 Modelling

3.4.1 Introduction

Thermo-hydraulic modelling of water redistribution in compacted bentonite blocks has earlier been made with good result. However, for the modelling of the pellet filled slot no good mathematical models are available. The pellet filling is very porous with large pores between the pellets, therefore air can move in the pellet filling. Due to the heat gradient that is present over the pellet slot there will be air convection. This air circulation will move vapour around in the pellets. It is also believed that this transport of vapour could be very large compared to the vapour diffusion and water transport due to suction gradients. Therefore, a first attempt to develop models for the pellet slot has been done and these models are described and tested against the laboratory scale tests in this chapter.

3.4.2 Models for the buffer blocks

To model the water transport in the buffer two processes are considered, water transport in porous materials which is modelled with the Richard equation, Equation 3-1, and vapour transport which is modelled with the diffusion equation, Equation 3-4

$$\frac{C_m}{g}\frac{\partial p_s}{\partial t} + \nabla \cdot \left(-\rho \frac{\kappa_r \kappa_s}{\mu} \nabla \mathrm{p}_s\right) = -M_w R_c \qquad (3\text{-}1)$$

Where C_m is the specific moisture capacity, g is the acceleration due to gravity, ρ is the density of water, μ is the viscosity, κ_s is the saturated permeability, κ_r is the relative permeability, M_w is the molar weight of water and R_c is the rate of evaporation in mol/s. The retention curve is described by Equation 3-2.

$$w = \frac{0.004}{1-RH} + 0.26RH + 0.035 \int_0^t \begin{pmatrix} -28.9\frac{dw}{dt}, if\ |w| \le 1 \\ 0, if\ |w| > 1 \end{pmatrix} dt - 0.035 \qquad (3\text{-}2)$$

Where w is the gravimetric water content and RH is the relative humidity. The relation between relative humidity and pressure is described by Kelvin equation.

The retention curve used is based on MX-80 data and is shown in Figure 3-12. The retention curve also includes a function to capture the effect of hysteresis when switching from drying conditions to wetting conditions. This hysteresis effect is important because it is likely that there will be both areas with drying conditions and wetting conditions. There is a large difference in equilibrium water content at the same relative humidity for these two conditions.

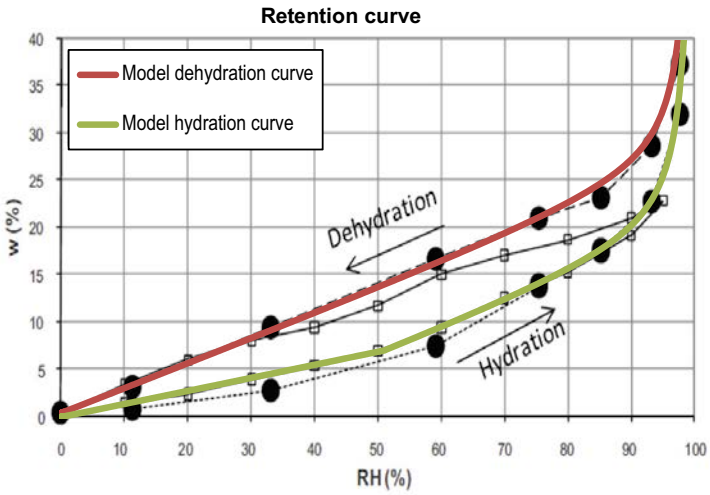

Figure 3-12. *Retention curve used in the model compared to data taken from Åkesson et al. (2010).*

For the saturated permeability, Equation 3-3, and vapour diffusion coefficient, Equation 3-5, relations from Åkesson et al. (2010) is used. The relative permeability is taken to be the cube of the degree of saturation.

$$\kappa_s = 1.21\ 10^{-21} e^{(21.3(\varphi - 0.363))} \tag{3-3}$$

Where φ is the porosity.

The diffusion equation is used to predict the water vapour movement in the bentonite.

$$\frac{\partial c}{\partial t} + \nabla \cdot (-D \nabla c) = R_c \tag{3-4}$$

$$D = \frac{5.9\ 10^{-6} T^{2.3}}{P_g} \tag{3-5}$$

Where T is the temperature and p_g is the gas pressure.

The heat transfer in the buffer blocks is modelled with the heat equation, Equation 3-6.

$$\rho C_p \frac{\partial T}{\partial t} + \nabla \cdot (-\lambda \nabla T) + \rho C_p \mathrm{u} \nabla \mathrm{T} = 0 \tag{3-6}$$

The thermal conductivity, λ, of the buffer blocks is a function of both water content and density. In this work it is assumed that the thermal conductivity is proportional to the normalized cross section area which is the area of the pores subtracted from the total area divided with the total area in one cross section. The thermal conductivity can then be expressed according to Equation 3-7.

$$\lambda = \big(1 - \varphi(1 - S_r)\big)\mathrm{a} - b \tag{3-7}$$

Where a and b are constants. When the expression is fitted to experimental data, see Figure 3-13, it can be seen that the Equation 3-7 describes the total thermal conductivity for a wide range of densities and water contents. When the Equation 3-7 is fitted to the data it suggests a thermal conductivity of the saturated clay material, a, is approximately 2.6 W/mK and the constant b is approximately 1.24 W/mK. This value of b suggests that the bulk density of the granulate is approximately 1 000 kg/m^3 which is close to what has been observed for bentonite before compaction.

3.4.3 Models for the pellet slot

As a first attempt to model the water transport in the pellet slot some simplifications are made. In this model it is assumed that the vapour will instantaneously go into equilibrium with the pellet and that the entire pellet will have the same water content. It is obvious that this is not the case in a real system were the surface of the pellet can have a different water content then in its centre. This would probably mean that this model will underestimate the transport of vapour due to air movements since the model assumes that no vapour can pass a point before full moisture equilibration has occurred with the pellet. Despite this simplification the model was used since they will assist in developing a better understanding of the system. Further development of the model is likely needed to better predict the water transport in the pellet filling.

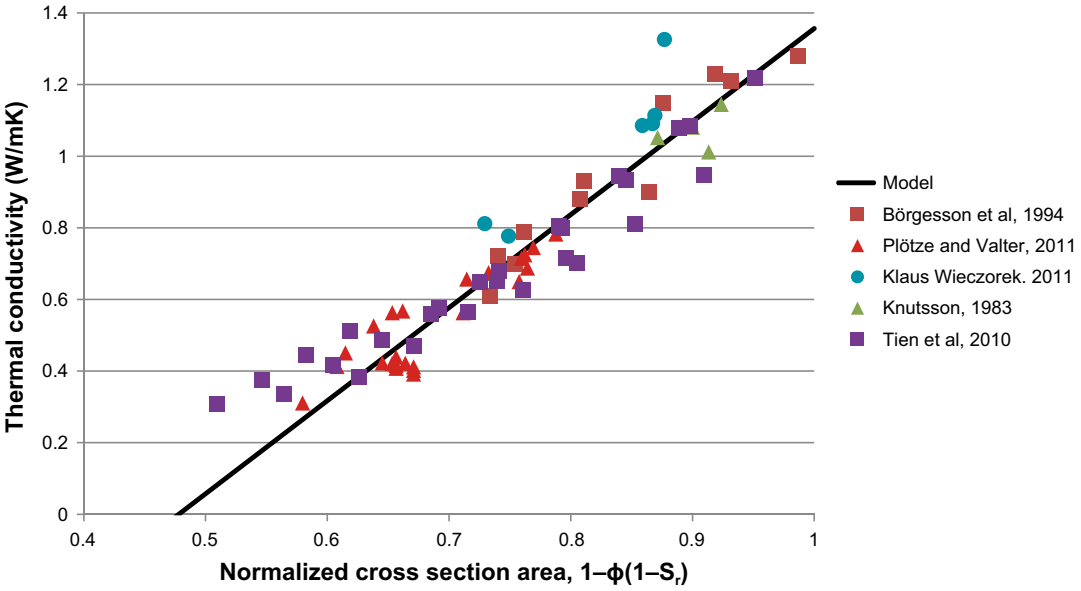

Figure 3-13. *Thermal conductivity model compared to data from different sources.*

For the water transport in porous material the same equation is used as for the blocks. To model the water vapour diffusion the convection diffusion equation, Equation 3-8, is used.

$$\frac{\partial c}{\partial t} + \nabla \cdot (-D\nabla c) + u\nabla c = R_c \qquad (3\text{-}8)$$

In Equation 3-8 there is a velocity term, u, which needs to be calculated. The air velocity is calculated with the Navier-Stokes equation, Equation 3-9.

$$\rho\left(\frac{\partial u}{\partial t} + u\nabla u\right) = -\nabla p + \nabla \cdot \left(\mu(\nabla u + (\nabla u)^T) - \frac{2}{3}\mu(\nabla \cdot u)I\right) + F \qquad (3\text{-}9)$$

However, the Navier-Stokes equation describes air flow in a system without pellets and therefore needs to be modified to accurately describe the flow in the pellet slot. The pellets will introduce a friction force, F, see Equation 3-9. This force has an opposite direction compared to the velocity of the air flow.

The magnitude of the friction force is described by Ergun equation, Equation 3-10, which was initially developed to predict pressure drop in chemical reactors with pellet filling.

$$\frac{dP}{dx} = F = d\frac{(1-\varphi_{ip})^2 V_s \mu}{{D_p}^2 {\varphi_{ip}}^3} + e\frac{{V_s}^2(1-\varphi_{ip})\rho}{D_p {\varphi_{ip}}^3} \qquad (3\text{-}10)$$

Where φ_{ip} is the inter-pellet porosity. d and e are constants.

The Ergun equation was initially developed for spherical pellets. However, the expression should be valid for any pellet shape if the sphere has the same volume to surface area ratio as the actual pellet. The equation predicts that the smaller the pellets, the smaller will be the inter-pellet porosity, see Figure 3-14, and higher air velocity all results in a higher friction force which is what is expected.

The same model used for predicting the thermal conductivity of the block is also used for the pellet filling but the constants a and b are changed to compensate for the low density of the loose pellet filling. Very little data on measurements of thermal conductivity on pellets filling is available. The thermal conductivity of the pellet filling has been measured to approximately 0.2 W/mK (Kivikoski et al. 2015).

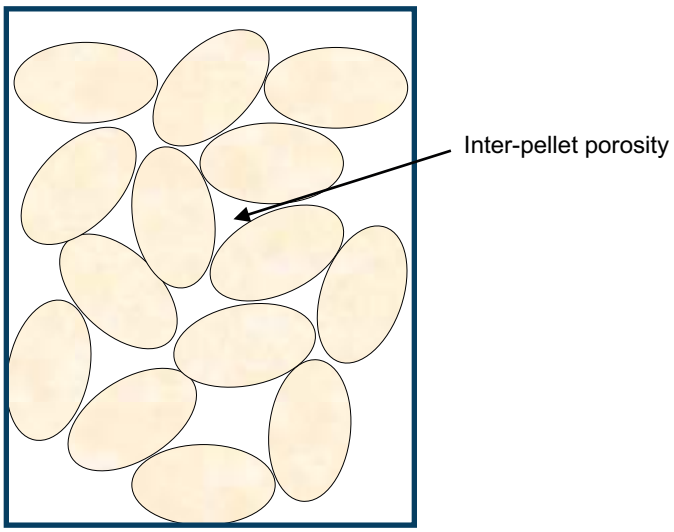

Figure 3-14. Sketch showing the inter pellet porosity used in Equation 3-9.

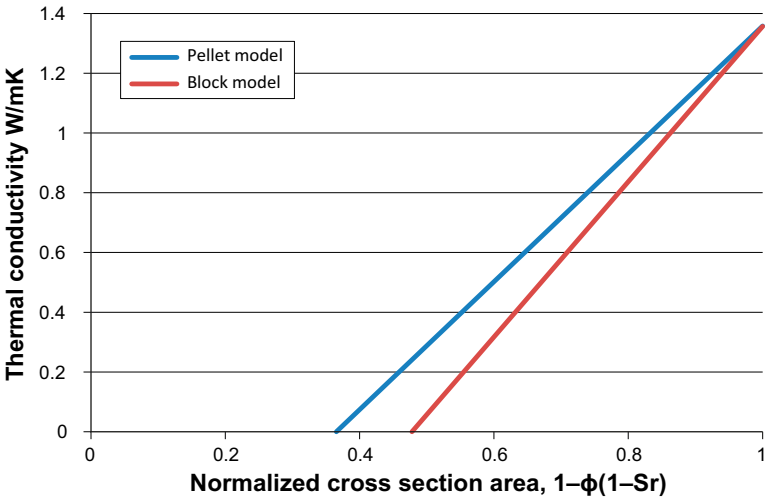

Figure 3-15. Expressions used for thermal conductivity of blocks and pellets.

3.4.4 Calibration of the pellet model against the air flow test

To find out how well the airflow resistance in the pellet filling can be determined by Equation 3-10, a test was done which is described in Section 3.2. In the original Ergun equation the constants d and e are 150 and 1.75 respectively it has been shown that the surface roughness affects the value of the constants in for example Jordi et al. (1990). Therefore some calibration needs to be done to get the correct values of the constants in the Ergun equation. This is done by fitting to the equation to experimental data. The equivalent spherical pellet diameter is calculated to be 12 mm based on the pellet size of 16 × 16 × 8 mm, see Figure 3-16. The pressure drop over the test can be calculated and a good fit is achieved, Figure 3-17, when the following values are used for the parameters in Equation 3-10, d = 150 and e = 8.75.

Figure 3-16. *Bentonite pellets used in the buffer.*

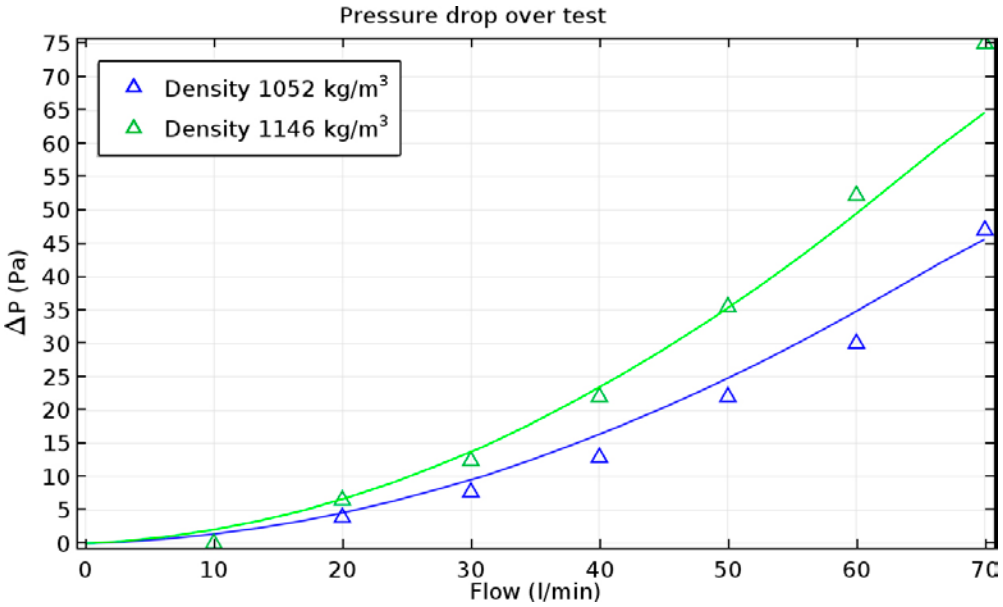

Figure 3-17. *The measured pressure drop over a pellet filling compared to model for two different densities.*

As the pellets swell, the inter pellet porosity will be reduced which leads to an increased flow resistance. The swelling model used assumes that the pellets swell or shrink according to the shrinkage curve described in Eriksson (2017). The inter pellet porosity can then be calculated according to Equation 3-11.

$$\varphi_{ip} = 1 - \rho_{d,pellet}\left(\frac{(1+2.8w)(0.5e^{-6w/0.5})}{2800}\right) \quad (3\text{-}11)$$

Where $\rho_{d,\,pellet}$ is the dry density of the pellet filling and w is the water content.

To test how well the models describes the swelling of the pellets a test where air with high relative humidity was passed through the pellets filling a tube during continuous measurement of the change in flow resistance with time. In Figure 3-18 the modelled values are compared with the experimental data.

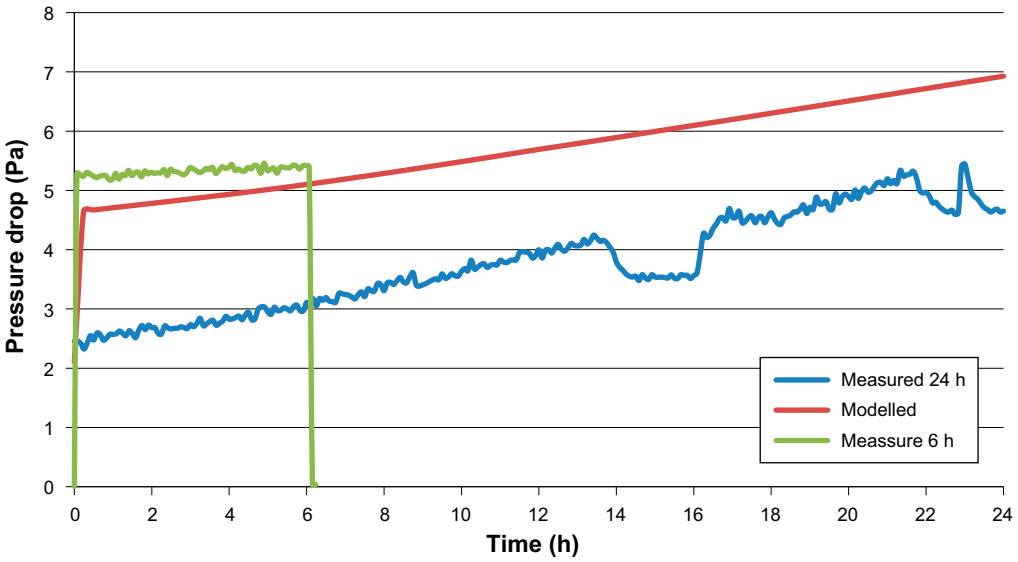

Figure 3-18. *Modelled values compared to measured values when air with 90 and 95 % relative humidity is blown through the pellet filling. The swelling of the pellet filling due to the water absorption is causing an increased pressure drop with time*

3.4.5 Modelling of the laboratory test with thermal gradient

To test the model developed and see how well it works, the laboratory test with thermal gradient was used, see Section 3.4. A rotational symmetric model is used and the geometry and boundary conditions are shown in Figure 3-19. The heat transfer coefficient, h, is chosen to fit the measured boundary conditions. The air flow equations developed in the earlier chapters is used in the pellet slot. The top of the slot is open to let air, water vapour and heat to pass that boundary. The convection in the inner slot is not included in the model because the slot is so small and that the modelling done in Section 4.2 shows that including this will have a very little affect.

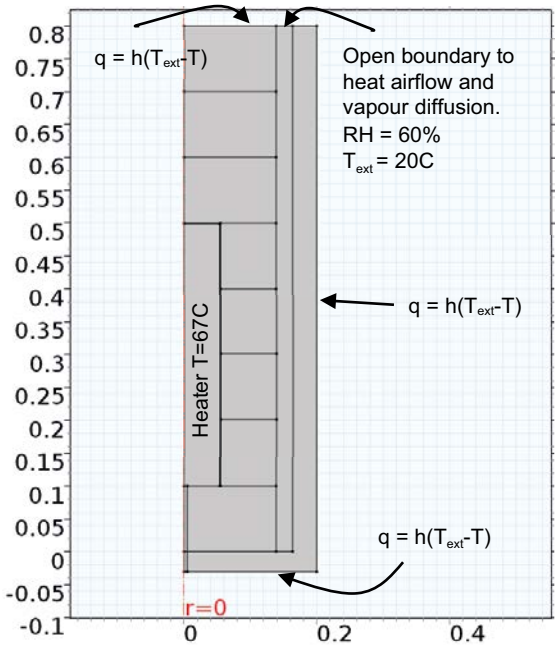

Figure 3-19. *Geometry of the modelled test.*

When the modelled temperature is plotted with the measured temperatures it can be seen that the model is predicting the temperatures well, see Figure 3-20. The largest difference between the modelling and the actual measurements are in T2, which is quite sensitive due to its placement. It is placed in the thin slot of approximately 1 mm. This small slot would also have a large temperature gradient which would mean that very small differences in position of the sensor would lead to large temperature differences in the measurements. In Figure 3-21 the measured and the modelled relative humidity in the pellet slot are shown. The modelled values seem to fit reasonable well with the measured ones. However, the increasing trend of sensor RH3 is not captured and sensor RH2 is underestimated somewhat.

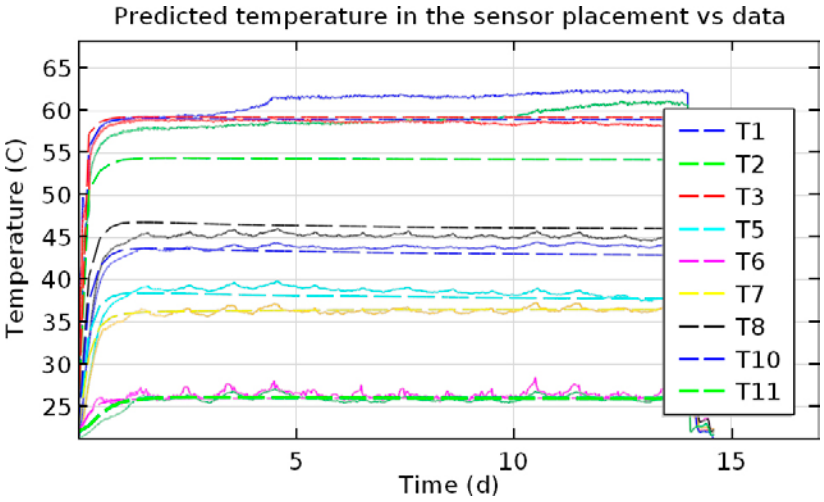

Figure 3-20. *Data from laboratory scale test compared to modelling result, dashed lines are modelled result and solid lines are measured.*

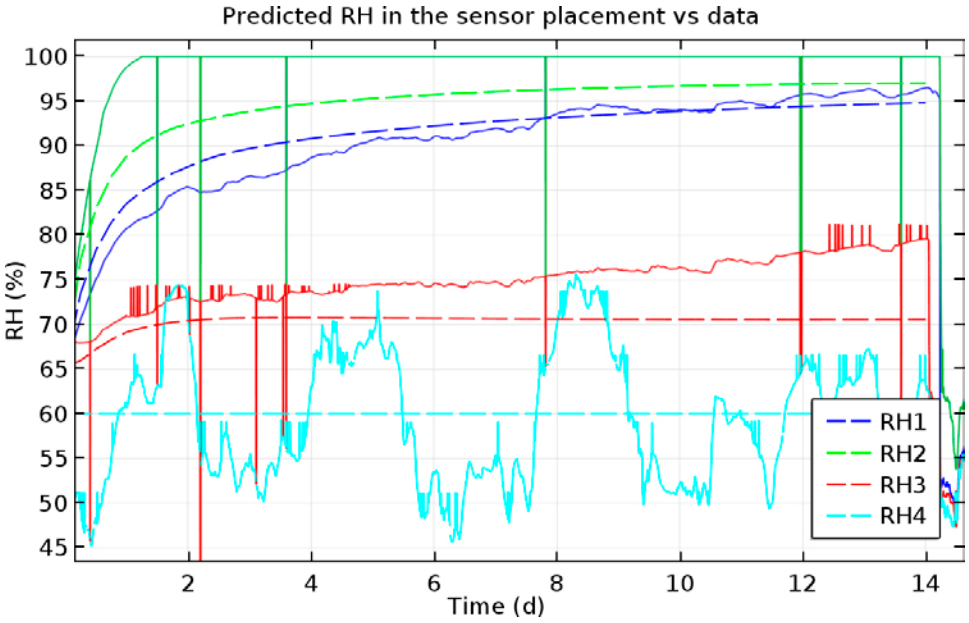

Figure 3-21. *Modelled relative humidity, dashed lines, compared to measured relative humidity, solid lines in the pellet-filled volume. Note that RH4 is located in the room outside the actual test. RH1 is placed in the lower part of the test RH2 is placed in centre of the canister and RH3 placed in the top part of the test.*

The model predicts the water content redistribution in the blocks and pellets quite well, see Figure 3-22. However there are small discrepancies between the modelling and the actual measurements mainly in the top and just above the canister. The result show that water has been lost from the blocks, which had an initial water content of 17 %, and moved into the pellet slot which had an initial water content of 15 %. The model predicts that approximately 630 g of water has been removed from the blocks and entered the pellets while the measurements showed that 760 g was actually lost

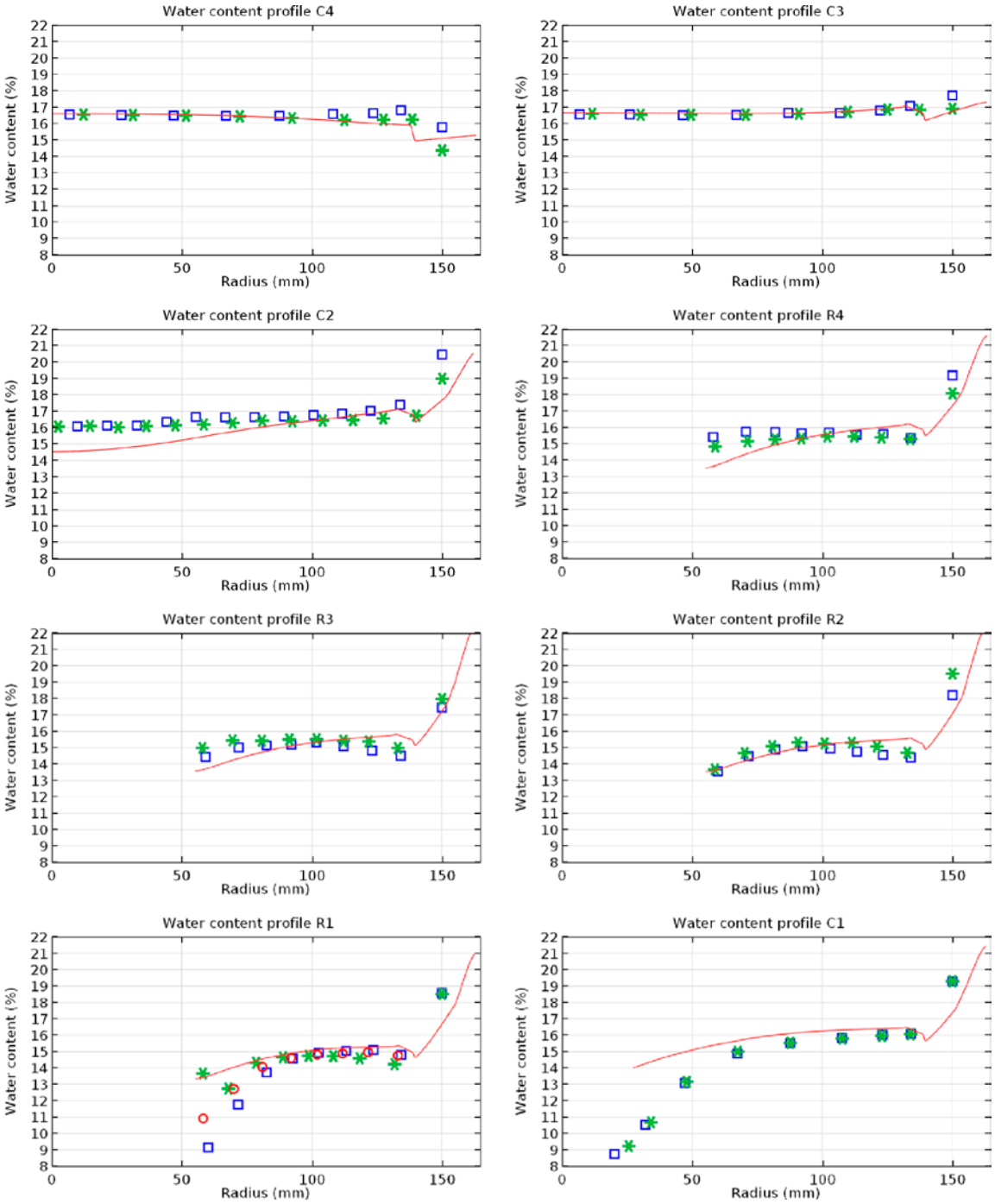

Figure 3-22. *Measured water content compared to the modelled result shown in red solid line. Squares are measured in 0° and astrix are measured in 180° according to Figure 3-7.*

Beyond the movement of water into the pellet-filled volume there was the movement of water out of this volume as the top boundary of the pellet slot is open and water vapour can be transported to the surrounding air due to the air flow. The amount of water that has left the pellet filled slot is measured to be 250 g while the modelling predicts approximately 70 g should have been removed. This suggests that the modelling is underestimating the vapour transport due to convection in the pellet slot. If the more water would leave the pellet slot in the model then the transport of water from the block into the pellet slot would increase due to the dryer pellet filling.

3.5 Conclusions

Laboratory tests have been made to build knowledge on how a system with pellet will act when a thermal gradient is applied and to help develop models that can describe the system. It can be concluded from the small scale test and modelling that the pellet slot influences the redistribution of water due to air movements in the pellet slot driven by convection and the difference in temperature over the slot. Modelling seems to predict the system reasonable well, however, the vapour transport in the pellet slot seems to be underestimated. The laboratory test with thermal gradient indicates that it would be possible to use a pellet filled slot in full scale to protect the buffer if the inflow of water from the rock to the deposition hole is low. It is difficult to draw conclusions regarding the full scale buffer system from the laboratory test due to scale factors. However the model used for the laboratory tests can be applied for the full scale to predict how the pellet filled slot would work in full scale. The model also needs to be developed further to better predict the movement of water vapour in the pellet slot.

The laboratory tests and modelling suggests that the installation method where buffer blocks and pellets are installed at the same time seems to be a promising method for protecting the blocks if the inflow of water is low. The pellet filling have a lower water content and can absorb rather large amounts of water before the blocks start to swell upwards.

4 Full scale installation Test 1 simulating a relatively dry hole

4.1 Description of buffer installation method

The installation of the buffer blocks, canister and the pellets are made in one sequence. The buffer is then left unsupported with the installed heat-generating canister in the deposition hole up to 90 days before the tunnel is backfilled and the buffer is confined vertically.

The proposed installation method has the following advantages and potential limitations/risks:

- The buffer blocks are installed without any protection sheets in the deposition hole. An installation of a protection sheet is an additional step at the installation phase but there are also risks involved at the removal of the sheet. There is an obvious risk that the sheet will get stuck in the deposition hole.
- Since all the buffer elements, blocks and pellets, and the canisters are installed at the same time and the installation of the backfill is made afterwards, the installation can be made in an efficient manner with a minimum of shifting of installation devices.
- The installed bentonite pellets may affect the risk of spalling due to the heating from the canister. The pellet filling is causing a small pressure on the wall of the deposition hole which will mitigate spalling.

Both laboratory tests and modelling, see section below, have shown that there will be changes of the water content and the dry density of the buffer caused both by the water uptake from the surrounding rock but also by the redistribution of the water in the buffer blocks due to the heating from the canister. These changes are assumed to cause both cracks and deformations of the buffer. However, if the inflow into the deposition hole is limited, these changes are assumed to be acceptable. The described test is performed to confirm this assumption is correct for the inflow in the test hole. The inflow was measured to 8E−4 l/min prior to the test

4.2 Pre-modelling and input to test design

4.2.1 Introduction

At the planning stage of test 1 it was decided to do pre-modelling as a part of the design of the test. A few questions regarding the test setup that needed to be answered are listed below.

- **How many buffer blocks are needed above the copper canister?**
  In a real case there would be 5 buffer blocks on top of the canister, but since clay blocks are expensive and broken blocks pose a risk of slowing down the disassembly of the test it would be favourable if some of the blocks could be replaced with concrete dummies.
- **Can the pellet slot be left open towards the deposition tunnel?**
  If the pellet slot is open to the deposition tunnel a large amount of water would escape the deposition hole as vapour. If the slot could be left open it would be easier to take out all the sensor cabling.
- **Were shall the sensors be placed?**
  It is important to know the expected temperature distribution to better optimise the position of the sensors to be installed in the test.
- **Does the time between the heaters are turned off until sampling can be done affect the result?**
  When the test is stopped the temperature is too high to start disassembly and sampling and the setup needs time to cool down. During the time it takes before the sampling can be made water can redistribute and give results that differ from what was present then when the power was turned off.
- **How does the initial temperature of the canister affect the final result?**
  In a real case the canister would have an elevated temperature, this could not be done during the test due to the problems associated with working with a hot canister. Would this difference in initial temperature affect the final result?

4.2.2 Geometry and boundary conditions

For the modelling of the full scale test the same numerical models described in Section 3.6 was used. The geometry of the model, which is the same as expected in Test 1, is shown in Figure 4-1. The thermal boundary condition on the outer boundary of the rock is an isolation boundary condition. To ensure that the boundary condition does not affect the result, a very large rock mass is included. This will ensure that the temperature at the rock-buffer boundary does not change enough to significantly affect the modelling results.

The actual water inflow from the rock in the test location is approximately 8×10^{-4} l/min. It seems that most of the inflow is located at the upper part of the borehole and enters from one direction. Since a rotational symmetric model is used this localized inflow cannot be captured in the modelling. Given this limitation and the very small inflow rate, it is assumed that there is no water inflow. An isolation hydraulic boundary condition towards the rock and towards the top of the block stack is used to set the no-inflow condition. This all means that the modelled result should be representative for the drier sections of the test but may not accurately capture overall behaviour.

The top of the pellet slot is modelled as an open boundary condition which allows heat, air and water vapour to enter or leave the system being modelled. To account for any transportation of moisture in vertical direction from the air movements in the inner slot, between the buffer blocks and the canister, this is included in the model.

To account for the period when the canister is cooling down after the test is turned off, the modelling is defined to cover a time period of 140 days. During this period the thermal power in the canister is modelled with a step function which is 1 700 W the first 90 days and after that the heater is turned off.

4.2.3 Modelling results

From the modelling of the test, the water content and temperature distribution has been calculated, see Figure 4-2 and Figure 4-3. The modelling results show that after 90 days of operation, the canister is expected to reach a maximum temperature of approximately 76 °C and the rock wall will reach a maximum temperature of approximately 46 °C. The difference in gravimetric water content between the inner part of the buffer block and the outer is predicted to be approximately 1.6 %. There seems to be no large redistribution in the inner slot due to the convection and this convection does not affect the result of the modelling.

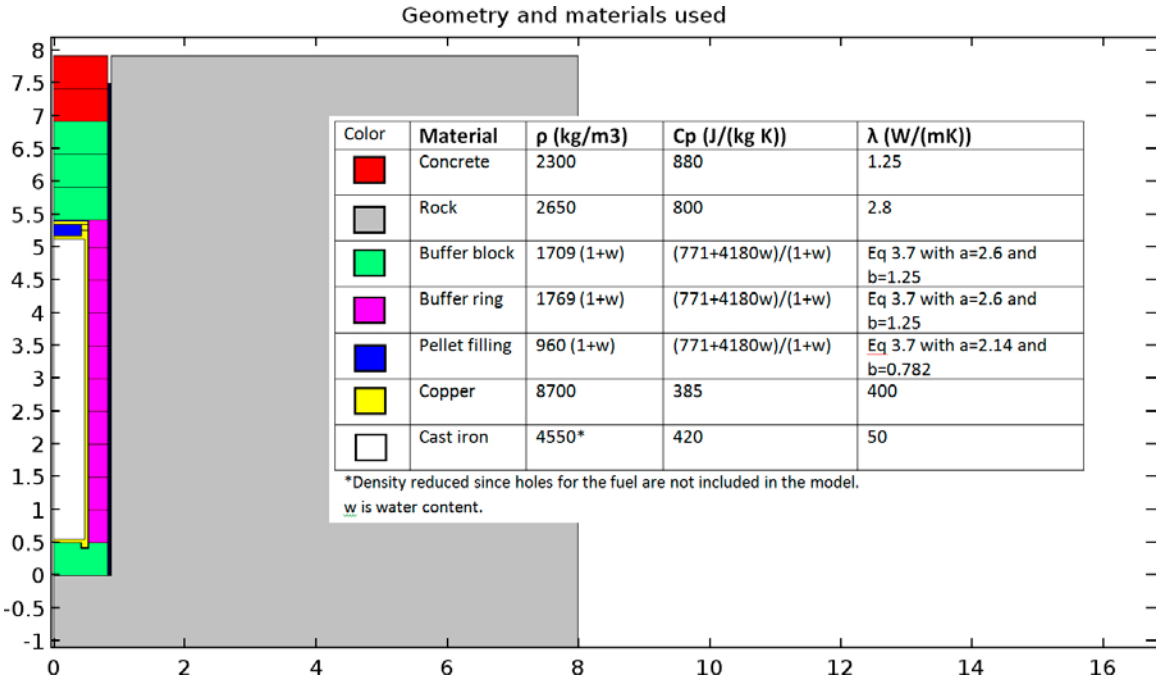

Figure 4-1. *Geometry and materials used in the model.*

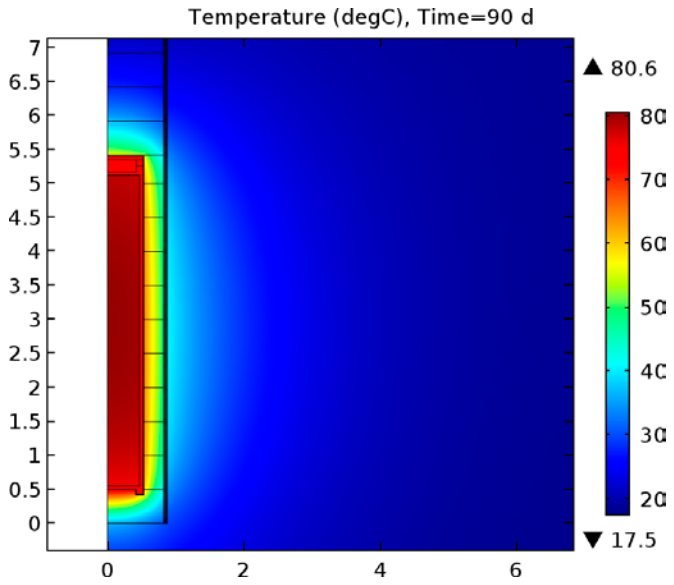

Figure 4-2. *Modelled temperature distribution for test 1.*

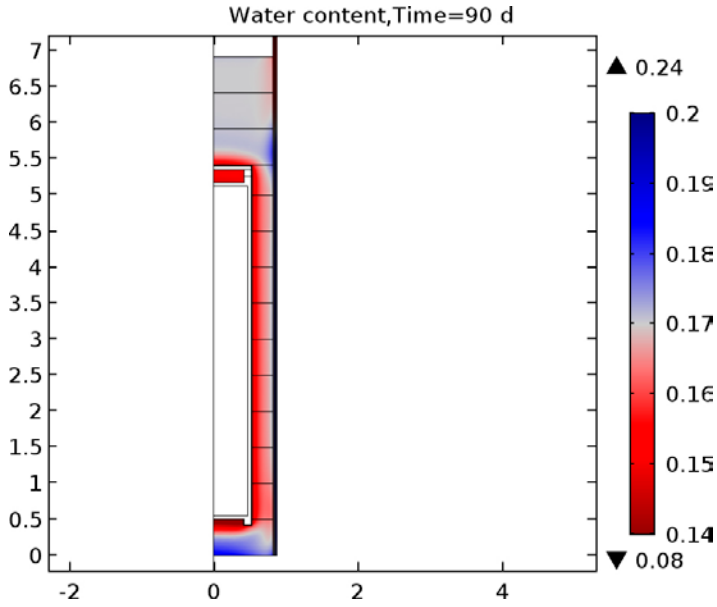

Figure 4-3. *Modelled final water content for test 1.*

The differences between using 3 or 5 blocks on top of the canister seem to be small. Very small changes in temperature and water content are predicted to be present in the two top blocks during the relatively short period of 90 days if the top surface is protected with a vapour barrier. The change in water content at the top of the third block is less than 0.1 percentage points if the area close to the dryer pellet slot is excluded. It is therefore concluded that if the two uppermost blocks are replaced with concrete

The model predicts that the air flow in the pellet filling it is quite small, approximately 3 mm/s. However, since the moving air can transport water vapour much faster than diffusion it is still a transport phenomenon that needs to be considered.

The air velocity is very low at the interface between the pellet slot and the tunnel since the thermal gradient is low at the interface. It is therefore expected that the loss of water to the tunnel will be low even if the slot is left open. The model predicts that only a very small amount of water will leave the pellet slot at the interface between the pellet-filled gap and the overlying open tunnel if the relative humidity in the tunnel is 70 %, see Figure 4-4. The effect of a higher initial temperature for the canister surface seems to have a very little effect on the moisture loss when the time span considered is as long as 90 days. In this case the initial temperature does not need to be considered due to the relatively long duration of the test, see Figure 4-5

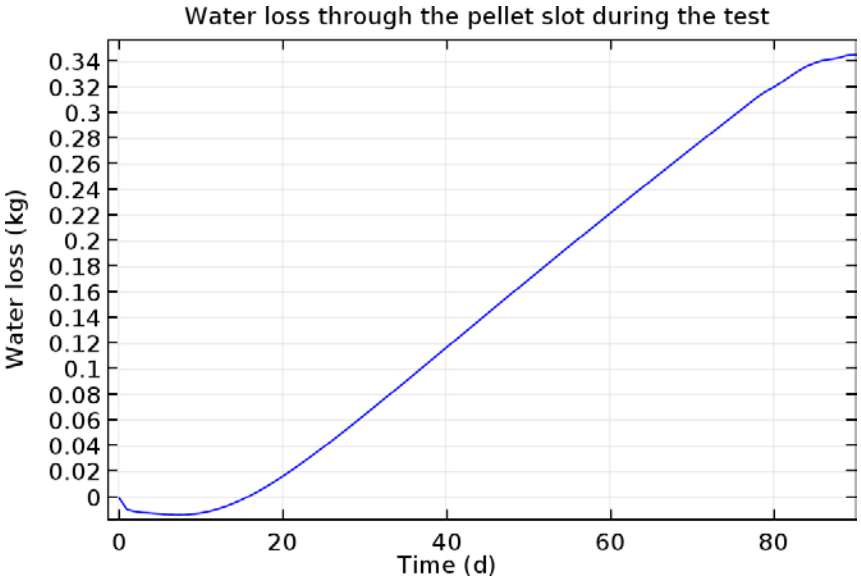

Figure 4-4. *Modelled water loss from a full-scale deposition borehole to the deposition tunnel. Note that it assumed that all moisture loss is via the surface of the pellet fill and no water enters the system from the surrounding rock.*

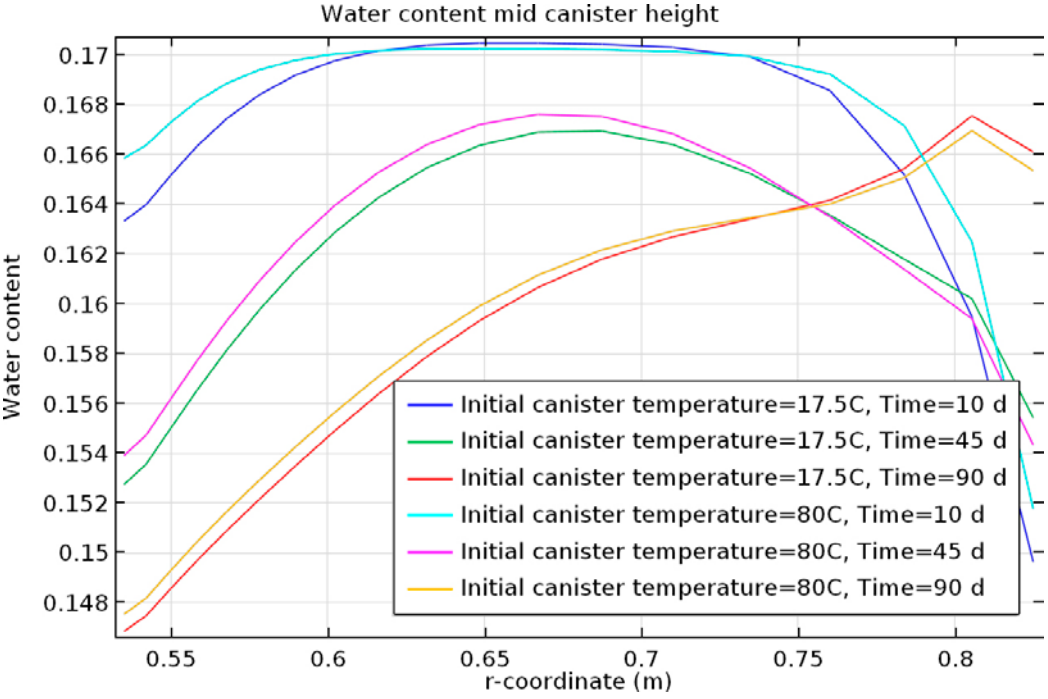

Figure 4-5. *Difference in water content of buffer blocks and pellet fill in radial direction from centreline of canister at mid height of canister comparing initial surface temperature of the canister of 17 °C and 80 °C for three different times.*

4.3 Description of Installation Test 1

This test simulated the technique where installing the buffer including the filling of pellets at the outer slot and the canister at the same time. It was also simulating the time from the installation of the buffer and the canister until the backfill is in place on top of the buffer. This time is assumed to be at maximum 90 days.

The installation of the test was made with both full size buffer blocks and canister in a deposition hole. However, the deposition hole used did not have the bevel close to the floor of the tunnel which is included in the reference design. Furthermore, the most upper two solid buffer blocks were replaced with two concrete blocks and finally was the installation made with a cold canister (heating supplied after installation). These deviations from the reference design were considered, not to affect the relevance of the test.

The canister was equipped with heater to simulate the power from the waste in a real canister with radio nuclear waste. The power in this test was set to 1 700 W. About 100 thermocouples and 10 Rh-sensors were installed in the buffer, on the canister surface and in the surrounding rock. These sensors were in operation and data was collected over the whole test period. The displacement of the upper part of the buffer was also continuously measured over the test period

Samples of the buffer were taken after the test period on which the water content and the density were determined. In total about 3 200 determinations of the water content and density were made.

4.4 Preparations and installation

4.4.1 Buffer manufacturing

The water content of the buffer material was first adjusted to a water content of 17 % in a large Eirich mixer at the SKB facility in Oskarshamn. The blocks for the test were compacted at a workshop in Ystad, Sweden. The blocks were compacted in a rigid mould in axial direction (uniaxial compaction), see Figure 4-6. Both ring shaped and solid blocks were compacted in the same manner. The idea was to compact the blocks to bulk densities consistent with the reference design shown in Table 4-1. The final shape, also in accordance with the reference design, was achieved by machining the blocks after the compaction. The height of the blocks after machining was however different to the reference design. The machining of the blocks was accomplished using an ordinary metal lathe.

The pellets used for the filling of the outer gap between the buffer blocks and the wall of the deposition hole was manufactured using the roller compaction technique also in accordance with the reference design, see Table 4-1.

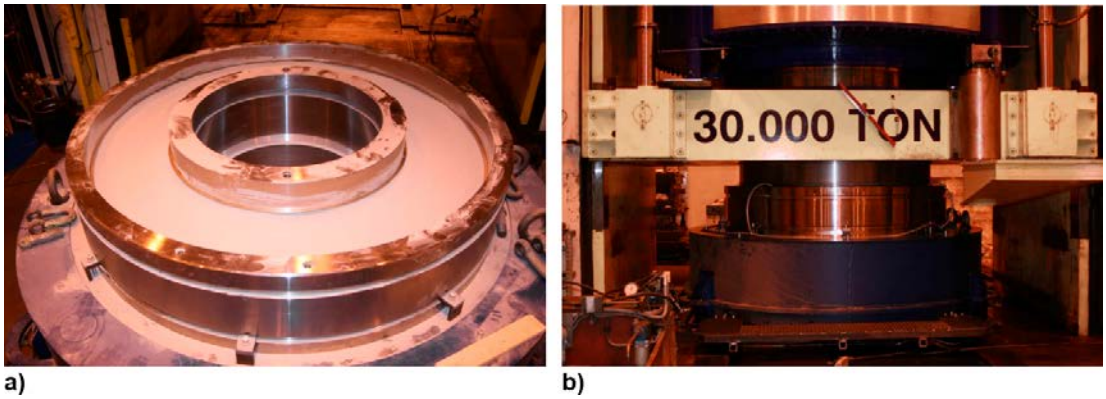

Figure 4-6. *Compaction of buffer blocks. a) The bentonite filled in a rigid mould. b) The mould placed in the press used at the compaction of the buffer blocks.*

Table 4-1. Reference design for the buffer blocks and pellets.

Design parameter	Nominal value	Acceptable variation
Solid block		
Bulk density (kg/m^3)	1 987	± 20
Water content (%)	17	± 1
Dimensions (mm)	Height:540.0 Outer diameter: 1 650.0	± 1
Ring shaped block		
Bulk density (kg/m^3)	2 057	± 20
Water content (%)	17	± 1
Dimensions (mm)	Height: 477.0 Inner diameter: 1 650.0 Outer diameter: 1 070.0	± 1
Pellets		
Dimensions (mm)	16 × 16 × 8	–
Bulk density loose filling (kg/m^3)	1 035	± 40
Water content (%)	15	± 1

4.4.2 Preparatory work on site

The deposition hole used for the test was DD0092G01 placed in the TASD-tunnel at Äspö (see Figure 4-7). The deposition hole was originally drilled for the Canister Retrieval Test (Thorsager et al. 2002). In order to minimize the risk of getting a stack of installed buffer blocks that were not properly aligned, the rock at the base of this borehole was checked. The inclination and unevenness of the base was adjusted through use of small amounts of concrete and putty. A last surveying of the bottom plate was then made and finally a thin steel base plate was placed on the floor of the borehole, covering the rock/concrete/putty surface where the buffer blocks were to be installed. The purpose of the steel base plate was to prevent water from being drawn into the buffer at this surface. Some unevenness of the rock wall in the deposition hole was also filled in with concrete. A sump was also made in the bottom of the deposition hole placed outside the bottom plate. The sump was used for pumping up water coming into the deposition hole at the installation (see pipe running down to the darker perimeter in Figure 4-7).

Figure 4-7. *Preparatory work inside the deposition hole a) The deposition hole with the concrete plate in the bottom. b) The plastic sheet used to allow measurement of the total inflow into the deposition hole. The plastic sheet is not a part of the installation method, but was necessary in the test to protect the blocks during the slow installation and instrumentation.*

Some water-bearing fractures were observed at the inspection of the deposition hole, see Figure 4-7a. No measurements of the inflow of water from single fractures were made but the total water inflow into the deposition hole was determined before the installation. This was made by covering the walls of the deposition hole with a plastic sheet to stop water from being transported out by convection of air, see Figure 4-7 b, and then pumping out all water from the sump. The inflow was measured on several occasions over several weeks by waiting for a couples of days between pumpings and determining the volume of the water entering the deposition hole. From this it was possible to calculate the total rate of water inflow. The measurements indicate a total flow into the borehole was about 8E−4 l/min (0.048 l/h or 1.152 l/day).

4.4.3 Installation sequence

The buffer consisted of total of 14 clay blocks, 10 ring shaped blocks, one bottom block and three solid blocks on top of the canister. In addition to these clay blocks another two solid blocks made of concrete were placed on top of the buffer. The concrete blocks had similar dimensions and weights to the solid buffer blocks. The numbering and naming of the blocks are shown in Figure 4-8.

The installation of the buffer the canister and sensors was made as follows:

1. The bottom plate in the deposition hole was evened out with concrete and putty. A pump was installed in the sump and the steel plate was placed in the deposition hole
2. Thermocouples were installed in the surrounding rock. The cables from the sensors were led up along the wall of the deposition hole to the tunnel floor.
3. A plastic sheet was installed inside the deposition hole and attached to the bottom plate with an O-ring. It was possible to remove the O-ring from the tunnel floor. The plastic sheet was used for protecting the buffer during the installation.
4. The bottom block (C1) was weighed and its dimensions were determined. A small sample of the block was taken in order to determine its actual water content. The block was then placed in the center of the deposition hole. The distance between the buffer block and the wall of the deposition hole was measured and the positon of the block in vertical direction was determined by geodetic surveying. A groove was machined at the top of the bottom block in order to fit the bottom of the canister. This was made with a drilling tool, see Figure 4-9. Holes for the sensors were drilled from the top of the block and the sensors were installed. The cables from the sensors were led in grooves at the top of the block towards the outer diameter of the block and further upwards to the tunnel.
5. The ten ring shaped blocks (R1–R10) were placed in the deposition hole after they were weighed and their dimensions were determined. The blocks were cantered in the deposition hole with the use of the block beneath. Sensors were installed in the same way as for the bottom block. Finally, the horizontal positions of the blocks were determined by measuring the distance between the outer diameter of the block and the wall of the deposition hole at eight locations and the vertical position by geodetic surveying.
6. All the cables from the sensors were led up to the tunnel along the stack of blocks as close as possible towards the outer diameter of the buffer blocks
7. The deposition machine with the canister-sized heater was transported from a nearby tunnel with a truck and placed over the deposition hole. The canister was put in place in the deposition hole using the deposition machine. The deposition machine was then removed from the tunnel. The cables coming from heating elements in the canister were arranged at the top. A ring of copper was put on the top of the canister. The volume inside the ring was then filled with pellets and an upper lid was placed on the copper ring. The cables coming from the heating elements in the canister was led in grooves on the top of block R10 towards its outer diameter and further upwards to the tunnel floor. The distance between the canister and the inner diameter of the upper block was determined and the vertical position of the top of the canister was measured by geodetic surveying.
8. The three upper solid buffer blocks (C2–C4) was put in place. The instrumentation and the measurements of the positions of the blocks were made in the same way as for the rest of the blocks.

9. Two blocks of concrete with same dimensions as the solid bentonite blocks were then installed.
10. The plastic sheet between the blocks and the rock was then removed from the deposition hole and the outer slot between the buffer blocks and the wall of the deposition hole was filled with pellets. The plastic sheet between the blocks and the rock was then removed from the deposition hole and the outer slot between the buffer blocks and the wall of the deposition hole was filled with pellets. A rubber sheet was placed on the top of the upper concrete block. This sheet was not covering the pellets filled outer slot
11. The power, 1 700 W, was applied on the heating elements in the canister and the data acquisition system for the installed sensors was started.

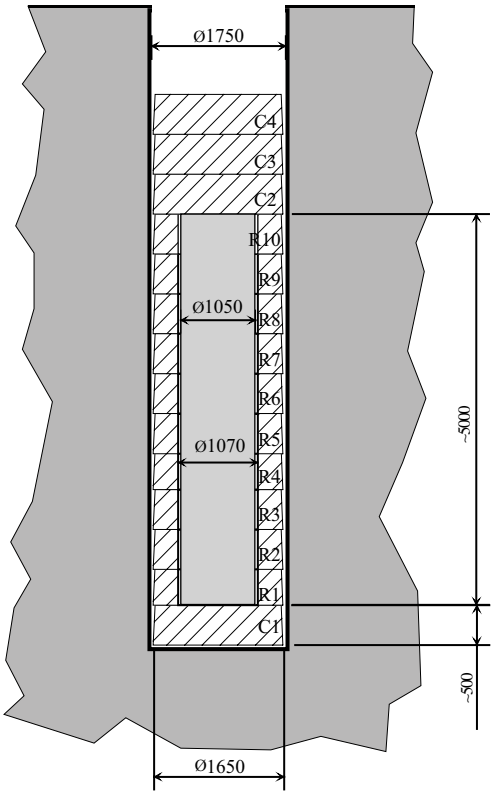

Figure 4-8. *Dimensions and numbering of the buffer blocks.*

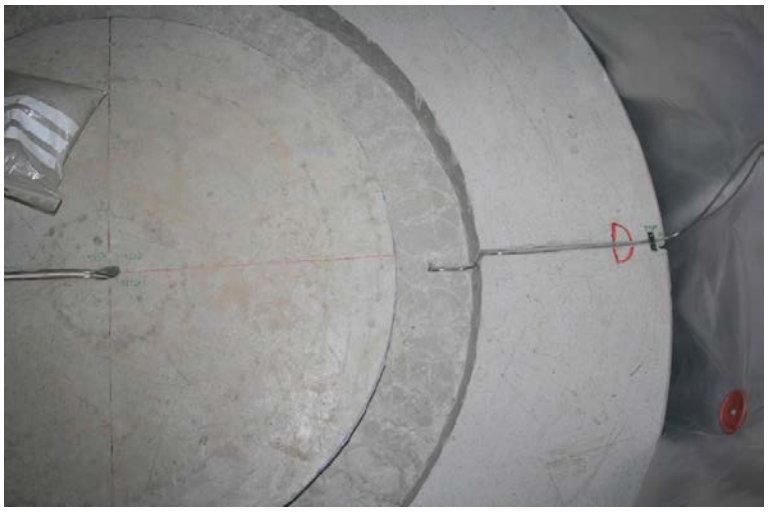

Figure 4-9. *The bottom block (C1) in the deposition hole. Note the groove for the bottom of the canister and the installed sensors.*

4.4.4 Installation of sensors

About 100 thermocouples and10 Rh-sensors were installed in the buffer, on the canister surface and in the surrounding rock. The solid blocks C1, C2, C3 and C4 and every second ring shaped buffer block were equipped with sensors (R1, R3, R5, R7 and R9), see Figure 4-8.

The position of the sensors were described in terms of radial distance from the centre of the deposition hole (r), the angle (α) and the depth from the surface of the installed blocks, see Figure 4-10. The installation of the sensors was made in four perpendicular directions (A, B, C and D). Direction A and C are placed in the tunnels axial direction with A headed against the end of the tunnel

4.4.5 Data from the installation

The weight and dimensions of the blocks were determined before they were installed in the deposition hole. From these data the bulk density (ρ) of each of the blocks was calculated. From a small sample taken from each of the blocks the water content (w) was determined. The data from these measurements are compiled in Table 4-2. The dry density (ρ_d) of each block is determined using the relationship:

$$\rho_d = \frac{\rho}{1 + w}$$

Table 4-2. Data from the installation of the buffer blocks in test 1.

Blok No	Outer diameter (mm)	Inner diameter (mm)	Average height (mm)	Weight (kg)	Bulk density (kg/m^3)	Water content (–)	Dry density (kg/m^3)
C1	1650.0		500.1	2142	2003	0.165	1719
R1	1650.0	1070.0	500.4	1275	2056	0.162	1769
R2	1650.4	1070.0	500.0	1280	2064	0.168	1768
R3	1650.1	1071.0	500.0	1279	2067	0.168	1770
R4	1650.2	1069.8	500.2	1278	2061	0.164	1770
R5	1650.2	1070.3	499.9	1275	2058	0.172	1757
R6	1650.5	1070.9	499.9	1276	2060	0.167	1766
R7	1650.5	1070.9	500.0	1276	2060	0.169	1763
R8	1650.1	1070.5	500.0	1277	2062	0.166	1769
R9	1650.0	1070.0	500.2	1280	2065	0.171	1764
R10	1650.4	1070.0	420.1	1077	2068	0.167	1772
C2	1650.1		498.8	2153	2019	0.168	1728
C3	1649.7		499.8	2158	2020	0.169	1727
C4	1650.0		498.6	2143	2010	0.167	1722

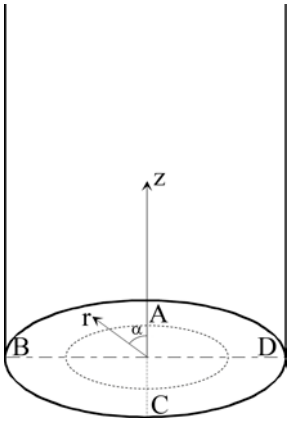

Figure 4-10. *The coordinate system used when describing the positions of the installed sensors.*

The water content for the 14 installed blocks varied between 0.165 and 0.169. The height of the blocks varied from 494–500 mm, except for block R10 that was adjusted to match the length of the canister and had a height of 420 mm. The dry density of the solid blocks varied between 1 719–1 728 kg/m^3 (average dry density 1 724 kg/m^3), while the dry density of the ring shaped blocks varied between 1 763–1 772 kg/m^3 (average dry density 1 767 kg/m^3).

The initial water content of the pellets was determined to be 15 % and the average dry density of the installed pellet filling was about 890 kg/m^3.

4.5 Running of test

4.5.1 Heating power

The power applied to the heating elements placed in the canister is shown in Figure 4-11. The power should according to the plan be 1 700 W during the whole test period. However, a problem with the electric power caused a reduction to half of the power over a period of about10 days about 80 days after the test was started, see Figure 4-11. The decrease in power has a marginal effect on the relevance of the test.

4.5.2 Temperature measurements

Data from the installed sensors were collected continuously during the whole test period. The installed thermocouples functioned well, while ten installed RH sensors failed. The reason for the failures is unclear. The data from all sensors are shown in Appendix 2.

The temperature measurements made on the canister surface are shown in Figure 4-12. The thermocouples were installed in two directions (B and C, see Section 4.4.4 how the directions are defined) close to the bottom, at mid height and close to the top of the canister. The maximum measured temperature was about 77 °C at the mid height of the canister. Furthermore, the maximum temperature at the top and bottom of the canister was about 5 °C lower than the maximum temperature at mid height of the canister. The temperature on the canister was, as expected, independent of the direction (B and C).

The temperature was also measured in the rock inside the deposition hole. This was made at three levels in the deposition hole, 400 mm, 2 900 mm and 4 900 mm from the bottom. The sensors were installed in two directions (B and C) at each level. Additionally, temperature sensors were installed about 50 and 150 mm into the rock (at a radial distance of 925 and 1 025 mm) at each of the three instrumentation elevations.

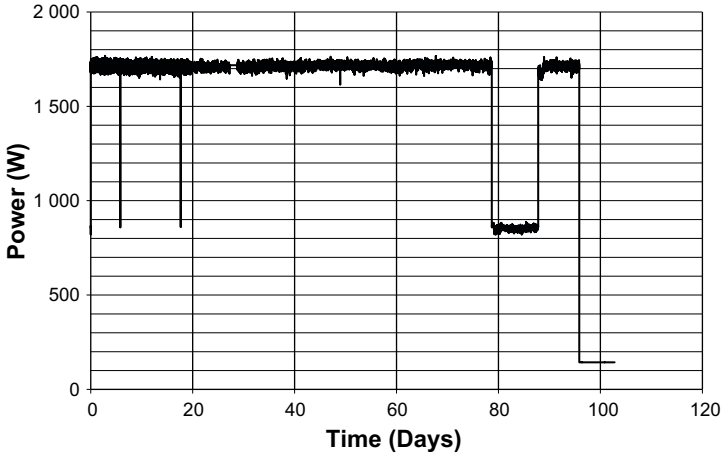

Figure 4-11. *The Applied power on the heaters in the canister.*

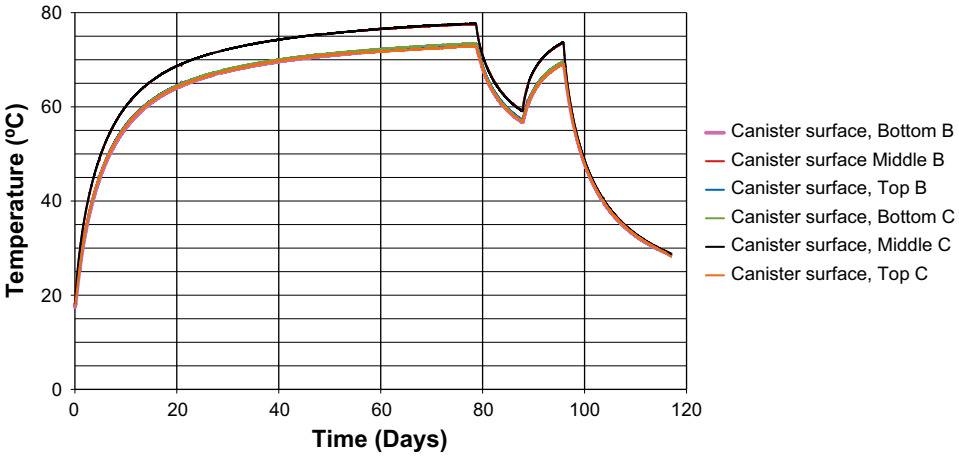

Figure 4-12. *The temperature evolution on the canister surface as function of time. The thermocouples are placed at the bottom, at mid height and at the top of the canister and at two radial directions B and C. The directions are defined in Section 4.4.4*

The results from the measurements at the three instrumentation levels are shown in Figure 4-13 and shows that the temperature was, as expected, highest at the level of 2 900 mm i.e. close to mid height of the canister. The lowest temperature was measured close to the bottom of the deposition hole. The plots also show that the temperature was lower towards the left wall of the tunnel, i.e. in direction B. The maximum temperature measured on the rock surface was just above 40 °C.

The temperature in the buffer was measured with thermocouples but also with the RH-sensors. The data from all sensors are shown in Appendix 2. Figure 4-14 shows the temperature measurements in buffer block R5 and the maximum temperature in the buffer was about 65 C. This was measured on the inside surface of the buffer ring. This figure shows that the temperature decrease across the inner gap i.e. between the canister surface and the inner surface of the buffer block was about 12–13 °C. The temperature decrease over the buffer block was about 15 °C in direction B, C and D and somewhat higher in direction A. The temperature fall over the pellets filled outer gap was about 10 C in direction B, C and D and about 6.5 °C in direction A.

4.5.3 Buffer displacement

The displacement of the buffer in axial (vertical) direction was measured by geodetic surveying of the upper surface of the most upper concrete block. This was made at least once a week in 9 positions of the block, two in each of the four directions and one in the centre. The results from the measurements are shown in Figure 4-15, where positive displacement means that the block has moved upwards. The following conclusions can be made from the measurements:

- The displacement reached its maximum at the end of test period, averaging about 40 mm.
- The displacement velocity was decreasing with time.
- The displacement of the surfaces varied between 30 and 50 mm.
- The largest displacement was observed in direction A–B which implies that the surface of the block was inclined (block had a slight tilt).

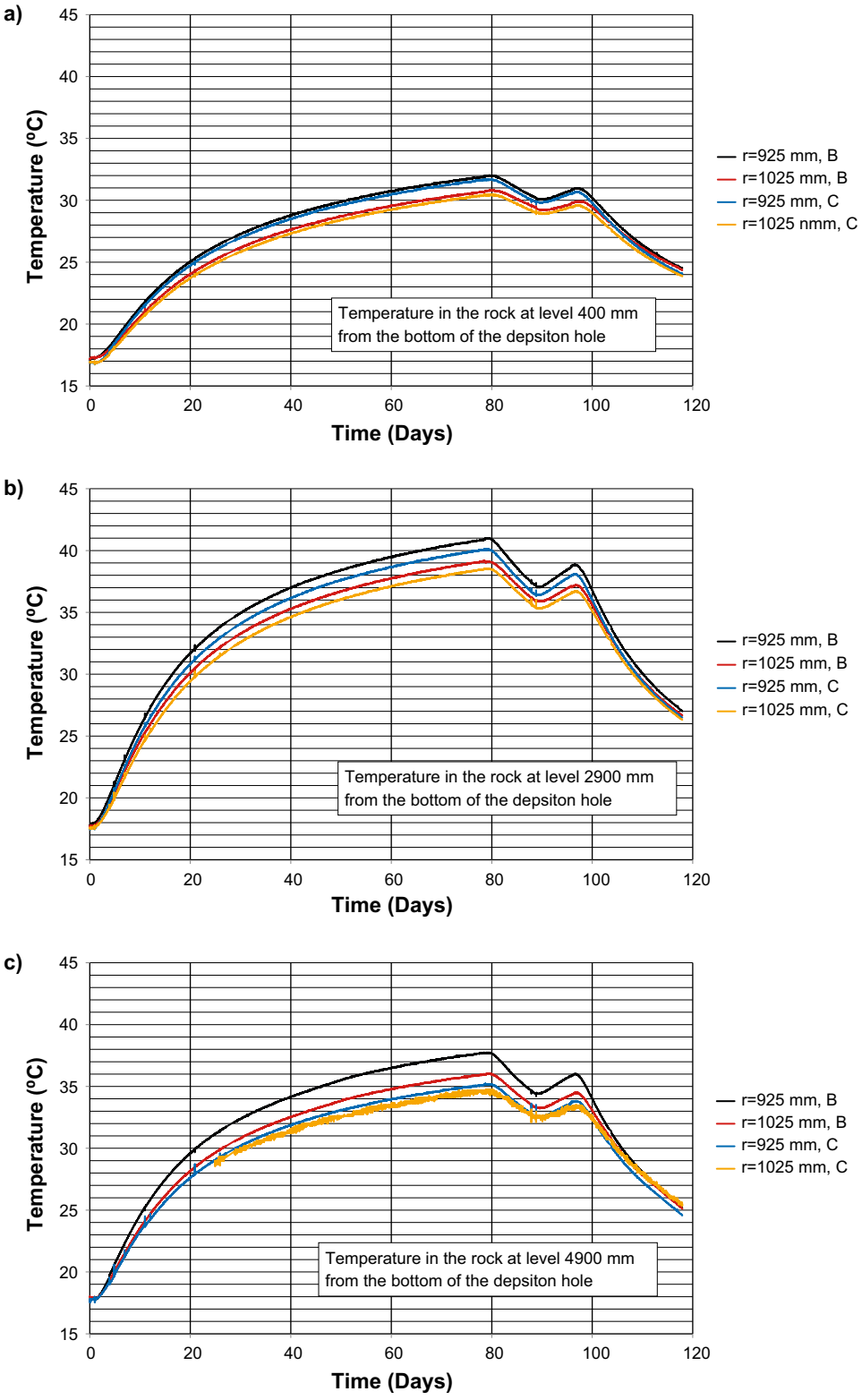

Figure 4-13. *The temperature evolution in the surrounding rock at three different levels in the deposition hole a) 400 mm b) 2 900 mm and c) 4 900 mm from the bottom and at two radial directions B and C. The directions are defined in Section 4.4.4.*

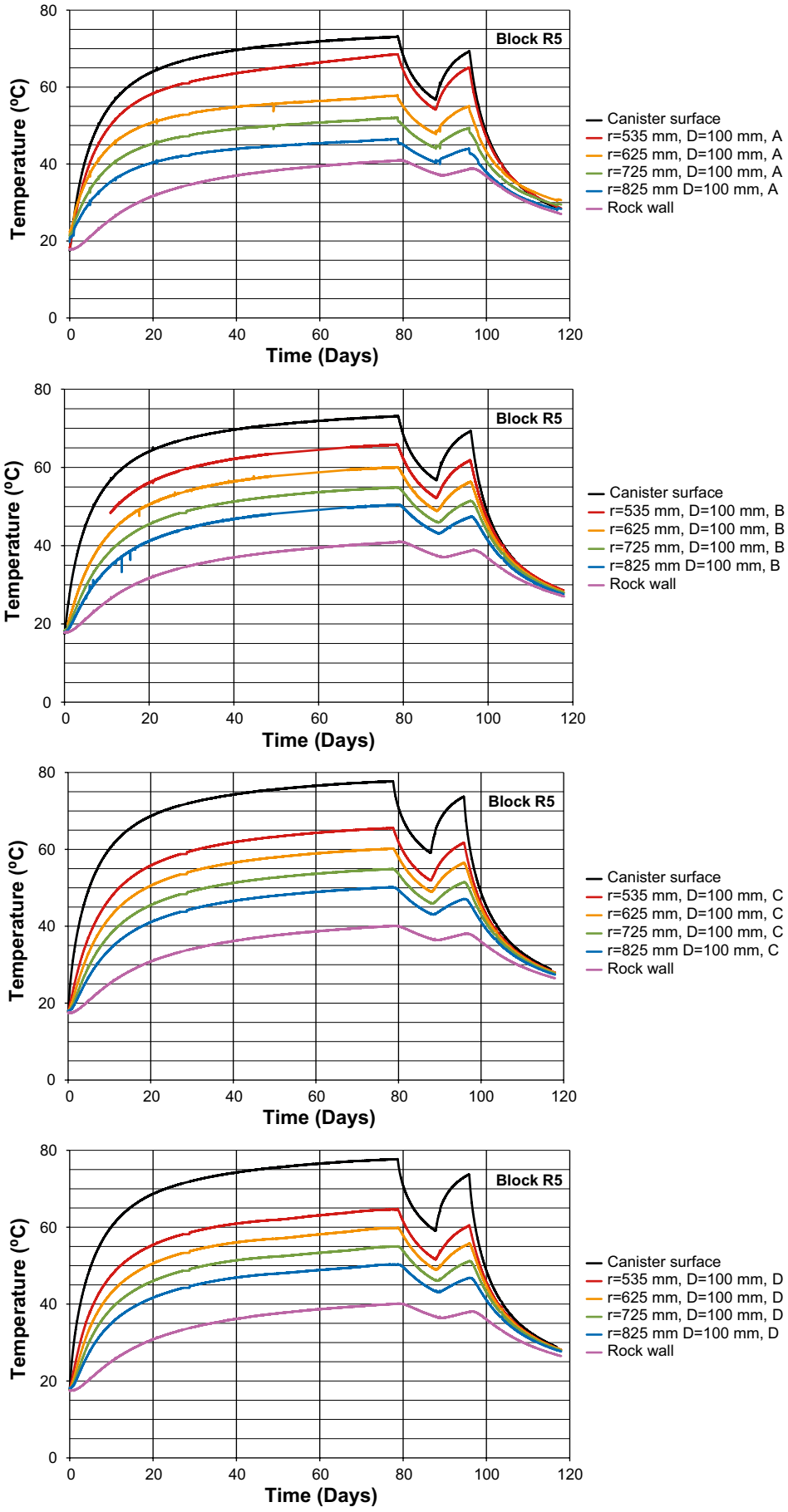

Figure 4-14. *The temperature evolution in buffer block R5. The measurements are made in the four directions A, B, C and D which are defined in Section 4.4.4.*

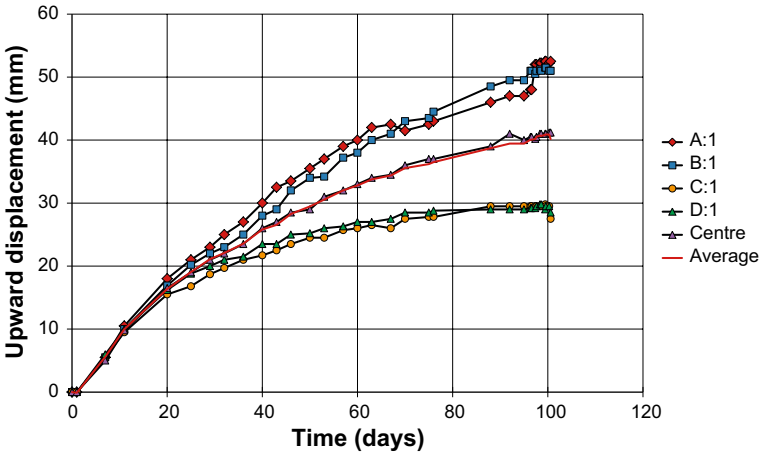

Figure 4-15. *The upward displacement of the upper concrete block. The measurements were made in four directions (A, B, C and D) and at the centre of the block. The average of the displacement (from measurements in nine points) is also given. The directions are defined in Section 4.4.4.*

4.6 Dismantling

4.6.1 Removal of the buffer and the canister

The power to the test was switched off after about 90 days. For a period of about 7 days after heater shutoff, the canister was allowed to passively cool and after that, the dismantling and sampling of the buffer started. The dismantling was made block by block. Samples were taken in four directions 15°, 105°, 195° and 285° respectively at each sampling elevation.

The dismantling sequence was as follows:

1. The two blocks of concrete (C5 and C6) were lifted out of the deposition hole. Samples of the pellets in the outer slot were taken in 8 directions (0°, 45°,…315°, see Figure 4-10 about the definition of the angle) The water content of the pellets was determined for each sample recovered. The distance between the blocks and the surface of the deposition hole was also measured at the same 8 directions and the position of the upper surface was measured by geodetic surveying
2. Samples of the three upper solid bentonite blocks (C2–C4) were taken by core drilling from the upper surface of the blocks, see Figure 4-16. The cores were transported to a laboratory on ground level where they were divided into smaller specimens for water content and density determinations. The water content of the pellets in the outer slot was also determined. The distance between the blocks and the surface of the deposition hole were also measured also in the same 8 directions as for the concrete blocks. The vertical positions of the upper surface of the blocks were measured by geodetic surveying.
3. The vertical position of the canister lid was measured after block C2 was removed.
4. The canister was then lifted up from the deposition hole and transported away to a nearby tunnel with the use of a deposition machine.
5. Samples were taken from the ten ring shaped blocks (R1–R10) by sawing out thin slices from the blocks in four perpendicular lines (at ~15°, 105°, 195° and 285°). The slices were transported to a laboratory on ground level where they were divided in smaller specimens on which water content and the density were determined. The water content of the pellets in the outer slot was also determined. Furthermore the distance between the block and the surface of the deposition hole were also measured in the same 8 directions as for previous locational measurements. The vertical positions of the upper surface of the blocks were measured by geodetic surveying.
6. The bottom block (C1) was removed and sampled in the same way as blocks C2–C4, see above

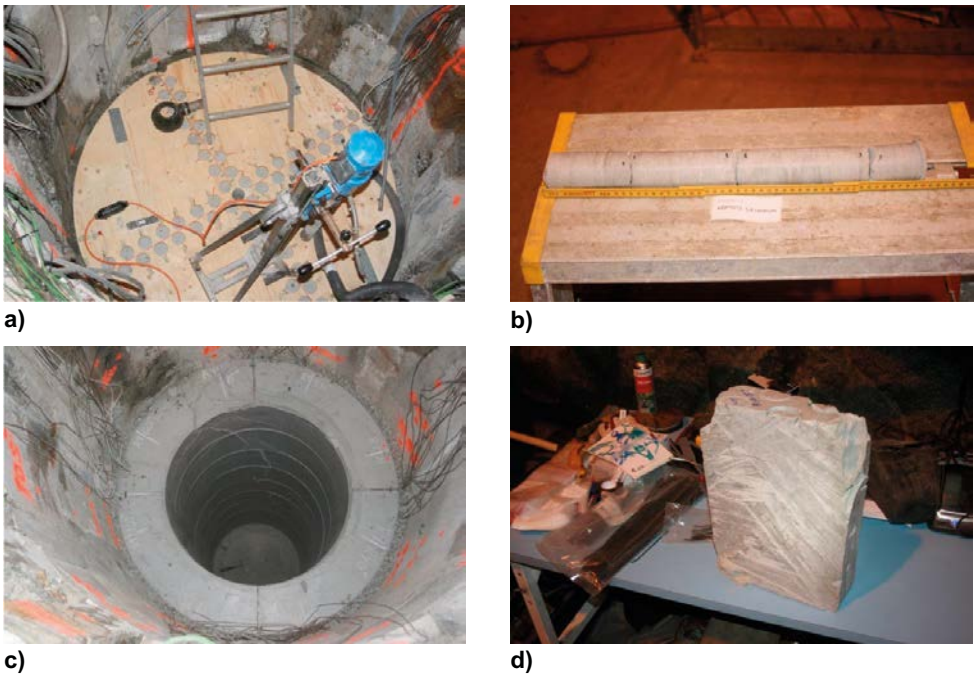

Figure 4-16. *Sampling of the buffer a) Core drilling from the upper surface of block C4. b) A core taken from a solid block. c) The stack of ring shaped blocks. d) A slice of bentonite sawn out from a ring shaped block.*

4.6.2 Observed cracks

In all of the removed buffer blocks cracks were observed, see Figure 4-17. Some of the cracks in the ring shaped blocks went through the whole blocks in radial direction. It is not ruled out that these cracks affected the redistribution of the water in the buffer, see Section 4.7 below. However, since the outer slot was filled with pellets and the installation processes is not affected by these post-installation features, the technical design requirements related to long term safety will be fulfilled

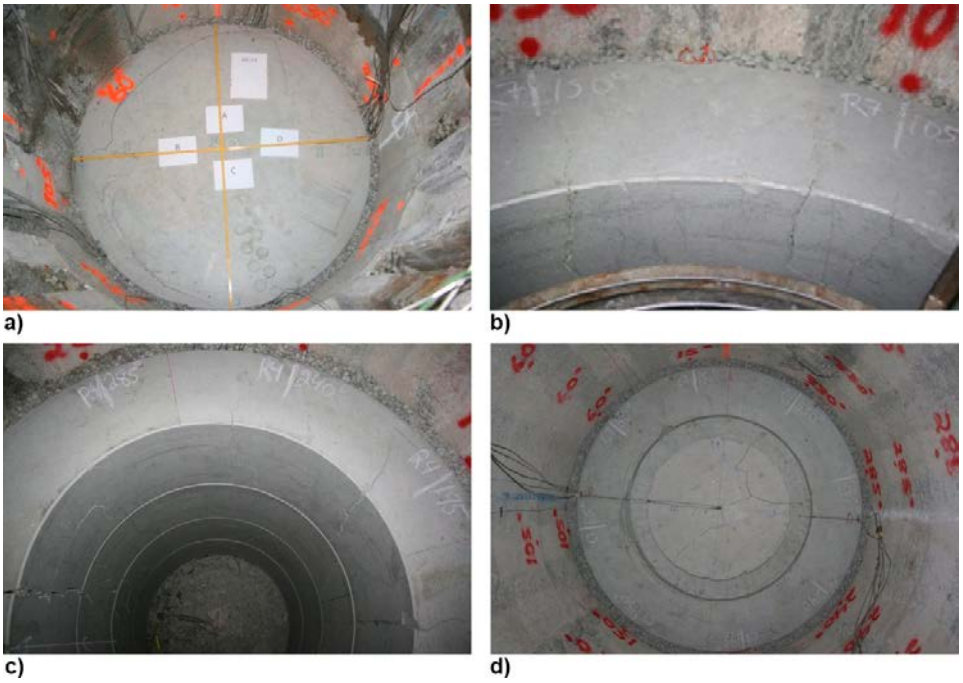

Figure 4-17. *Observed cracks on the blocks at the time of dismantling a) in block C3 b) block R4 c) block R7 d) and in the bottom block C1.*

4.7 Water content and density of the buffer

4.7.1 Preparation of the samples

From the samples taken from the solid blocks by core drilling in four perpendicular directions (see Figure 4-18), smaller specimens were taken on five levels and their bulk density and water content were determined. Corresponding preparations of the specimens from the slices taken from the ring shaped blocks is shown in Figure 4-19. From each slice ideally 50 smaller specimens were sawn out and had their water content, bulk density and dry density determined.

Samples were also taken from the pellet filling at eight directions and at three different depths measured from the upper surface of the individual buffer blocks, 50, 250 and 450 mm respectively. These samples were representing the whole pellets filling in radial direction. Only the water content was determined on these samples.

Altogether more than 3 200 determinations of the water content and density were made.

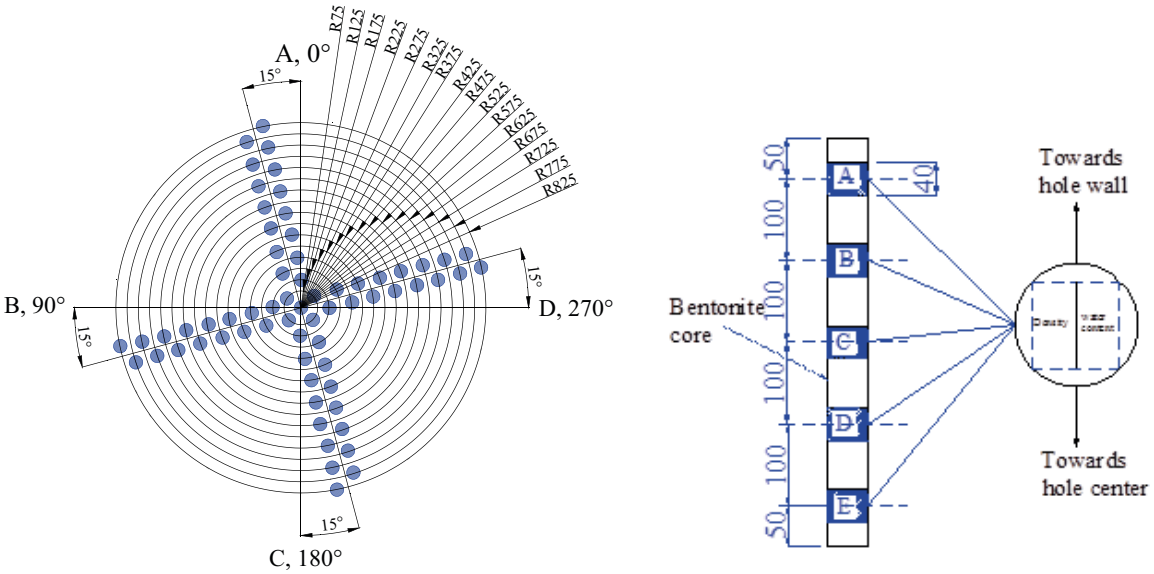

Figure 4-18. *Specimens sawn out from the cores drilled in the solid blocks.*

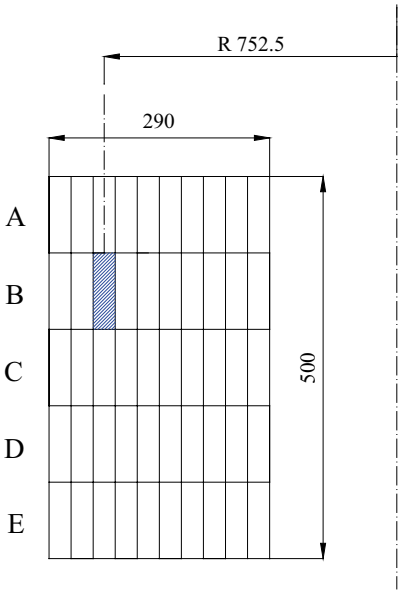

Figure 4-19. *Specimens sawn out from the slices taken from the ring shaped blocks.*

4.7.2 Determination of density and water content

The determination of the water content was made in the following way:

1. The balance was checked with reference weights before the starting of the measurements
2. A small baking tin of aluminum was placed on the balance and the weight (m_{bt}) was noted in a protocol.
3. The sample was placed in the baking tin and the weight of sample and tin is noted in a protocol ($m_{bt}+m_{bulk}$).
4. The tin with the sample was placed in an oven with a temperature of 105 °C for 24 h.
5. After the drying the weight of the baking thin and the sample ($m_{bt}+m_{solid}$) was measured and noted in a protocol.

The mass of water dried from the sample was determined according to Equation 4-1:

$$m_{water} = m_{bulk} = m_{solid} \tag{4-1}$$

and the water content (w) was calculated according to Equation 4-2.

$$w = \frac{m_{water}}{m_{solid}} \tag{4-2}$$

The bulk density of the samples was determined by weighing the samples both in air and immersed in paraffin oil with known density. The determination was made as follows:

1. A piece of thread was weighed.
2. The sample was weighed hanging on the thread underneath the balance (m_{bulk}).
3. The sample was then submerged in the paraffin oil with the density $\rho_{paraffin}$ and the weight ($m_{paraffin}$) was noted

The volume of the sample (V_{bulk}) and the density (ρ_{bulk}) were calculated according to Equations 4-3 and 4-4.

$$V_{bulk} = (m_{bulk} - m_{paraffin})/\rho_{paraffin}) \tag{4-3}$$

$$\rho_{bulk} = \frac{m_{bulk}}{V_{bulk}} \tag{4-4}$$

The dry density (ρ_{dry}) and the degree of saturation (S_r) can be calculated according to Eqns 4-5 and 4-6.

$$\rho_{dry} = \frac{\rho_{bulk}}{(1+w)} \tag{4-5}$$

$$S_r = \frac{w \times \rho_{bulk} \times \rho_s / \rho_w}{\rho_s \times (1+w) - \rho_{bulk}} \tag{4-6}$$

For calculating the degree of saturation the values of the density of the solid particles $\rho_s = 2\,780$ kg/m^3 and the density of water to $\rho_w = 1\,000$ kg/m^3 are used. The void ratio (e) can be calculated according to Equation 4-7.

$$e = \frac{\rho_s - \rho_{bulk}}{\rho_{bulk} - \rho_w \times S_r} \tag{4-7}$$

4.7.3 Results

The data from the determinations of the water content and the bulk density together with the positions of the taken specimens are used for analysing the buffer after the test.

Pellet filling

The determinations of the water content of the pellets filling in the outer slot are summarised in Figure 4-20. The figure is showing the following:

- All parts of the filling had taken up water since the initial water content of the pellets was 15 %, see Section 4.4.5.
- The water content of the pellets filling varied between 0.15 and 0.65.
- The highest water content values were observed in a band going from direction B at the top of the filling (90°) towards direction D–A (320°) at the bottom of the deposition hole.
- The figure is indicating that water in the filling was entered the deposition hole from water bearing fractures in the wall of the deposition hole since the highest water content values were very local.
- It cannot be ruled out that some of the increase in water content of the pellet filling was caused by redistribution of the water in the buffer blocks due to the heating from the canister surface.

Above the canister

The water content and the density of the buffer, were as mentioned above determined in four profiles in each buffer block. In Figure 4-21 the densities and the water contents of one profile in block No C3 are plotted as function of the distance from the centre of the deposition hole. The figure shows that the water content at the centre of the block was close to the initial conditions although close to the top of the block the water content was about 1 % lower than the initial condition. This resulted in a somewhat higher dry density in these part of the block compared to the initial conditions. Close to the outer diameter of the block the plot shows that a significant increase in water content has occurred. This is also seen in adjacent pellet filling where the water content increased from the initial value of 0.15 to as much as 0.27. Furthermore, there was a decrease in the dry density of the block close to the pellets filling. Thus, the plot indicates that in the central part of the block drying occurred, causing an increase in dry density. Finally, there was water uptake in both the pellets and in the outer part of the block, causing a swelling of the bentonite with a subsequent decrease in dry density. Corresponding plots for the rest of the investigated sections of the solid blocks above the canister are shown in Appendix 3.

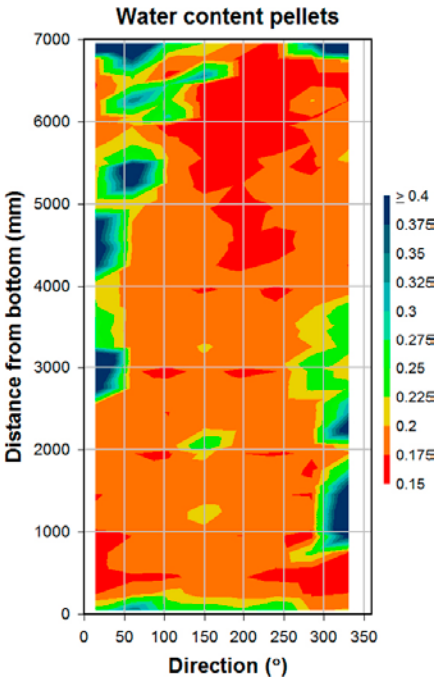

Figure 4-20. *Water content in the pellets filling after the test.*

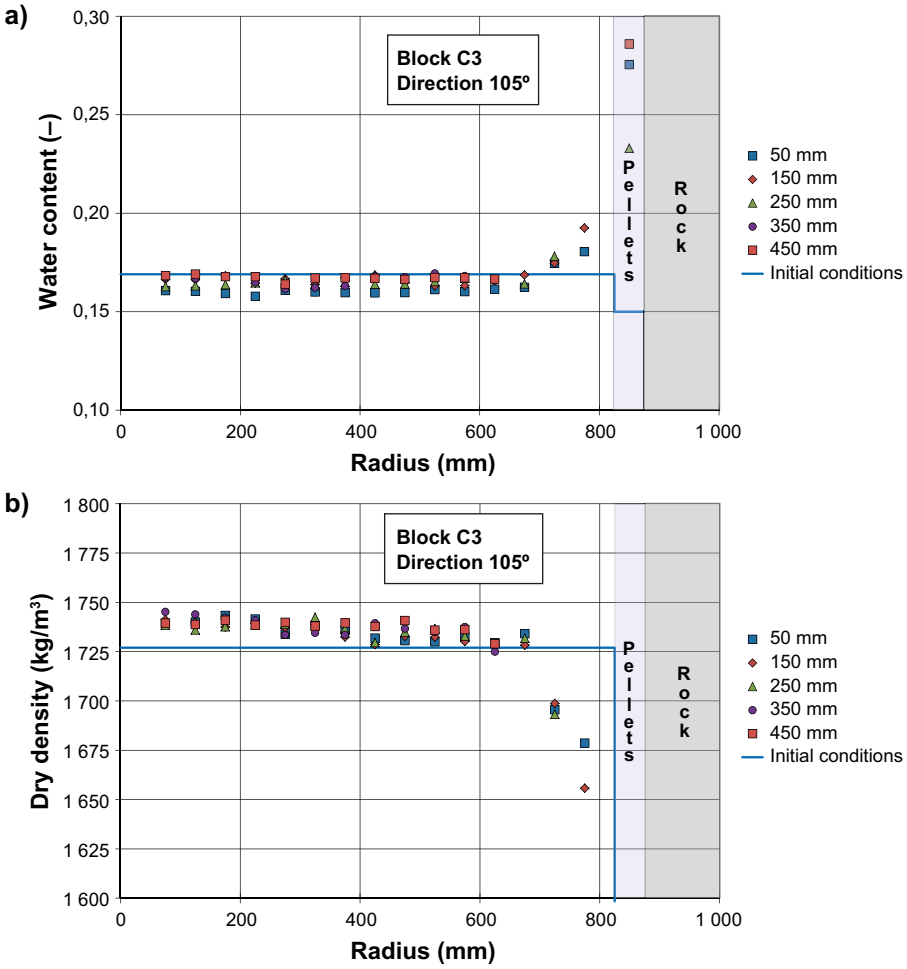

Figure 4-21. *Determination of a) water content and b) dry density of the bentonite in block C3 as function of distance from the center of the deposition hole. The determinations are made at five different depths from the upper surface of the block.*

Around the canister

The densities and the water contents of one profile in block No R6 are plotted in Figure 4-22. The figure shows that there was a drying of all parts of the block, resulting in an increasing of the dry density in most parts, compared to the initial conditions. Corresponding plots for all of the investigated sections are shown in Appendix 3.

Below the canister

The water content and the density of the buffer were, as mentioned above, determined in four profiles in each buffer block. The densities and the water contents of one profile in block No C1 are plotted in Figure 4-23. The figure shows that the water content at the center of the block was almost the same as the initial, although the close to the top of the block the water content was about 2 % lower. This resulted in a somewhat higher dry density in dryer part of the block compared to the initial conditions. Close to the outer diameter of the block the plot shows a small increase in the water content. This was also seen for the pellet filling where the water content increased to up to 0.23 from the initial value of 0.15. Additionally, there was a decrease in the dry density of the block from the radius 600 mm towards the pellet filled region.

Figure 4-23 indicates that in the central part of the block there was drying occurring, causing an increase in dry density and there was water content increase in both the pellets and the outer part of the block that caused a swelling of the bentonite with a subsequent decrease in dry density in that region. Corresponding plots for the rest of the investigated sections of the solid blocks below the canister are shown in Appendix 3.

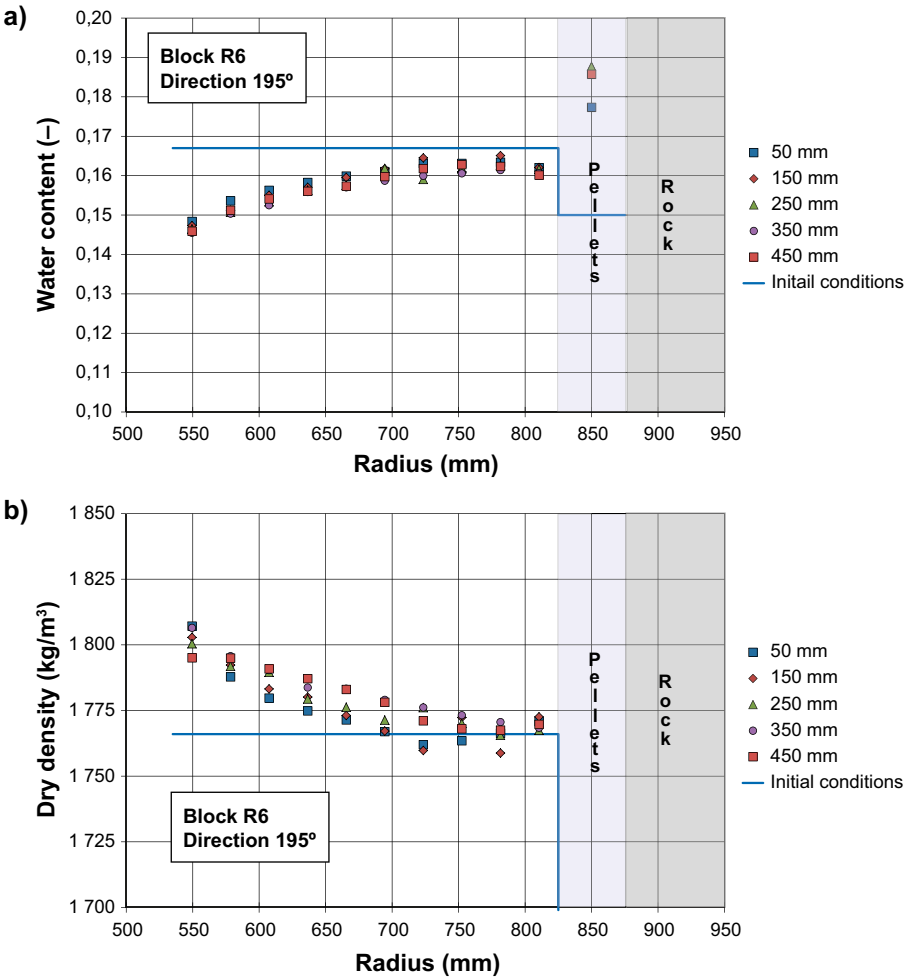

Figure 4-22. *Determination of a) water content and b) dry density of the bentonite in block R6 as function of distance from the center of the deposition hole. The determinations are made at five different depths from the upper surface of the block.*

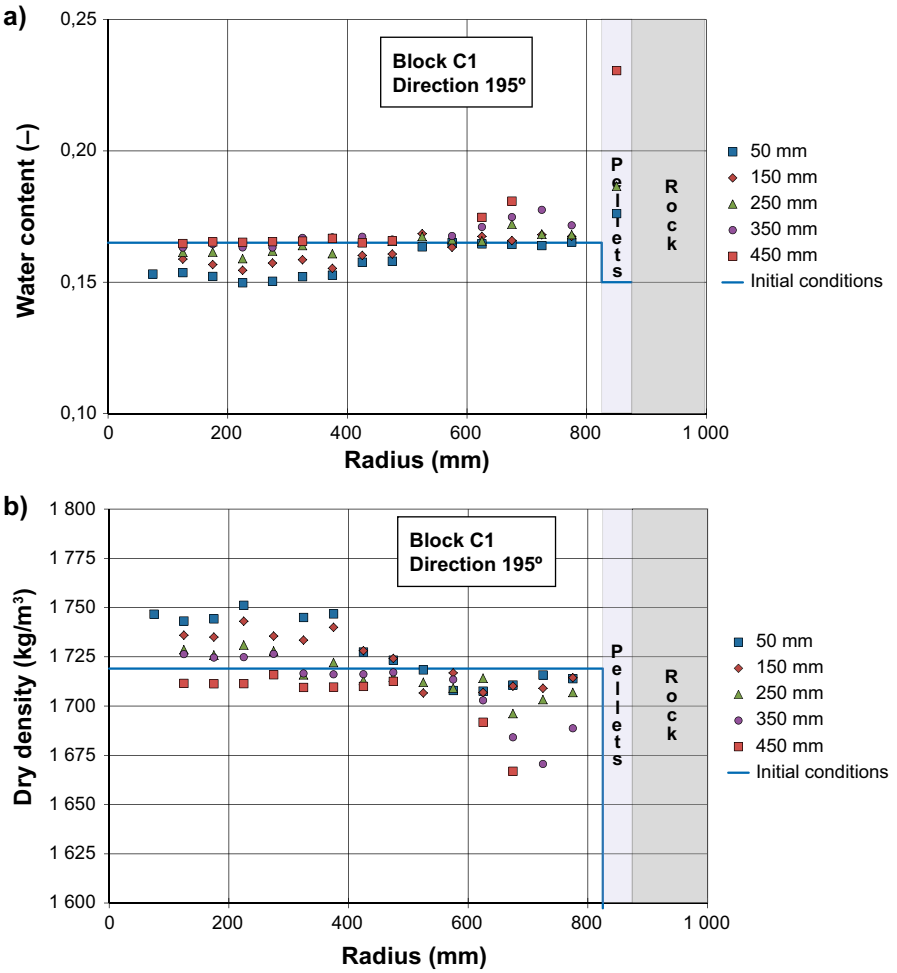

Figure 4-23. *Determination of a) water content and b) dry density of the bentonite in block C1 as function of distance from the center of the deposition hole. The determinations are made at five different depths from the upper surface of the block*

Overall response of the buffer

The data from all the determinations of the water content and density are summarised in Figure 4-24 and Figure 4-25. The initial water content of the buffer blocks was about 0.165 and for the pellets filling 0.150. The dry densities for the blocks at the installation were about 1 725 kg/ m^3 for the solid blocks and 1 767 kg/m^3 for the ring shaped blocks, see Section 4.4.5.

The figures show that the water uptake was relatively axisymmetric. There was an increase of the water content close to the top of the canister which indicates that there has been condensation of water vapour in that region of the buffer. There was a corresponding drying of the buffer close to the canister surface from about 500 mm below the top of the canister to the bottom of the canister. In the direction 105°–195° and at the distance between 2 500 and 6 000 mm from the bottom of the deposition hole there was a significant increase in the water content of the pellets and the outer part of the blocks. These depths, where this behaviour was evident, corresponds to blocks R5 to C2. At the bottom of block C1, close to the wall of the deposition hole, there was an increase in the water content.

The plots of the density show a decrease in the dry density of the buffer at locations of water uptake and an increase of the dry density at those parts of the buffer where a drying has occurred.

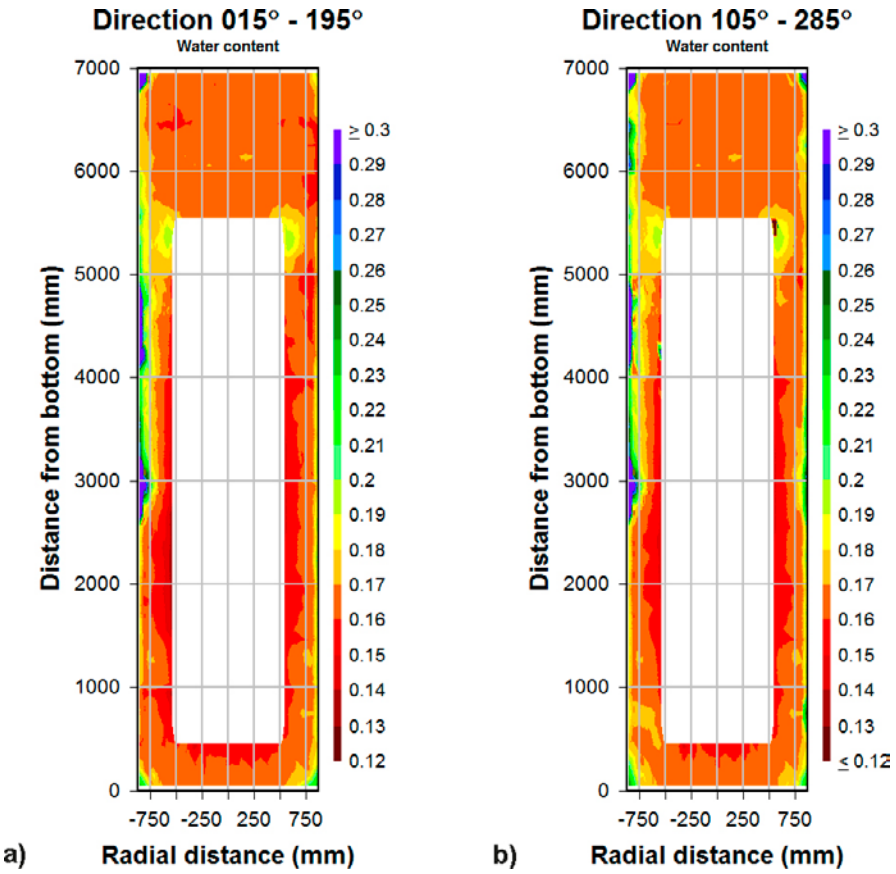

Figure 4-24. *Water content for the buffer a) in section 015–195° and b) in section 105–285°.*

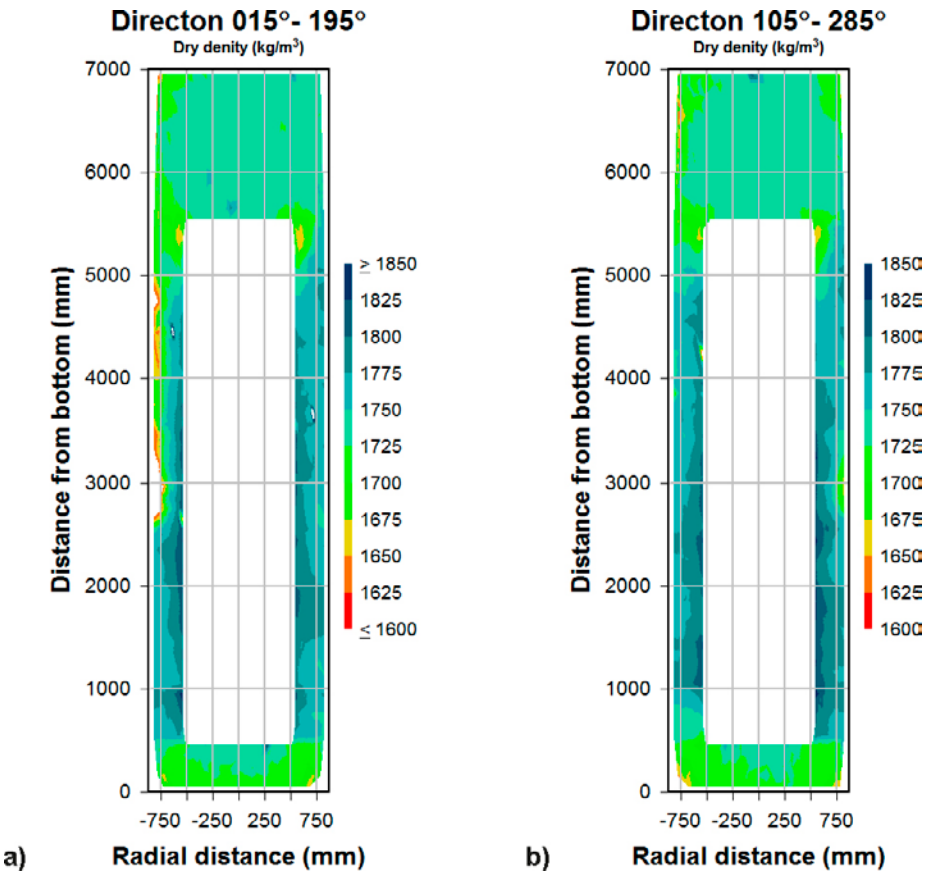

Figure 4-25. *Dry density for the buffer a) in section 015–195° and b) in section 105–285°.*

4.8 Deformations of the individual buffer blocks

The vertical coordinate for the individual buffer blocks were determined by geodetic surveying at the retrieval of the test. The measurements were made at 8 locations on top of each block. From these data it was possible to determine an average vertical coordinate for each block and then from this data calculate the average height of the blocks after the tests. Corresponding calculations could be made with data coming from the installation of the buffer blocks. By comparing these two data sets it was possible to calculate the changes in height of each individual buffer block, see Figure 4-26. A positive value corresponds to an increase of the block height. The following conclusions can be drawn from the calculations:

- The plot shows that all blocks except block C1, R1 and R2 increased in height during the test period. This coincides with the observed increase of water content for block R4 to C2, see Section 4.7.3.
- The largest swelling was observed for blocks R8 – R10 and C2.
- The sum of the swelling measurements for the individual blocks (37 mm), corresponds well with the measured deformation of the upper concrete block measured during operation of the test, see Section 4.5.3.
- The deformation of the blocks was measured after the cooling of the canister and the buffer. It is likely that, due to thermal contraction, there was a decrease in height of both the buffer blocks and the canister during the cooling phase.

4.9 Results and discussion

The measurements of water content in the pellets showed a large variation, indicating that this part of the buffer also absorbed water from the surrounding rock and its water bearing fractures (inflow estimated to be ~1.152 l/d, corresponding to ~115.2 l over the 100 days of Test 1 operation. The buffer around the canister showed a decrease in water content close to the canister. The combination of water uptake by the pellets and a drying of the inner part of the buffer blocks probably caused the cracking of the ring shaped blocks, see Figure 4-27. The figure indicates that the visible crack on the inside of the ring shaped blocks were following the wet fracture on the wall of the deposition hole.

An increase in water content close to the lid of the canister was also observed. This is probably due to condensation of water in that region. The effect of water redistribution on the solid blocks above and below the canister was small and the frequency and extent of cracks were much lower than in the rings.

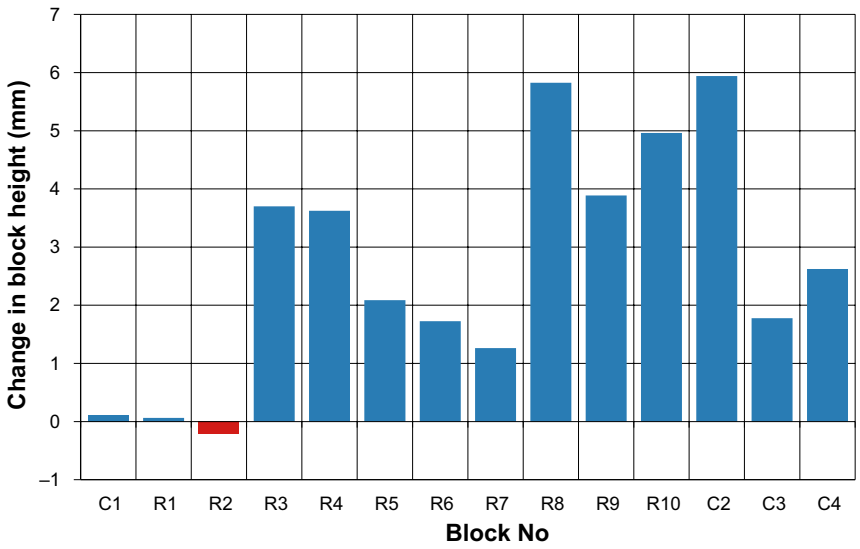

Figure 4-26. *Change in height of the 14 installed buffer block in test 1.*

Radial cracks were observed in all buffer blocks, some of them passing through the entire block. However, since the outer slot was filled with pellets the buffer installation processes is not affected by such post-installation cracking. No requirement limiting allowable crack has been formulated considering long term safety since such cracks would seal during saturation and homogenisation. The technical design requirements considering long term safety hence will be fulfilled.

The observed total deformation of about 40 mm is considered to be acceptable and has been taken into account in buffer design.

The conclusion from the installation test is that the chosen installation technique is feasible in boreholes where there is low water inflow. In Test 1 the total water inflow was about 8E−4 l/min, making it a very dry location. However, from this test it is not possible to evaluate the limits on the acceptable water inflow for this installation technique. Joyce et al. (2013) calculated that 88 % of the deposition holes have an inflow lower than E−4 l/min. Based on this it can, with some safety margin, be stated that at least 90 % of the deposition holes in Forsmark will have an inflow lower than the deposition hole in the test.

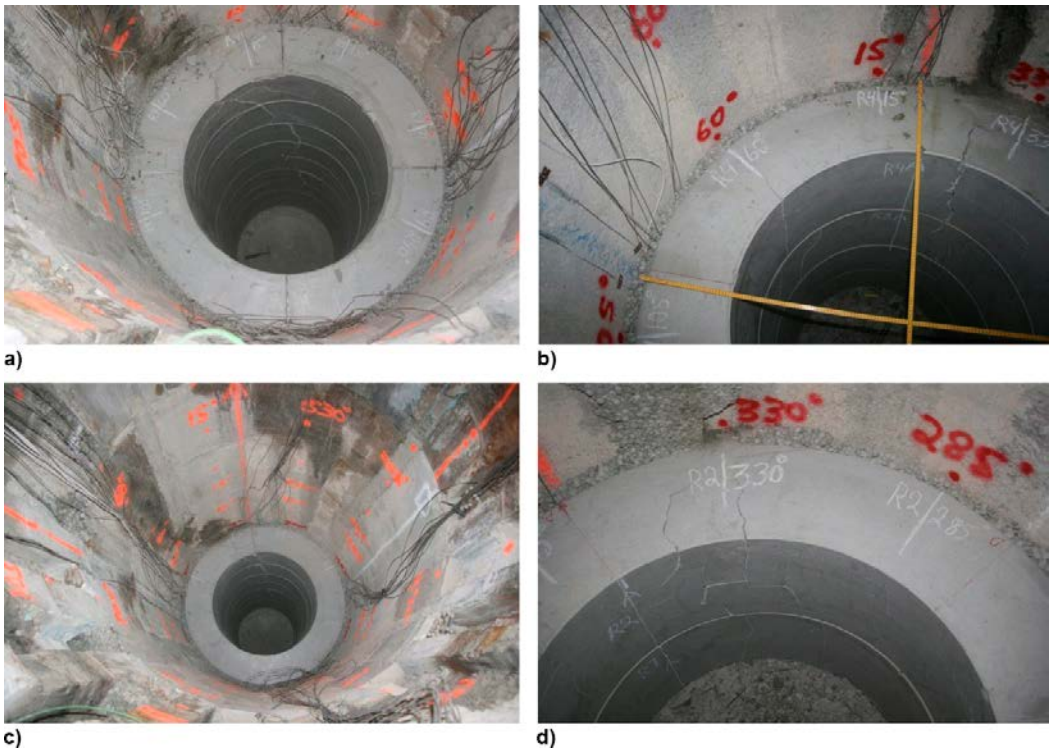

Figure 4-27. *Observed cracks in the ring shaped blocks in position closed to water bearing fractures.*

5 Full scale installation Test 2 simulating a relatively wet hole

5.1 Description of buffer installation method

This installation method was intended for use with wet deposition holes. A buffer protection hood is installed from the top of the buffer to approximately the top of the canister. This hood is removed just before the outer slot is filled with pellets. During the time period before the pellets are installed and the tunnel section above is backfilled, the water entering in the deposition hole is pumped out through a pipe installed at the bottom of the deposition hole. The buffer protection is intended to maintain its function for 90 days.

This installation method has the following advantages and risks:

- The buffer blocks are installed with a protection hood at most upper part of the buffer. Compared to a protection sheet that covers the whole buffer, this is assumed to be easier to remove and so poses less risk to an installation where a canister is present.
- This installation method was to be able to handle higher water inflows than could be accomplished using an unprotected buffer assembly.

Modelling, see Section 5.2, has shown that during the 90 days following buffer and canister installation, there will be changes of the water content and the dry density of the buffer. This is caused by the redistribution of the water in the buffer blocks due to the heating from the canister as well as limited water uptake. However, if the protection hood placed on the top of the buffer is used, these changes are, according to the made modelling, assumed to be small.

5.2 Pre-modelling and input to installation method and test set-up

The basic idea behind Test 2 is to let the thermal gradient protect the majority of the buffer from incoming moisture. If the thermal gradient across the outer slot is large enough then the outer part of the buffer should experience drying conditions. These drying conditions are not as detrimental to block integrity as wetting conditions. It is anticipated that the blocks will develop cracks on their surfaces but no material loss into the outer slot is expected. The upper part, above the canister, will be cooler than in regions closer to the canister and so water vapour will condense and wet the materials in this region. To protect the blocks from this wetting a modified buffer protection sheet covering only the upper part of the buffer is suggested. A modelling exercise to determine how such a cover would work has been done as a part the design and optimization of this buffer protection concept. A number of different layouts of the buffer protection have been modelled, see Figure 5-1, with the intent of identifying the best solution for use and identifying the geometry to be physically tested. The same models as described in Section 3.4 is used with the exception that all the air filled slots are considered to have free convection and the air flow is calculated with the Navier-Stokes equation.

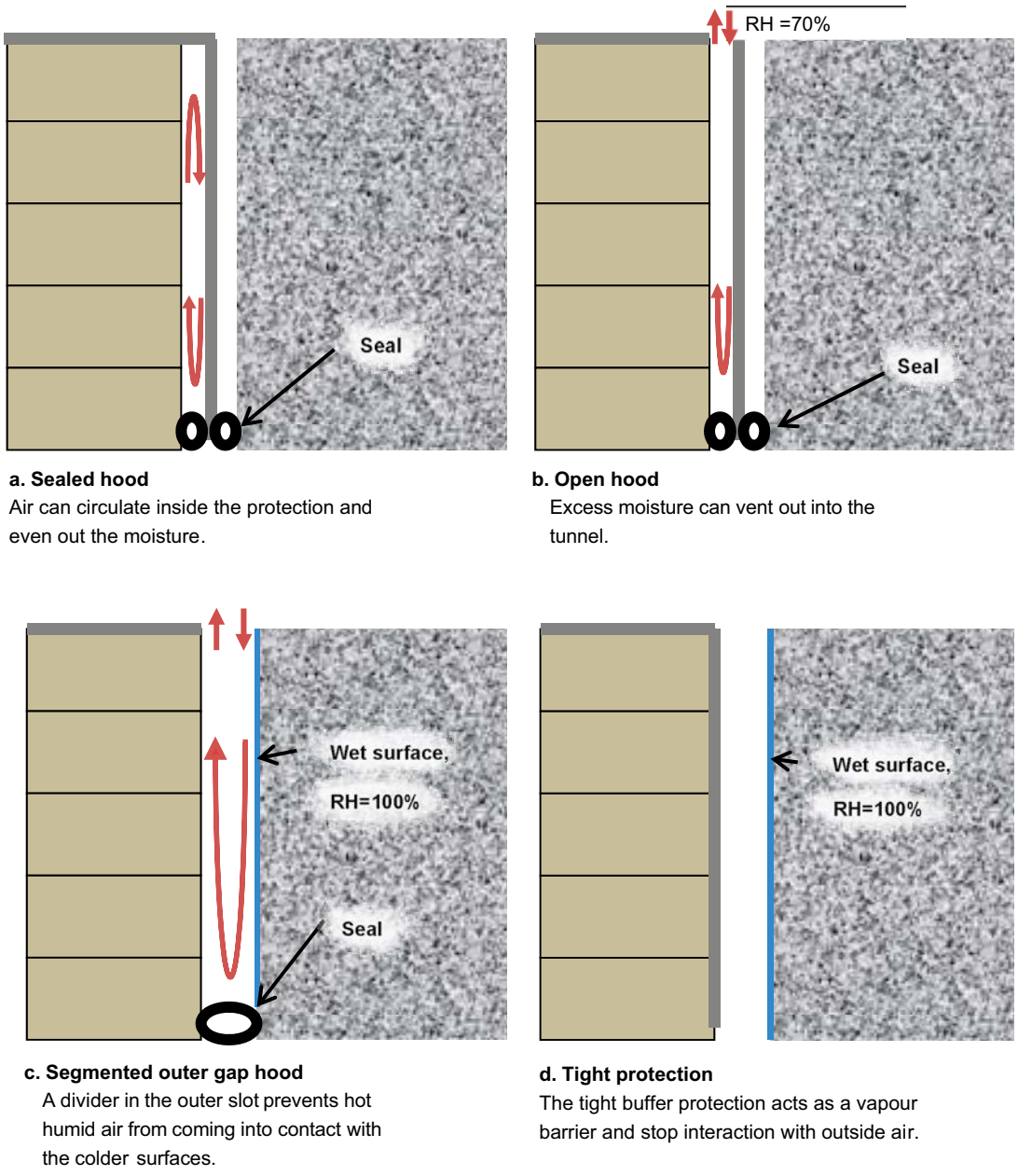

a. Sealed hood
Air can circulate inside the protection and even out the moisture.

b. Open hood
Excess moisture can vent out into the tunnel.

c. Segmented outer gap hood
A divider in the outer slot prevents hot humid air from coming into contact with the colder surfaces.

d. Tight protection
The tight buffer protection acts as a vapour barrier and stop interaction with outside air.

Figure 5-1. *Suggested alternative to protect the buffer.*

From the modelling of the four alternatives the following were concluded:

Alternative a. Seemed to work quite well and very little wetting is expected.

Alternative b. This alternative yielded approximately the same results as alternative a, but it is sensitive to the relative humidity in the tunnel and therefore is deemed to be less robust than alternative 1.

Alternative c. Due to the high relative humidity close to the rock wall, approximately 100 %, and the lack of a thermal gradient the relative humidity will be high in the interface between the buffer blocks and the slot. This will result in wetting of the buffer which is likely to cause problems.

Alternative d. A tight buffer protection over the buffer blocks has the disadvantage that when a thermal gradient is present, the water content will increase in the outer parts of the block. It was not possible to determine an optimal length for the protection and there was always an area close to the top of the canister that developed an increased water content (from 17 % to approximately 18.5 %).

For the reasons listed above it was decided to continue the design of alternative a, and try to optimize the length and the thickness of the slot between the blocks and the buffer protection by numerical simulation means.

The most optimal design, according to the modelling and installation considerations, is to have a protection sheet that protects the buffer down to the top of the canister and to have it positioned in the middle of the outer slot diameter. The modelling of the water content, see Figure 5-2, suggests that drying cracks will develop in the buffer rings and the top blocks. However, these cracks are not considered to have any major effect on the subsequent installation of pellets. The bottom block will take up some moisture and is likely to crack but this is also not considered to cause any major problems regarding pellet installation or canister stability.

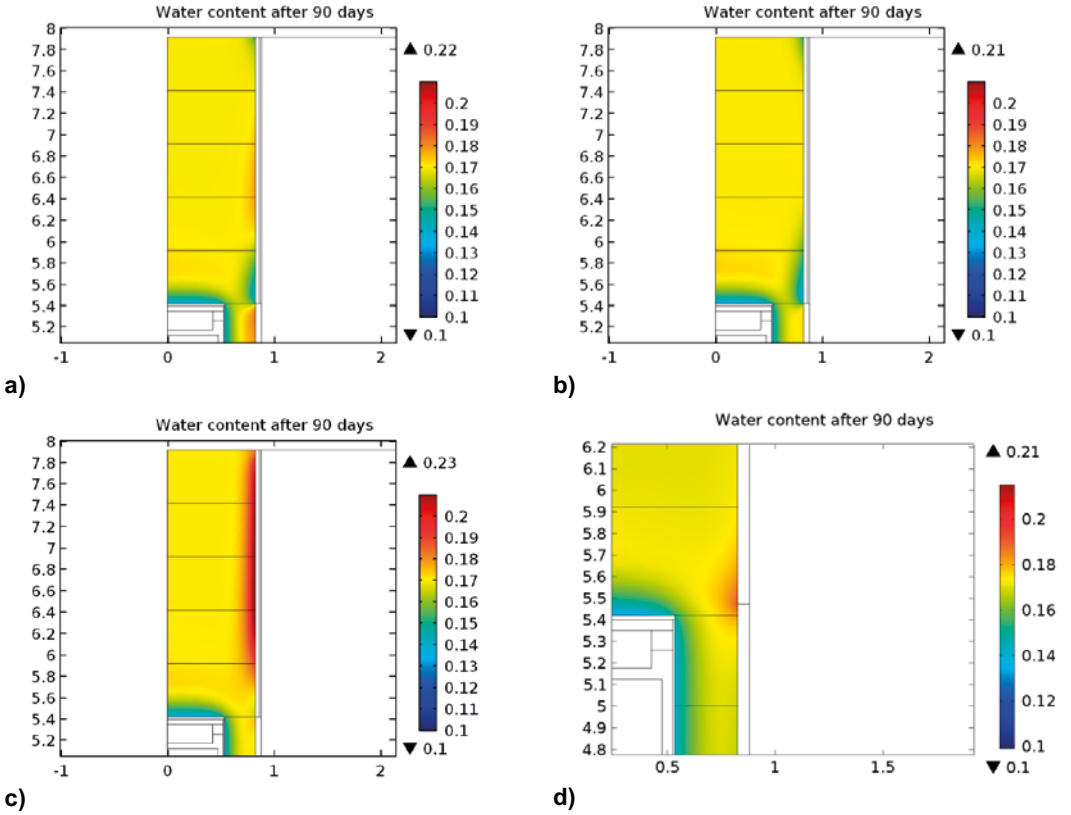

Figure 5-2. *Modelled final water content for the different alternatives.*

5.3 Installation

5.3.1 Buffer manufacturing

The buffer blocks and the pellets used for this test were made in the same way as described in Section 4.4.1.

5.3.2 Preparatory work on site

The preparation of the site was made in the same way as described in Section 4.4.2.

5.3.3 Installation sequence

The buffer consisted in total of 14 bentonite blocks, 10 ring shaped blocks, one disk-shaped bottom block and three solid cylindrical blocks on top of the canister. In addition to the bentonite blocks another two solid blocks made of concrete were placed on top of the buffer to fill the remaining volume in the deposition borehole. The concrete blocks had similar dimensions and weights as the solid buffer blocks. The numbering and naming of the blocks are shown in Figure 4-8.

The installation of the buffer the canister and sensors was made as follows:

1. The bottom plate in the deposition hole was evened out with concrete and putty. A pump was installed in the sump and the steel plate was placed in the deposition hole
2. Thermocouples were installed in the surrounding rock. The cables from the sensors were led on the wall of the deposition hole up to the tunnel floor.
3. A plastic sheet was installed inside the deposition hole and attached to the bottom plate with an O-ring. It was possible to remove the O-ring from the tunnel floor. The plastic sheet was used for protecting the buffer during the installation.
4. The bottom block (C1) was weighed and its dimensions were determined. A small sample of the block was taken on which the water content was determined. The block was then placed in the centre of the deposition hole. The distance between the buffer block and the wall of the deposition hole was measured and the positon of the block in vertical direction was determined by geodetic surveying. A groove was machined at the top of the bottom block in order to fit the bottom of the canister, see Figure 4-9. This was made with a drilling tool. Holes for the sensors were drilled from the top of the block and the sensors were installed. The cables from the sensors were led in grooves at the top of the block towards the outer diameter of the block and further upwards to the tunnel.
5. The ten ring shaped blocks (R1–R10) were placed in the deposition hole after they were weighed and their dimensions were determined. The blocks were centred in the deposition hole with the use of the block beneath. Sensors were installed in the same way as for the bottom block. Finally, the horizontal positions of the blocks were determined by measuring the distance between the outer diameter of the block and the wall of the deposition hole at eight locations and the vertical position by geodetic surveying.
6. All the cables from the sensors were led up to the tunnel along the stack of blocks as close as possible towards the outer diameter of the buffer blocks.
7. The deposition machine with a canister-sized heater was transported from a nearby tunnel with a truck and placed over the deposition hole. The canister was put in place in the deposition hole and the deposition machine was then removed with the truck. The cables coming from the heating elements in the canister was arranged at the top. A ring of copper was put on the top of the canister. The volume inside the ring was then filled with pellets and an upper lid was placed on the copper ring. The cables coming from the heating elements in the canister was led in grooves on the top of block R10 towards its outer diameter and further upwards to the tunnel floor. The distance between the canister and the inner diameter of the upper block was determined. The vertical position of the top of the canister was then measured by geodetic surveying.
8. A protection tube, made of tarpaulin was attached to the outer diameter of block R10 at the distance of about 100 mm from the top of the block, see Figure 5-3.
9. The three upper solid blocks (C2–C4) was put in place inside the protection tube, see Figure 5-3. The instrumentation and the measurements of the positions of the blocks were made in the same way as for the rest of the blocks.

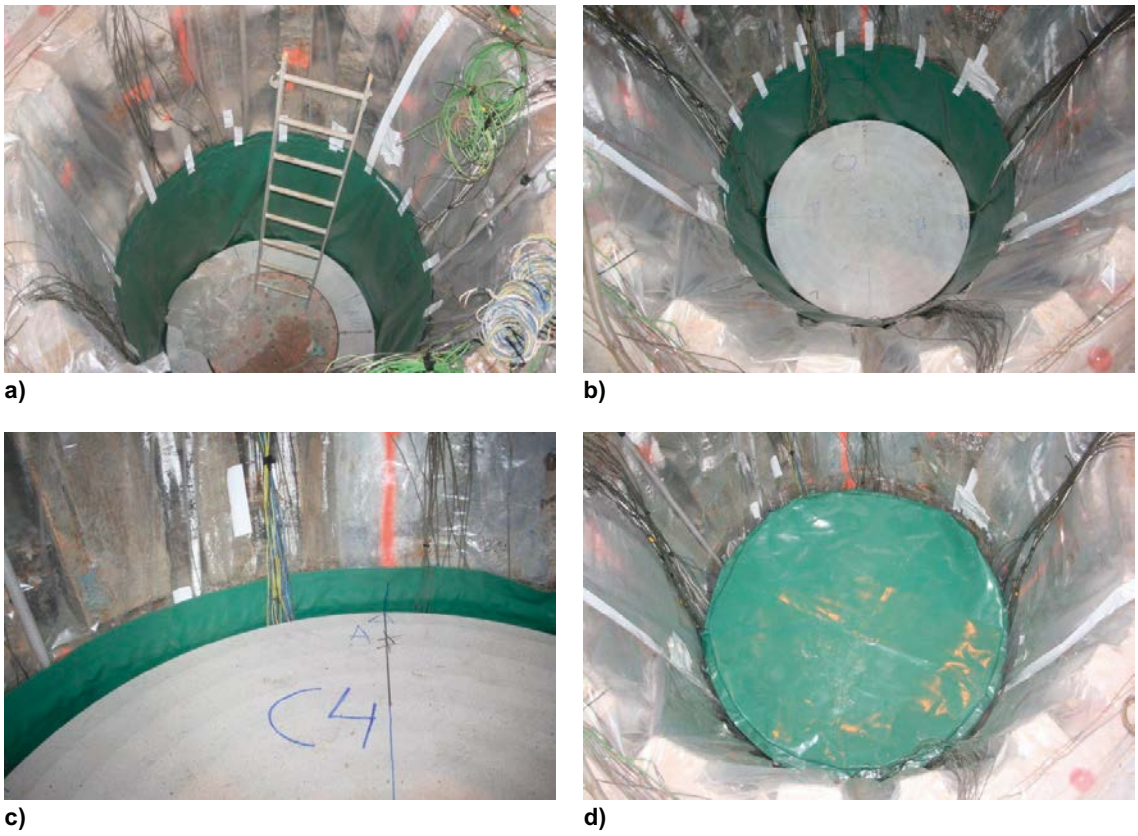

Figure 5-3. *Installation of the protection tube in the deposition hole a) the tube is in place b) block C2 inside the protection tube c) block C4 in place inside the protection tube d) a sheet placed on top of block C4.*

10. A sheet of rubber was placed on the top of block C4 and attached to the installed protection tube, see Figure 5-3.
11. Two blocks of concrete with same dimensions as the solid bentonite blocks was put in place.
12. The installed plastic sheet was then removed from the deposition hole. A rubber sheet was place on the upper concrete block.
13. The power required to generate 1 700 W of heating was supplied to the heating elements in the canister and the data acquisition system for the installed sensors was started.

5.3.4 Installation of sensors

The installation of the sensors in this test (Test 2) was done in the same way as in Test 1. This is described in Section 4.4.4.

5.3.5 Data from the installation

The weight and dimensions of the installed blocks were determined before they were installed in the deposition hole. From these data the bulk density (ρ) of the blocks was calculated. Using a small sample taken from each of the blocks, the water content (w) was determined. The data from these measurements are compiled in Table 5-1. The dry density (ρ_d) of each block is determined as:

$$\rho_d = \rho/(1+w)$$

The water content for the 14 blocks varied between 0.165 and 0.169. The height of the blocks varied between 494 and 500 mm, except for block R10 which was adjusted to match the remaining length of the canister and thus had a height of about 420 mm. The dry density of the solid blocks varied between 1 711–1 733 kg/m^3 (average dry density 1 722 kg/m^3) while the dry density of the ring shaped blocks varied between 1 758–1 788 kg/m^3 (average dry density 1 776 kg/m^3).

Table 5-1. Data from the installation of the buffer blocks in Test 2.

Blok No	Outer diameter (mm)	Inner diameter (mm)	Average height (mm)	Weight (kg)	Bulk density (kg/m^3)	Water content (–)	Dry density (kg/m^3)
C1	1650.0		496.5	2147	2022	0.165	1736
R1	1650.0	1071.0	500.0	1284	2075	0.167	1779
R2	1650.0	1071.0	500.0	1288	2082	0.165	1787
R3	1650.0	1070.0	500.0	1285	2074	0.168	1775
R4	1650.0	1070.0	500.0	1285	2074	0.166	1778
R5	1650.0	1070.0	500.0	1288	2079	0.168	1780
R6	1650.0	1070.0	502.8	1287	2066	0.169	1768
R7	1650.0	1070.0	502.8	1290	2071	0.169	1771
R8	1650.0	1070.0	500.0	1291	2084	0.166	1788
R9	1650.0	1070.0	501.0	1273	2051	0.167	1758
R10	1650.0	1070.0	420.8	1084	2079	0.167	1781
C2	1650.0		493.7	2139	2026	0.169	1733
C3	1650.0		500.0	2137	1999	0.168	1711
C4	1650.0		500.0	2136	1998	0.168	1711

5.4 Running of test

5.4.1 The power on the canister

The power applied to the heating elements placed in the canister is shown in Figure 5-4. A power of 1 700 W was applied to the heating elements during the whole test period.

5.4.2 Temperature and RH measurements

The RH-sensors which failed during the first test were checked before they were installed in Test 2. The tests were made at a constant temperature and the readings from the sensors looked reasonable. Tests were also made were the sensors were placed in bentonite with good results. Data from the installed sensors was collected continuously during the whole test period. The installed thermocouples functioned well, while readings from the ten installed RH showed, as in Test 1, large scattering. The reason for this is unclear. The temperature was also measured with the RH-sensors and these measurements gave reliable values. The data from all sensors are shown in Appendix 4.

The temperature measurements made on the canister surface are shown in Figure 5-5. The thermocouples were installed in two directions (B and C) close to the bottom, at mid-height and close to the top of the canister. The four directions A, B, C and D are defined in Section 4.4.4. The figure shows that the maximum measured temperature was about 70 °C at the mid-height of the canister.

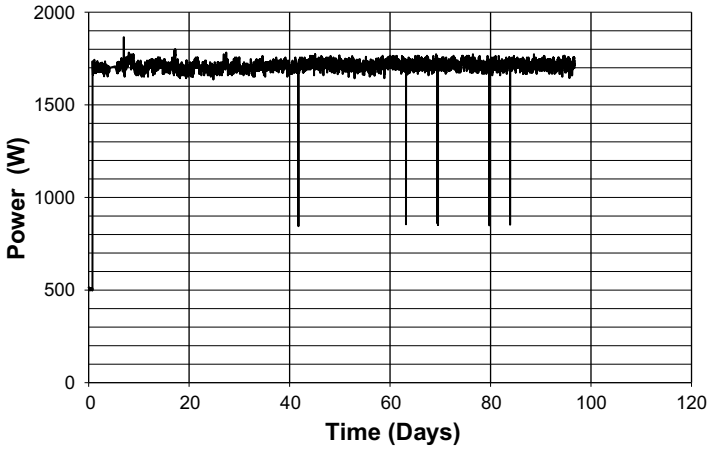

Figure 5-4. *The applied power on the heaters in the canister.*

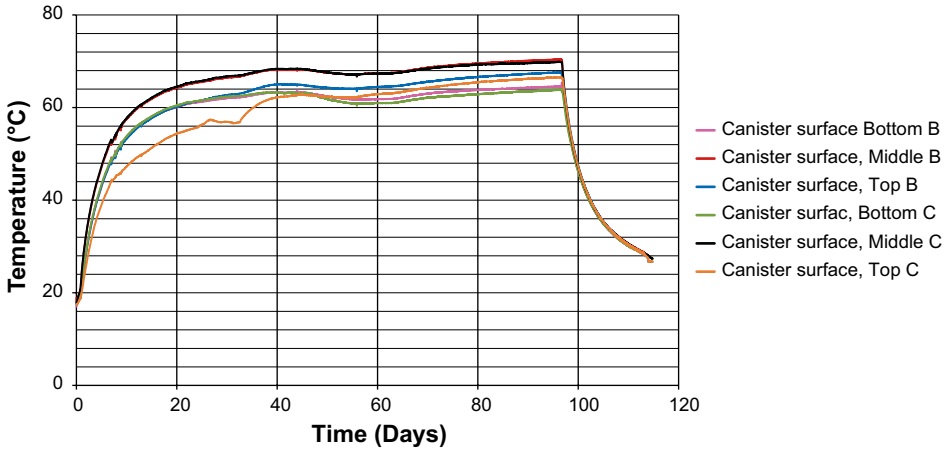

Figure 5-5. *The temperature evolution on the canister surface as function of time. The thermocouples are placed at the bottom, at mid height and at the top of the canister.*

The maximum temperature at the bottom of the canister was about 6 °C lower than the maximum temperature at the mid-height of the canister. The temperature on the canister was, as expected, almost independent of the direction (B and C).

The temperature was also measured in the rock inside the deposition hole. This was made at three levels in the deposition hole, 400 mm, 2 900 mm and 4 900 mm from the bottom. The sensors were installed in two directions at each level. Sensors were also installed about 50 and 150 mm into the rock (radial distance of 925 and 1 025 from the centerline of the heater). The results from the measurements at these three levels are presented in Figure 5-6 and show that the temperature was, as expected, highest at the level of 2 900 mm i.e. close to mid-height of the canister. The lowest temperature was measured close to the bottom of the deposition hole. The plots also indicate that the temperature was lower towards the left wall of the tunnel, i.e. in direction B. The maximum temperature measured on the rock surface was about 38 °C.

The temperature in the buffer was measured with thermocouples but also with the thermocouples associated with the RH-sensors. The data from all sensors are shown in Appendix 4. The measurements made in buffer block R5 are shown in Figure 5-7 and shows that the maximum temperature in the buffer was about 64 °C. This was measured on the inside surface of the buffer ring. The figure also shows that the temperature decrease over the inner gap i.e. between the canister surface and the inner surface of the buffer block was about 10–17 °C expect for direction B where the temperature fall was much less, about 1 °C. This indicates that the canister in that direction was in direct contact with the buffer block rather than having a small gap between them. The temperature decrease over the buffer block was about 20 °C in directions A, B and C, and somewhat lower in direction D. The temperature decrease over outer gap was about 6–10 °C.

5.4.3 Buffer displacement

The displacement of the buffer in axial direction was measured by geodetic surveying of the upper surface of the uppermost concrete block. This measurement was made at least once a week in 9 positions on the block, two in each of the four main directions and one in the centre. The four directions A, B, C and D are defined in Section 4.4.4. The results from the measurements are shown in Figure 5-8, where positive displacement means that the block has moved upwards. The following conclusions can be made from the measurements:

- The maximum average displacement was reached at around day 30, about 30 mm.
- After day 30 the displacement decreased to about 10 mm during a period of 30 days.
- During the next 30 days the displacement was relatively constant.
- The maximum displacement of the surfaces varied between 27 and 32 mm.
- The largest displacement was observed in direction A–D which implies that the surface of the block was somewhat inclined.

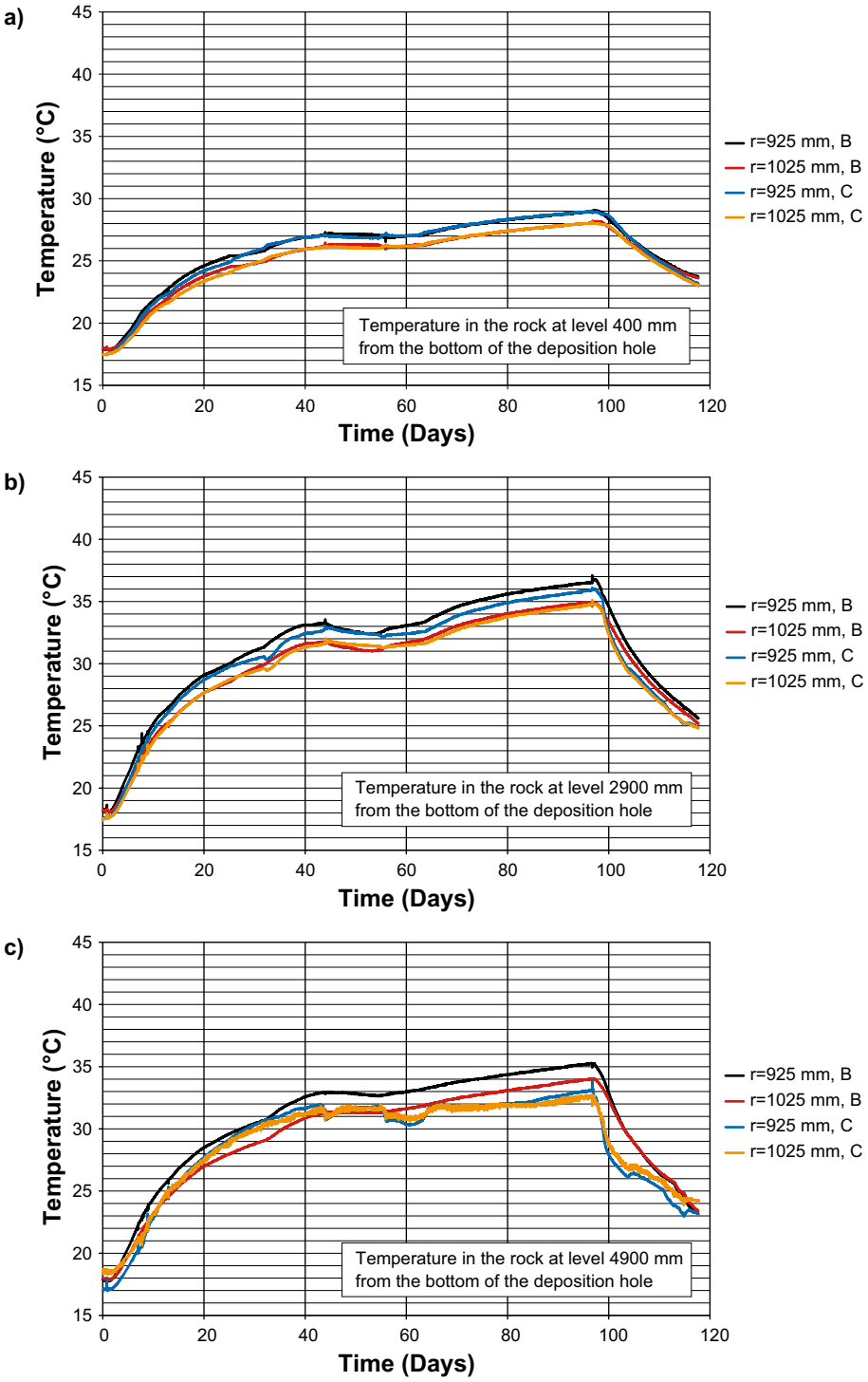

Figure 5-6. *Test 2 temperature evolution in the surrounding rock at three different levels in the deposition hole a) 400 mm b) 2 900 mm and c) 4 900 mm from the bottom.*

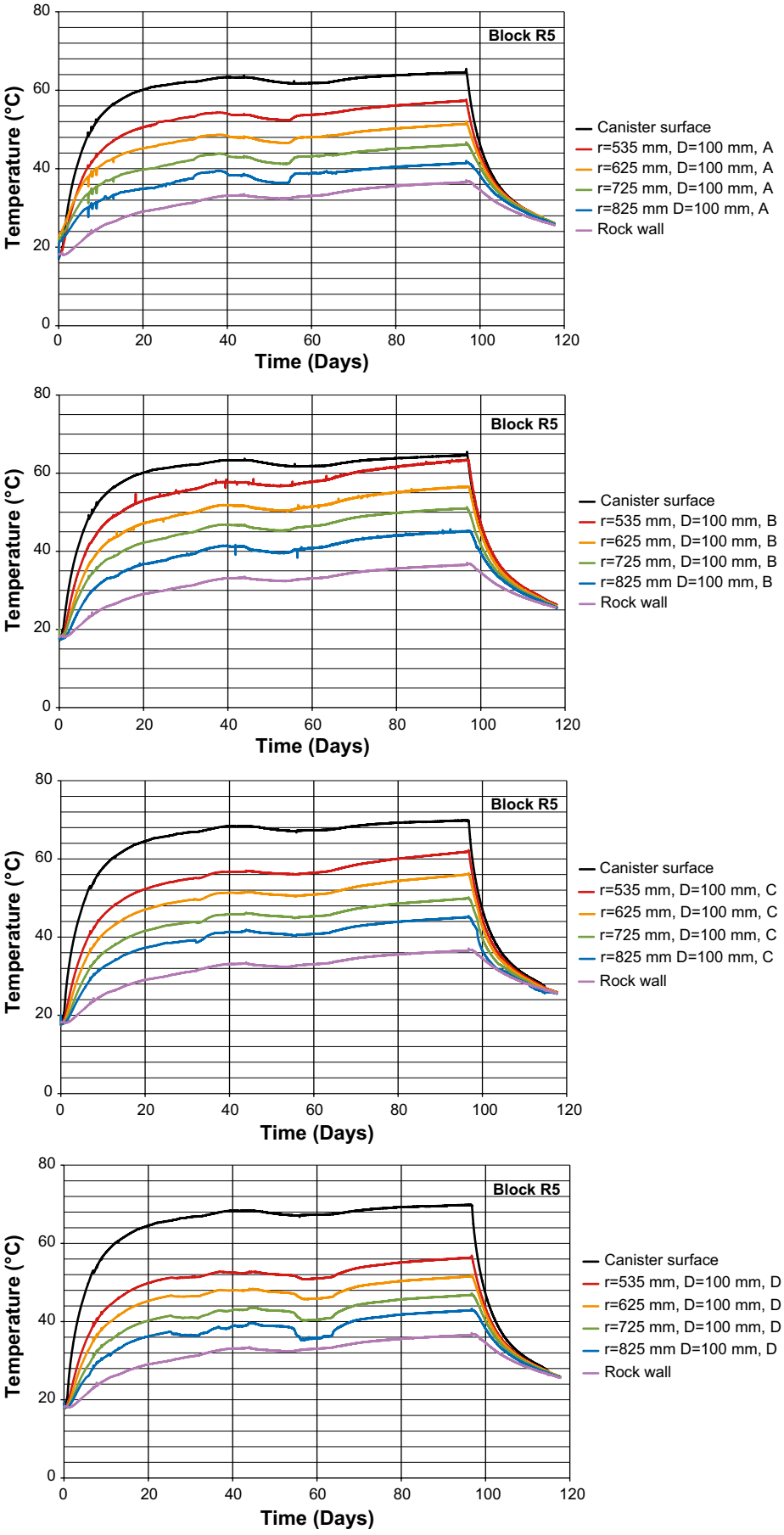

Figure 5-7. *The temperature evolution in buffer block R5 of Test 2. The measurements are made in four directions A, B, C and D.*

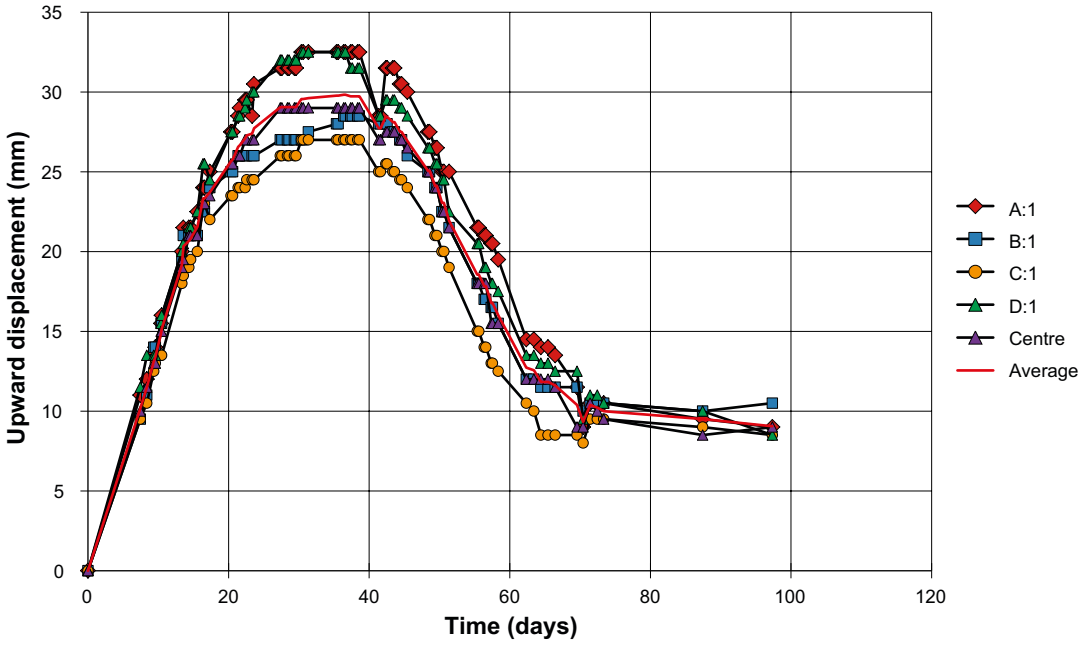

Figure 5-8. *The upward displacement of the upper concrete block. The measurements were made in four perpendicular directions and at the centre of the block. The average of the displacement (from measurements in nine points) is also given.*

5.4.4 Observed damage on the buffer blocks during the running of the test

With a camera that was sent down into the outer gap between the buffer blocks and the wall of the deposition hole, observations of cracks and how they were developed during the test period on the outer periphery of the buffer blocks could be made. Due to the small gap between the buffer blocks and the wall of the deposition hole and the installed buffer protection could the observations only be made on small parts of the blocks. At the investigation three zones where cracks were observed could be recognized, see Figure 5-9:

1. **At the bottom of the deposition hole, position I.** These cracks and damages were observed very early in the test period and consisted of flakes of bentonite which were loosened from the bottom block. The damage seemed not to get worse with the time and it is assumed that the damage was caused by high relative humidity at the bottom of the outer gap before the temperature pulse from the warm canister had reached the outer slot.
2. **At mid height of the canister, position II.** The cracks were both horizontal and vertical and had a width of some mm. The cracks did not cause fallouts of bentonite into the outer gap. The cracks had most likely occurred due to the warm canister causing a dehydration of the bentonite, with a subsequent shrinkage.
3. **Around block R9 and R10, position III.** Large cracks with widths of several centimeters were observed. Furthermore, large pieces of the blocks were seen to be detached from the two blocks. The damage to these blocks increased with time.

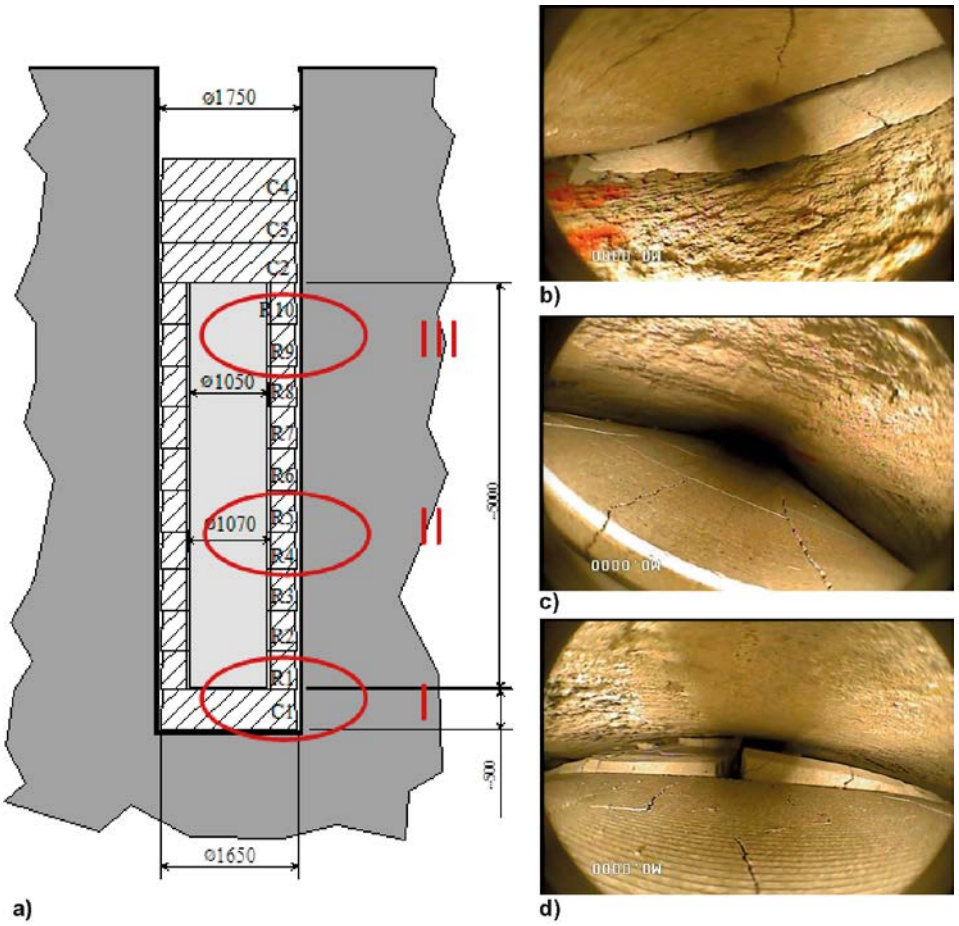

Figure 5-9. *Cracks observed at the running of the test a). The three different positions where phots have been taken. b). A photo taken at the bottom of the deposition hole, position I. c) A photo taken at mid height of the canister, position II. d) A photo of the joint between block R9 and R10, position III.*

5.5 Dismantling

5.5.1 Removal of the buffer and the canister

The power to the test was switched off after about 90 days and was followed by 7 days of passive cooling of the canister, after which sampling of the buffer started. The dismantling was done block by block. Samples were taken in two directions 15° and 195° respectively in all blocks. In two additional directions (105° and 285°) samples were taken of the solid blocks.

The dismantling was done according the following sequencing:

1. The two blocks of concrete (C5 and C6) were lifted out of the deposition hole. Samples of the pellets in the outer slot were taken in 8 directions (0°, 45°,…315°, see Figure 4-10 about the definition of the angle). The water content of the pellets was determined for each sample recovered. The distance between the blocks and the surface of the deposition hole was also measured at the same 8 directions and the position of the upper surface was measured by geodetic surveying.
2. Samples of the three upper solid bentonite blocks (C2–C4) were taken by core drilling from the upper surface of the blocks. The cores were transported to a laboratory on ground level where they were divided in smaller specimens for water content and the density determinations. The distance between the block and the surface of the deposition hole was measured in 8 directions. The vertical positions of the upper surface of the blocks were measured by geodetic surveying.
3. After block C2 was removed the buffer protection tube was also removed and the vertical position of the top of the canister was measured.

4. In order to minimize the possible changes on the remaining blocks at the dismantling, i.e. their water content and dry density, the outer slot was filled with bentonite pellets.
5. The canister was then lifted up from the deposition hole and transported away to a nearby tunnel with the use of a deposition machine.
6. Samples were taken from the ten ring shaped blocks (R1–R10) by sawing out thin slices from the blocks in two directions. The slices were transported to a laboratory on ground level where they were divided in smaller specimens on which the water content and the density were determined. The distance between the block and the surface of the deposition hole were measured in 8 directions. The vertical positions of the upper surface of the blocks were measured by geodetic surveying.
7. The bottom block (C1) was removed and sampled in the same way as blocks C2–C4, see above.

5.5.2 Observed cracks

Cracks were observed in all of the removed buffer blocks, see Figure 5-10. Some of the cracks in the ring shaped blocks went through the whole blocks in radial direction. These cracks have most likely affected the redistribution of the water in the installed buffer, see Section 5.7.

5.6 Water content and density of the buffer

5.6.1 Preparation of the samples

From the samples taken from the solid blocks by vertically drilling out core samples at four locations on the surface of the blocks, see Figure 4-18, smaller specimens were taken on five levels on which the bulk density and water content were determined. Corresponding preparations of the specimens from the slices taken from the ring shaped blocks is shown in Figure 4-19. In Test 2, these slices were taken only in two directions. From each slice, ideally 50 smaller specimens were sawn out to obtain water content, density and the bulk density values.

Altogether more than 1 500 determinations of the water content and density were made.

5.6.2 Determination of density and water content

The determination of the water content was made in the same way as for Test 1, described in Section 4.7.2.

5.6.3 Results

The data from the determinations of the water content and the bulk density together with the positions of the samples are used for analysing the buffer after the test.

Above the canister

The water content and the density for the buffer, were as mentioned above determined in four profiles in each solid buffer block. The densities and the water contents of one profile in block No C3 (middle clay block above the canister), are plotted as function of the distance from the centre of the deposition hole in Figure 5-11. The figure shows that:

- The water content and hence dry density at the center of the block was close to the initial conditions.
- Close to the outer diameter of the block the plot shows that a significant increase in water content has occurred.
- There has been a decrease in the dry density of the block close to the outer surface of the block. Thus, the plot is indicating that there has been a water uptake at the outer part of the block causing a swelling of the bentonite with a subsequent decrease in dry density.

Corresponding plots for the rest of the investigated sections of the solid blocks above the canister are shown in Appendix 5.

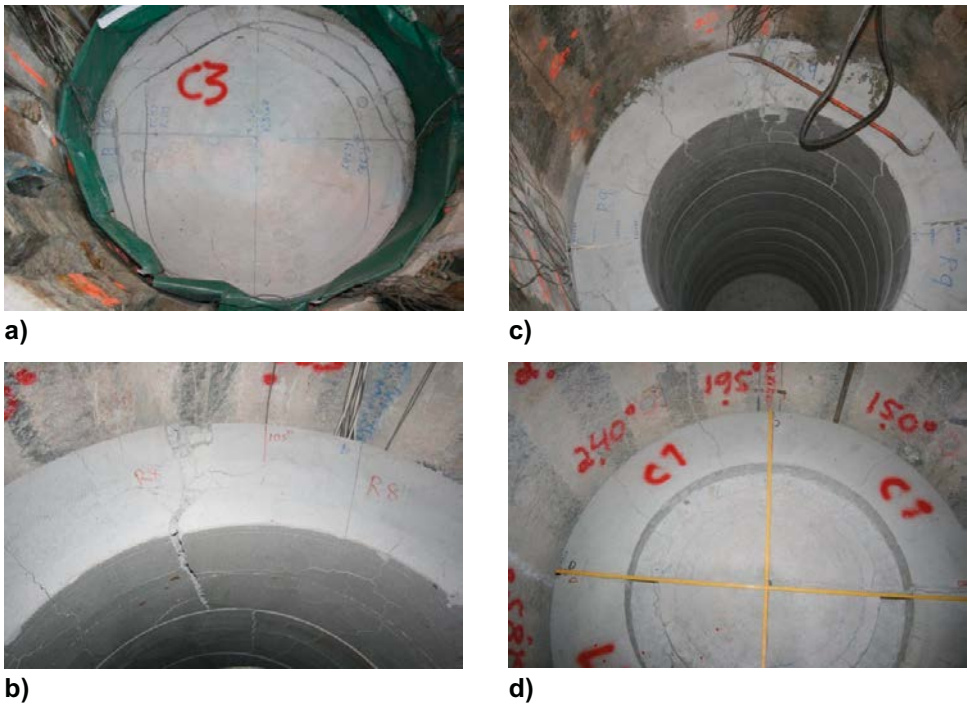

Figure 5-10. *Observed cracks on the blocks at the dismantling a) in block C3 b) block R9 c) block R8 d) and in the bottom block C1.*

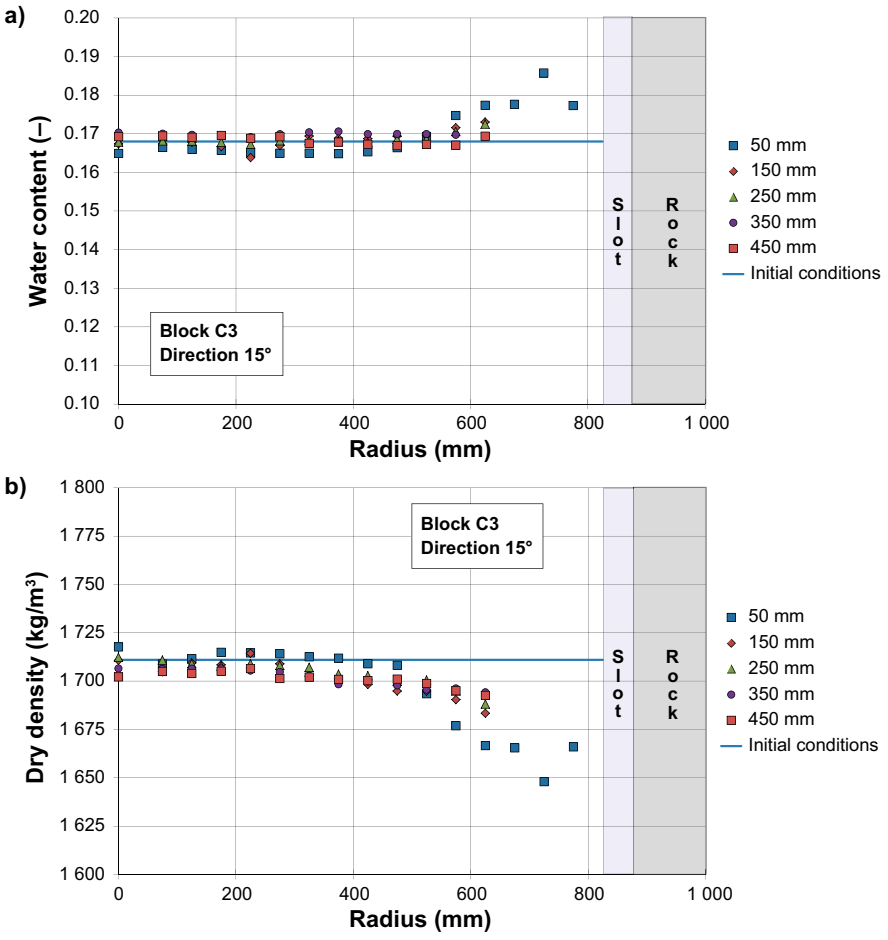

Figure 5-11. *Determination of a) water content and b) dry density of the bentonite in block C3 as function of distance from the center of the deposition hole. The determinations are made at five different depths from the upper surface of the block.*

Around the canister

The densities and the water contents of one profile in block No R6 are plotted in Figure 5-12. The figure shows that there has been a drying of all parts of the block resulting in an increasing of the dry density in most parts, compared to the initial conditions. This is valid for the buffer at mid-height of the canister. Corresponding plots for all of the investigated sections are shown in Appendix 5.

Below the canister

The water content and the density of the buffer were, as mentioned above, determined in four profiles in each solid buffer block. The densities and the water contents of one profile in block No C1 are plotted in Figure 5-13. The figure shows that

- the water content at the mid-height and lower portions of the block (250, 350 and 450 mm), was almost the same as the initial,
- close to the top of the block (50 and 150 mm) the water content was about 2 % lower compared to the initial conditions and drying was greatest close to the radial midpoint,
- there is a somewhat higher overall dry density in the upper part of the block compared to the initial conditions.

Corresponding plots for the rest of the investigated sections of the solid blocks above the canister are shown in Appendix 5.

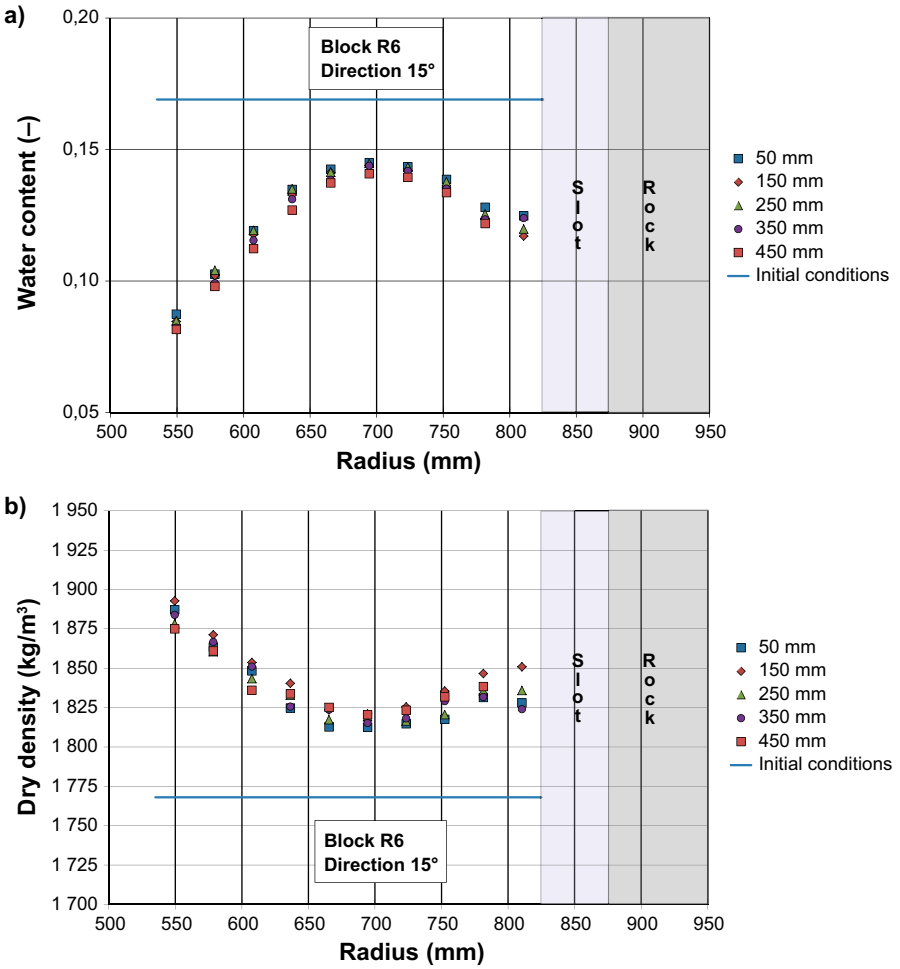

Figure 5-12. *Determination of a) water content and b) dry density of the bentonite in block R6 as function of distance from the center of the deposition hole. The determinations are made at five different depths from the upper surface of the block*

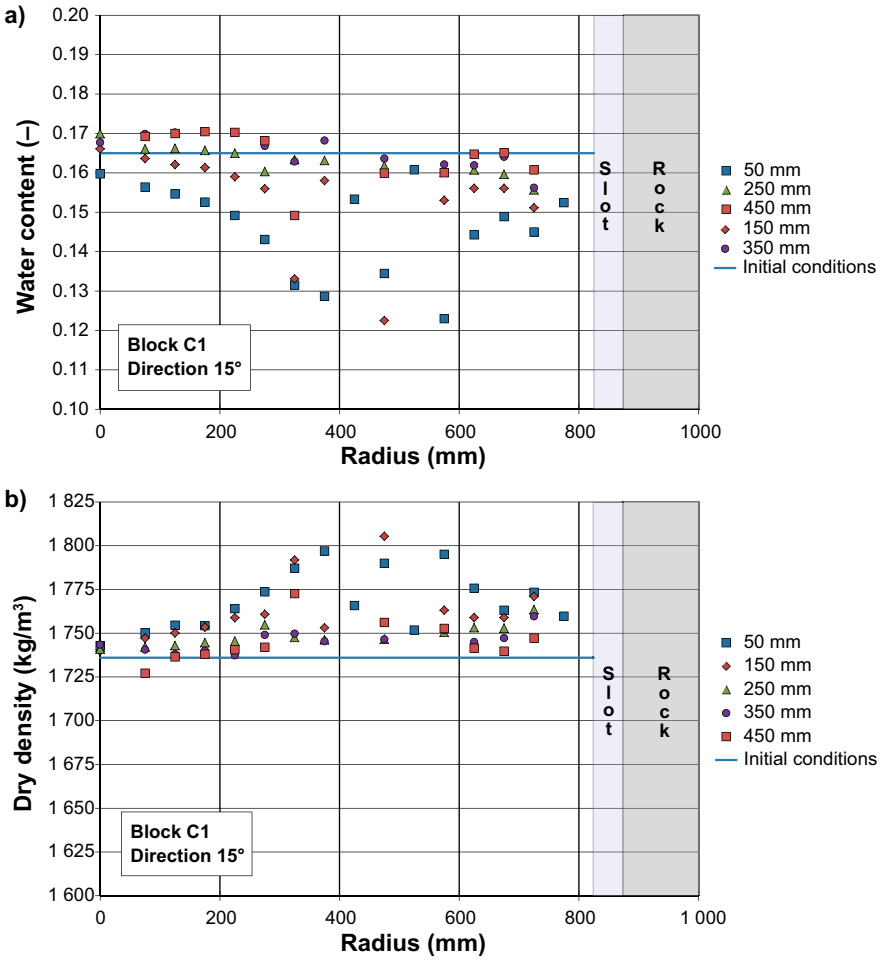

Figure 5-13. *Determination of a) water content and b) dry density of the bentonite in block C1 as function of distance from the center of the deposition hole. The determinations are made at five different depths from the upper surface of the block.*

The whole buffer

The data from all the determinations of the water content and density in the two directions 15° and 195° are summarised in Figure 5-14. The initial water content of the buffer blocks was about 0.167. The dry densities for the blocks at the installation were about 1 723 kg/m^3 for the solid blocks and 1 776 kg/m^3 for the ring shaped blocks, see Section 5.4.5.

The figures are indicating that most of the buffer had experienced some degree of drying. This was most pronounced around the canister and especially close to the canister surfacefer had dried. This was most pronounced around the canister and especially close to the canister surface.

The drying was, as expected symmetric. The drying of the buffer caused shrinkage of the buffer blocks and thus an increase of the dry density of the buffer occurred. As a result of this shrinkage, the height of the stack of ring shaped blocks decreased. One effect of this was that at the time of dismantling of the test there was a gap between the tenth ring shaped block (R10) and the first solid clay block placed on top of the canister (C2) of about 80 mm. At time of installation the upper surface of block R10 was about 20 mm higher than the upper lid of the canister, see Figure 5-15. This means that the solid clay block was resting on the canister lid rather than being in contact with the underlying ring-shaped block R10. The result would be a large gap connecting the inner slot between the canister and the buffer with the outer slot between the buffer and the rock surface of the deposition hole. It is likely that this gap has affected the drying of the buffer during the test.

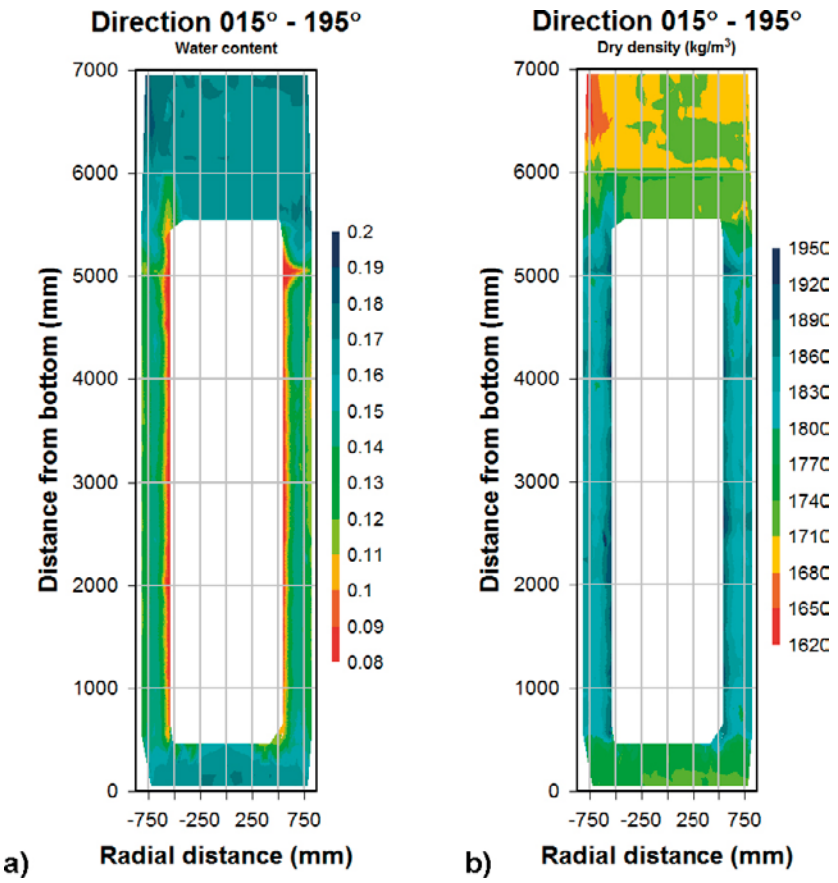

Figure 5-14. *a) The water content for the buffer in section 015–195° and b) the dry density for the same section.*

Figure 5-15. *Block R10 and the canister lid a) at the installation and b) at the retrieval.*

5.7 Deformations of the individual buffer blocks

The vertical coordinate for the individual buffer blocks were determined by geodetic surveying at the retrieval of the test. The measurements were made at 8 locations on top of each block. From these data it was possible to determine an average vertical coordinate for each block and then from this data calculate the average height of the blocks after the tests. Corresponding calculations could be made with data coming from the installation of the buffer blocks. By comparing these two data sets it was possible to calculate the changes in height of each individual buffer block, see Figure 5-1. A positive value implies an increase of the block height. The accuracy in these calculations is limited since large cracks were observed on all blocks after the test, which made the upper surfaces uneven and effected the measurements. This is especially the case for block C2, i.e. the block placed on top of the canister. The following conclusions can be made:

- The plot is indicating that all blocks below block R10 had decreased in height.
- The decrease in height coincides with the observed increase in dry density observed for blocks R1–R10, see Section 5.7.3.
- A comparison of the total deformation of the buffer stack (Section 5.5.3), with the deformation of the individual blocks indicates that first a swelling of the blocks occurred. After that there was shrinkage of the ring shaped blocks. This evolution can be observed in the measurement of the total displacement of the stack of blocks, where first an upward displacement was observed with a subsequent downward displacement. This downwards displacement ended at ~70 days (Figure 5-8), perhaps when block C2 lost contact with the ring-shaped blocks below it and was resting directly on the canister lid.
- The measurement of deformation of the blocks was made after the cooling of the canister and the buffer. It is likely that, due to thermal contraction there was a decrease in height of both the buffer blocks and the canister during the cooling phase.

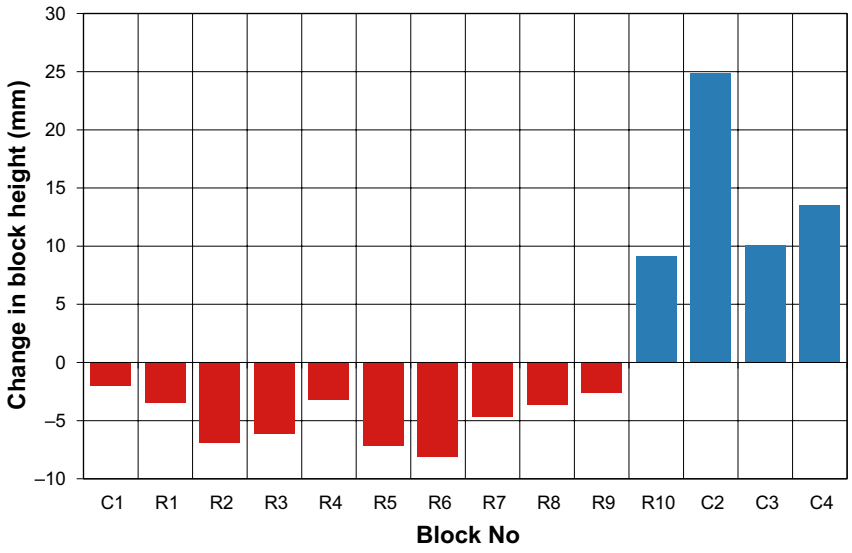

Figure 5-16. *Change in height of the 14 installed buffer block in test 2.*

5.8 Results and discussion

The test performed showed that technique used to maintain a stable environment for a buffer block-canister installation without pellet filling or tunnel backfilling for a period of 90 days was not feasible. The main reason for this was the large drying and subsequent shrinkage and cracking of the buffer blocks which would cause problems at the time of removal of the protection hood but also at the installation the pellets in the outer slot.

6 Post modelling and analysis

A post modelling of Test1 was made in order to evaluate how well the model works. To do the modelling the same models as described in Section 3.4 was used. These models are also the same as was used in the pre-modelling and the difference from the pre-modelling was that the boundary conditions were updated to better fit the data. The data obtained from the tests were analysed and compared with modelling results. In general, the model predicts both the temperature and the water content well, see Figure 6-1 and Figure 6-2. The model cannot be compared with data from wetter sections were there is inflow from the rock this is because the model has no water inflow. But if the model is used to predict behaviour in the dryer regions, the results are quite good. This in turn suggests that the thermal and hydraulic model in the buffer blocks works.

However, there are two things in the model that need to be improved. The first one is as mentioned earlier that the model of the pellet slot seems to underestimate the transport rate of water vapour.

The second thing that was noticed during the test is that there was an increase of water content close to the top of the canister, see Figure 6-3. It was suggested that this could be caused by hot humid air from the inner slot leaking between the blocks to the outer pellet filled slot. As the warm air cools down it deposits moisture in the surface between the blocks. To test this hypothesis a small slot between the top ring and the block above the canister was introduced into the model. The slot width is kept constant during the modelled time although it is likely that the slot width changes with time as the blocks take up water or dry and therefore changes density. The result from introducing this slot between the blocks can be seen in Figure 6-3. In Figure 6-3 it can be seen that the water content around the pathway between the inner and outer slot increases. However, after longer times when the bentonite dries out enough the pathway will start to dry out again. In Test 2 where there was no pellet filling, the air movements are much faster and the process speeds up. This is likely what happened in Test 2, the water content increased which caused the blocks to crack which in turn increased the air flow between the inner and outer slot. The top block then started to dry out again resulting in the problems seen in Test 2.

It should be noted that the model without leakage between the blocks was used for designing the buffer protection that was tested in buffer installation test 2. The improved model with leakage between the blocks shows a quite different HM behaviour which can explain the result from test 2.

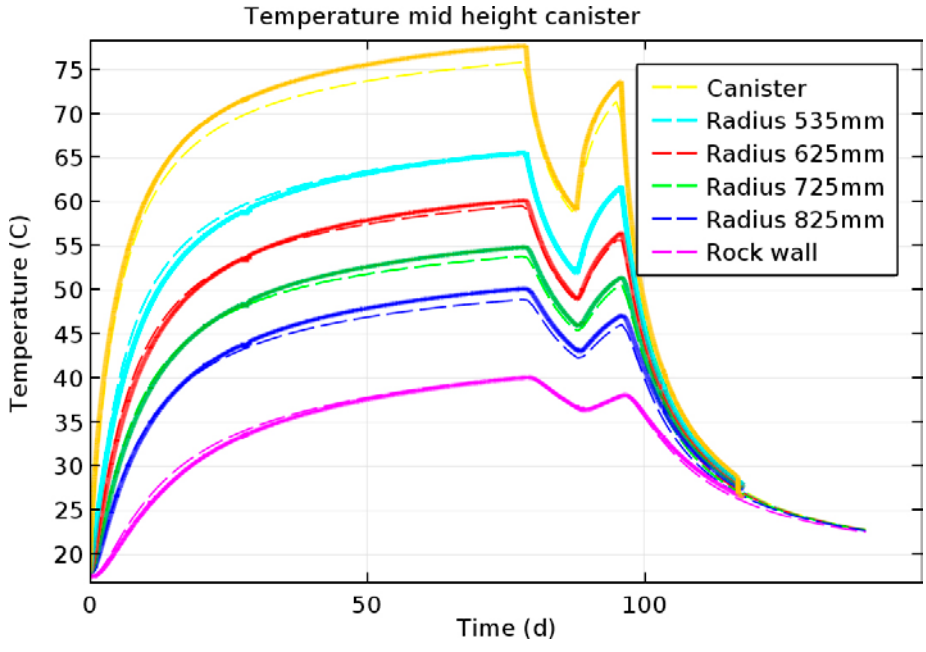

Figure 6-1. *Measured temperatures for test 1(solid lines) compared to modelling results (Dashed lines) at mid height of the canister.*

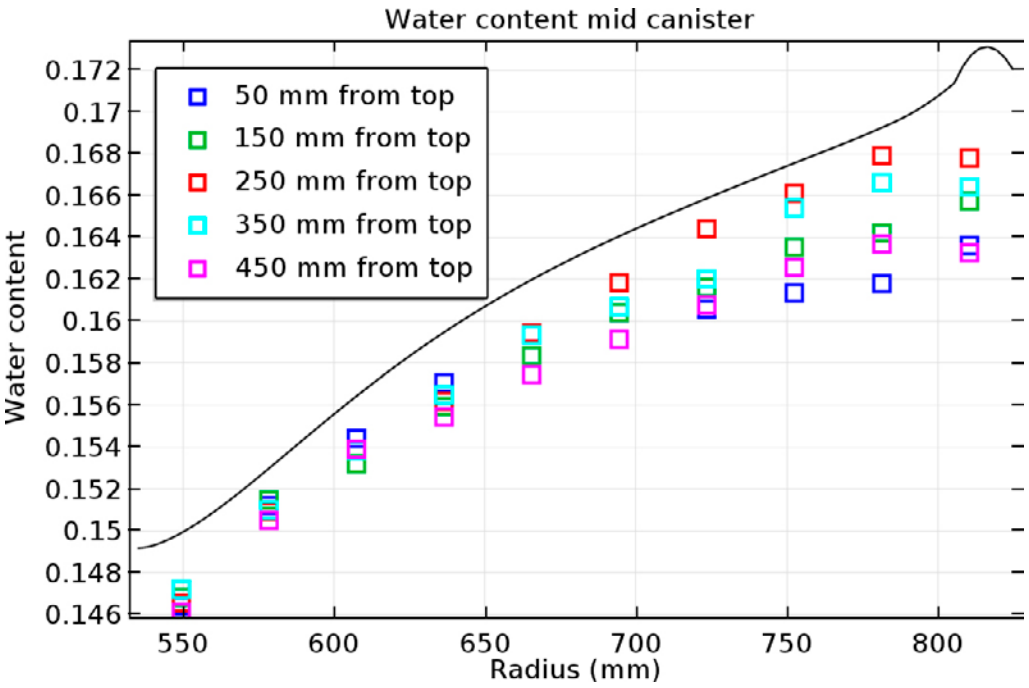

Figure 6-2. *Measured water content at block R5 (squares) compared to modelling result (solid line).*

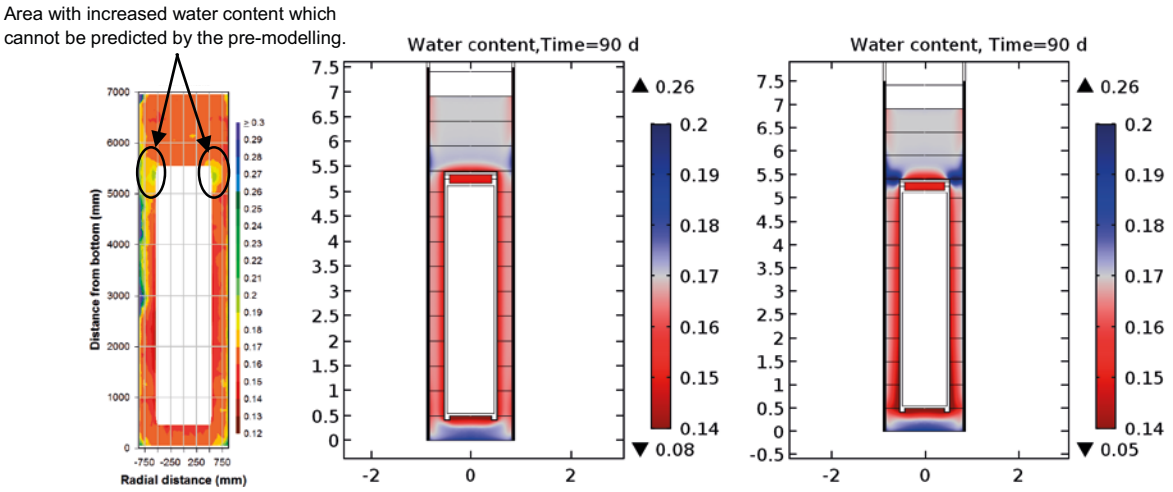

Figure 6-3. *Data from test 1 (left figure) compared with models without a slot between the blocks (middle figure) and with a slot between the blocks (right figure).*

7 Buffer design and installation procedure

7.1 Buffer requirements

The requirements set on the buffer is presented by Posiva and SKB (Posiva SKB 2017). The text in this chapter is based on this report.

The buffer shall protect and preserve the containment of the radionuclides by limiting the transport and availability of corrosion-inducing materials at the canister surface at the canister surface. Further, to preserve the containment the buffer must be designed with respect to the mechanical integrity of the canister. If canisters are breached the buffer shall contribute to retain radionuclides and retard their dispersion into the environment. With respect to this, the buffer is assigned the safety functions to:

- limit advective mass transfer,
- limit microbial activity,
- filter colloids,
- protect the canister from detrimental mechanical loads
  - rock shear load,
  - pressure load,
- resist transformation,
- keep the canister in position,
- retain sufficient mass over life cycle.

These safety functions are resulting in several technical design requirements on the buffer which are summarised below.

7.1.1 Technical design requirements

The technical requirements on the buffer are described below. The requirements together with the related safety functions are summarised in Table 7-1.

The technical design requirements that govern the design of the buffer and backfill are divided into:

1. Requirement for a number of geophysical properties, such as swelling pressure, that is measured with specified measurement methods.
2. Some of the properties, such as swelling pressure, depend on the bentonite density. The requirement is expressed as a density range where the required properties according to 1) are met. The density range is controlled by measuring the volume and mass of installed bentonite.

Swelling pressure

The lower limit for the swelling pressure for the specified laboratory tests is 3 MPa and the upper limit for the swelling pressure is 10 MPa.

Hydraulic conductivity

The hydraulic conductivity measured in a specified laboratory test shall be less than 10E−12 m/s.

Shear strength

Rock shear movements may occur when stresses in the bedrock are released. Depending on the mechanical properties of the buffer, the rock shear movements may cause the insert to collapse or deform to such an extent that the deformation of the copper shell will result in a breach and loss of the containment.

High shear strength as well as too high swelling pressure are undesired characteristics of the buffer, since they will result in high stresses on the canister in the case of rock shear. The technical requirements on the shear strength, defined as unconfined compressive strength at failure, is set to maximum 4 MPa. The unconfined compressive strength of a buffer material is determined according to a specific laboratory procedure where the preparation of the samples and deformation rate.

Installed buffer material mass

For the buffer to maintain its safety functions, the installed buffer dry density shall lie within the material-specific limits specified for swelling pressure, hydraulic conductivity and shear strength (see above). The installed mass of blocks and pellets, together with their water contents and the deposition hole dimensions, are used to calculate the average installed dry density of the buffer. The requirement based on average buffer density in a deposition hole is based on the assumption of complete homogenization.

The mass shall be distributed so that the variations of density within the deposition hole are as small as possible. However, there will inevitably be an uneven density within the hole. This is caused by

- different initial density of the materials (installed blocks and pellets),
- unevenness in the walls of the deposition hole and variation of the deposition holes within the acceptable tolerances,
- expansion of the buffer up into the backfill,
- rock fallout in the wall of the deposition hole,
- un-centred installation of buffer blocks or deposition of the canister.

The mass and water content of the buffer components, the positions of the buffer blocks and the dimensions of the deposition holes will be determined during the production so that the variation in installed density can be determined.

Buffer thickness and volume

A buffer thickness of at least 30 cm around the canister and a thickness of at least 50 cm below and above the canister has been shown to be sufficient for assuring safety. The thicknesses around, above and below the canister are together with the dimensions of the canister determine the buffer volume, see Figure 7-1. The stated technical design requirements for the buffer are valid for this minimum volume.

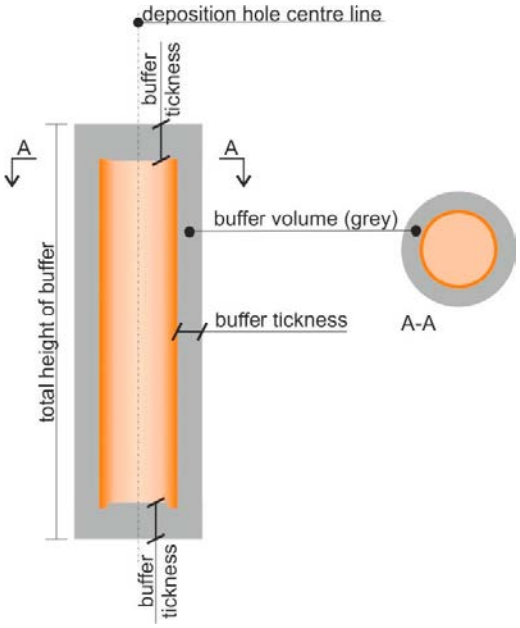

Figure 7-1. *The buffer thickness and volume.*

The entire volume of the deposition hole except the canister and the bevel is defined as buffer although the requirements are only valid for the minimum buffer volume.

The buffer components and their geometrical configuration in the deposition hole as well as the dimensions of the deposition hole shall, in addition to the required installed density, be determined with respect to the required thickness. This basically sets a requirement on the dimensions of the blocks. The required thickness sets a limit on the volume within which the average dry density must lie, see above.

Content of impurities

The clay materials used for the buffer should not include substances or impurities that may impair the safety functions of the repository. Carbon, sulphide and sulphur are impurities occurring in clay materials that may adversely affect the maintaining of favourable chemical conditions in the repository. The chemical composition of the buffer should be such that it has limited potential to act as a source of sulphides, which may corrode the copper canister.

The buffer consists of natural materials and the chemical composition is variable depending on the supplier but also within the same bentonite quarry. The content of organic carbon, sulphide and total sulphur will be determined as part of the approval of buffer materials and qualification of buffer material suppliers. The approval and qualification include characterisation of sulphur-containing minerals or sources of microbial nutrients that could enhance production of sulphides during the long-term evolution of the buffer. At delivery the material must be inspected to verify that delivered material conforms to specification.

Thermal conductivity

The thermal evolution of the near field is of importance for the safety functions of the engineered barriers. As a performance target for the buffer to resist transformation and for providing favourable thermal conditions in the repository, the peak buffer temperature must not exceed 100 °C.

The thermal evolution of the repository depends on the allowed decay power in the canister, the thermal properties of the canister, rock, buffer blocks and the pellets filling and on the canister spacing. The thermal evolution is also depending on the properties of the initially air filled gap between the canister and the buffer.

In order to analyse the temperature development in the repository, the thermal conductivity over the installed buffer must be known. The thermal conductivity of the buffer depends on the degree of saturation and the dry density.

Gas transport properties

Corrosion processes in the near field, or in a breached canister, will result in the production of hydrogen gas. If the gas production exceeds the ability of the surrounding groundwater to take it into solution and transport it away from the canister, a separate gas phase will develop and pressure will build up. Unless the evolved gas can escape via the buffer and the fractures in the rock, there will be a further build-up of gas pressure to levels that may impair the safety functions of the canister or rock.

The buffer and rock must have sufficient capability to transport gas. Gas can escape through the fractures of the rock. The gas transport properties of the buffer are related to its swelling pressure where a lower swelling pressure is an advantage. The bentonite is assumed to ultimately open by fracturing if the pressure increase is large enough.

The produced gas can then escape through the buffer and the fractures in the rock. The outflow through the buffer is expected to proceed until the pressure falls to levels at which the swelling pressure of the buffer would act to seal the formed passage.

Table 7-1. The technical requirements on the buffer together with the related safety functions (Posiva SKB 2017).

Characteristic	Technical design requirement	Related safety functions
Material specific relation between dry density and swelling pressure	The minimum dry density yielding a swelling pressure > 3 MPa when determined with a specific laboratory test procedure.	Limit advective mass transfer
		Limit microbial activity
		Keep the canister in position
	The maximum dry density yielding a swelling pressure < 10 MPa when determined with a specific laboratory test procedure.	Limit pressure on the canister
Material specific relation dry density – hydraulic conductivity	The minimum dry density yielding a hydraulic conductivity in saturated state < 10^{-12} m/s when determined with a specific laboratory test procedure.	Limit advective mass transfer
Material specific relation between dry density and shear strength	The maximum dry density yielding an unconfined compressive strength at failure < 4 MPa at a deformation rate of 0.8 %/min when determined with a specific laboratory test procedure, and for material specimens in contact with waters with less favourable characteristics than site-specific groundwater.	Mitigate the impact of rock shear on the canister
Installed buffer material mass	The installed buffer material mass shall in average in the buffer volume (Figure 7-1) result in a dry density ≥ the least required dry density determined for the specific buffer material.	Limit advective mass transfer
		Limit microbial activity
		Filter radiocolloids
		Keep the canister in position
		Retain sufficient mass over life cycle
Installed buffer material mass	The installed buffer material mass shall in average in the buffer volume (Figure 7-1) result in a dry density ≤ the highest allowed dry density determined for the specific buffer material.	Mitigate rock shear Limit pressure on the canister
Thickness	The buffer thickness, i.e. the distance between the canister and the deposition hole wall, shall be at least 30 cm.	Overall functions of the buffer
	The thickness of the buffer below the canister bottom shall be at least 50 cm.	
	The thickness of the buffer above the canister shall be at least 50 cm.	
Volume	The buffer volume shall be cylindrical and determined from its cross section area in the deposition hole and its height, i.e. the sum of its thickness above and below the canister and the distance between the surface of the canister lid and bottom, minus the canister volume (Figure 7-1).	
Material composition	The content of organic carbon shall be less than 1 wt-%.	Compatibility and reliability of production (chemically favourable conditions)
	The sulphide content shall not exceed 0.5 wt-% of the total mass, corresponding to approximately 1 wt-% of pyrite.	
	The total sulphur content (including the sulphide) shall not exceed 1 wt-%.	

7.1.2 Other requirements

Based on the buffer design, the following requirements are put on the geometry of the deposition hole and the canister:

1. Deposition hole depth from a theoretical tunnel floor varies between 7 935 ± 30 mm.
2. Deposition hole nominal *average* diameter of 1 750 ± 5 mm.
3. Local rock fallout may not result in the deposition hole total volume exceeding the volume given by a diameter of 1 755 mm.
4. Deposition hole minimum diameter > 1 745 mm.

5. Deposition hole maximum inclination of 25 mm over the total depth.
6. The maximum inclination of the bottom of the deposition hole: 3.6/1 650. This requirement does not apply 25 mm from the deposition hole wall.
7. The bottom should be flat enough not to risk cracking of the bottom buffer block.
8. The total length and outer diameter of the canister is assumed to be 4 841 mm and 1 051.5 mm respectively.

7.2 Buffer design

7.2.1 Introduction

The design of the buffer for the KBS3-concept includes the following demands:

1. The restrictions on the impurities of the buffer material (carbon, sulphur and sulphide) must be fulfilled
2. The requirements described in Section 7.1 on the buffer must be fulfilled. The most important are the requirements on the minimum and maximum swelling pressure, the minimum hydraulic conductivity and the maximum shear strength. These parameters are functions of both the bentonite type and the density of the buffer. Furthermore, the requirements are stated to be fulfilled after homogenisation and fully saturation of the buffer. The parameters are determined with a specific preparation and test procedure where the bentonite are tested at extreme conditions.
3. The requirements on the thickness of the buffer, thus the minimum distance between the surface of the canister and the wall of the deposition hole must be fulfilled.
4. The requirement No 2 above must be fulfilled even if a swelling upwards of the buffer in a deposition hole has occurred.
5. The buffer components must be possible to manufacture and install with high quality.

The above listed requirements are the input for the design of the buffer. At the design, also the variation in the production of the buffer, blocks and pellets filling and the variation in the dimensions of the deposition hole are considered.

7.2.2 Design procedure

The first step in the design of the buffer is to ensure that the requirements concerning the geochemical composition of the chosen bentonite are fulfilled, Item 1 above. This is checked by laboratory tests which are described in detail in Svensson et al. (2017).

The next step in design process is to calculate the nominal density of the buffer based on the requirements described in Section 7.1. These requirements can be summarised as the following:

1. The maximum swelling pressure.
2. The minimum swelling pressure.
3. The maximum shear strength.
4. The highest required hydraulic conductivity.
5. The highest required average density of the buffer.
6. The lowest required average density of the buffer.

Analyses made on the bentonite MX-80 show that the key dimensioning requirement on the density of the buffer is the swelling pressure. The other requirements, i.e. the requirements on the shear strength and the hydraulic conductivity are, for most bentonites, considered to be fulfilled if the demands on the swelling pressure are fulfilled. However, these requirements must be checked when the density of the buffer has been determined.

The calculation of the nominal buffer density is made by an iterative process including the following:

a) Determination of the swelling pressure as function of the dry density of the buffer bentonite. The determination is made with de-ionized water and with 1 M $CaCl_2$ solution.

b) A heaving of the buffer of totally 175 mm is considered. The heaving includes two parts. The first part occurs at the installation of the buffer is assumed to be 40 mm, see Section 4.5.3. The second part is caused by the compression of the backfill above the buffer at the saturation of the buffer. This part of the total heaving of the buffer has been estimated to be 135 mm (Börgesson and Hernelind 2017). Several cases of buffer densities and geometric configurations of the buffer are analysed in the report. This is made by numerical modelling (FEM) and the results are determined as a change in the void ratio of the buffer from the bottom of the deposition hole to the level 500 mm above the top of the canister. In this report, the case where the final void ratio of the buffer is assumed to be 0.806 is used (Börgesson and Hernelind 2017, Table 5-5, Case 2b). From the determined change in void ratio, the heaving of the buffer is calculated to about 135 mm.

c) Based on experience from the Prototype Repository the standard deviation of the dry density is assumed to be 6 kg/m^3 (Birgersson and Johannesson 2006). This value includes both the variation in the block density and the variation in the diameter of the deposition hole.

d) The diameter of the deposition hole is assumed to be vary with ± 5 mm.

The first part of the analysis is with the data from the determination of the swelling pressure as function of the dry density determine the lowest and highest density in order to fulfil the requirement concerning the swelling pressure ($3 < \sigma_s < 10$ MPa). At the determination of swelling pressure the measurements are first made with de-ionized water and then with a 1 M $CalC_2$ solution. The reason for choosing the two solutions is to get the swelling pressure of the bentonite at extreme conditions. At the test with de-ionized water the highest swelling pressure is expected while the tests made with 1 M $CaCl_2$ solution gives information of the lowest expected swelling pressure. The measuring and the technique used for determining the swelling pressure as function of the density are described in detail in Svensson et al. (2017). The data from the investigation made on MX-80 which was used in the previous described large scale tests are shown in Figure 7-2. The figure shows that, in order to fulfil the requirements concerning the swelling pressure the nominal dry density of the buffer should lie between 1 486 kg/m^3 and 1 591 kg/m^3.

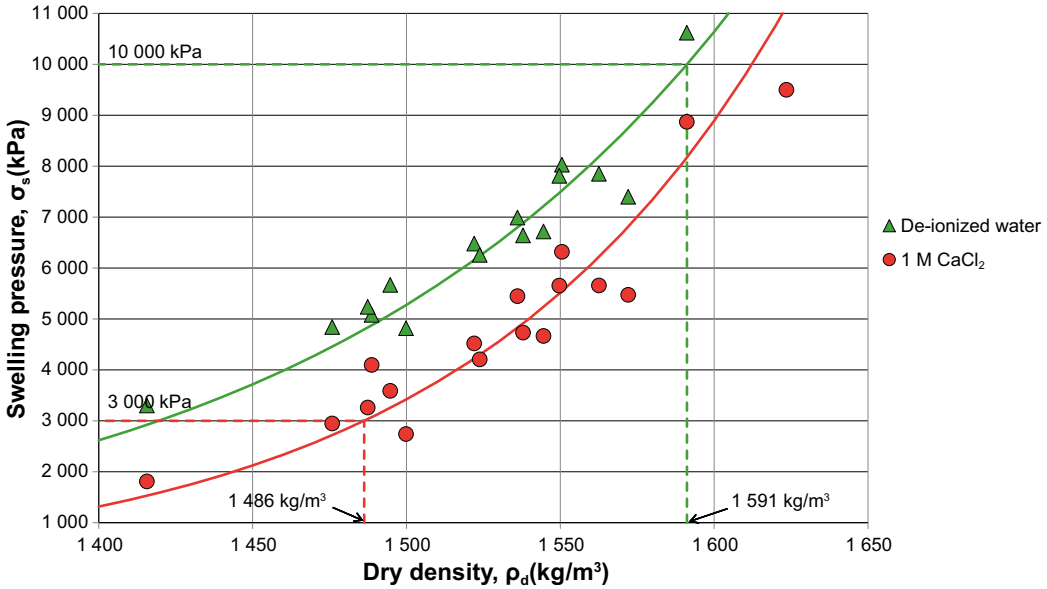

Figure 7-2. *Measured swelling pressure as function of the dry density for the bentonite MX-80 together with the upper and lower limits for the dry density in order to fulfil the requirements on the swelling pressure.*

As a first step in the iteration process, the nominal dry density for the buffer is set to 1 570 kg/m^3. At this dry density the swelling pressure is assumed to vary between 6 745 kPa and 8 686 kPa, see Figure 7-3.

At an assumed total upward expansion of 175 mm for the buffer in the deposition hole, the average dry density will decrease from 1 570 kg/m^3 to 1 520 kg/m^3, see Figure 7-4. If also the assumed standard deviation of the average dry density for the buffer, 6 kg/m^3, is taken into account by plotting the 95 % confidence interval around both the upper dry density of 1 570 kg/m^3 and the lower dry density of 1 520 kg/m^3 the expected minimum swelling pressure will thus be 3 596 kPa, see Figure 7-4. Corresponding maximum swelling pressure will be 9 449 kPa. These swelling pressures correspond to the dry densities 1 510 kg/m^3 and 1 580 kg/m^3 respectively.

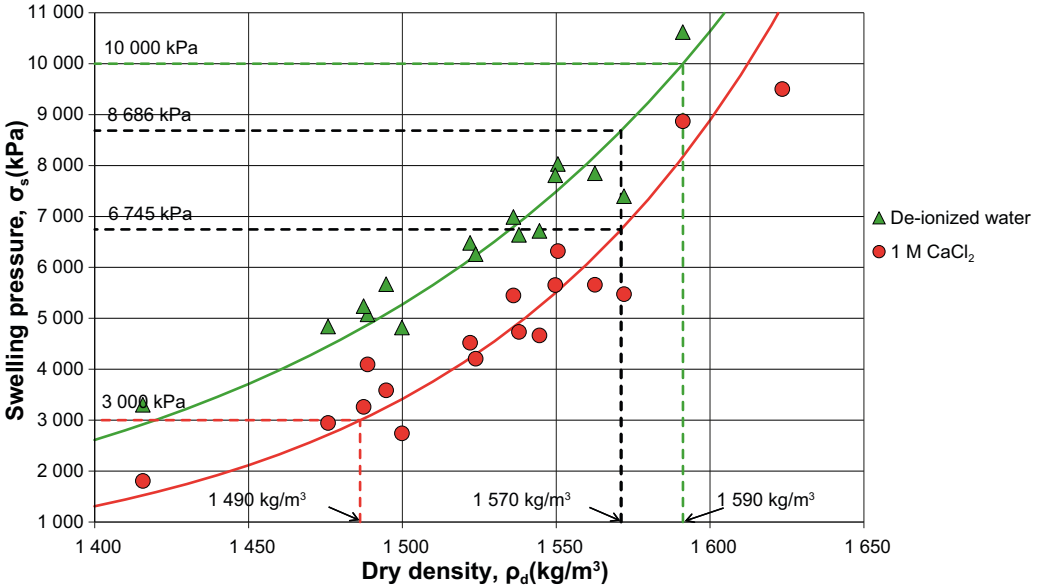

Figure 7-3. Measured swelling pressure as function of the dry density for the bentonite MX-80 together with the expected swelling pressure at a nominal dry density of 1 570 kg/m^3.

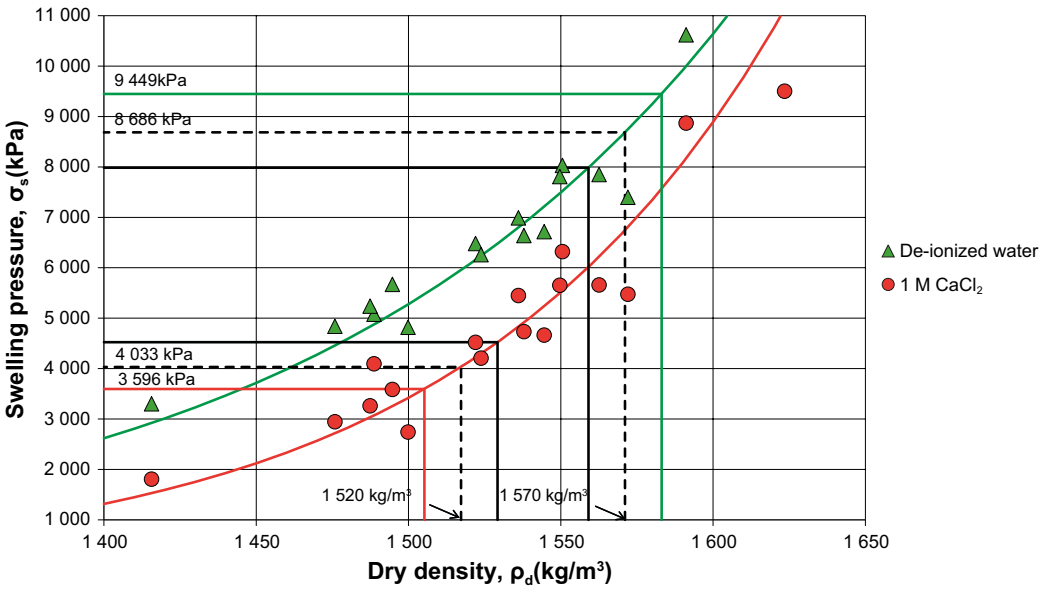

Figure 7-4. Measured swelling pressure as function of the dry density for the bentonite MX-80 together with the expected swelling pressure at a nominal dry density of 1 570 kg/m^3 and after an upward swelling of the buffer of 175 mm resulting in a density of 1 520 kg/m^3. The 95 % confidence intervals around the upper and lower densities are also indicated.

The next part in the design of the buffer is to check whether the buffer can fulfil the demands on the highest acceptable hydraulic conductivity i.e. 1E−12 m/s. The hydraulic conductivity as function of the dry density for bentonite used in the test, MX-80, is shown in Figure 7-5. At the lowest expected dry density of 1 510 kg/m^3 the hydraulic conductivity is lower than 1E−13 m/s and thus the requirement is fulfilled.

The demands on the maximum acceptable shear strength of 4 000 kPa should also be checked in the same way. The shear strength is determined by unconfined compression tests or triaxial tests which are described in detail in Dueck et al. (2010). Data from tests made on both Ca-and Na-bentonites are plotted in Figure 7-6. This data and the performed tests are described in Dueck et al. (2010). At this step of the analysis it is assumed as a worst case scenario, independent of the initial state of the buffer material, that it is converted to a Ca-bentonite. In Figure 7-6 the red line is representing the uniaxial compressive strength of a Ca-bentonite (DeponitCAN) while the blue line is representing a Na-bentonite (MX-80). At the highest expected dry density of 1 580 kg/m^3 the shear strength is lower than 4 000 kPa and thus the requirement is fulfilled, see Figure 7-5.

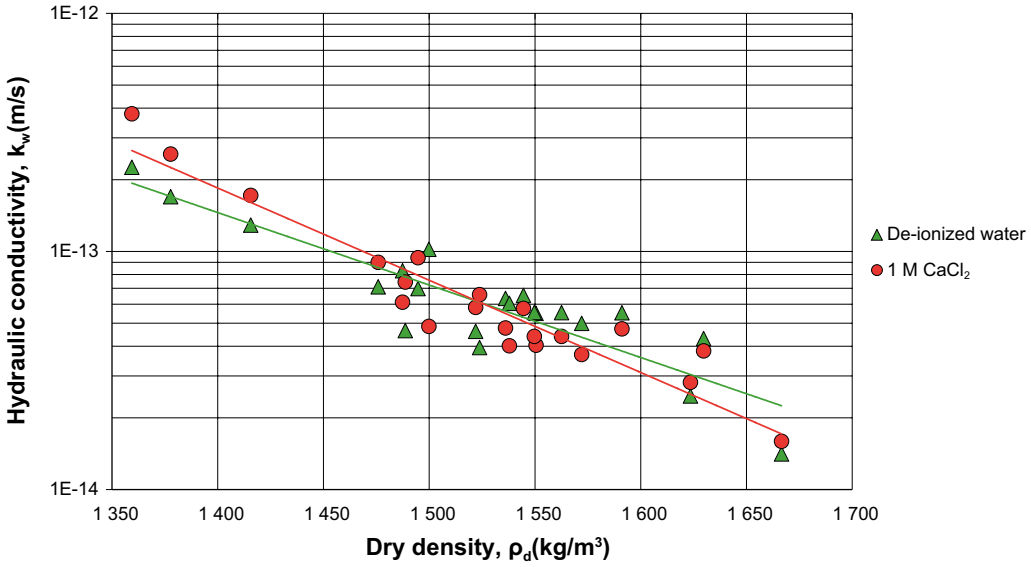

Figure 7-5. *Measured hydraulic conductivity as function of the dry density for the bentonite MX-80.*

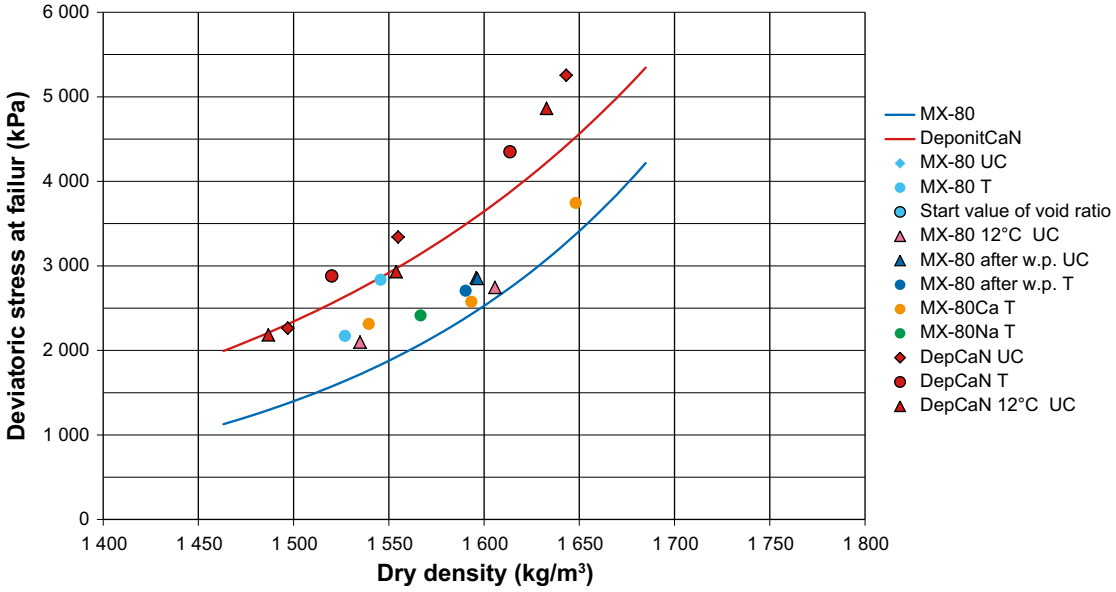

Figure 7-6. *Results from unconfined compression tests (UC) and triaxial tests (T) on MX-80 (blue), MX-80Na (green), MX-80Ca (orange) and DepCaN (red) (Dueck et al. 2010).*

7.2.3 Design of blocks and pellets

The output from the design of the buffer from Section 7.2.2 is the nominal dry density of 1 570 kg/m^3. The next step is to design the buffer blocks and the pellets in detail. The detail design of the buffer components are made at the following conditions:

1. The dimensions of the buffer blocks are according to Figure 7-7.
2. The water content for the bentonite in the blocks are, for MX-80 set to be 17 %.
3. The maximum compaction pressure at the manufacturing of the buffer blocks is set to 100 MPa. This restriction is chosen for optimizing the construction of the mould and the press used at the production of buffer blocks.
4. The minimum compaction pressure is set to 25 MPa. This restriction is chosen to ensure that the strength of the blocks is enough so the blocks can be handled and installed in a safe manner.
5. The bulk density of the pellets filling is set to 1 035 kg/m^3 and the water content of the bentonite for the pellets is set to 15 % and thus the dry density of the pellets filling is 900 kg/m^3.
6. The nominal diameter of the deposition hole is set to 1 750 mm.
7. The demands on the minimum and maximum average dry density, see Section 7.2.1, is assumed to be valid for the buffer volume counted from the bottom of the deposition hole to a distance of 500 mm from the top of the canister.

Under these conditions a detail design of the blocks can been done. The design of the buffer with the bentonite used in previous described tests, is shown in Table7-2. The dry densities of the blocks together with needed compaction pressure to get the required dry density of the blocks are shown in the table. Furthermore, the calculated final dry density of the buffer at two locations i.e. around and below/above the canister and the expected swelling pressure are shown. Note that the calculated dry density for the buffer around the canister is lower compare to the density under and above the canister although the density of the ring shaped blocks is higher compare to the solid blocks. This is due to the fact that the dry density of the buffer is a function of the dry density of the block, there volume and the volume and density of the pellets filling. The swelling pressures shown in the table are determined from Figure 7-2. The higher value of the swelling pressure is determined from the tests made with de-ionized water while the lower value is determined from the tests made with 1 M $CaCl_2$ solution. The values are showing that the calculated swelling pressures are within the limits ($3 < \sigma_s < 10$ MPa) except for the buffer under and above the canister when assuming de-ionized water.

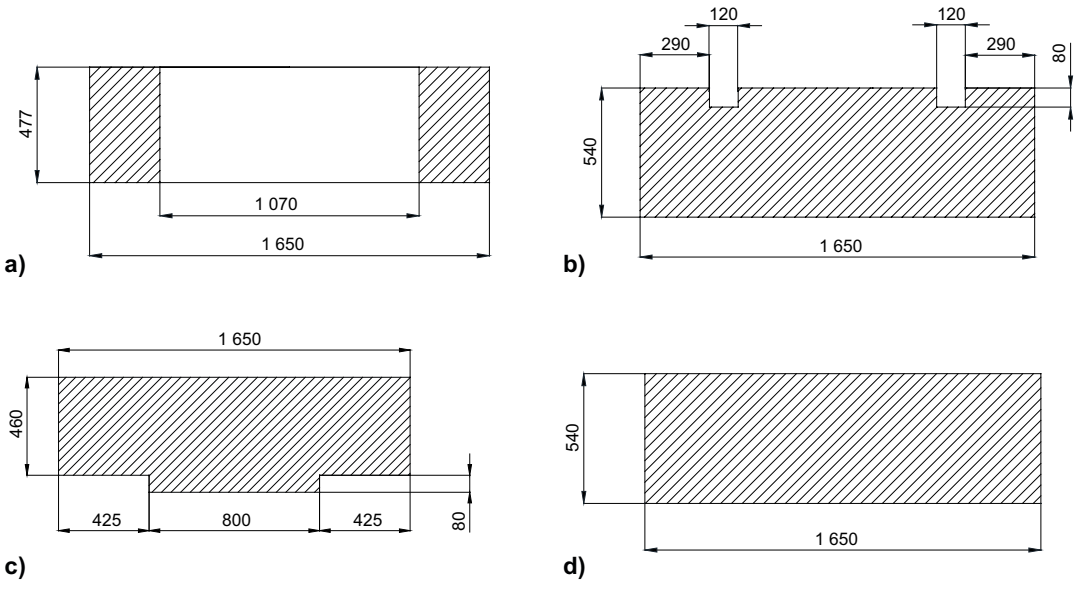

Figure 7-7. *Nominal dimensions of the buffer blocks for a) the ten ring shaped blocks placed around the canister b) the solid bottom block c) the block on top of the canister d) the four uppermost solid blocks in the deposition hole.*

In Table 7-2 the expected average dry density of the buffer is calculated for the buffer volume from the bottom of the deposition hole up to 500 mm above the top of the canister. The same analysis is also made where the diameter of the deposition hole is assumed to be 5 mm higher and smaller than the nominal diameter of 1 750 mm. The calculated swelling pressures are within the limits.

Finally is the average dry density and corresponding swelling pressure is determined assuming a diameter of the deposition hole of 1 755 mm plus a rock fall-out of 6 dm^3 on the wall of the deposition hole has occurred. In this case it is assumed that the volume of the fall-out is filled with pellets. Also these calculations show that the swelling pressure is within the limits.

Table 7-2. The design of the buffer in a deposition hole together with the expected average density and swelling pressure.

Part of the buffer	Diameter dep. hole (mm)	Dry density block (kg/m^3)	Compaction stress (MPa)	Dry density buffer (kg/m^3)	Swelling pressure***) (max/min) (kPa)
Around the canister	1 750	1 758	50	1 570	8 690/6 750
Under/above the canister	1 750	1 699	30	1 610	11 410/9 780
The whole buffer*)	1 750	1 758/1 699	50/30	1 574	8 870/6 940
The whole buffer*)	1 745	1 758/1 699	50/30	1 579	9 180/7 270
The whole buffer*)	1 755	1 758/1 699	50/30	1 515	5 860/3 950
The whole buffer **)	1 755	1 758/1 699	50/30	1 514	5 820/3 910

*) The buffer volume calculated from the bottom of the deposition hole up to 500 mm above the top of the canister.

**) The buffer volume calculated from the bottom of the deposition hole up to 500 mm above the top of the canister plus a rock fall-out of 6 dm^3.

***) For distilled and saline water.

7.3 Early TH evolution

7.3.1 Introduction

Since there is a requirement that the temperature in the buffer should not exceed 100 °C the suggested design needs to be evaluated for its compliance with this limit. The thermal conductivity of the bentonite is primarily a function of density and water content. Therefore there is a need to predict the how water will redistribute in the buffer since this will affect the maximum temperature of the buffer. The model used here are the models that were developed in this report. They include convection in the pellet slot; however more work is needed to validate the model. The model does not consider that the surface of the pellets can have different water content than the centre of the pellets and therefore the transport of vapour might be higher than predicted. The model used here does not include the leakage in fractures that have been seen in the large scale tests.

The case were the buffer would reach its highest temperature is if the deposition tunnel and deposition hole is dry. Therefore this case is modelled.

7.3.2 Strategy and assumptions

The model is very complex and detailed in order to capture the different processes observed in the tests. Due to this and that the model is geometrically large, simplifications are needed to be able to get a result in reasonable computation times. To be able to use the desired resolution a rotational symmetric model is used. To get appropriate thermal boundary conditions to the rotational symmetric model a thermal analysis is done in 3D which is then compared to the rotational symmetric model and a diameter is chosen to fit the 3D model.

To simplify the boundary conditions an infinite repository is used. Therefore then result should be representative for a canister in the center of the repository. It is also assumed that the distance between the canisters are 6 m and that the distance between the deposition tunnels are 40 m.

The canister will be have a high surface temperature due to the decay heat from the spent nuclear fuel inside them. The power of the canister will be 1 700 W at disposal but will decrease with time. To predict the thermal power in the canister with time an expression used in Hökmark et al. (2009) is used.

7.3.3 Conversion from a 3D model to a 2D model

To be able to use a rotational symmetric model suitable thermal boundary conditions need to be selected to get a representative thermal field. This is done by doing a thermal modelling both in 3D and in 2D, see Figure 7-8 and then adjusting the diameter to get the same response from the rock in the 2D case as in the 3D case. Both the 3D model and the 2D model use isolation boundary condition on all surfaces but the length in z direction is large enough that no heating will take place during the modelled time. If the temperatures in the point shown in Figure 7-8 are compared there are very little difference between the 3d and the 2D model as can be seen in Figure 7-9. This shows that the rotational model will represent the 3D very well. To make the model even smaller the model is cut approximately 12 meters above and under the bottom of the canister. To get a god boundary condition for these boundaries an analytical expression, Equation 7-1, this fits well with the modelled result see Figure 7-10.

$$T(t) = \frac{40t}{(t+22)} + 11.6 \qquad (7\text{-}1)$$

Were t is the time in Years.

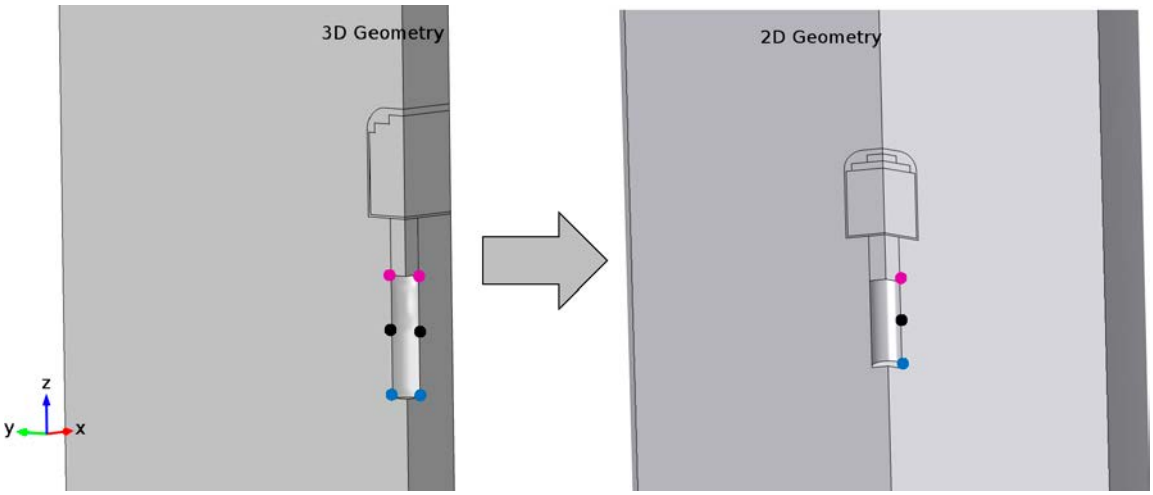

Figure 7-8. *The 3D and 2D geometry used in the models. Black, blue and purpur point shows were models are compared to each other.*

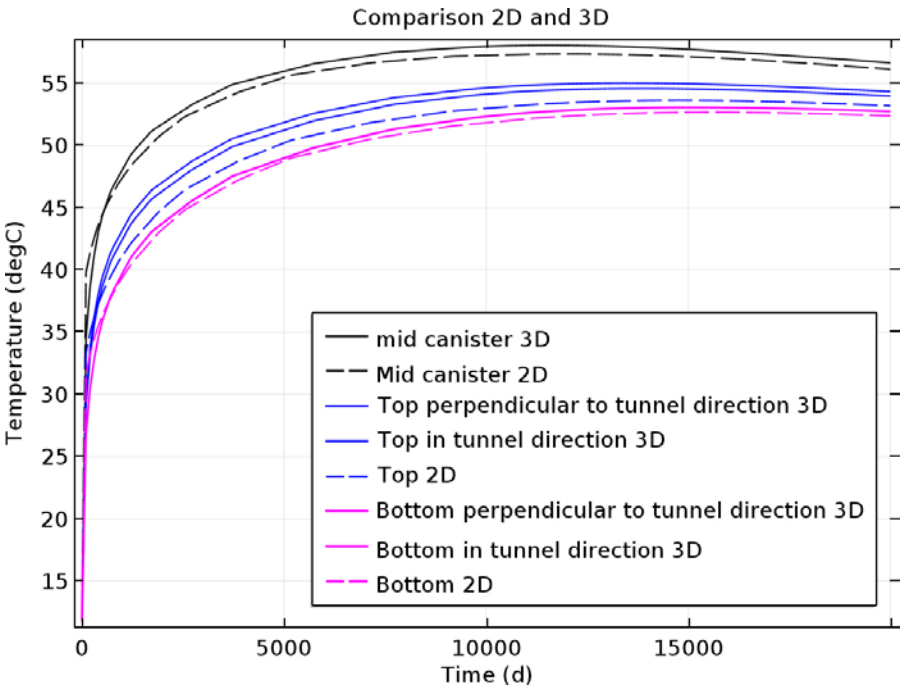

Figure 7-9. *Comparison between 3D and 2D geometry in the points shown in Figure 7-8. 2D and 3D gives similar result.*

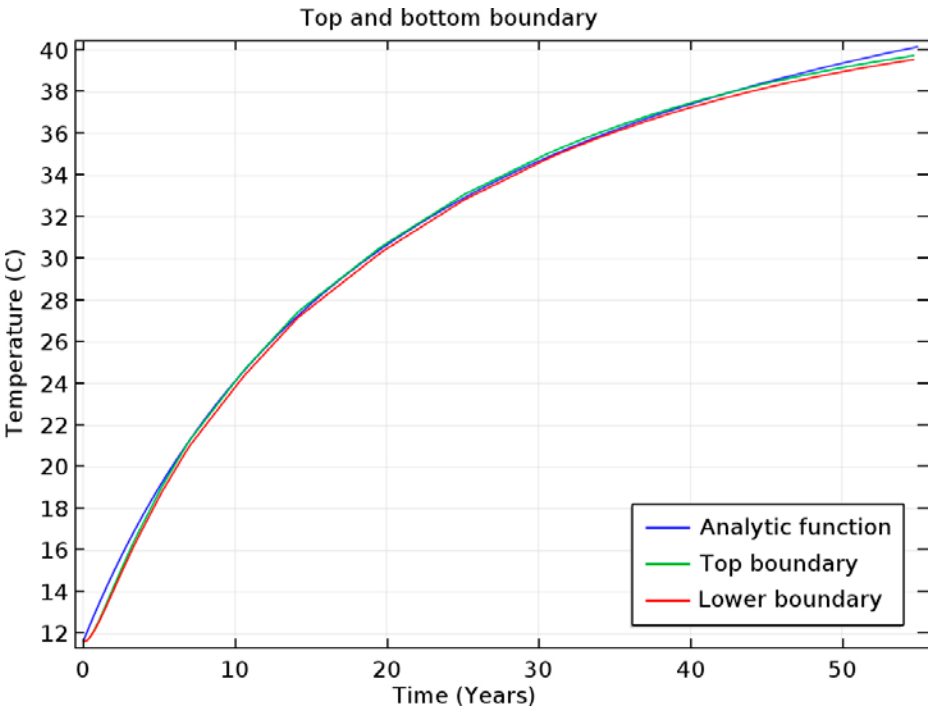

Figure 7-10. *Comparison between the boundary condition used in the 2D model and the temperature in the larger 3D model.*

7.3.4 Result of the TH modelling

The modelling results show that the moisture content will start to decrease in the buffer close to the canister after a very short time. The water that is removed from the inner part of the buffer is transported as vapour through the buffer block and in to the pellet slot. Since there is a thermal gradient over the pellet slot there will be convective air circulation in the pellet slot. The air will rise close to the buffer block and will be transported downwards close to the rock wall. This circulation will transport the water vapour upwards until it rises above the canister, there the buffer blocks will be cooler and the vapour will condense. This process will transport water from the lower parts of the buffer to the area above the canister. As the water content is lowered in the bottom of the hole the thermal conductivity of the buffer will decrease. This redistribution, see Figure 7-12, will go on until the canister starts to cool down as a result of decreasing heat generation and the suction difference in the bentonite will start to even out the water content again. According to the modelling the temperature of the canister starts to decrease after approximately 10 years, see Figure 7-13. Although the redistribution of water is rather large the maximum temperature in the buffer is 85 °C which is well below the requirement of 100 °C. If the thermal conductivity of the buffer material was lower the maximum temperature in the buffer would increase. However, if the saturated thermal conductivity is lowered with approximately 25 % from 1.35 W/(mK) to 1.05 W/(mK) then the maximum temperature would only increase approximately 5 °C, see Figure 7-14

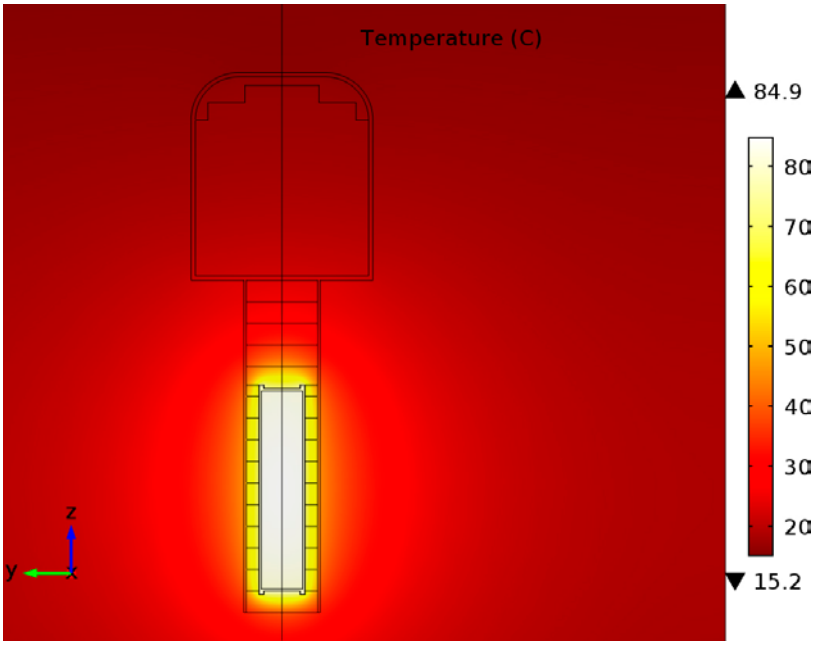

Figure 7-11. *Temperature field around the canister when maximum temperature is reached.*

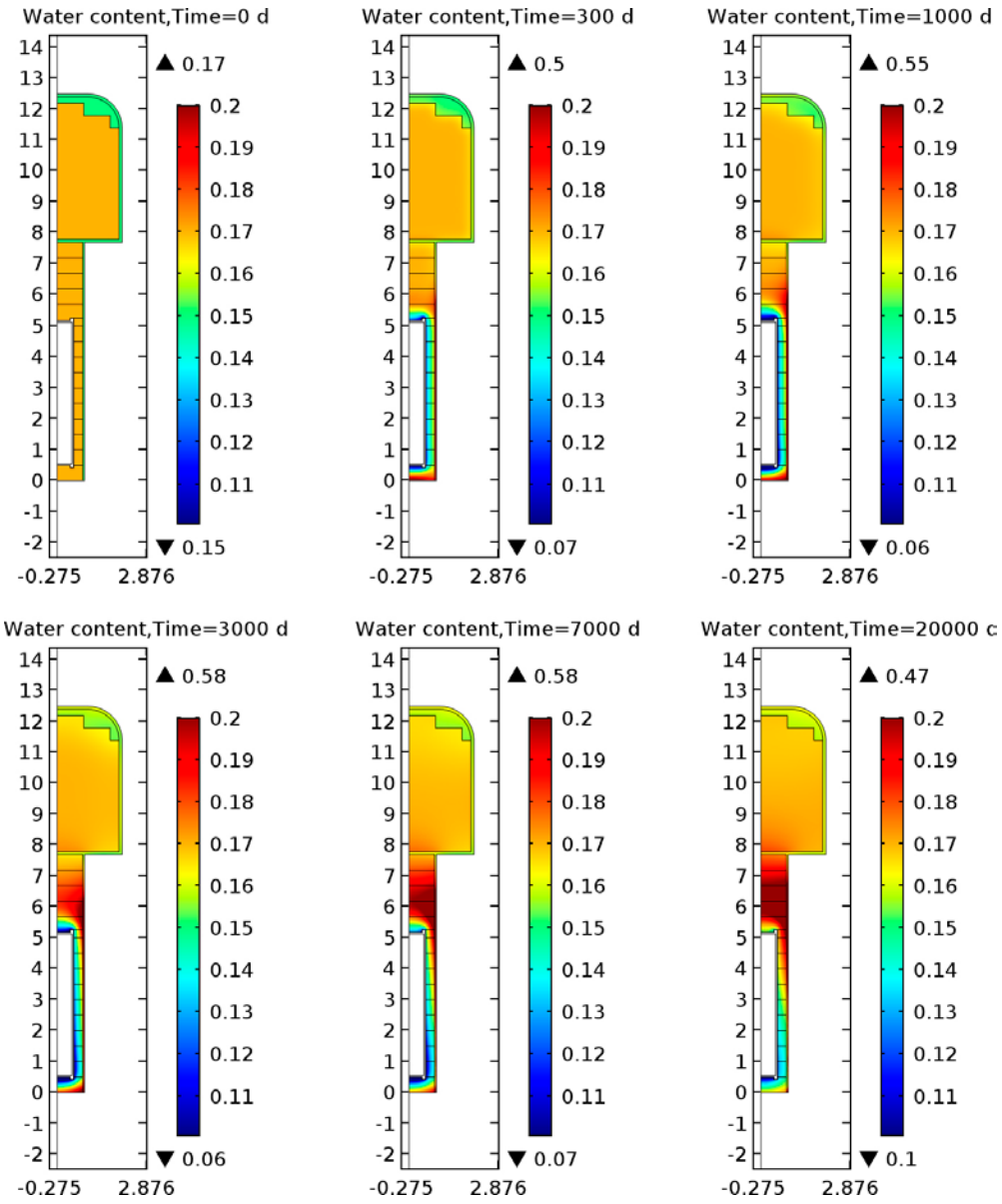

Figure 7-12. *Modelled water content distribution at different times.*

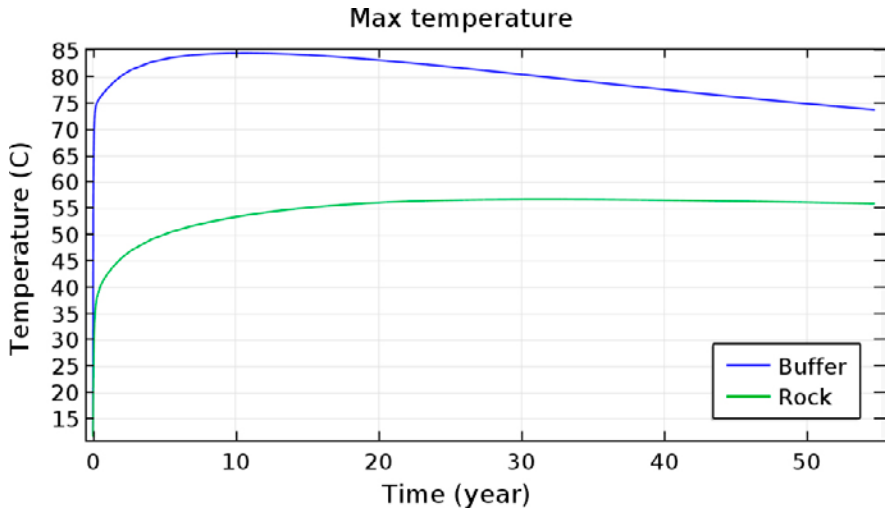

Figure 7-13. *Maximum temperature in the rock and buffer as a function of time.*

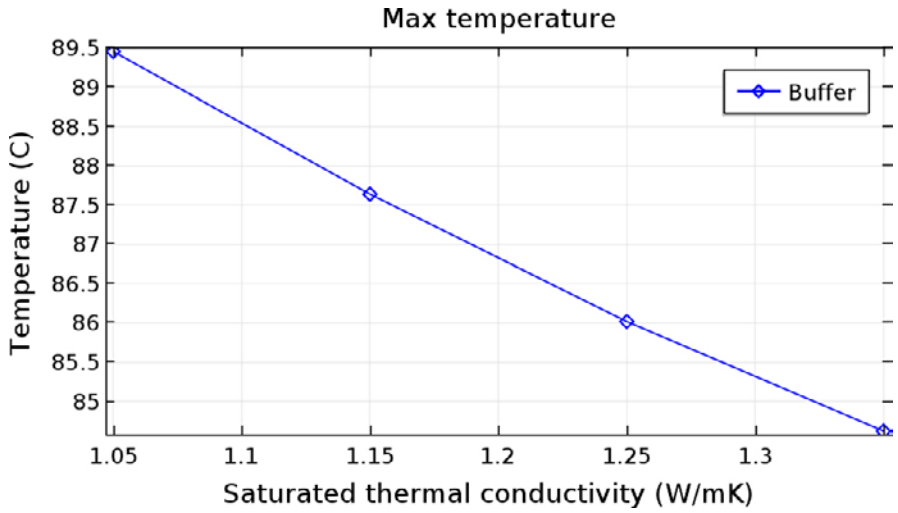

Figure 7-14. *Influence of the thermal conductivity of the buffer on the peak temperature.*

8 Conclusions and Recommendations

The buffer design developed in Chapter 7 is recommended. The geometry of the buffer blocks is shown in Figure 8-1 and the resulting dry density and corresponding swelling pressure is presented in Table 8-1.

Table 8-1. The design of the buffer in a deposition hole together with the expected average density and swelling pressure.

Part of the buffer	Diameter dep. hole (mm)	Dry density block (kg/m^3)	Compaction stress (MPa)	Dry density buffer (kg/m^3)	Swelling pressure **) (max/min) (kPa)
The whole buffer*)	1 750	1 758/1 699	50/30	1 574	8 870/6 940

*) The buffer volume calculated from the bottom of the deposition hole up to 500 mm above the top of the canister.
**) For distilled and saline water.

The results from buffer installation Test 2 in combination with the increased understanding of the early THM processes make it evident that the buffer protection concept does not result in a robust installation process.

Based on the predicted water inflow to the deposition holes (Joyce at al. 2013) and the results from Test 1, this installation method will give a robust installation for about 90 % of all assessed potential deposition holes corresponding to about 6 000 deposition holes in the planned repository in Forsmark. If the installation sequence is modified so that the wet deposition holes are installed in conjunction with the backfilling of the tunnel the majority of the remaining deposition holes can also be used for deposition. The recommended installation method is hence simultaneous installation of blocks, canister and pellets without any buffer protection.

The developed model for describing the early THM evolution is in good agreement with the results from the full scale tests. However there are remaining development needs considering the modelling of the pellet water uptake. The influence of fines in the pellet filling has not been investigated and is an uncertainty.

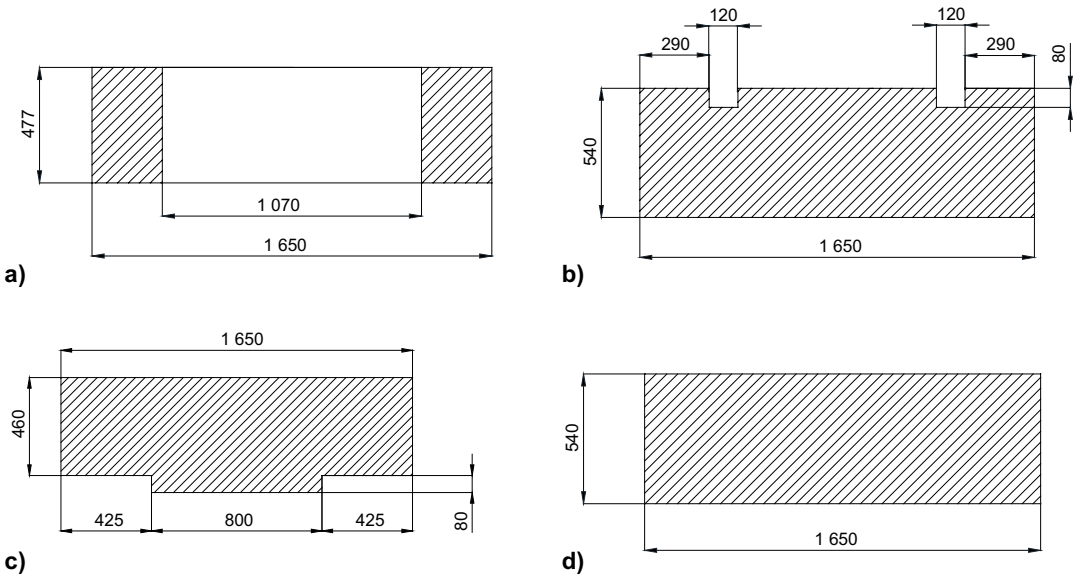

Figure 8-1. *Nominal dimensions of the buffer blocks for a) the ten ring shaped blocks placed around the canister b) the solid bottom block c) the block on top of the canister d) the four uppermost solid blocks in the deposition hole.*

The installation method where buffer blocks and pellets are installed in direct sequence works well for the water inflow equal or less than in the test deposition hole (8E−4 l/min). The exact limit for how much water inflow can be handled with this method remains to be determined.

The upward swelling of the buffer and the deformation of backfill has a significant influence on the fulfilment of the technical design requirements stated for the buffer. The understanding and modelling of this process needs to be further developed and verified.

References

SKB's (Svensk Kärnbränslehantering AB) publications can be found at www.skb.com/publications.

Birgersson M, Johannesson L-E, 2006. Äspö Hard Rock Laboratory. Prototype Repository. Statistical evaluation of buffer density. SKB IPR-06-15, Svensk Kärnbränslehantering AB.

Börgesson L, Hernelind J, 2017. Modelling of the mechanical interaction between the buffer and the backfill in KBS-3V. Modelling results 2015. SKB TR-16-08, Svensk Kärnbränslehantering AB.

Börgesson L, Fredriksson F, Johannesson L-E, 1994. Heat conductivity of buffer materials. SKB TR 94-29, Svensk Kärnbränslehantering AB.

Dueck A, Börgesson L, Johannesson L-E, 2010. Stress-strain relation of bentonite at undrained shear. Laboratory tests to investigate the influence of material composition and test technique. SKB TR-10-32, Svensk Kärnbränslehantering AB.

Eriksson P, 2017. Investigation of alternatives to the buffer protection. SKB P-16-07, Svensk Kärnbränslehantering AB.

Hökmark H, Lönnqvist M, Kristensson O, Sundberg J, Hellström G, 2009. Strategy for thermal dimensioning of the final repository for spent nuclear fuel. SKB R-09-04, Svensk Kärnbränslehantering AB.

Johannesson L-E, Kristensson O, Åkesson M, Eriksson P, Hedin M, 2014. Tests and simulations of THM processes relevant for the buffer installation. SKB P-14-22, Svensk Kärnbränslehantering AB.

Jordi R G, Young B D, van Vliet B M, 1990. The effect of surface roughness on pressure drop in a packed bed. Chemical Engineering Communications 89, 137–146.

Joyce S, Swan D, Hartley L, 2013. Calculation of open repository inflows for Forsmark. SKB R-13-21, Svensk Kärnbränslehantering AB.

Kivikoski H, Heimonen I, Hyttinen H, 2015. Bentonite pellet thermal conductivity techniques an measurements. Posiva Working Report 2015-09, Posiva Oy, Finland.

Knutsson S, 1983. On the thermal conductivity and thermal diffusivity of highly compacted bentonite. SKB TR 83-72, Svensk Kärnbränslehantering AB.

Plötze M, Valter M, 2011. Bentonite as barrier material – Thermal conductivity of compacted bentonite. Nagra Arbeitsbericht NAB 11-16, Nagra, Switzerland.

Posiva SKB, 2017. Safety functions, performance targets and technical design requirements for a KBS-3V repository. Conclusions and recommendations from a joint SKB and Posiva working group. Posiva SKB Report 01, Posiva Oy, Svensk Kärnbränslehantering AB.

Svensson D, Lundgren C, Johannesson L-E, Norrfors K, 2017. Developing strategies for acquisition and control of bentonite for a high level radioactive waste repository. SKB TR-16-14, Svensk Kärnbränslehantering AB.

Thorsager P, Börgesson L, Johannesson L-E, Sandén T, 2002. Äspö Hard Rock Laboratory. Canister Retrieval Test. Report on installation. SKB IPR-02-30, Svensk Kärnbränslehantering AB.

Tien Y-M, Chu C-A, Wu P-L, Chuang W-S, Chung Y-J, 2010. Improved measurement and predictive model for thermal conductivity of sand-bentonite mixtures. Journal of Geoengineering 5, 51–60.

Wieczorek K, Miehe R, 2013. Measurement of thermal parameters of the HE-E buffer materials. PEBS report, Deliverable D-No:2.2-9, European Commission.

Åkesson M, Börgesson L, Kristensson O, 2010. SR-Site Data report. THM modelling of buffer, backfill and other system components. SKB TR-10-44, Svensk Kärnbränslehantering AB.

Appendix 1

Pictures from the installation and dismantling of the laboratory test

Installation

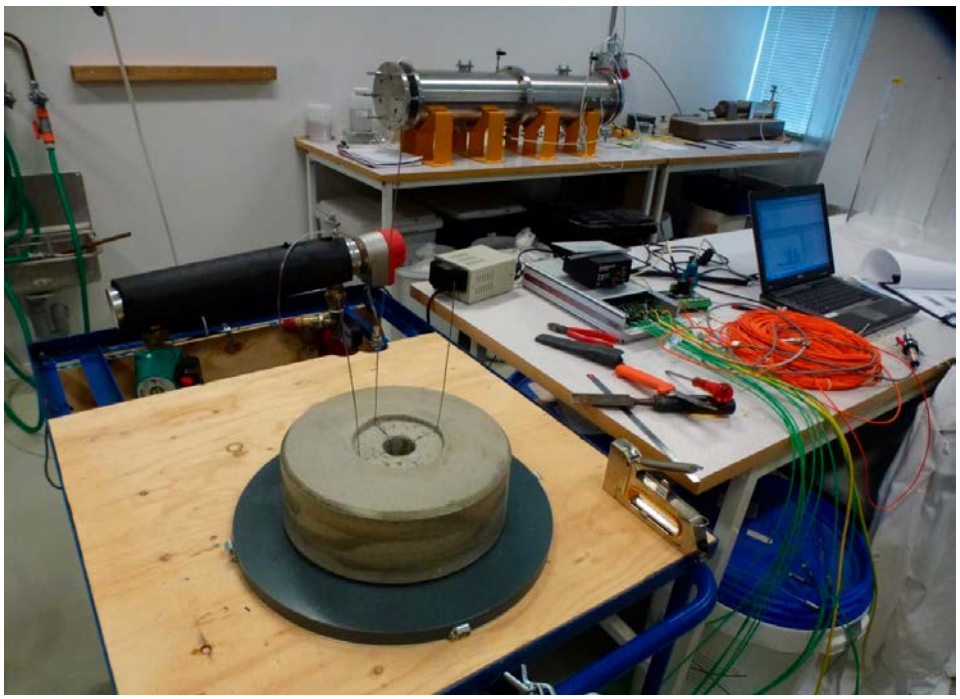

A1-1. *Block C1 with the thermocouples T1–T4.*

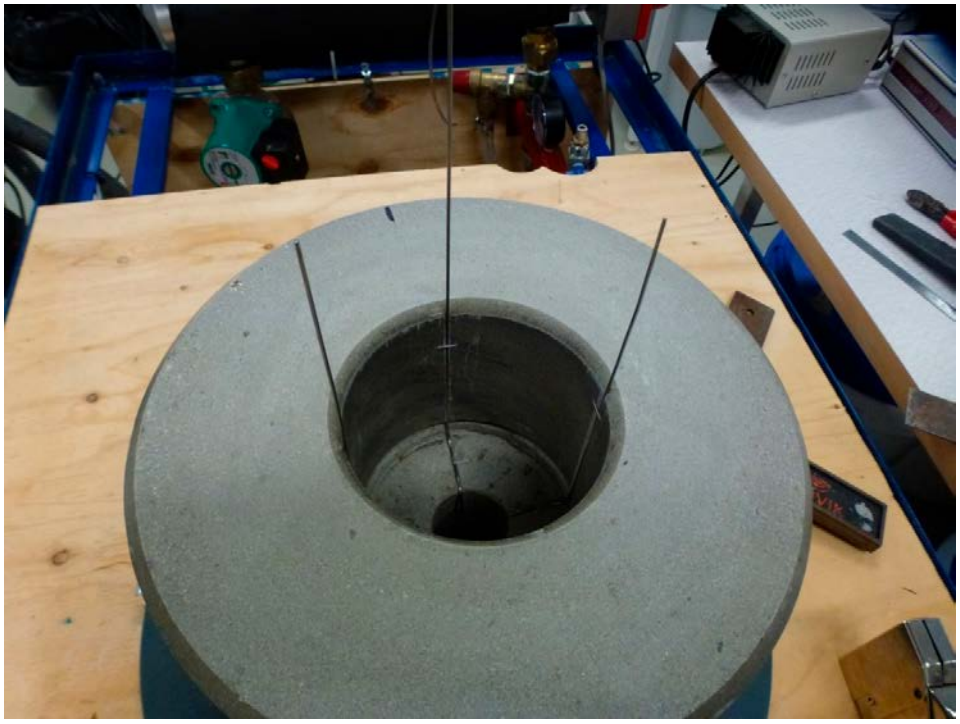

A1-2. *Block C1 and R1 installed with the thermocouples T1, T2 and T4.*

A1-3. *Block C1 –R3 with the heater in place.*

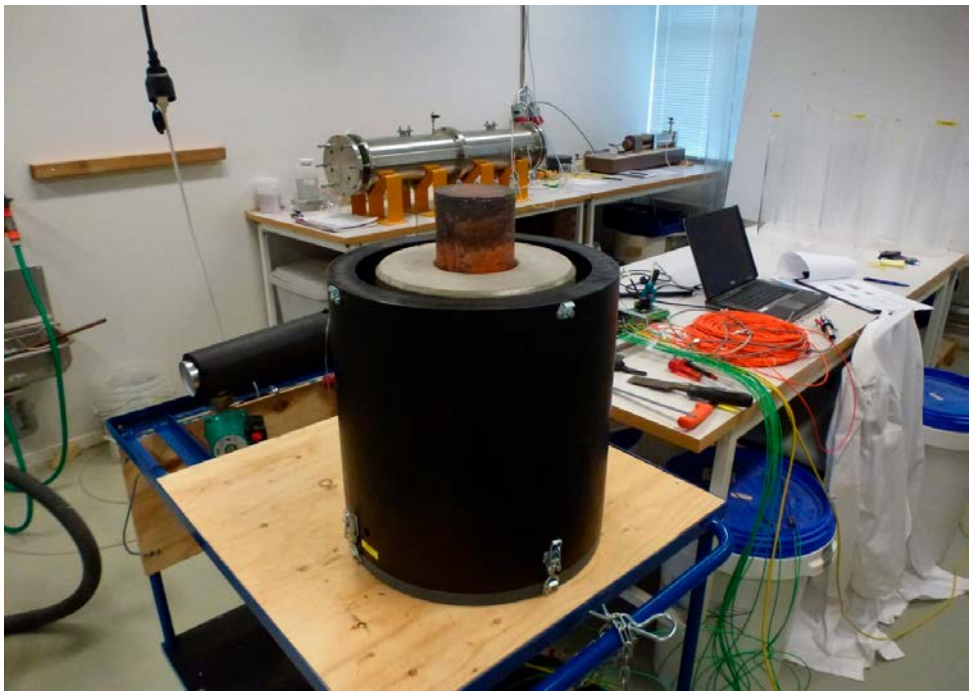

A1-4. *The first part of the outer tube put in place.*

A1-5. *Block R4 mounted and the outer slot filled with pellets. Thermocouples T2 and T10 with the heater are visible.*

A1-6. *The test setup with the rubber sheet on top and thermocouples C4 and T11 in place.*

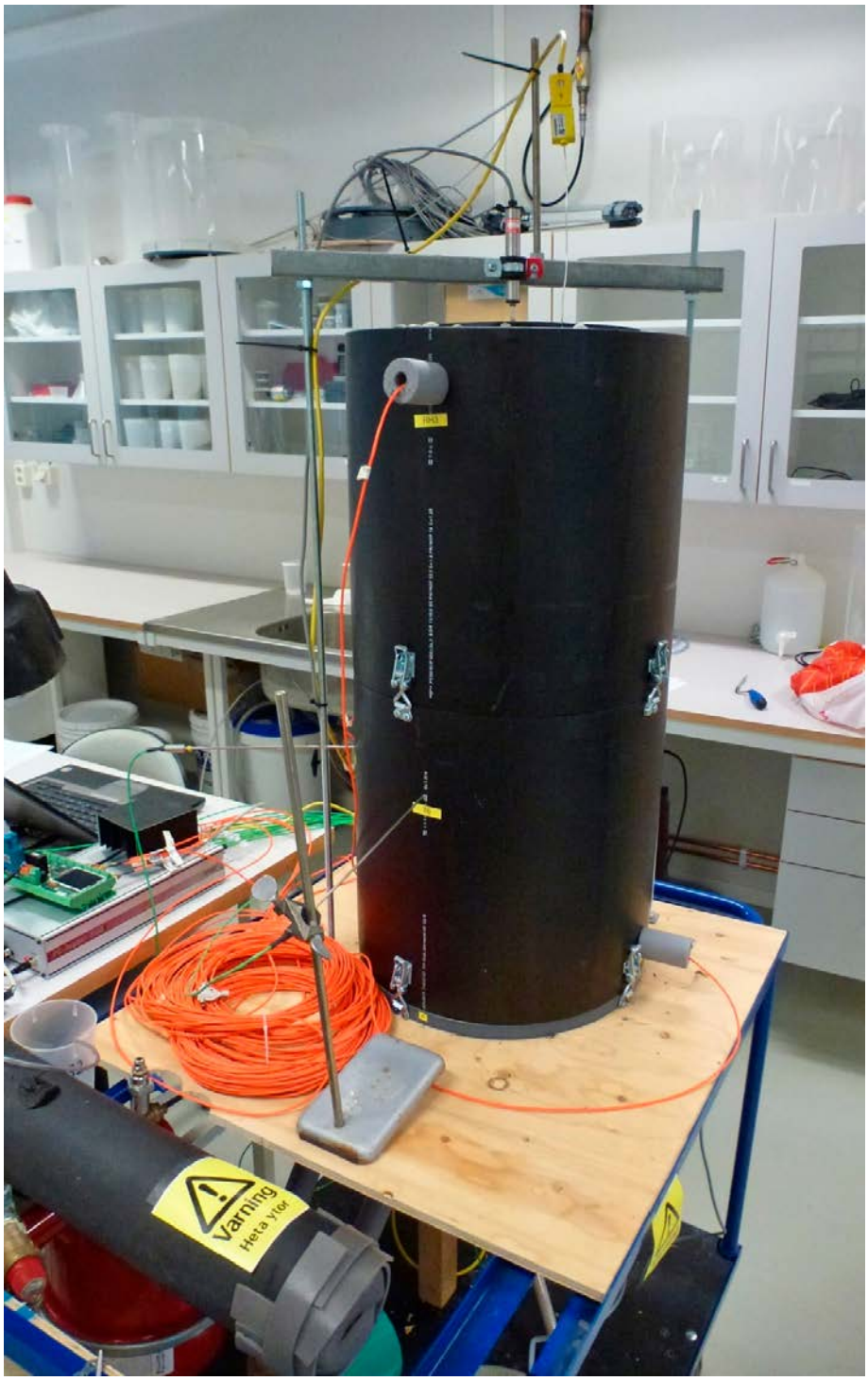

A1-7. *The test at the start of the heating.*

Dismantling

A1-8. *Block R4 removed from the test (direction 0° upwards). No visible cracks.*

A1-9. *Block R3 from below. A small crack is shown on the inside of the block.*

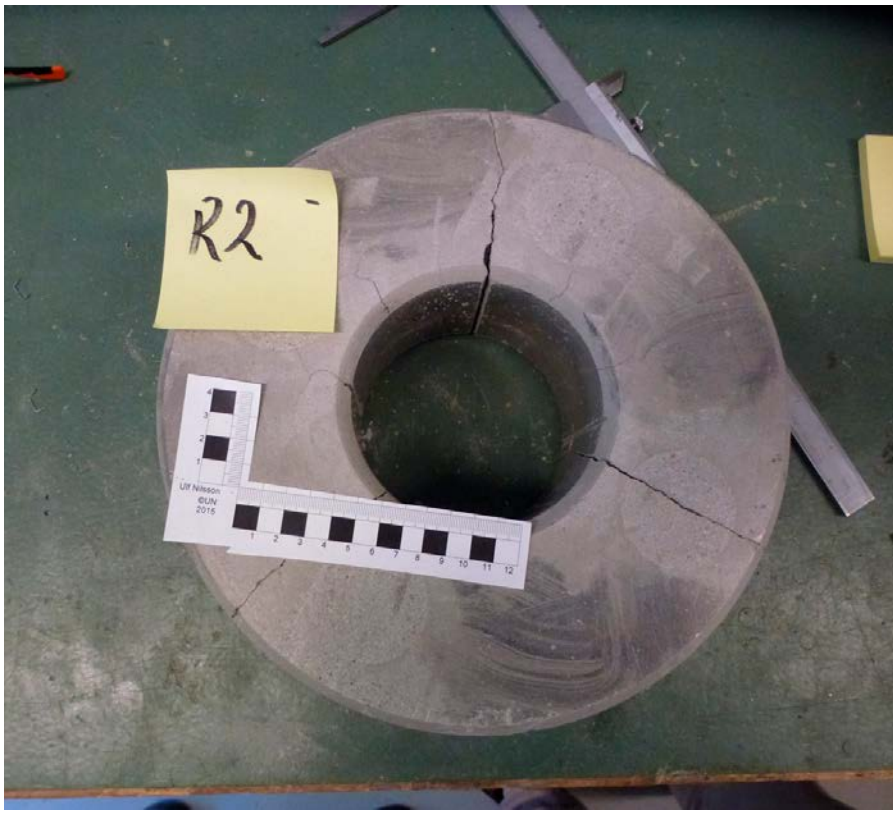

A1-10. *Block R2 from below (direction 0° upwards). Several visible cracks.*

A1-11. *Block R1 before the heater was removed. Several cracks are visible although not opened.*

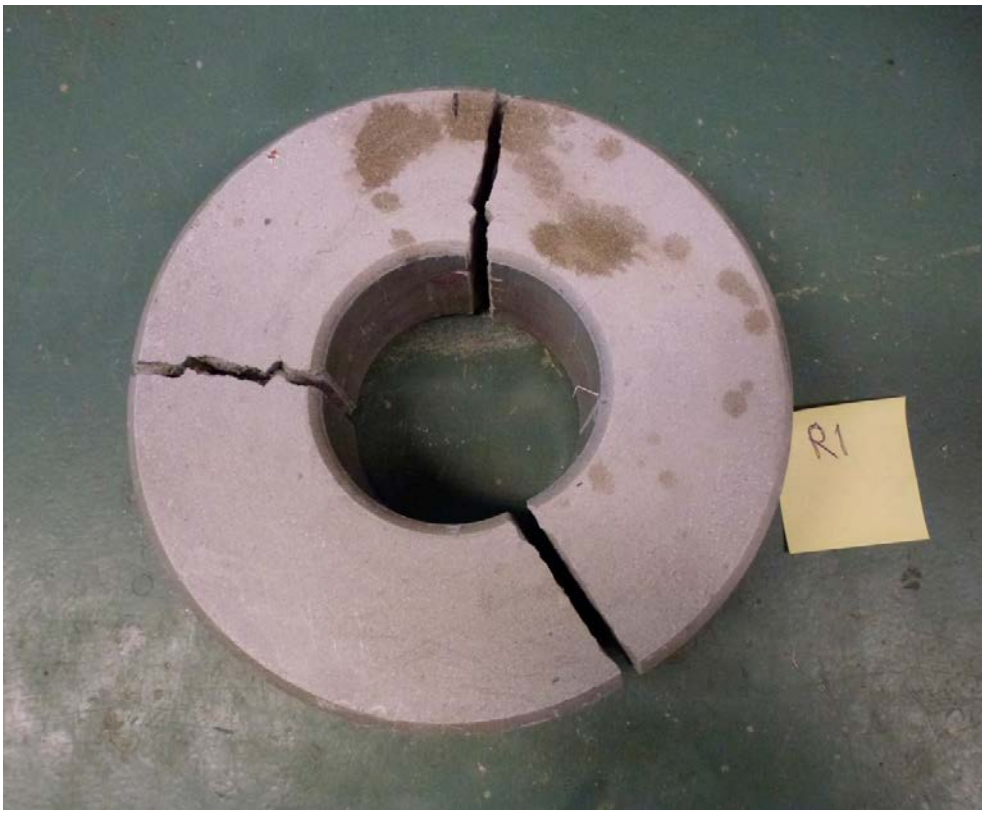

A1-12. *Block R1 from above (direction 0° upwards). Several visible cracks.*

A1-13. *Specimen taken from Block R1.*

Appendix 2

Temperature measurements made in Test 1

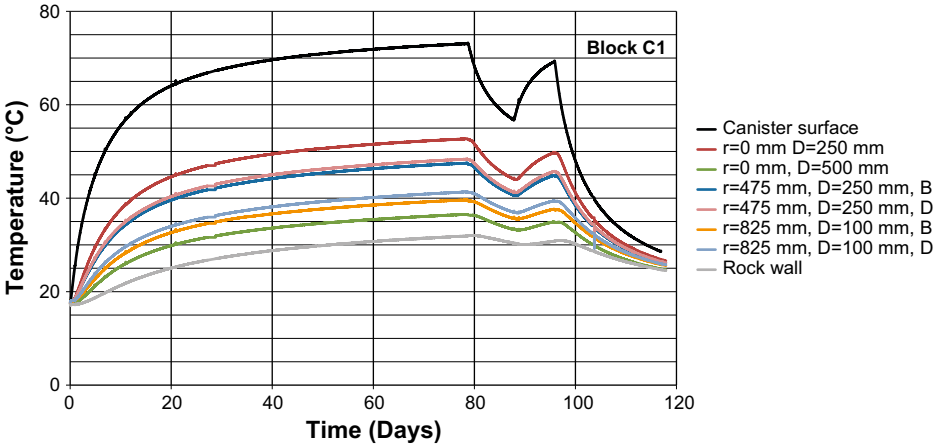

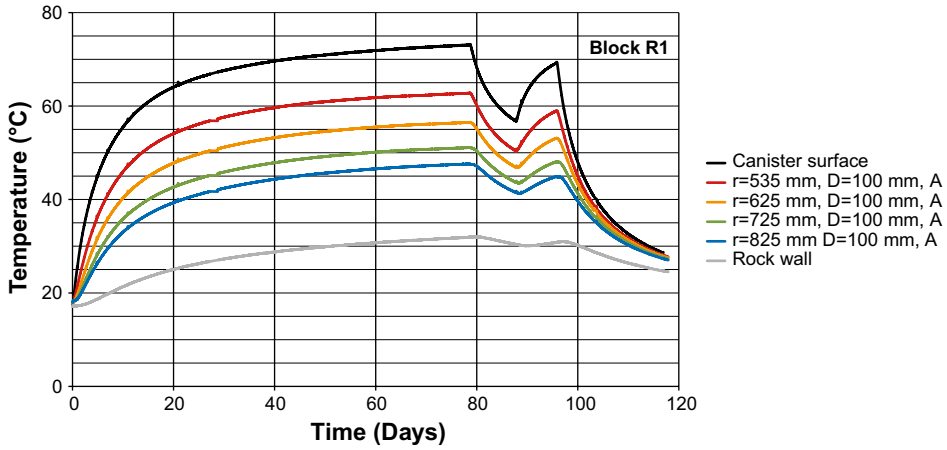
Block R1
Temperature (°C)
Time (Days)
0
20
40
60
80
100
120
Canister surface
r=535 mm, D=100 mm, A
r=625 mm, D=100 mm, A
r=725 mm, D=100 mm, A
r=825 mm D=100 mm, A
Rock wall

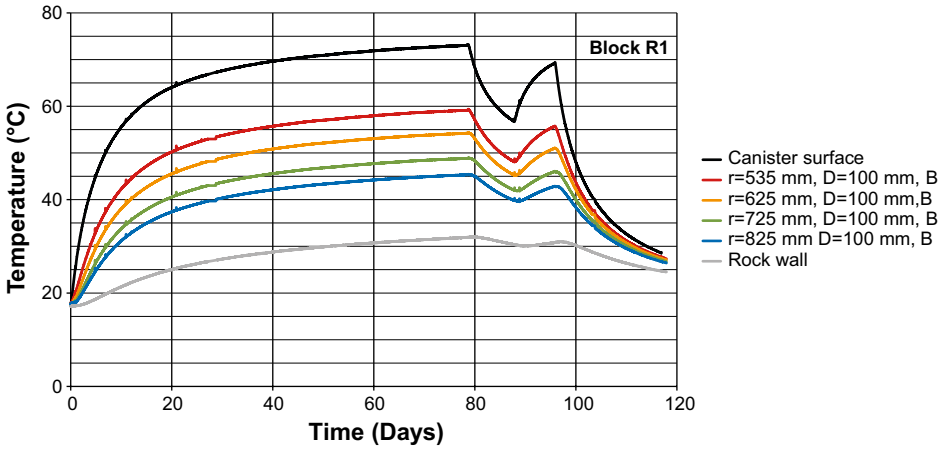
Block R1
Temperature (°C)
Time (Days)
0
20
40
60
80
100
120
Canister surface
r=535 mm, D=100 mm, B
r=625 mm, D=100 mm,B
r=725 mm, D=100 mm, B
r=825 mm D=100 mm, B
Rock wall

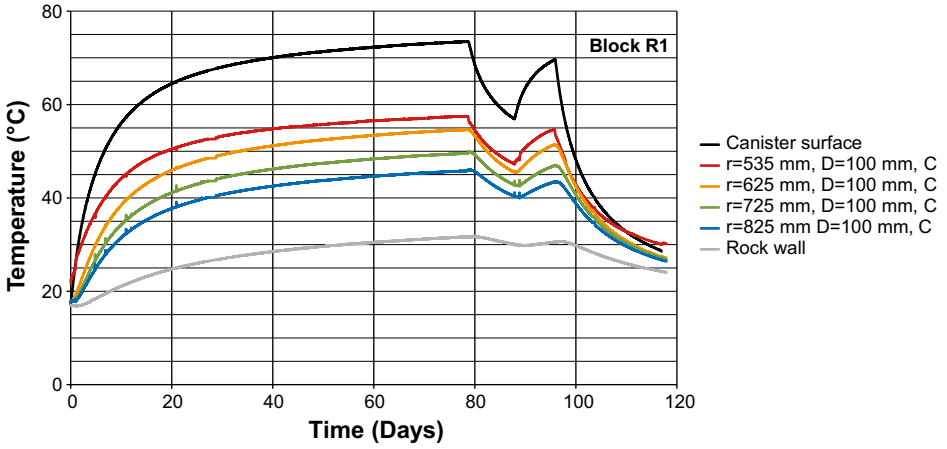
Block R1
Temperature (°C)
Time (Days)
0
20
40
60
80
100
120
Canister surface
r=535 mm, D=100 mm, C
r=625 mm, D=100 mm, C
r=725 mm, D=100 mm, C
r=825 mm D=100 mm, C
Rock wall

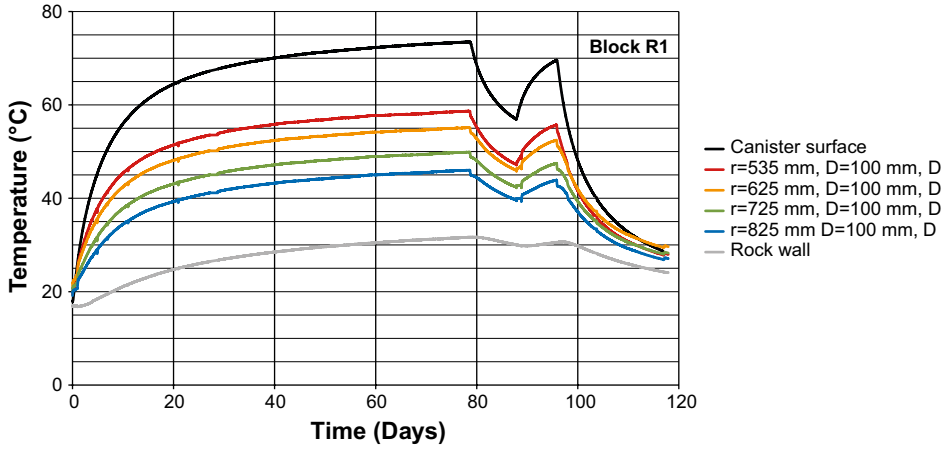
Block R1
Temperature (°C)
Time (Days)
0
20
40
60
80
100
120
Canister surface
r=535 mm, D=100 mm, D
r=625 mm, D=100 mm, D
r=725 mm, D=100 mm, D
r=825 mm D=100 mm, D
Rock wall

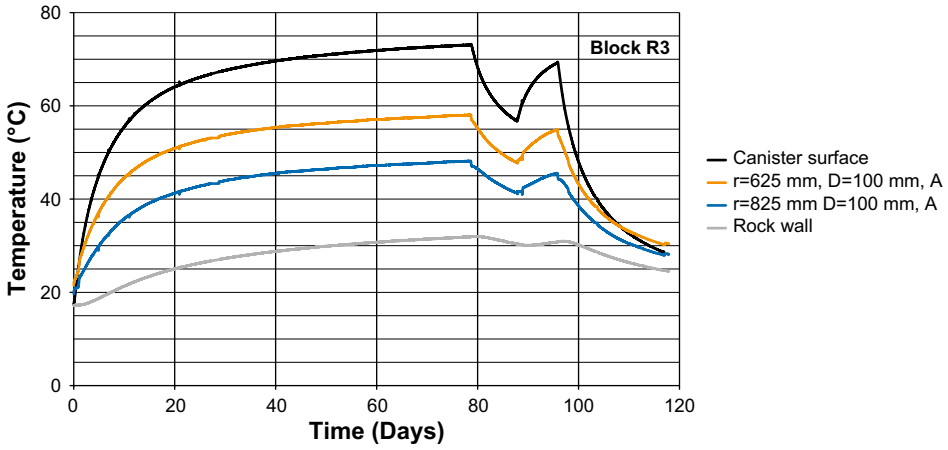
Block R3
Temperature (°C)
Time (Days)
0
20
40
60
80
100
120
Canister surface
r=625 mm, D=100 mm, A
r=825 mm D=100 mm, A
Rock wall

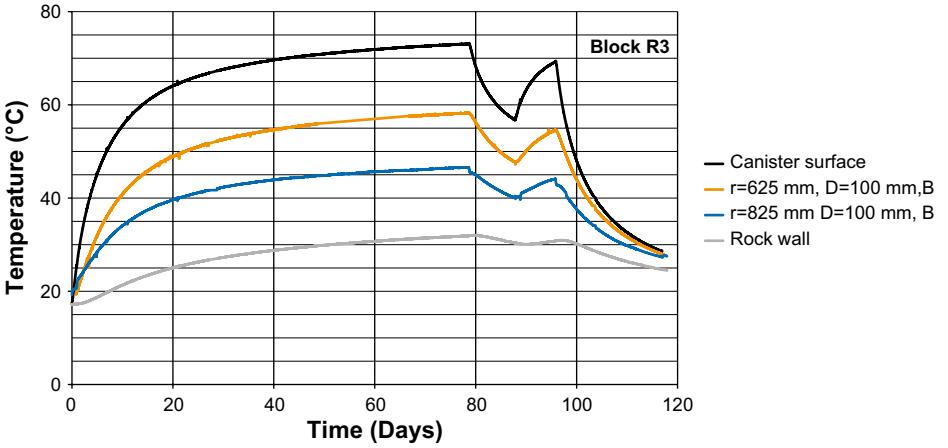
Block R3
Temperature (°C)
Time (Days)
0
20
40
60
80
100
120
Canister surface
r=625 mm, D=100 mm,B
r=825 mm D=100 mm, B
Rock wall

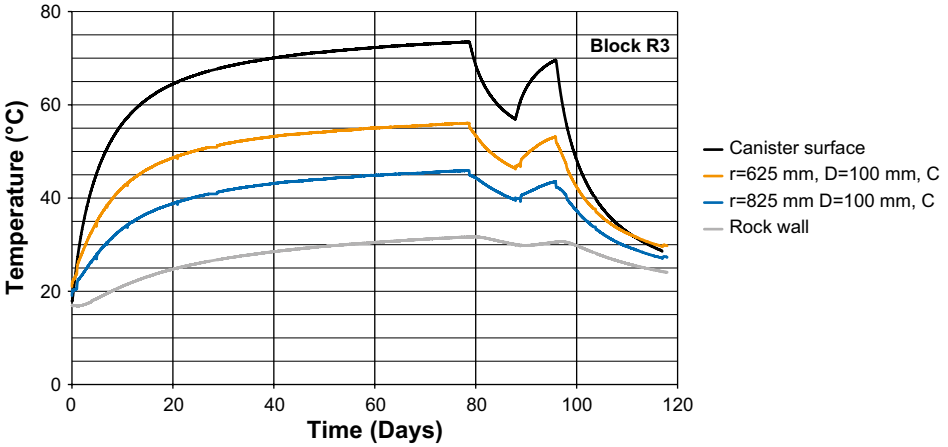
Block R3
Temperature (°C)
Time (Days)
0
20
40
60
80
100
120
Canister surface
r=625 mm, D=100 mm, C
r=825 mm D=100 mm, C
Rock wall

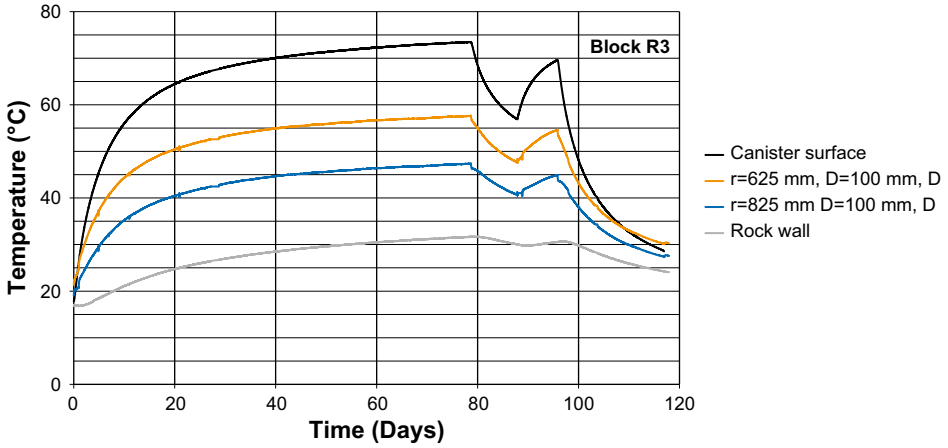
Block R3
Temperature (°C)
Time (Days)
0
20
40
60
80
100
120
Canister surface
r=625 mm, D=100 mm, D
r=825 mm D=100 mm, D
Rock wall

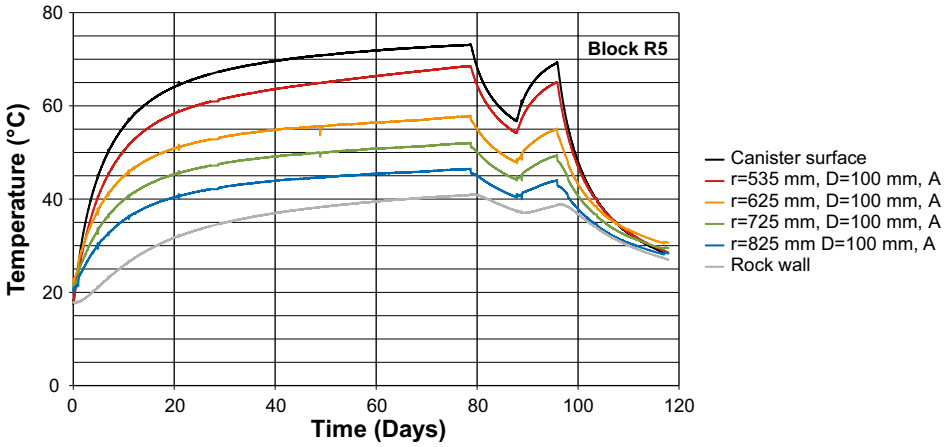
Block R5
Temperature (°C)
Time (Days)
0
20
40
60
80
100
120
Canister surface
r=535 mm, D=100 mm, A
r=625 mm, D=100 mm, A
r=725 mm, D=100 mm, A
r=825 mm D=100 mm, A
Rock wall

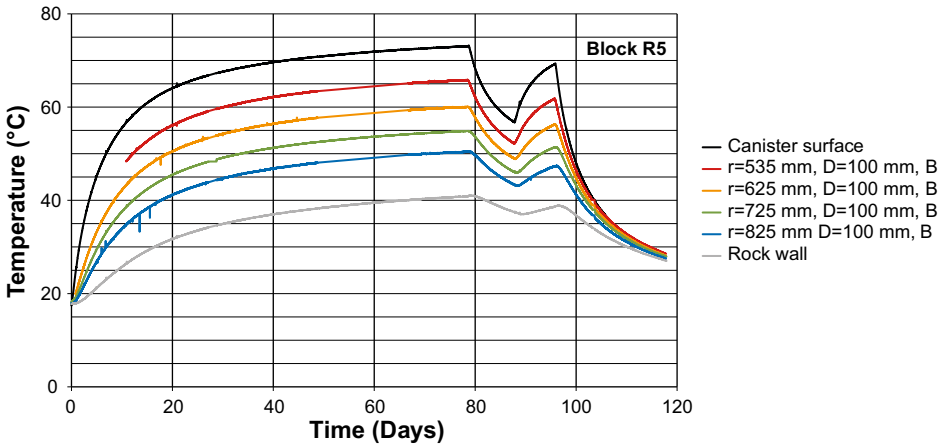
Block R5
Temperature (°C)
Time (Days)
0
20
40
60
80
100
120
Canister surface
r=535 mm, D=100 mm, B
r=625 mm, D=100 mm, B
r=725 mm, D=100 mm, B
r=825 mm D=100 mm, B
Rock wall

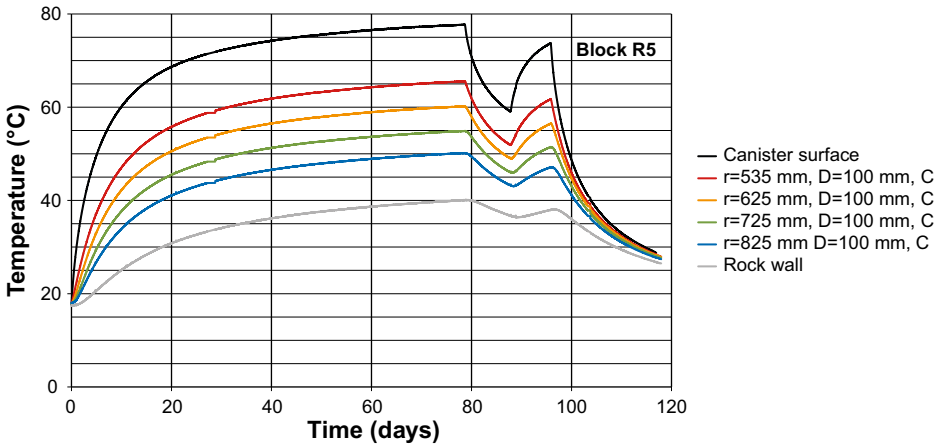
Block R5
Temperature (°C)
Time (days)
0
20
40
60
80
100
120
Canister surface
r=535 mm, D=100 mm, C
r=625 mm, D=100 mm, C
r=725 mm, D=100 mm, C
r=825 mm D=100 mm, C
Rock wall

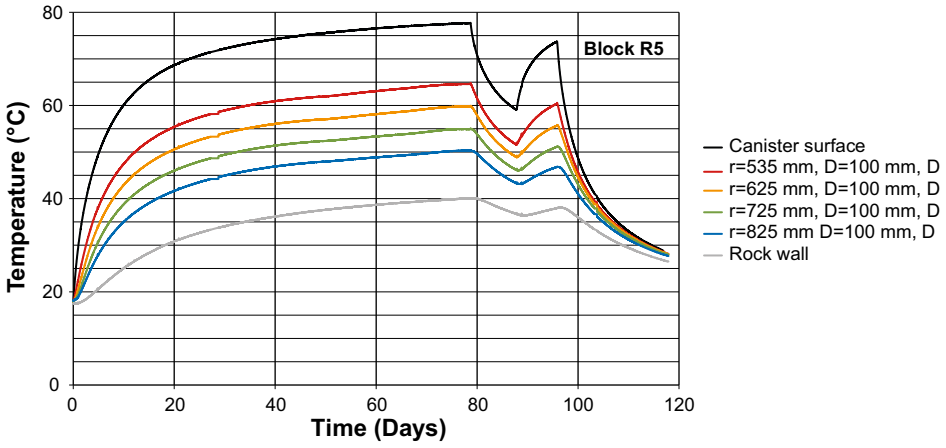
Block R5
Temperature (°C)
Time (Days)
0
20
40
60
80
100
120
Canister surface
r=535 mm, D=100 mm, D
r=625 mm, D=100 mm, D
r=725 mm, D=100 mm, D
r=825 mm D=100 mm, D
Rock wall

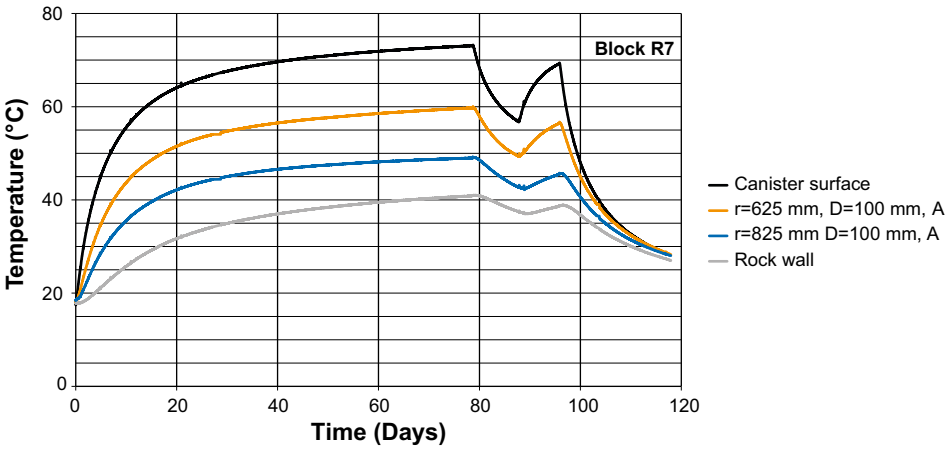
Block R7
Temperature (°C)
Time (Days)
0
20
40
60
80
100
120
Canister surface
r=625 mm, D=100 mm, A
r=825 mm D=100 mm, A
Rock wall

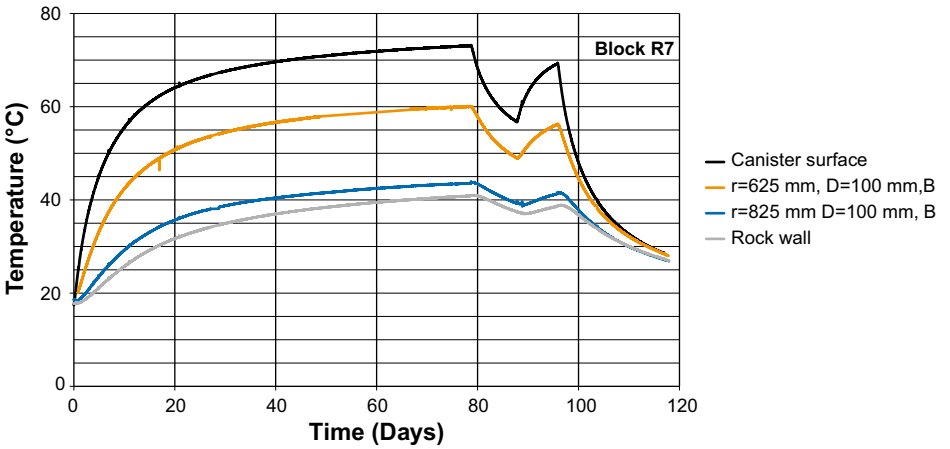
Block R7
Temperature (°C)
Time (Days)
0
20
40
60
80
100
120
Canister surface
r=625 mm, D=100 mm,B
r=825 mm D=100 mm, B
Rock wall

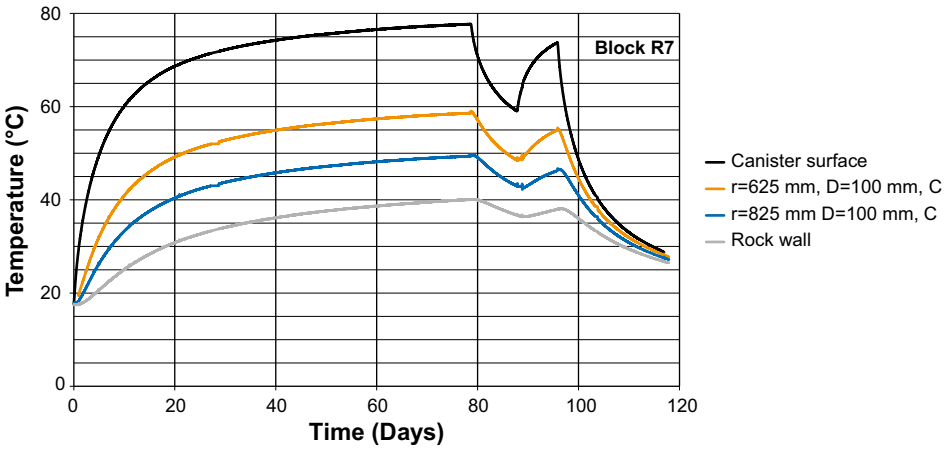
Block R7
Temperature (°C)
Time (Days)
0
20
40
60
80
100
120
Canister surface
r=625 mm, D=100 mm, C
r=825 mm D=100 mm, C
Rock wall

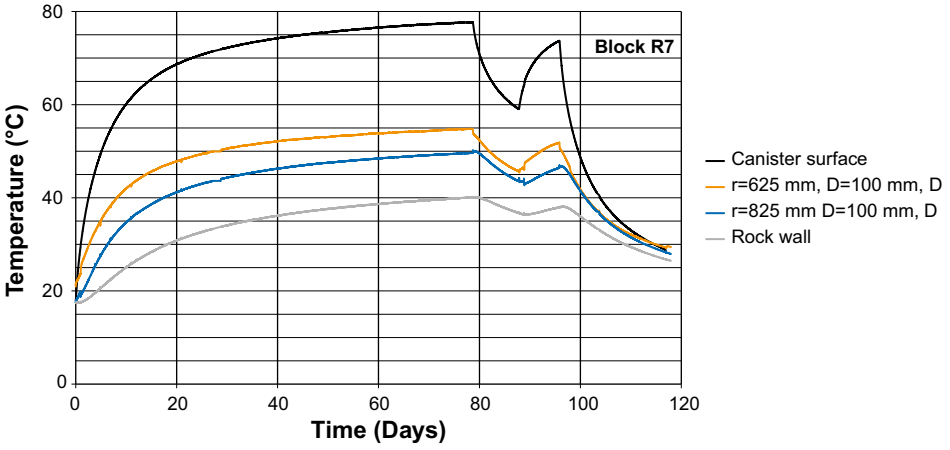
Block R7
Temperature (°C)
Time (Days)
0
20
40
60
80
100
120
Canister surface
r=625 mm, D=100 mm, D
r=825 mm D=100 mm, D
Rock wall

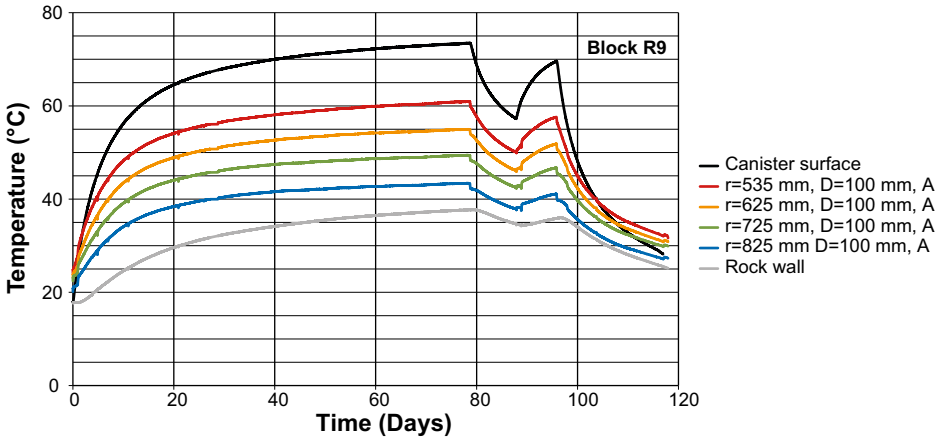
Block R9
Temperature (°C)
Time (Days)
0
20
40
60
80
100
120
Canister surface
r=535 mm, D=100 mm, A
r=625 mm, D=100 mm, A
r=725 mm, D=100 mm, A
r=825 mm D=100 mm, A
Rock wall

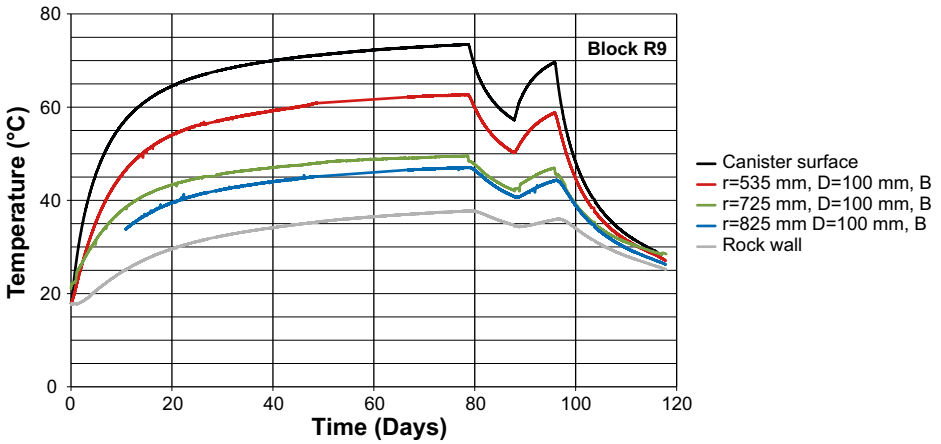
Block R9
Temperature (°C)
Time (Days)
0
20
40
60
80
100
120
Canister surface
r=535 mm, D=100 mm, B
r=725 mm, D=100 mm, B
r=825 mm D=100 mm, B
Rock wall

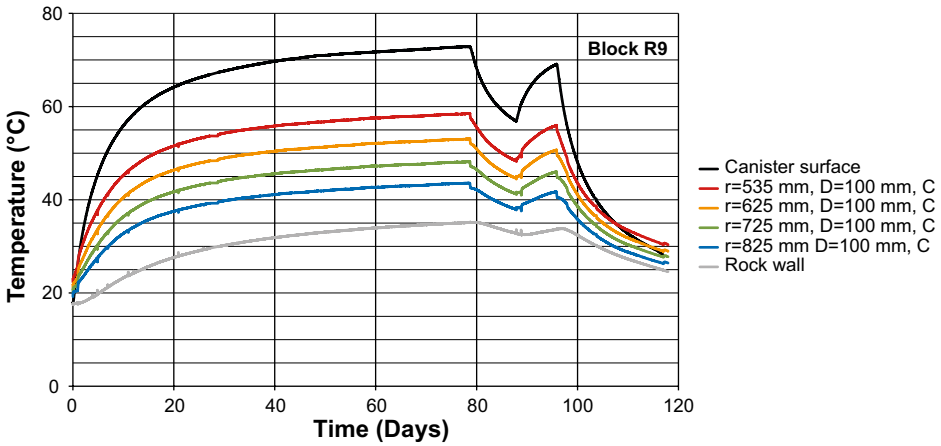
Block R9
Temperature (°C)
Time (Days)
0
20
40
60
80
100
120
Canister surface
r=535 mm, D=100 mm, C
r=625 mm, D=100 mm, C
r=725 mm, D=100 mm, C
r=825 mm D=100 mm, C
Rock wall

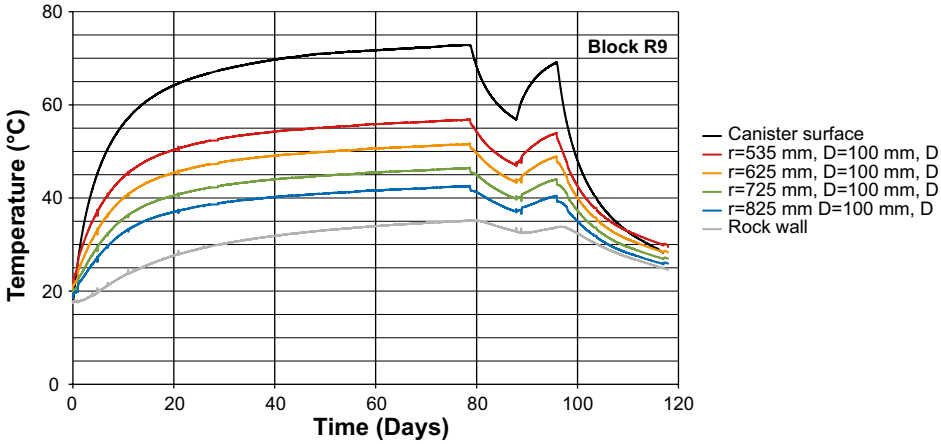
Block R9
Temperature (°C)
Time (Days)
0
20
40
60
80
100
120
Canister surface
r=535 mm, D=100 mm, D
r=625 mm, D=100 mm, D
r=725 mm, D=100 mm, D
r=825 mm D=100 mm, D
Rock wall

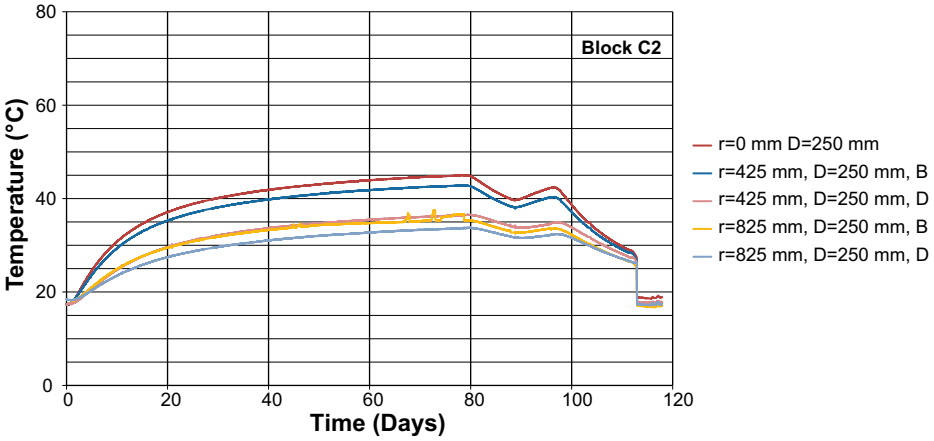
Block C2
Temperature (°C)
Time (Days)
0
20
40
60
80
100
120
r=0 mm D=250 mm
r=425 mm, D=250 mm, B
r=425 mm, D=250 mm, D
r=825 mm, D=250 mm, B
r=825 mm, D=250 mm, D

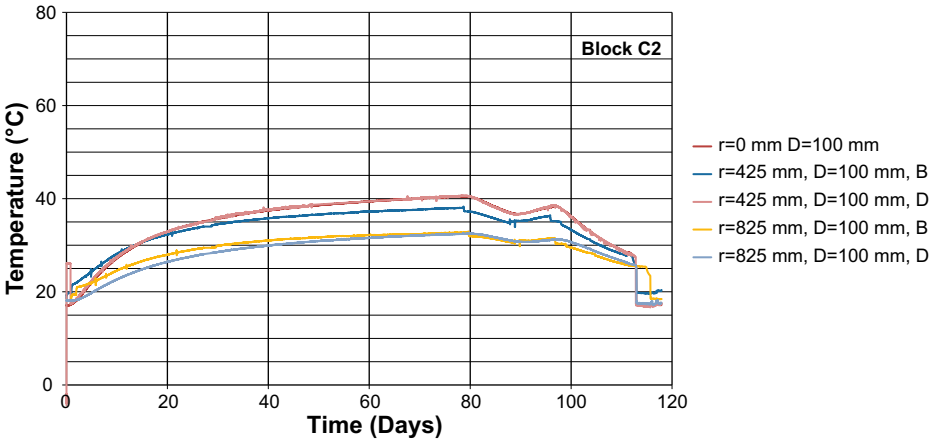
Block C2
Temperature (°C)
Time (Days)
0
20
40
60
80
100
120
r=0 mm D=100 mm
r=425 mm, D=100 mm, B
r=425 mm, D=100 mm, D
r=825 mm, D=100 mm, B
r=825 mm, D=100 mm, D

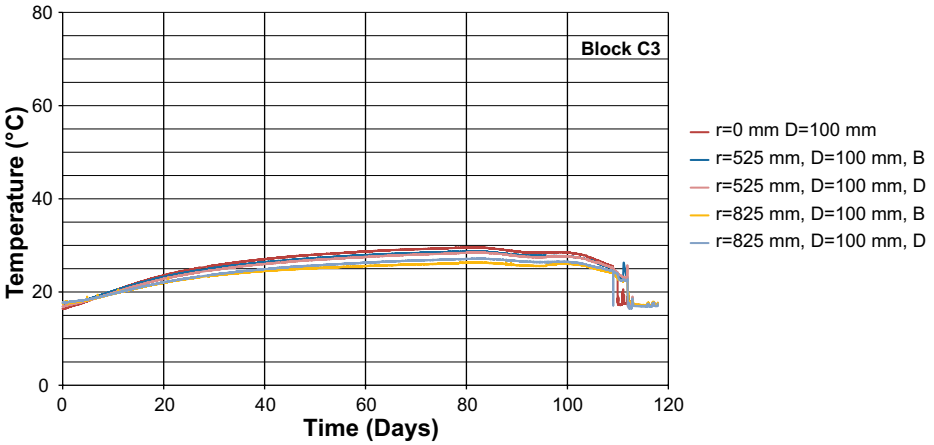
Block C3
Temperature (°C)
Time (Days)
0
20
40
60
80
100
120
r=0 mm D=100 mm
r=525 mm, D=100 mm, B
r=525 mm, D=100 mm, D
r=825 mm, D=100 mm, B
r=825 mm, D=100 mm, D

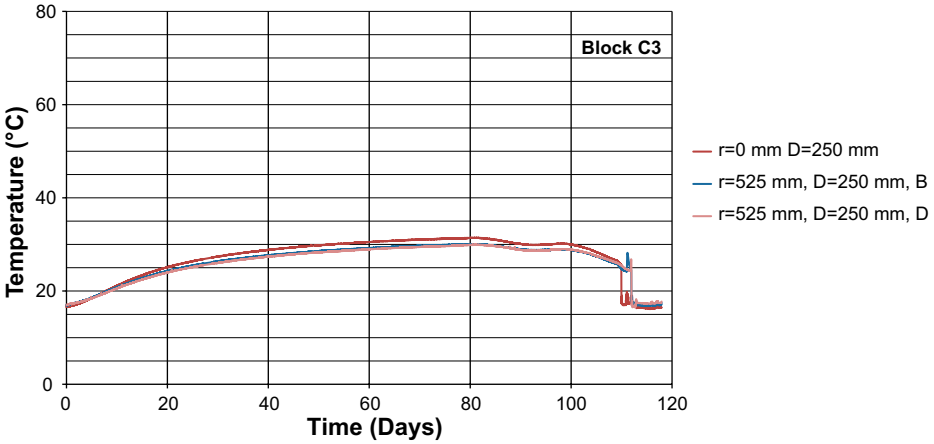
Block C3
Temperature (°C)
Time (Days)
0
20
40
60
80
100
120
r=0 mm D=250 mm
r=525 mm, D=250 mm, B
r=525 mm, D=250 mm, D

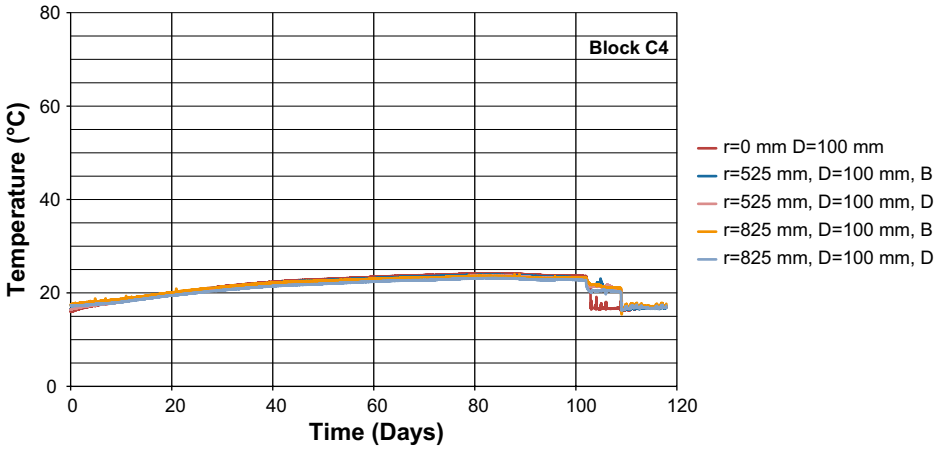
Block C4
Temperature (°C)
Time (Days)
0
20
40
60
80
100
120
r=0 mm D=100 mm
r=525 mm, D=100 mm, B
r=525 mm, D=100 mm, D
r=825 mm, D=100 mm, B
r=825 mm, D=100 mm, D

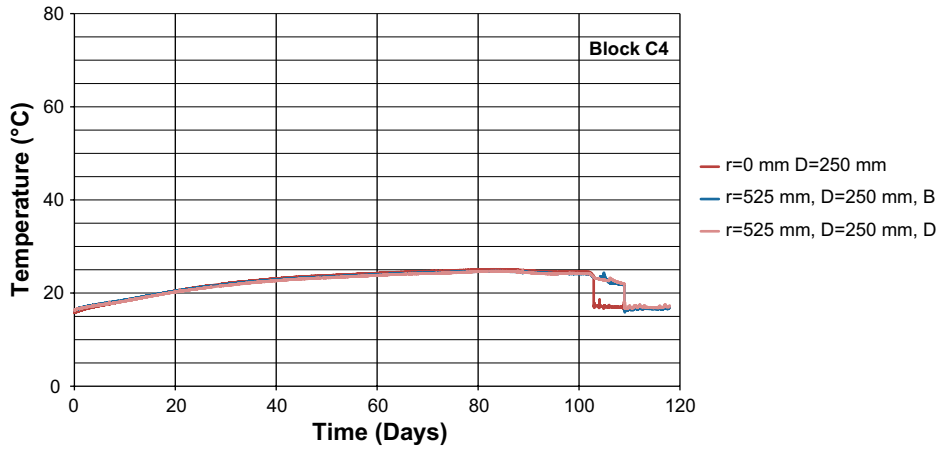
Block C4
Temperature (°C)
Time (Days)
0
20
40
60
80
100
120
r=0 mm D=250 mm
r=525 mm, D=250 mm, B
r=525 mm, D=250 mm, D

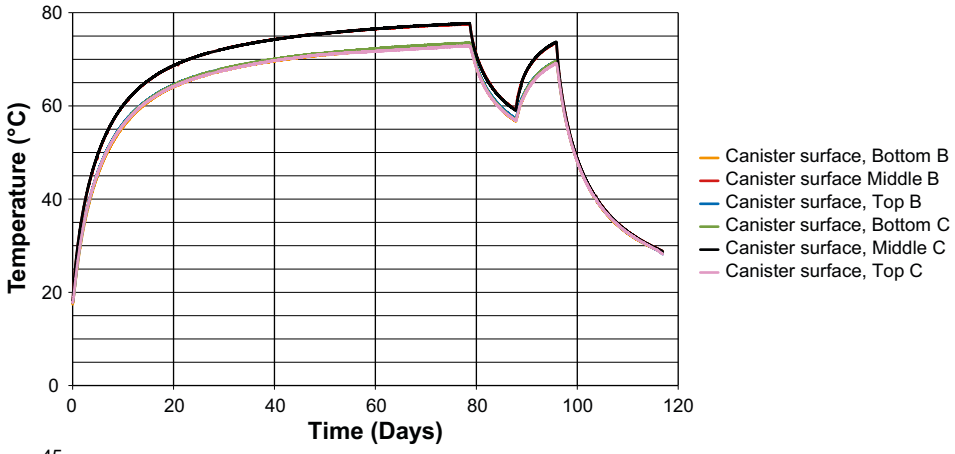
Temperature (°C)
Time (Days)
Canister surface, Bottom B
Canister surface Middle B
Canister surface, Top B
Canister surface, Bottom C
Canister surface, Middle C
Canister surface, Top C

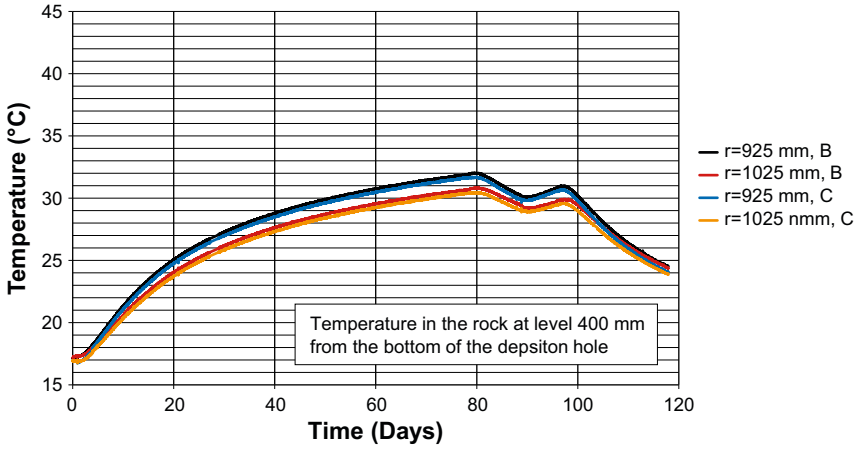
Temperature (°C)
Time (Days)
r=925 mm, B
r=1025 mm, B
r=925 mm, C
r=1025 nmm, C
Temperature in the rock at level 400 mm
from the bottom of the depsiton hole

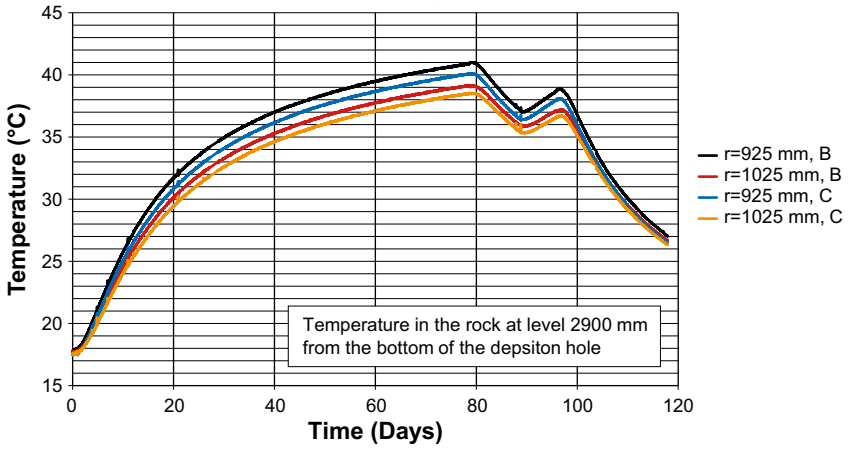
Temperature (°C)
Time (Days)
r=925 mm, B
r=1025 mm, B
r=925 mm, C
r=1025 mm, C
Temperature in the rock at level 2900 mm
from the bottom of the depsiton hole

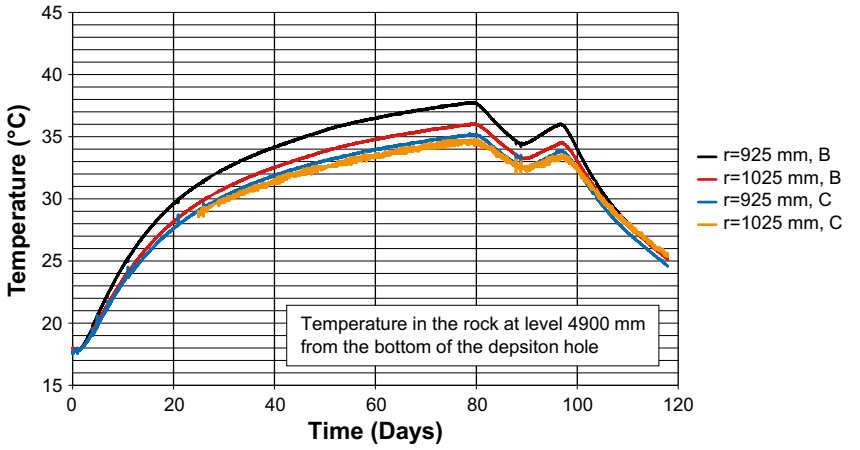
Temperature (°C)
Time (Days)
r=925 mm, B
r=1025 mm, B
r=925 mm, C
r=1025 mm, C
Temperature in the rock at level 4900 mm
from the bottom of the depsiton hole

Water content and dry density of the buffer Test 1

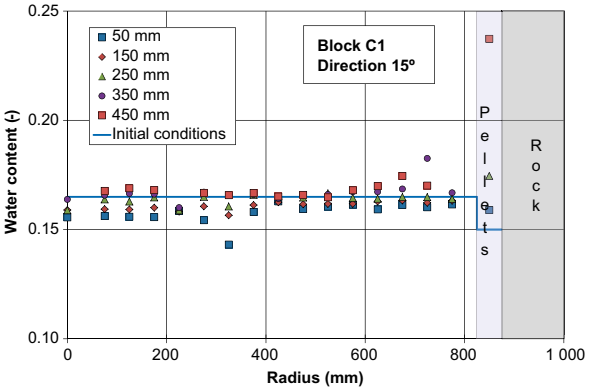

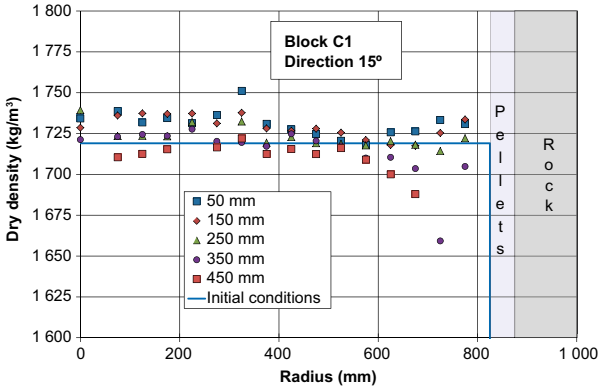

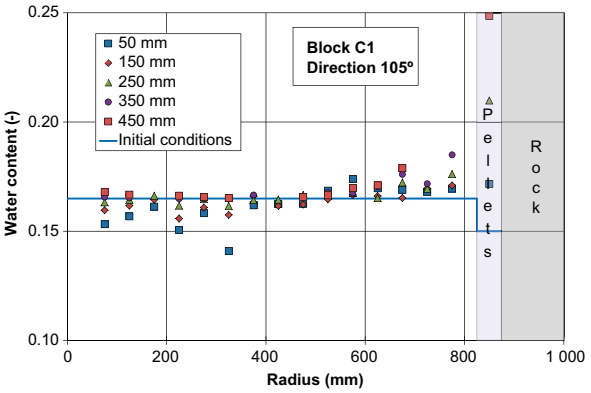

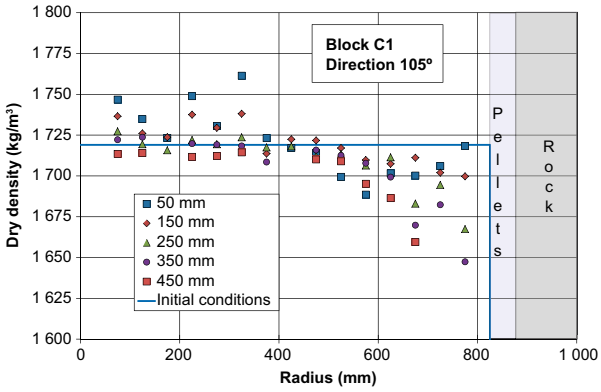

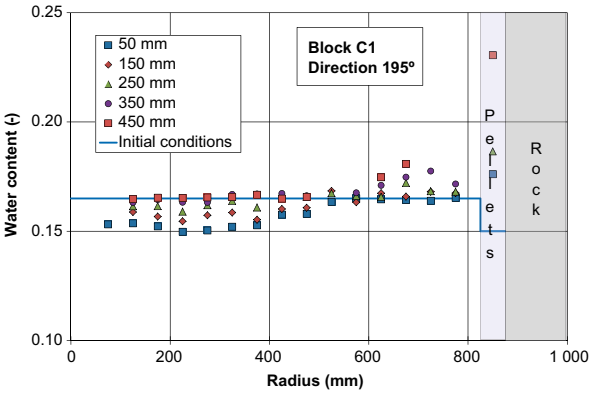

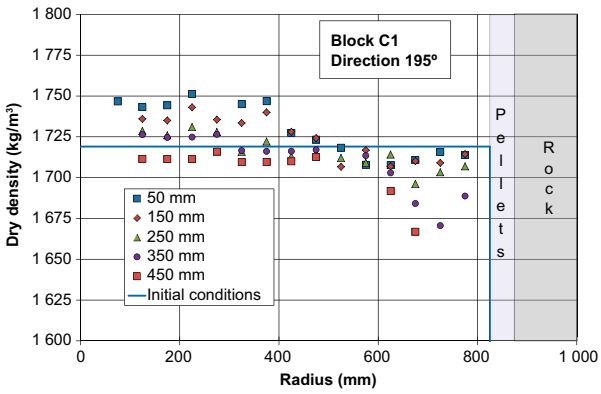

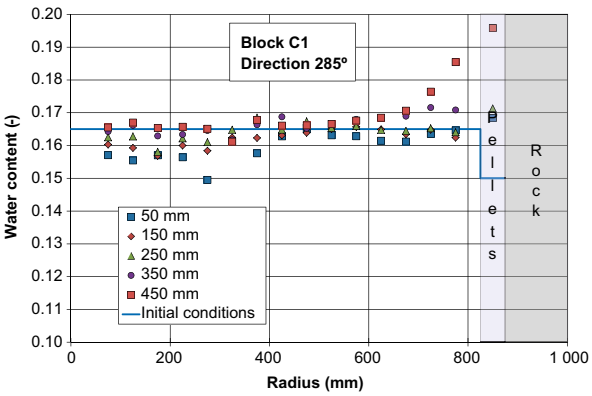

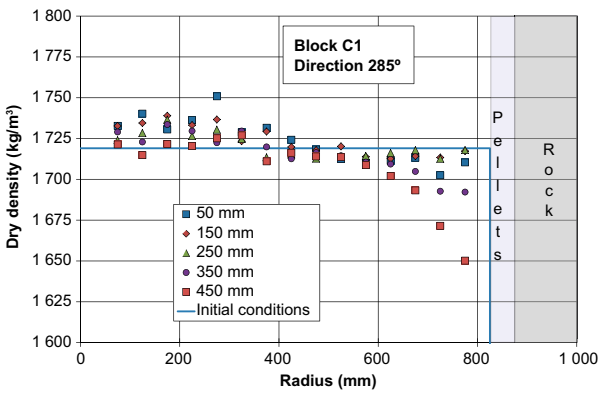

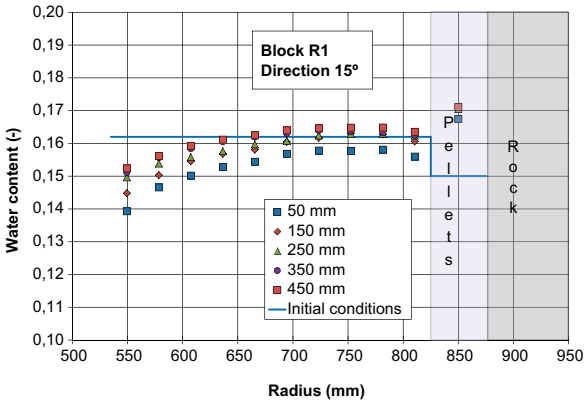
Block R1
Direction 15º
Water content (-)
Radius (mm)
50 mm
150 mm
250 mm
350 mm
450 mm
Initial conditions
Pellets
Rock

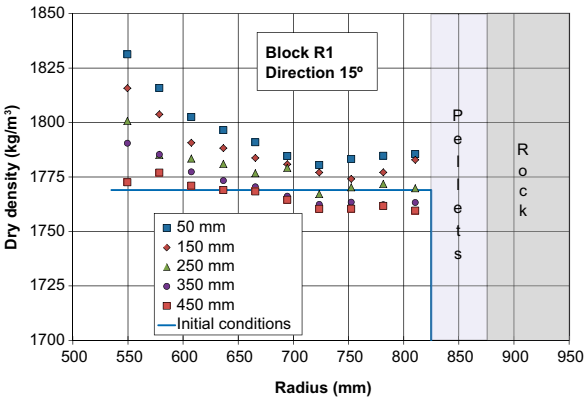
Block R1
Direction 15º
Dry density (kg/m³)
Radius (mm)
50 mm
150 mm
250 mm
350 mm
450 mm
Initial conditions
Pellets
Rock

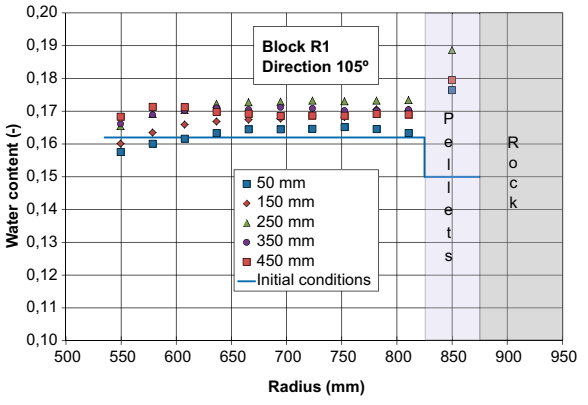
Block R1
Direction 105º
Water content (-)
Radius (mm)
50 mm
150 mm
250 mm
350 mm
450 mm
Initial conditions
Pellets
Rock

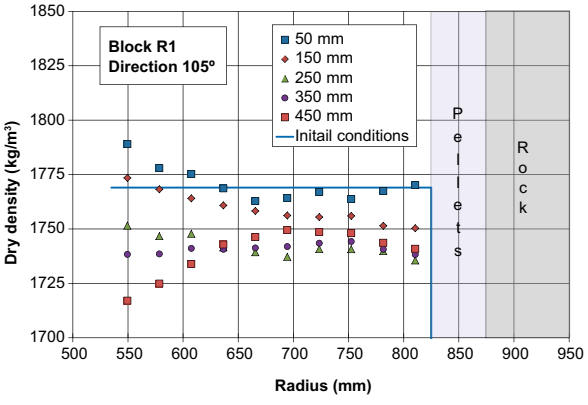
Block R1
Direction 105º
Dry density (kg/m³)
Radius (mm)
50 mm
150 mm
250 mm
350 mm
450 mm
Initail conditions
Pellets
Rock

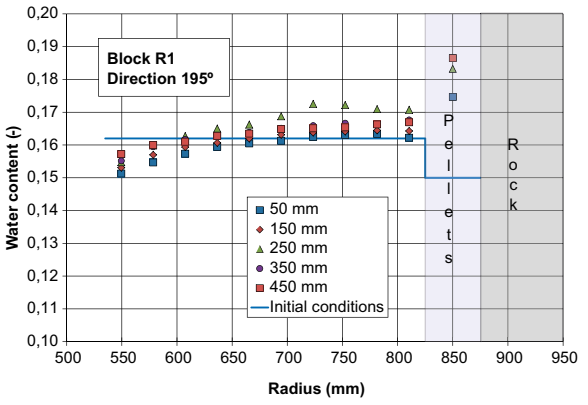
Block R1
Direction 195º
Water content (-)
Radius (mm)
50 mm
150 mm
250 mm
350 mm
450 mm
Initial conditions
Pellets
Rock

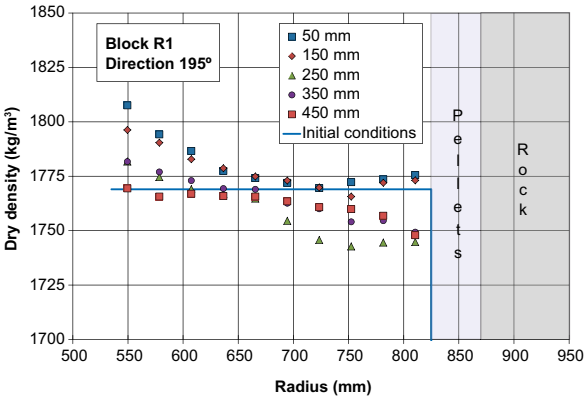
Block R1
Direction 195º
Dry density (kg/m³)
Radius (mm)
50 mm
150 mm
250 mm
350 mm
450 mm
Initial conditions
Pellets
Rock

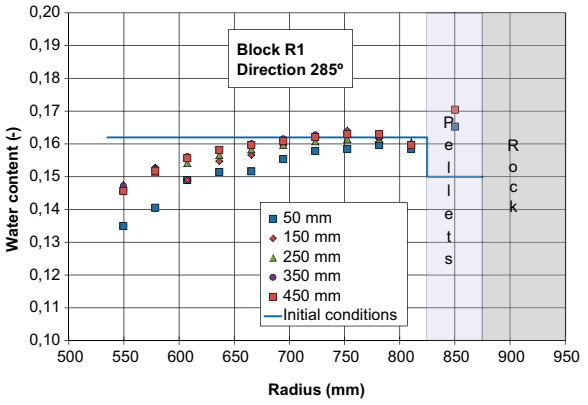
Block R1
Direction 285º
Water content (-)
Radius (mm)
50 mm
150 mm
250 mm
350 mm
450 mm
Initial conditions
Pellets
Rock

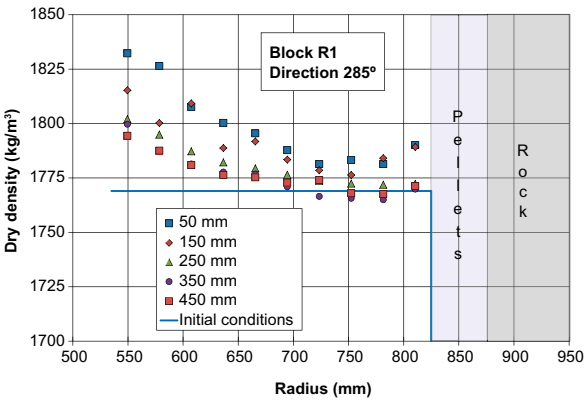
Block R1
Direction 285º
Dry density (kg/m³)
Radius (mm)
50 mm
150 mm
250 mm
350 mm
450 mm
Initial conditions
Pellets
Rock

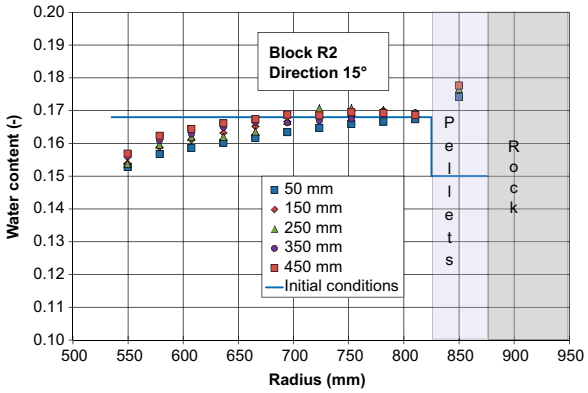
Block R2
Direction 15°
Water content (-)
Radius (mm)
50 mm
150 mm
250 mm
350 mm
450 mm
Initial conditions
Pellets
Rock

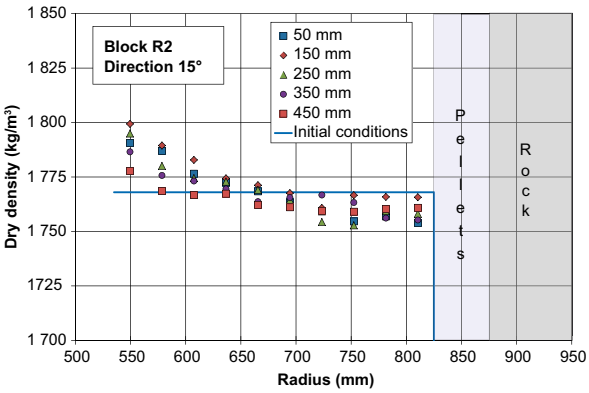
Block R2
Direction 15°
Dry density (kg/m³)
Radius (mm)
50 mm
150 mm
250 mm
350 mm
450 mm
Initial conditions
Pellets
Rock

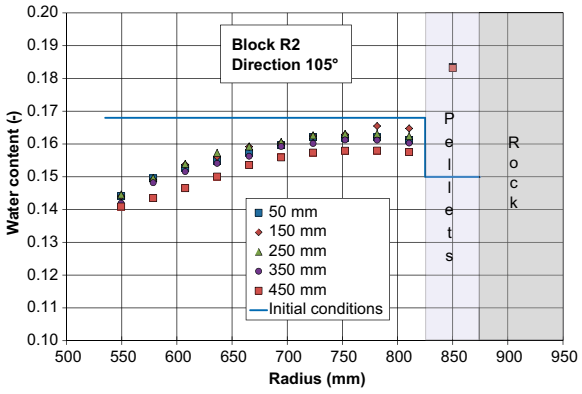
Block R2
Direction 105°
Water content (-)
Radius (mm)
50 mm
150 mm
250 mm
350 mm
450 mm
Initial conditions
Pellets
Rock

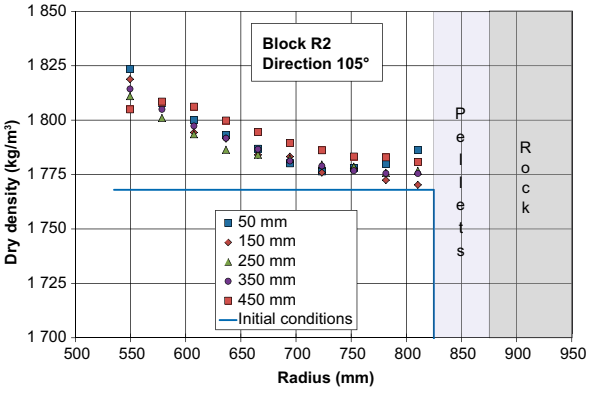
Block R2
Direction 105°
Dry density (kg/m³)
Radius (mm)
50 mm
150 mm
250 mm
350 mm
450 mm
Initial conditions
Pellets
Rock

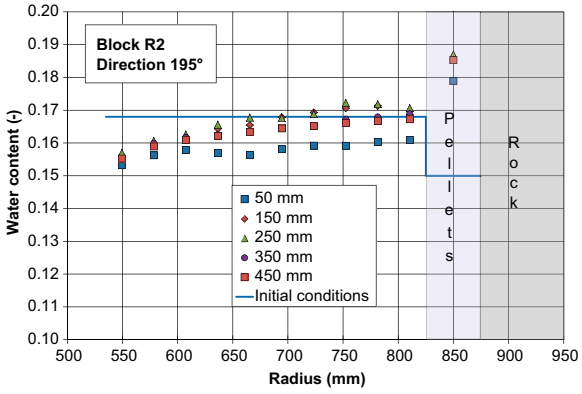
Block R2
Direction 195°
Water content (-)
Radius (mm)
50 mm
150 mm
250 mm
350 mm
450 mm
Initial conditions
Pellets
Rock

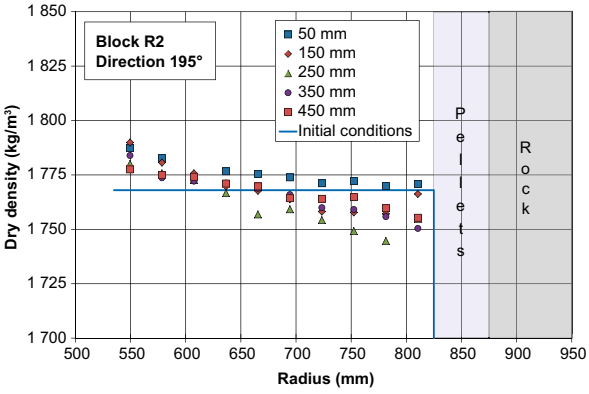
Block R2
Direction 195°
Dry density (kg/m³)
Radius (mm)
50 mm
150 mm
250 mm
350 mm
450 mm
Initial conditions
Pellets
Rock

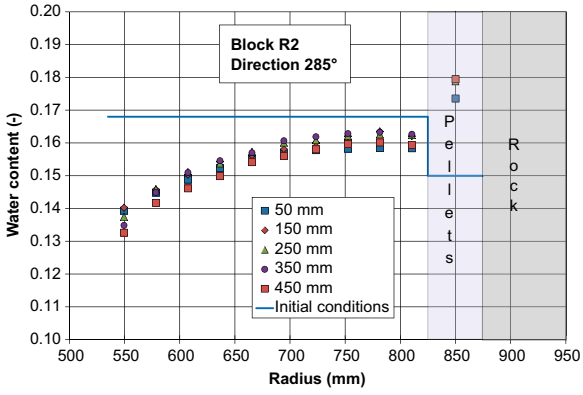
Block R2
Direction 285°
Water content (-)
Radius (mm)
50 mm
150 mm
250 mm
350 mm
450 mm
Initial conditions
Pellets
Rock

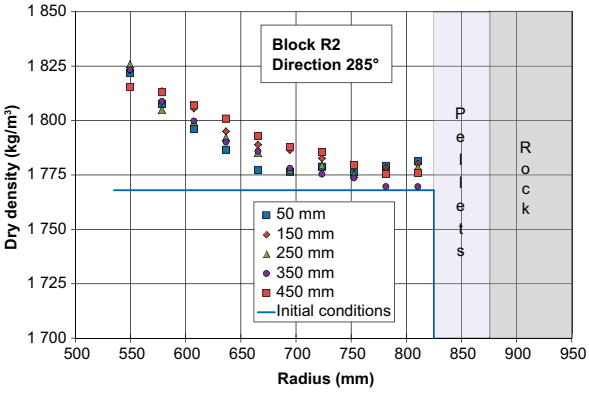
Block R2
Direction 285°
Dry density (kg/m³)
Radius (mm)
50 mm
150 mm
250 mm
350 mm
450 mm
Initial conditions
Pellets
Rock

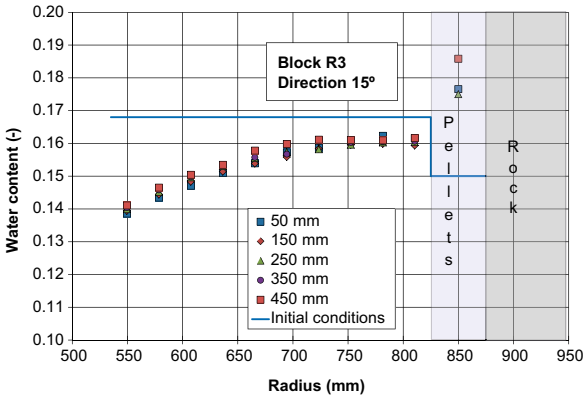
Block R3
Direction 15º
Water content (-)
Radius (mm)
50 mm
150 mm
250 mm
350 mm
450 mm
Initial conditions
Pellets
Rock

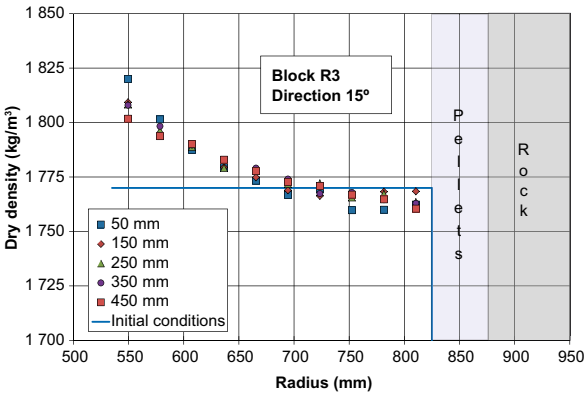
Block R3
Direction 15º
Dry density (kg/m³)
Radius (mm)
50 mm
150 mm
250 mm
350 mm
450 mm
Initial conditions
Pellets
Rock

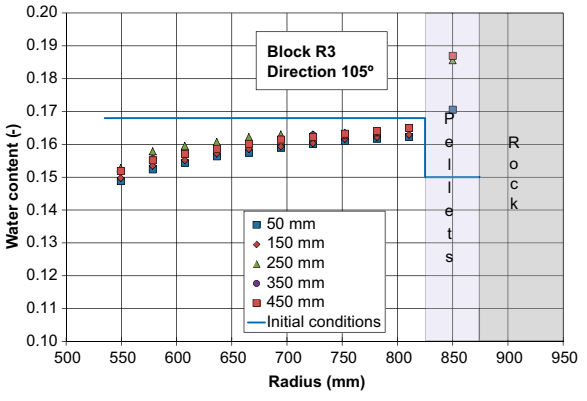
Block R3
Direction 105º
Water content (-)
Radius (mm)
50 mm
150 mm
250 mm
350 mm
450 mm
Initial conditions
Pellets
Rock

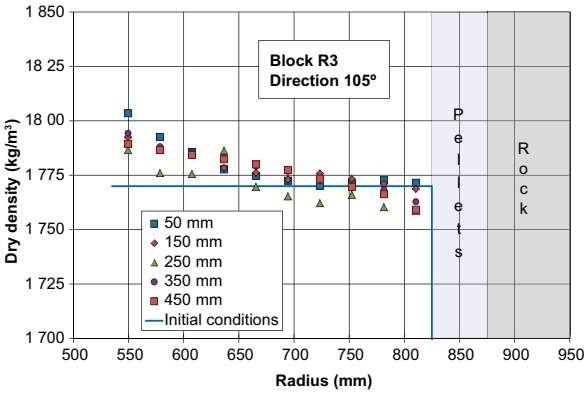
Block R3
Direction 105º
Dry density (kg/m³)
Radius (mm)
50 mm
150 mm
250 mm
350 mm
450 mm
Initial conditions
Pellets
Rock

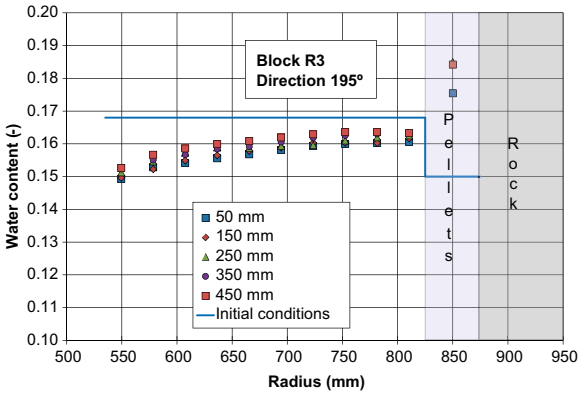
Block R3
Direction 195º
Water content (-)
Radius (mm)
50 mm
150 mm
250 mm
350 mm
450 mm
Initial conditions
Pellets
Rock

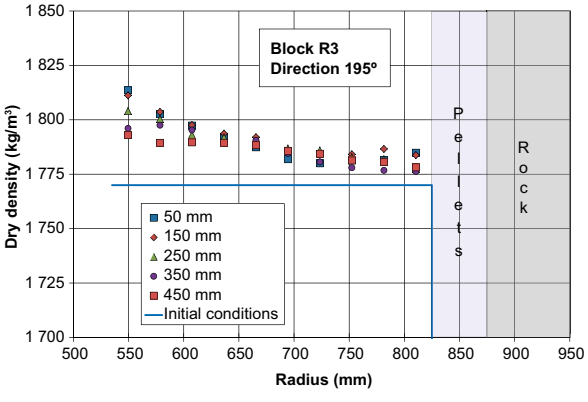
Block R3
Direction 195º
Dry density (kg/m³)
Radius (mm)
50 mm
150 mm
250 mm
350 mm
450 mm
Initial conditions
Pellets
Rock

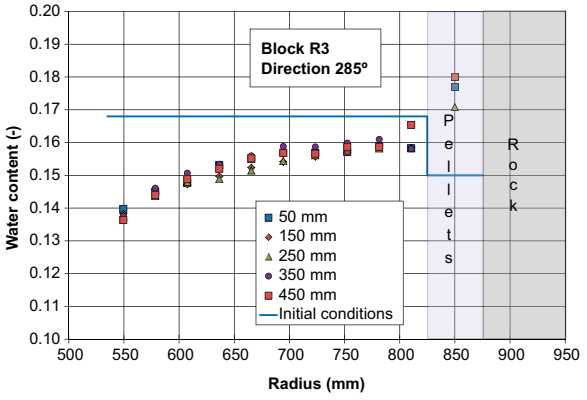
Block R3
Direction 285º
Water content (-)
Radius (mm)
50 mm
150 mm
250 mm
350 mm
450 mm
Initial conditions
Pellets
Rock

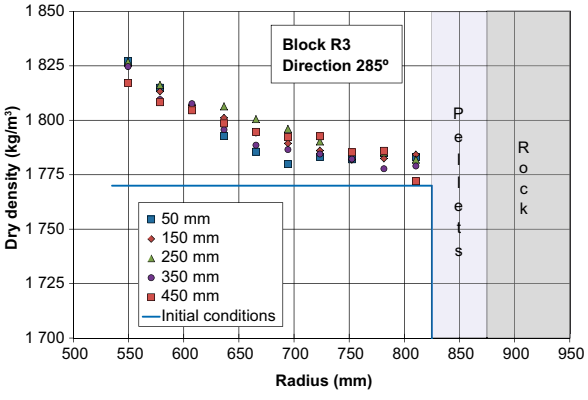
Block R3
Direction 285º
Dry density (kg/m³)
Radius (mm)
50 mm
150 mm
250 mm
350 mm
450 mm
Initial conditions
Pellets
Rock

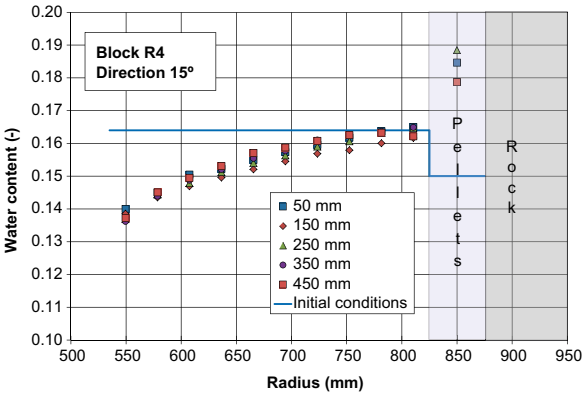
Block R4
Direction 15º
Water content (-)
Radius (mm)
50 mm
150 mm
250 mm
350 mm
450 mm
Initial conditions
Pellets
Rock

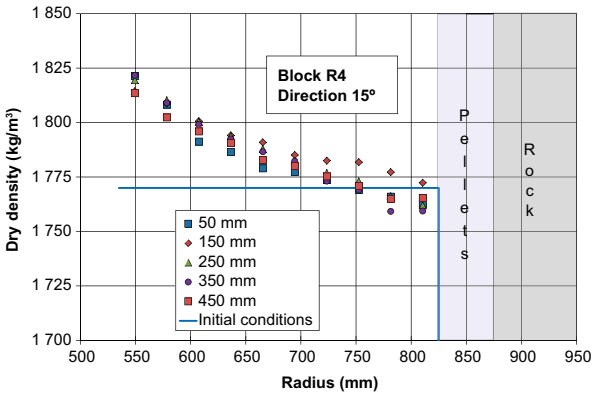
Block R4
Direction 15º
Dry density (kg/m³)
Radius (mm)
50 mm
150 mm
250 mm
350 mm
450 mm
Initial conditions
Pellets
Rock

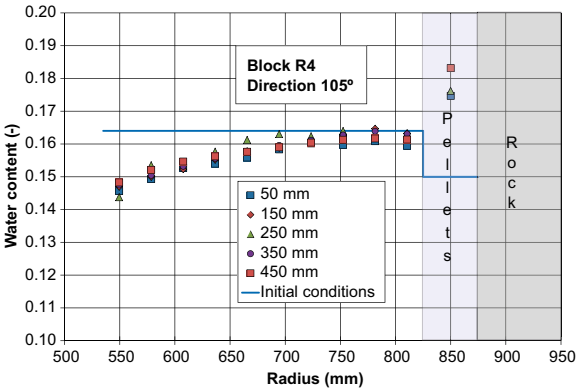
Block R4
Direction 105º
Water content (-)
Radius (mm)
50 mm
150 mm
250 mm
350 mm
450 mm
Initial conditions
Pellets
Rock

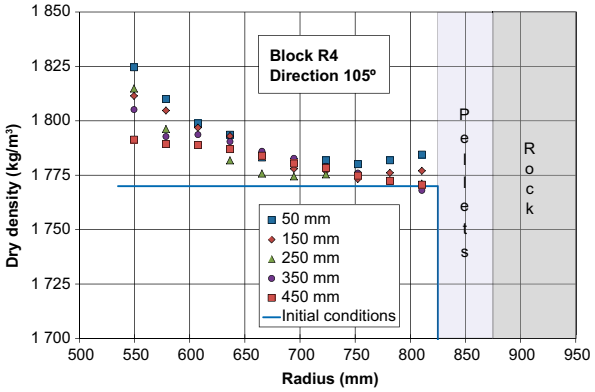
Block R4
Direction 105º
Dry density (kg/m³)
Radius (mm)
50 mm
150 mm
250 mm
350 mm
450 mm
Initial conditions
Pellets
Rock

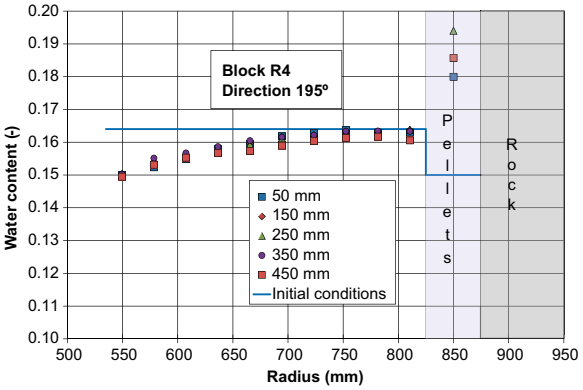
Block R4
Direction 195º
Water content (-)
Radius (mm)
50 mm
150 mm
250 mm
350 mm
450 mm
Initial conditions
Pellets
Rock

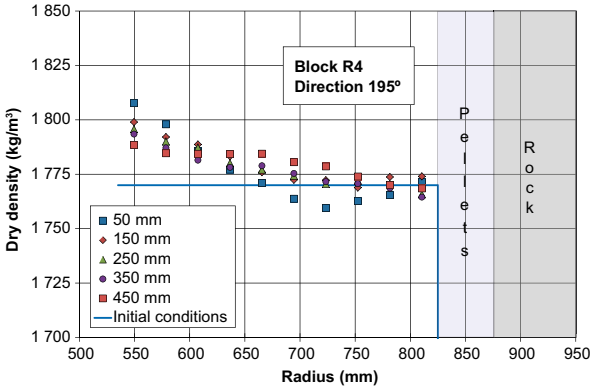
Block R4
Direction 195º
Dry density (kg/m³)
Radius (mm)
50 mm
150 mm
250 mm
350 mm
450 mm
Initial conditions
Pellets
Rock

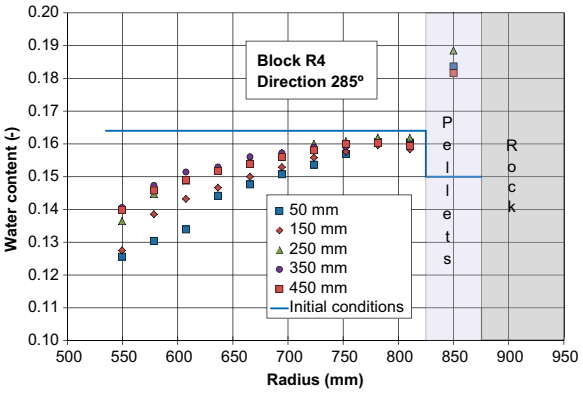
Block R4
Direction 285º
Water content (-)
Radius (mm)
50 mm
150 mm
250 mm
350 mm
450 mm
Initial conditions
Pellets
Rock

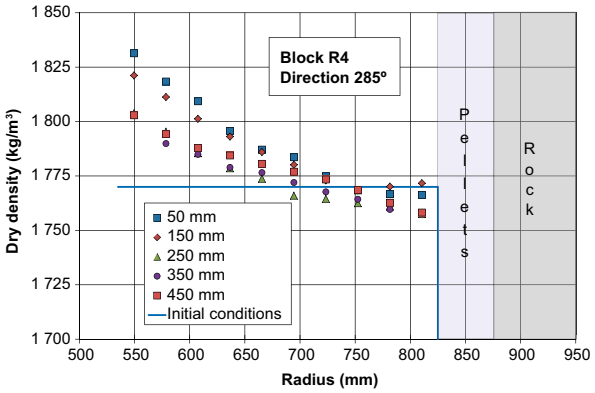
Block R4
Direction 285º
Dry density (kg/m³)
Radius (mm)
50 mm
150 mm
250 mm
350 mm
450 mm
Initial conditions
Pellets
Rock

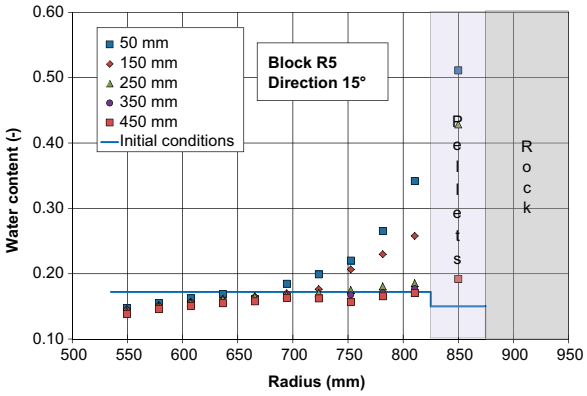
Block R5
Direction 15°
50 mm
150 mm
250 mm
350 mm
450 mm
Initial conditions
Water content (-)
Radius (mm)
Pellets
Rock

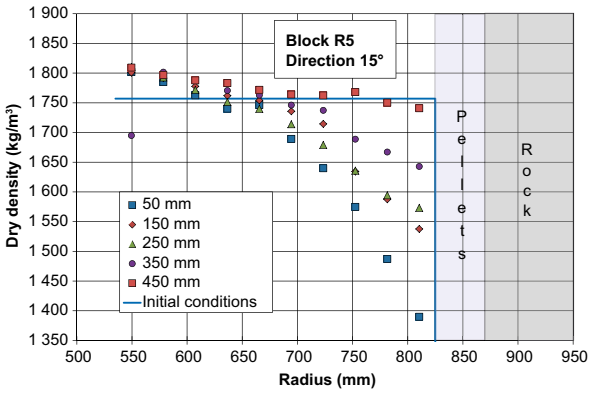
Block R5
Direction 15°
50 mm
150 mm
250 mm
350 mm
450 mm
Initial conditions
Dry density (kg/m³)
Radius (mm)
Pellets
Rock

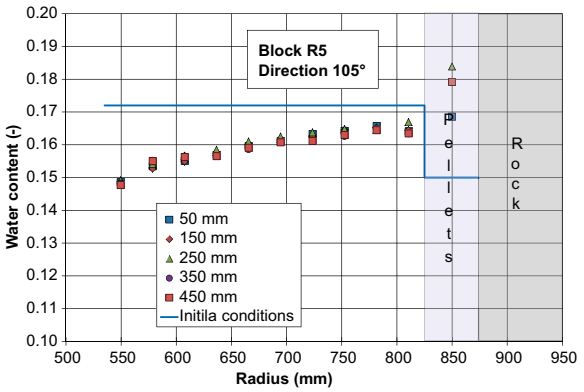
Block R5
Direction 105°
50 mm
150 mm
250 mm
350 mm
450 mm
Initila conditions
Water content (-)
Radius (mm)
Pellets
Rock

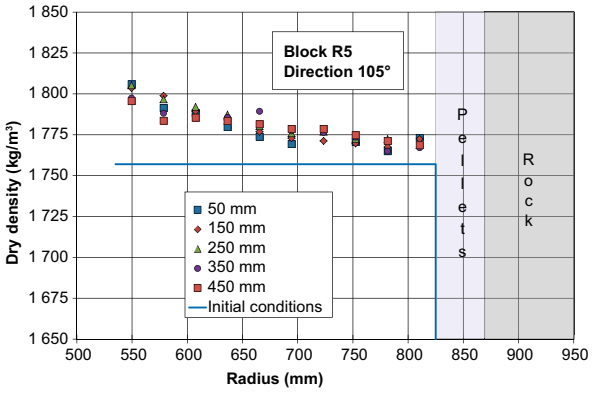
Block R5
Direction 105°
50 mm
150 mm
250 mm
350 mm
450 mm
Initial conditions
Dry density (kg/m³)
Radius (mm)
Pellets
Rock

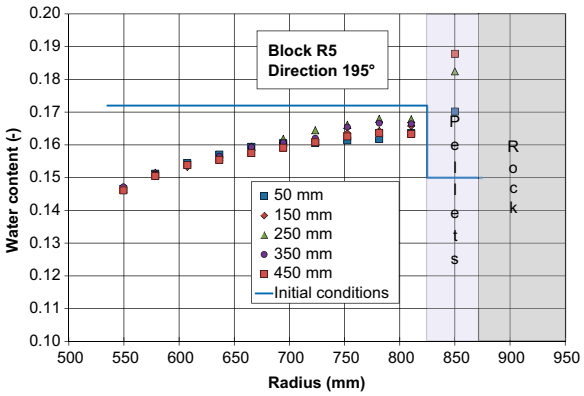
Block R5
Direction 195°
50 mm
150 mm
250 mm
350 mm
450 mm
Initial conditions
Water content (-)
Radius (mm)
Pellets
Rock

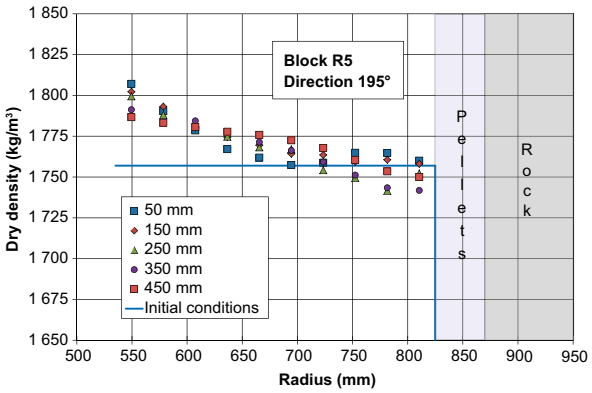
Block R5
Direction 195°
50 mm
150 mm
250 mm
350 mm
450 mm
Initial conditions
Dry density (kg/m³)
Radius (mm)
Pellets
Rock

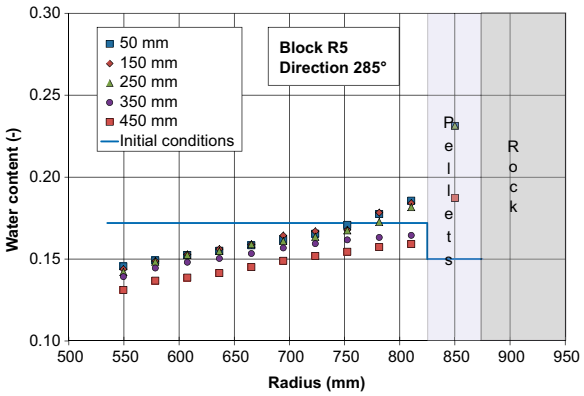
Block R5
Direction 285°
50 mm
150 mm
250 mm
350 mm
450 mm
Initial conditions
Water content (-)
Radius (mm)
Pellets
Rock

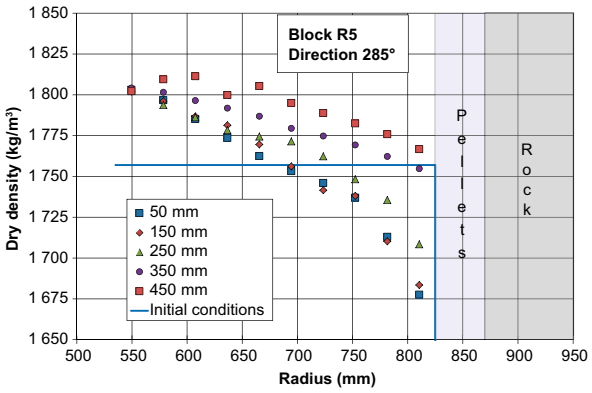
Block R5
Direction 285°
50 mm
150 mm
250 mm
350 mm
450 mm
Initial conditions
Dry density (kg/m³)
Radius (mm)
Pellets
Rock

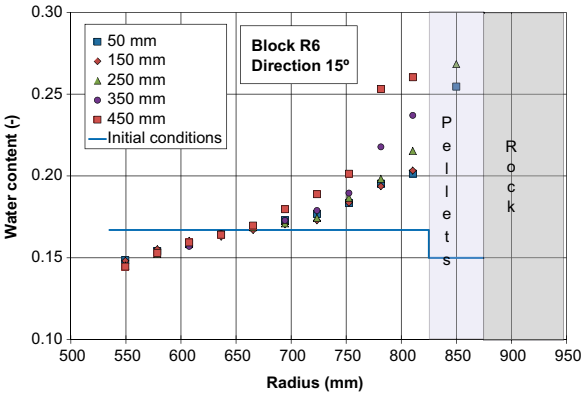
Block R6
Direction 15º
50 mm
150 mm
250 mm
350 mm
450 mm
Initial conditions
Water content (-)
Radius (mm)
Pellets
Rock

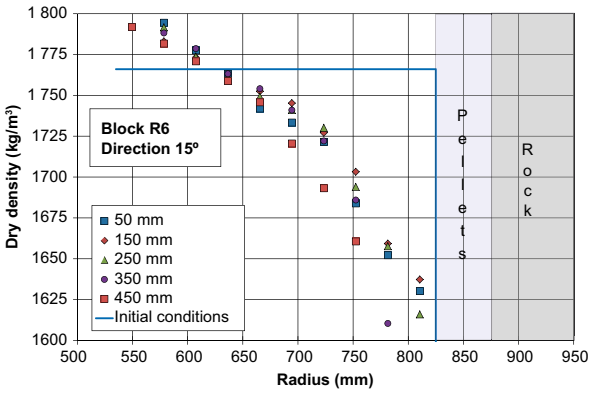
Block R6
Direction 15º
50 mm
150 mm
250 mm
350 mm
450 mm
Initial conditions
Dry density (kg/m³)
Radius (mm)
Pellets
Rock

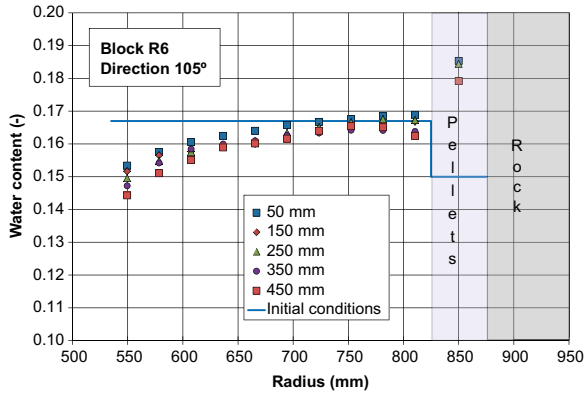
Block R6
Direction 105º
50 mm
150 mm
250 mm
350 mm
450 mm
Initial conditions
Water content (-)
Radius (mm)
Pellets
Rock

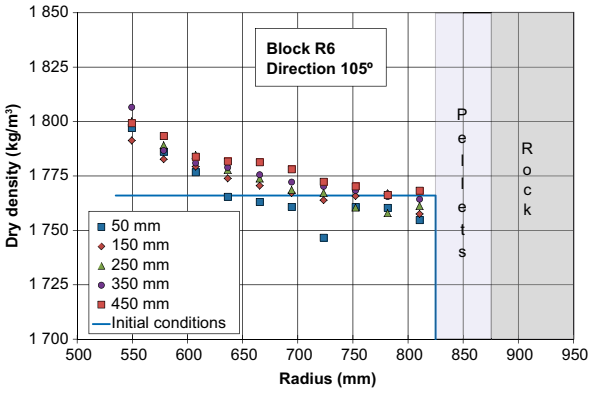
Block R6
Direction 105º
50 mm
150 mm
250 mm
350 mm
450 mm
Initial conditions
Dry density (kg/m³)
Radius (mm)
Pellets
Rock

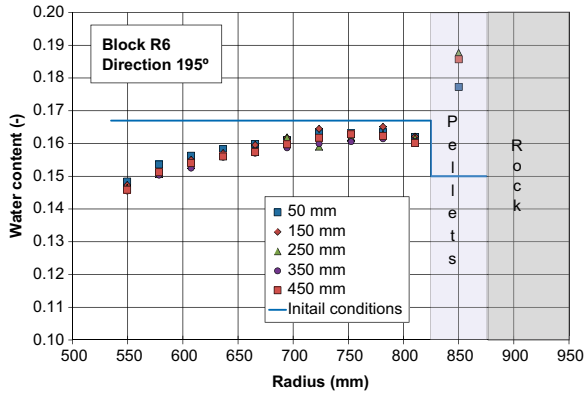
Block R6
Direction 195º
50 mm
150 mm
250 mm
350 mm
450 mm
Initail conditions
Water content (-)
Radius (mm)
Pellets
Rock

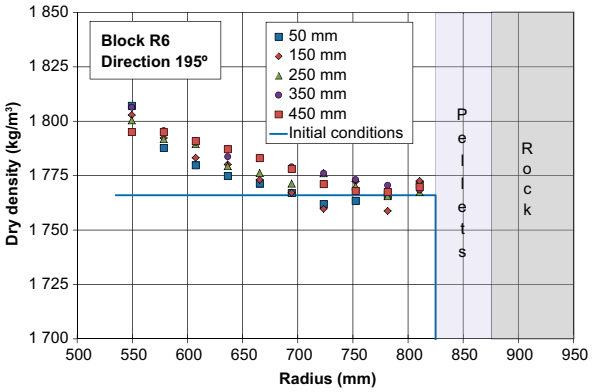
Block R6
Direction 195º
50 mm
150 mm
250 mm
350 mm
450 mm
Initial conditions
Dry density (kg/m³)
Radius (mm)
Pellets
Rock

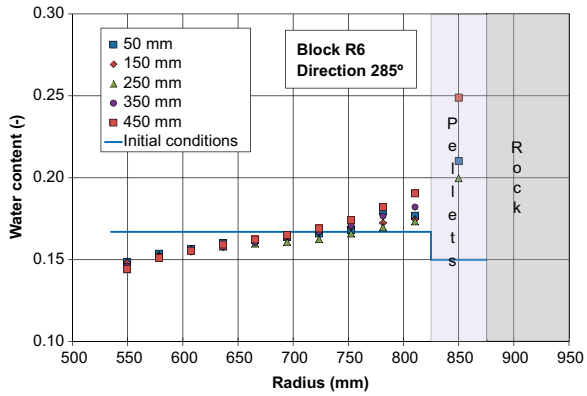
Block R6
Direction 285º
50 mm
150 mm
250 mm
350 mm
450 mm
Initial conditions
Water content (-)
Radius (mm)
Pellets
Rock

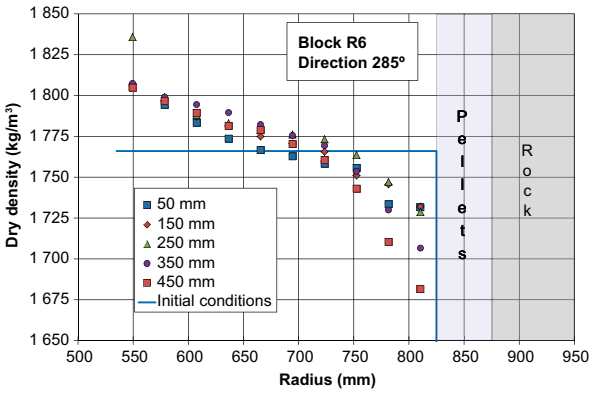
Block R6
Direction 285º
50 mm
150 mm
250 mm
350 mm
450 mm
Initial conditions
Dry density (kg/m³)
Radius (mm)
Pellets
Rock

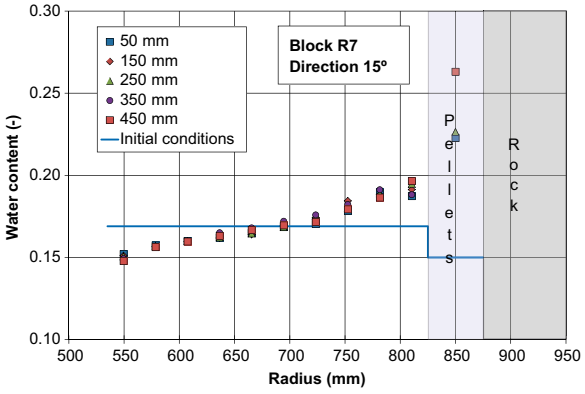
Block R7
Direction 15º
50 mm
150 mm
250 mm
350 mm
450 mm
Initial conditions
Water content (-)
Radius (mm)
Pellets
Rock

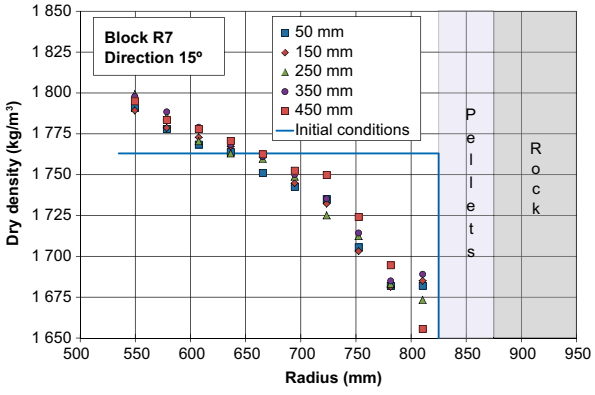
Block R7
Direction 15º
50 mm
150 mm
250 mm
350 mm
450 mm
Initial conditions
Dry density (kg/m³)
Radius (mm)
Pellets
Rock

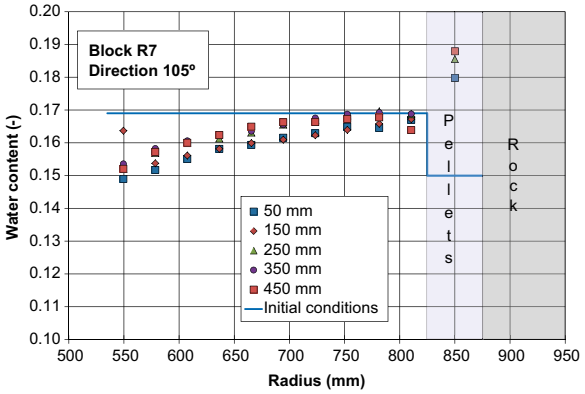
Block R7
Direction 105º
50 mm
150 mm
250 mm
350 mm
450 mm
Initial conditions
Water content (-)
Radius (mm)
Pellets
Rock

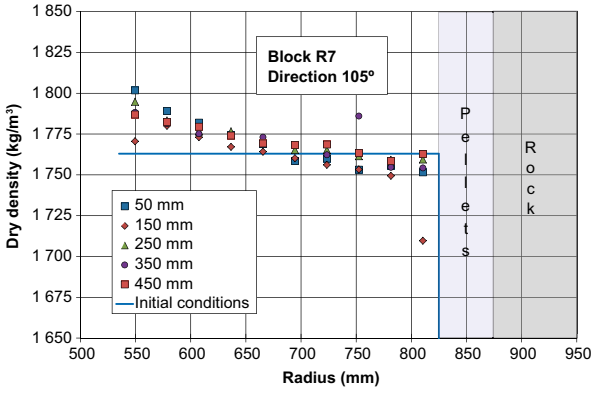
Block R7
Direction 105º
50 mm
150 mm
250 mm
350 mm
450 mm
Initial conditions
Dry density (kg/m³)
Radius (mm)
Pellets
Rock

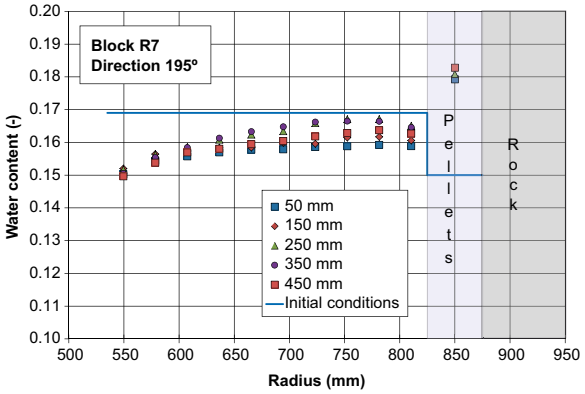
Block R7
Direction 195º
50 mm
150 mm
250 mm
350 mm
450 mm
Initial conditions
Water content (-)
Radius (mm)
Pellets
Rock

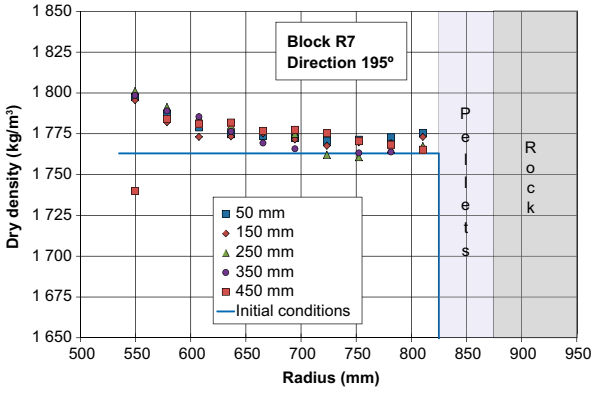
Block R7
Direction 195º
50 mm
150 mm
250 mm
350 mm
450 mm
Initial conditions
Dry density (kg/m³)
Radius (mm)
Pellets
Rock

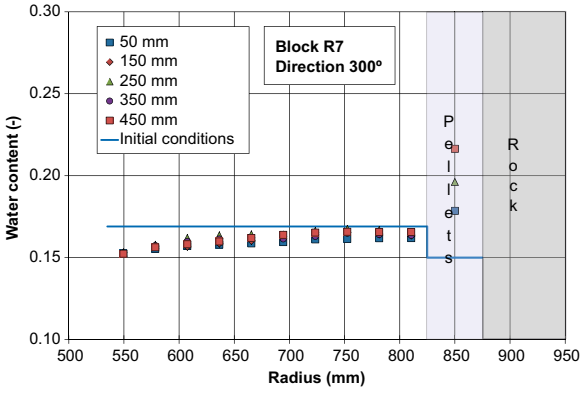
Block R7
Direction 300º
50 mm
150 mm
250 mm
350 mm
450 mm
Initial conditions
Water content (-)
Radius (mm)
Pellets
Rock

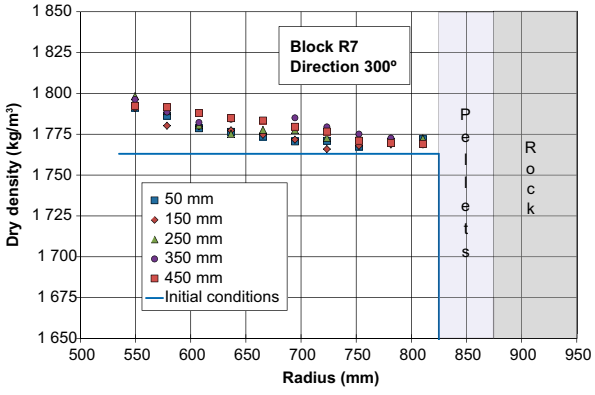
Block R7
Direction 300º
50 mm
150 mm
250 mm
350 mm
450 mm
Initial conditions
Dry density (kg/m³)
Radius (mm)
Pellets
Rock

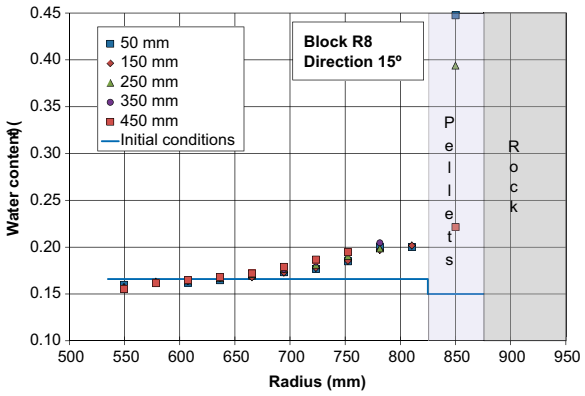
Block R8
Direction 15º
50 mm
150 mm
250 mm
350 mm
450 mm
Initial conditions
Pellets
Rock
Water content (-)
Radius (mm)

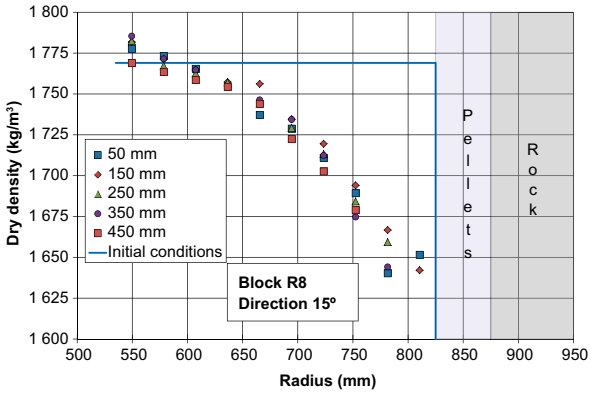
Block R8
Direction 15º
50 mm
150 mm
250 mm
350 mm
450 mm
Initial conditions
Pellets
Rock
Dry density (kg/m³)
Radius (mm)

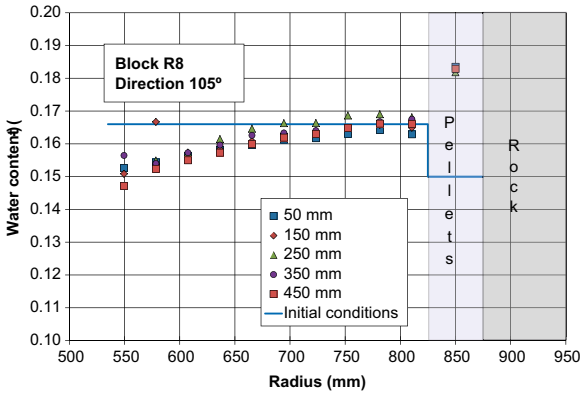
Block R8
Direction 105º
50 mm
150 mm
250 mm
350 mm
450 mm
Initial conditions
Pellets
Rock
Water content (-)
Radius (mm)

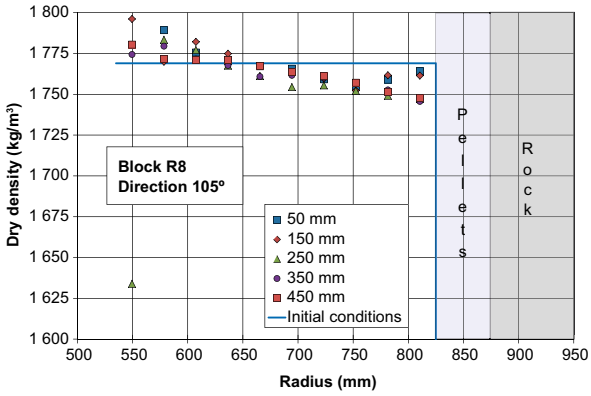
Block R8
Direction 105º
50 mm
150 mm
250 mm
350 mm
450 mm
Initial conditions
Pellets
Rock
Dry density (kg/m³)
Radius (mm)

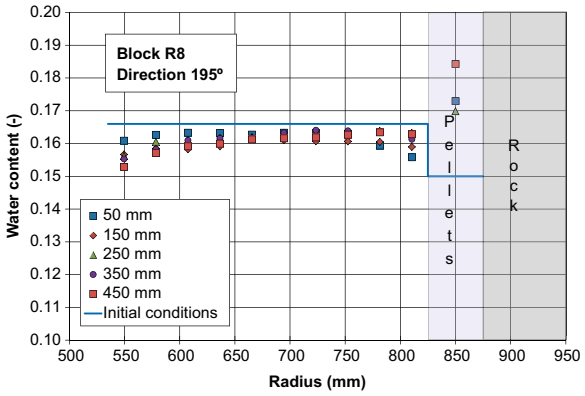
Block R8
Direction 195º
50 mm
150 mm
250 mm
350 mm
450 mm
Initial conditions
Pellets
Rock
Water content (-)
Radius (mm)

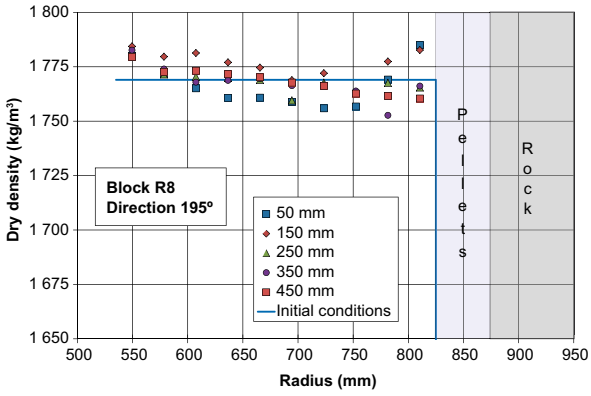
Block R8
Direction 195º
50 mm
150 mm
250 mm
350 mm
450 mm
Initial conditions
Pellets
Rock
Dry density (kg/m³)
Radius (mm)

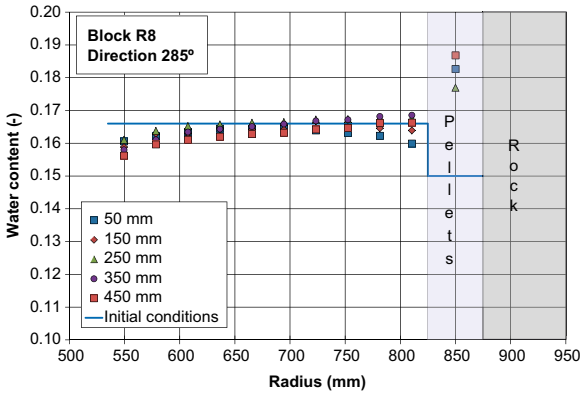
Block R8
Direction 285º
50 mm
150 mm
250 mm
350 mm
450 mm
Initial conditions
Pellets
Rock
Water content (-)
Radius (mm)

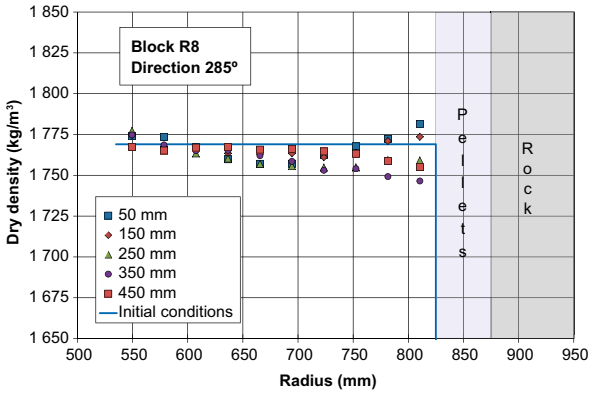
Block R8
Direction 285º
50 mm
150 mm
250 mm
350 mm
450 mm
Initial conditions
Pellets
Rock
Dry density (kg/m³)
Radius (mm)

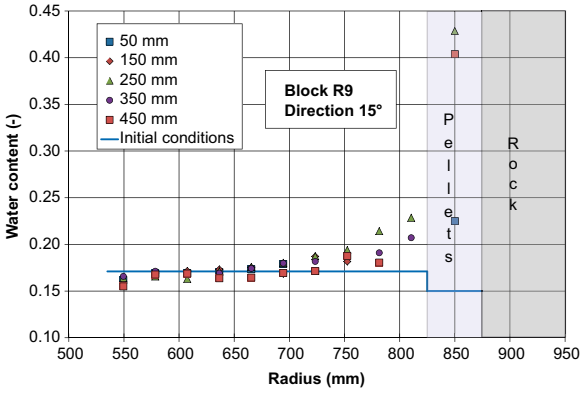
Block R9
Direction 15°
50 mm
150 mm
250 mm
350 mm
450 mm
Initial conditions
Pellets
Rock
Water content (-)
Radius (mm)

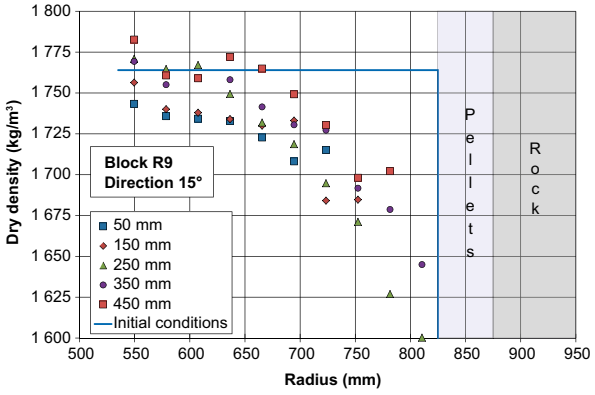
Block R9
Direction 15°
50 mm
150 mm
250 mm
350 mm
450 mm
Initial conditions
Pellets
Rock
Dry density (kg/m³)
Radius (mm)

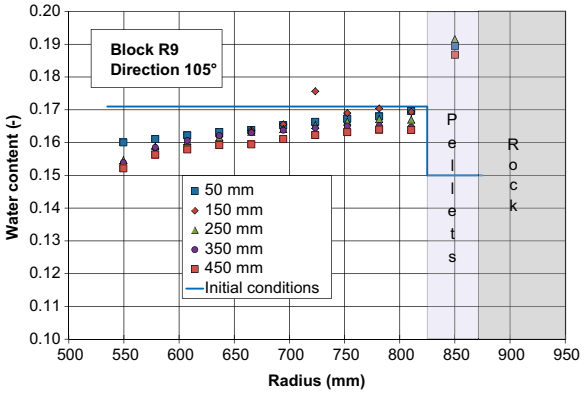
Block R9
Direction 105°
50 mm
150 mm
250 mm
350 mm
450 mm
Initial conditions
Pellets
Rock
Water content (-)
Radius (mm)

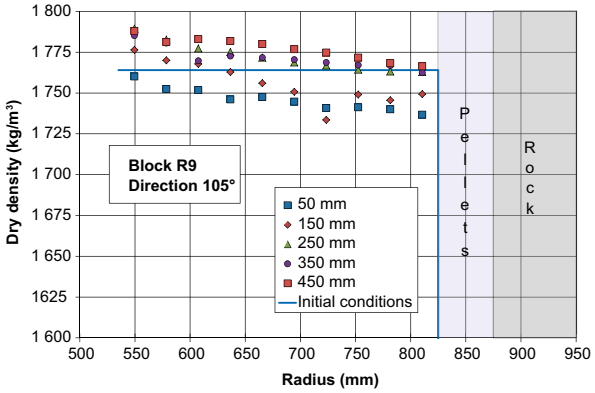
Block R9
Direction 105°
50 mm
150 mm
250 mm
350 mm
450 mm
Initial conditions
Pellets
Rock
Dry density (kg/m³)
Radius (mm)

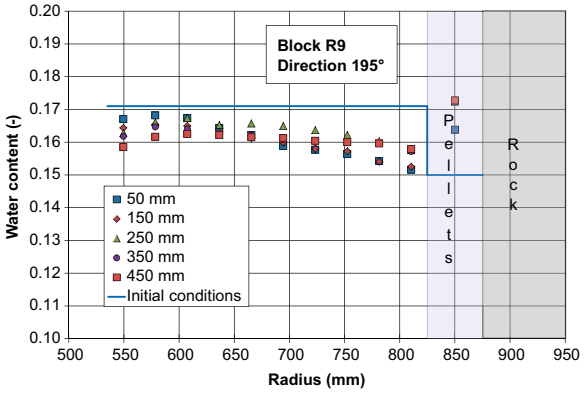
Block R9
Direction 195°
50 mm
150 mm
250 mm
350 mm
450 mm
Initial conditions
Pellets
Rock
Water content (-)
Radius (mm)

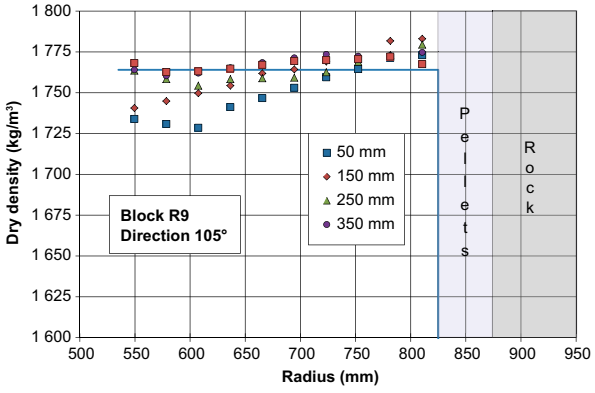
Block R9
Direction 105°
50 mm
150 mm
250 mm
350 mm
Pellets
Rock
Dry density (kg/m³)
Radius (mm)

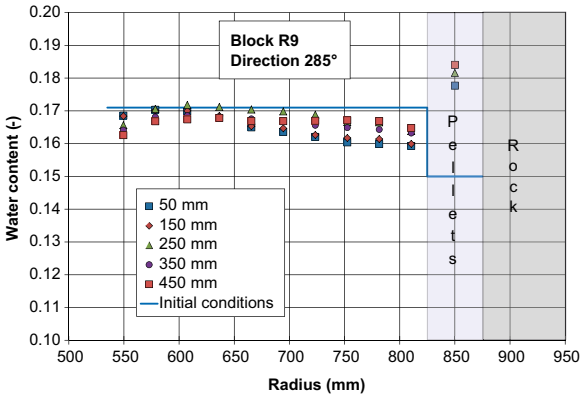
Block R9
Direction 285°
50 mm
150 mm
250 mm
350 mm
450 mm
Initial conditions
Pellets
Rock
Water content (-)
Radius (mm)

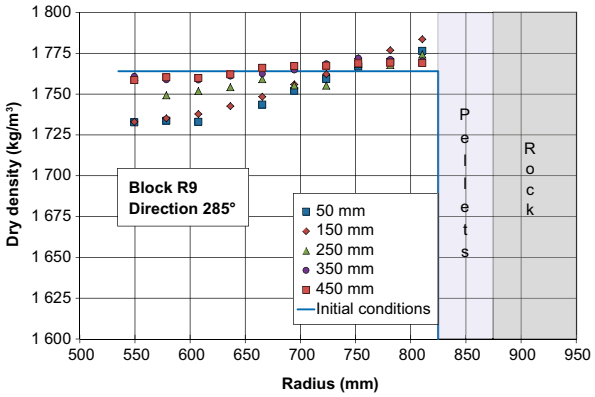
Block R9
Direction 285°
50 mm
150 mm
250 mm
350 mm
450 mm
Initial conditions
Pellets
Rock
Dry density (kg/m³)
Radius (mm)

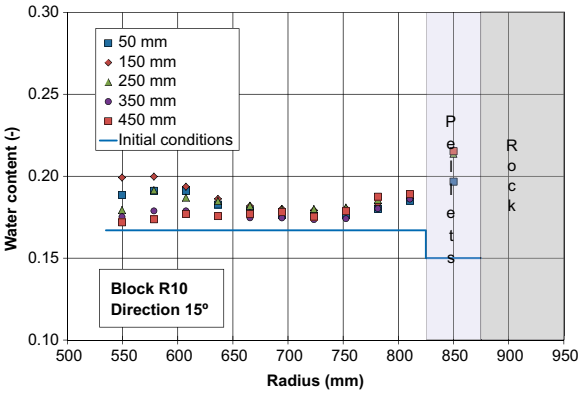
Water content (-)
Radius (mm)
50 mm
150 mm
250 mm
350 mm
450 mm
Initial conditions
Block R10
Direction 15º
Pellets
Rock

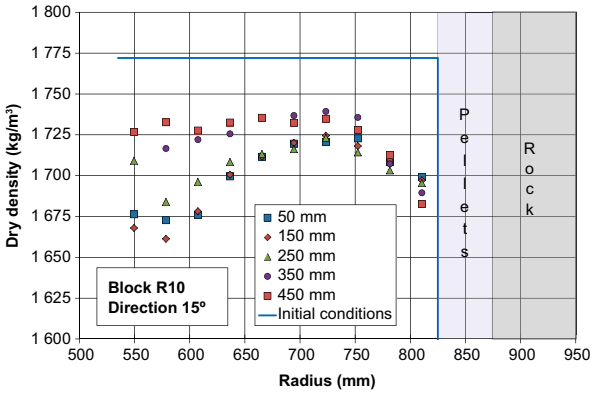
Dry density (kg/m³)
Radius (mm)
50 mm
150 mm
250 mm
350 mm
450 mm
Initial conditions
Block R10
Direction 15º
Pellets
Rock

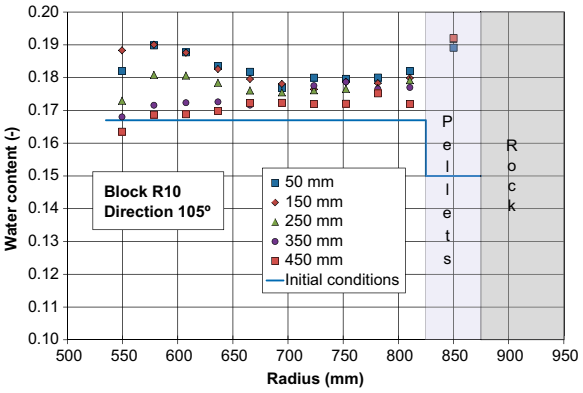
Water content (-)
Radius (mm)
50 mm
150 mm
250 mm
350 mm
450 mm
Initial conditions
Block R10
Direction 105º
Pellets
Rock

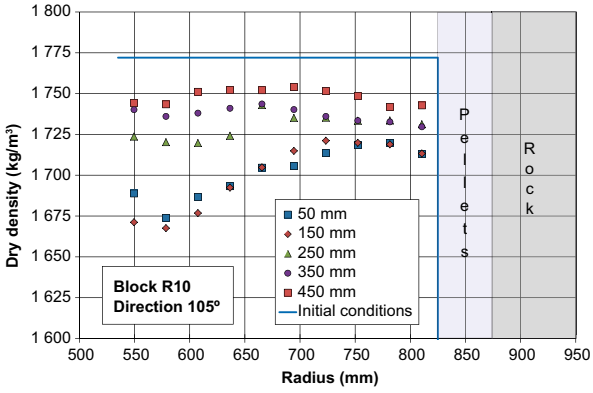
Dry density (kg/m³)
Radius (mm)
50 mm
150 mm
250 mm
350 mm
450 mm
Initial conditions
Block R10
Direction 105º
Pellets
Rock

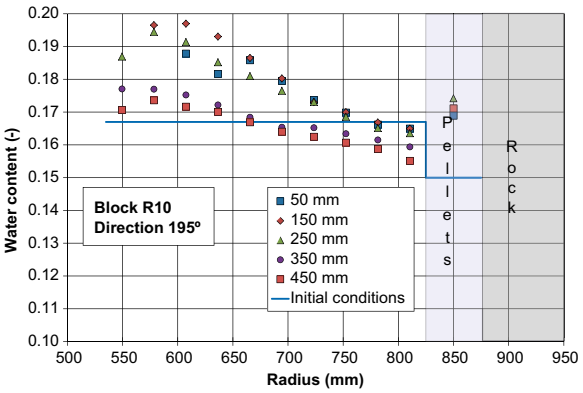
Water content (-)
Radius (mm)
50 mm
150 mm
250 mm
350 mm
450 mm
Initial conditions
Block R10
Direction 195º
Pellets
Rock

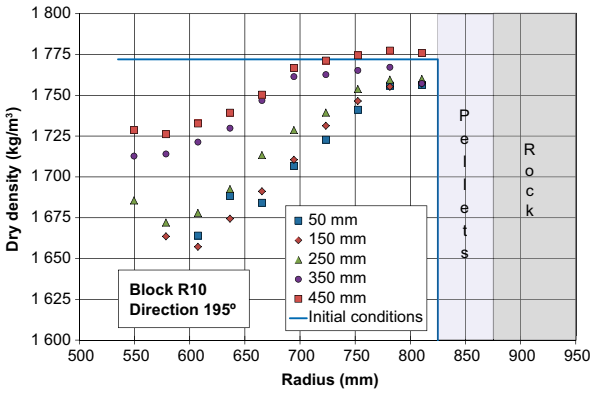
Dry density (kg/m³)
Radius (mm)
50 mm
150 mm
250 mm
350 mm
450 mm
Initial conditions
Block R10
Direction 195º
Pellets
Rock

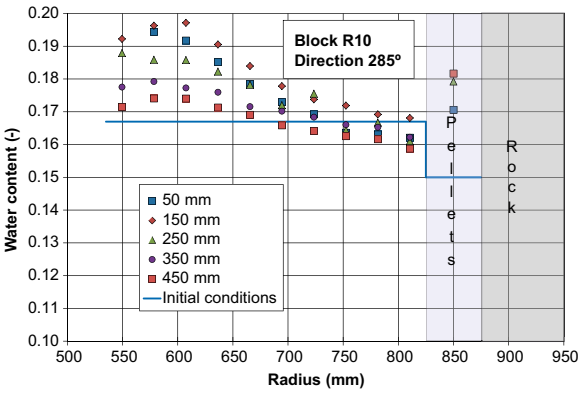
Water content (-)
Radius (mm)
50 mm
150 mm
250 mm
350 mm
450 mm
Initial conditions
Block R10
Direction 285º
Pellets
Rock

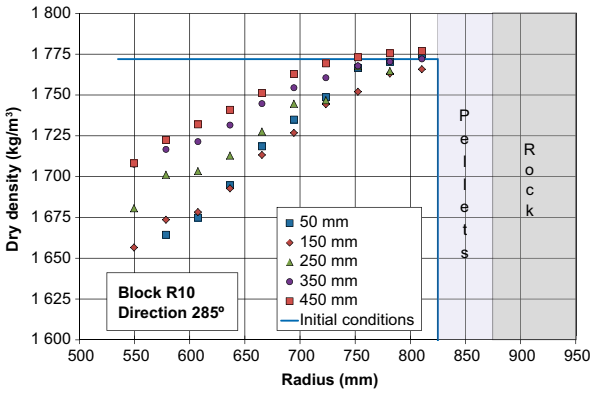
Dry density (kg/m³)
Radius (mm)
50 mm
150 mm
250 mm
350 mm
450 mm
Initial conditions
Block R10
Direction 285º
Pellets
Rock

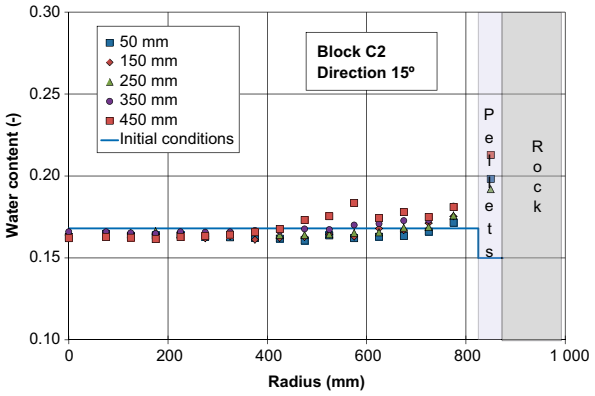
Block C2
Direction 15º
50 mm
150 mm
250 mm
350 mm
450 mm
Initial conditions
Water content (-)
Radius (mm)
Pellets
Rock

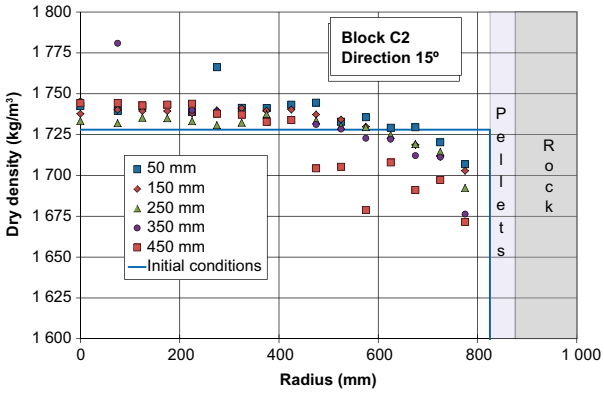
Block C2
Direction 15º
50 mm
150 mm
250 mm
350 mm
450 mm
Initial conditions
Dry density (kg/m³)
Radius (mm)
Pellets
Rock

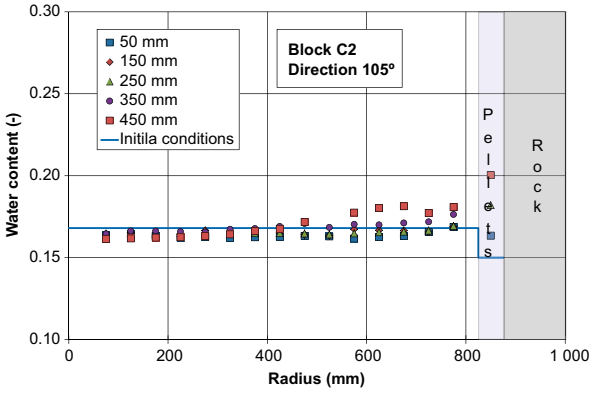
Block C2
Direction 105º
50 mm
150 mm
250 mm
350 mm
450 mm
Initila conditions
Water content (-)
Radius (mm)
Pellets
Rock

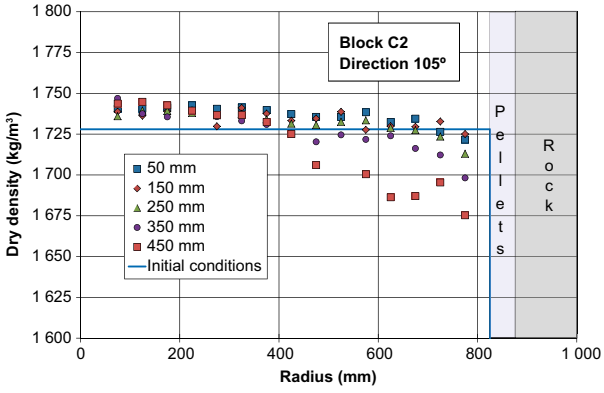
Block C2
Direction 105º
50 mm
150 mm
250 mm
350 mm
450 mm
Initial conditions
Dry density (kg/m³)
Radius (mm)
Pellets
Rock

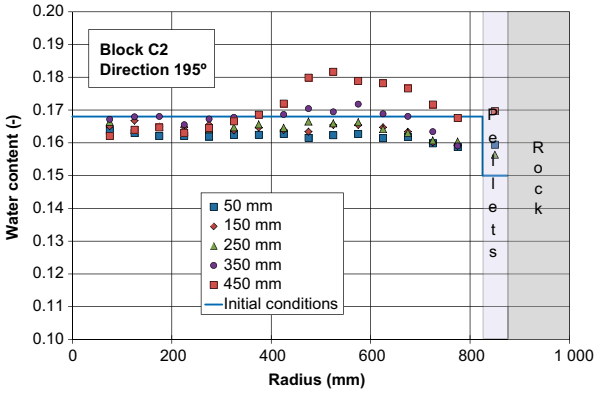
Block C2
Direction 195º
50 mm
150 mm
250 mm
350 mm
450 mm
Initial conditions
Water content (-)
Radius (mm)
Pellets
Rock

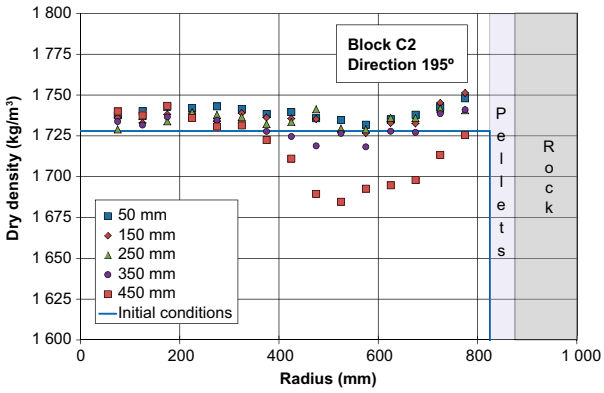
Block C2
Direction 195º
50 mm
150 mm
250 mm
350 mm
450 mm
Initial conditions
Dry density (kg/m³)
Radius (mm)
Pellets
Rock

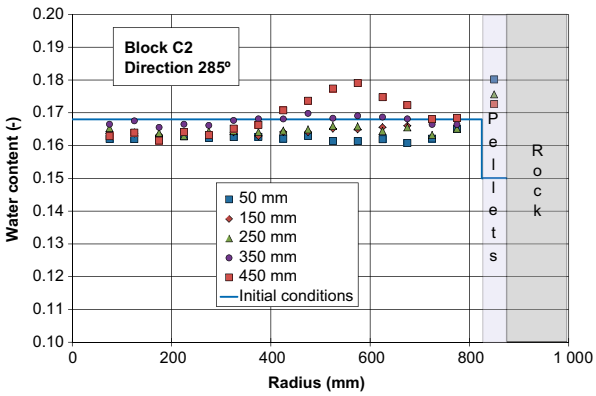
Block C2
Direction 285º
50 mm
150 mm
250 mm
350 mm
450 mm
Initial conditions
Water content (-)
Radius (mm)
Pellets
Rock

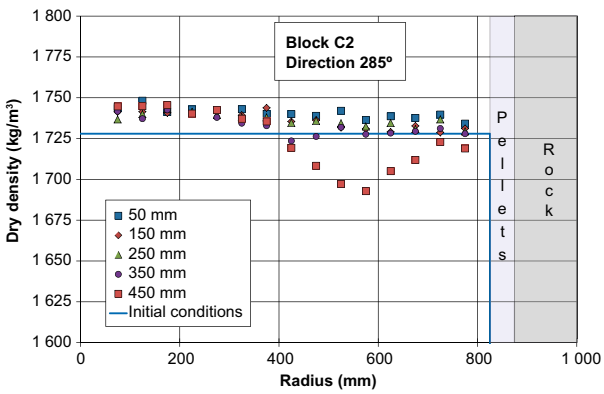
Block C2
Direction 285º
50 mm
150 mm
250 mm
350 mm
450 mm
Initial conditions
Dry density (kg/m³)
Radius (mm)
Pellets
Rock

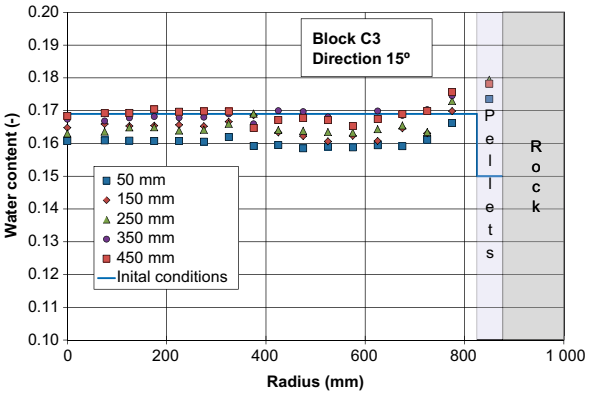
Block C3
Direction 15º
Water content (-)
Radius (mm)
50 mm
150 mm
250 mm
350 mm
450 mm
Inital conditions
Pellets
Rock

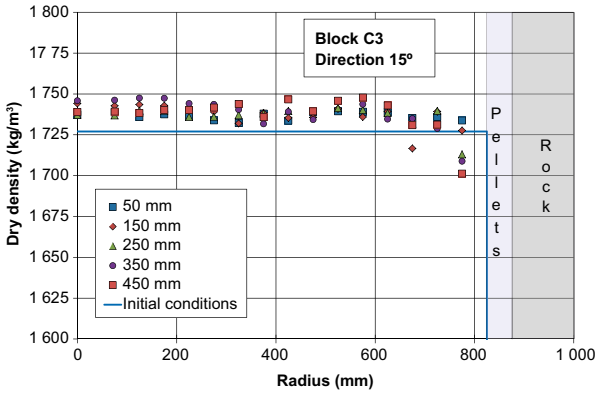
Block C3
Direction 15º
Dry density (kg/m³)
Radius (mm)
50 mm
150 mm
250 mm
350 mm
450 mm
Initial conditions
Pellets
Rock

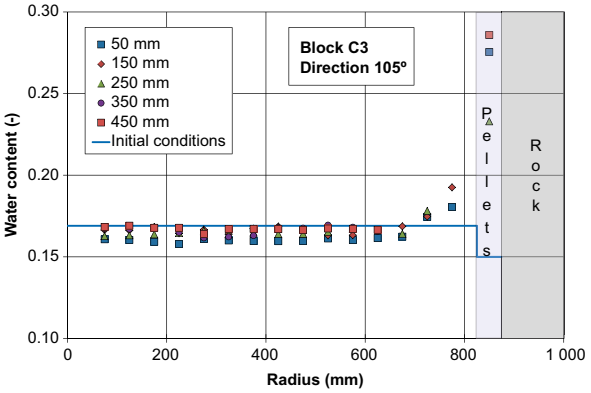
Block C3
Direction 105º
Water content (-)
Radius (mm)
50 mm
150 mm
250 mm
350 mm
450 mm
Initial conditions
Pellets
Rock

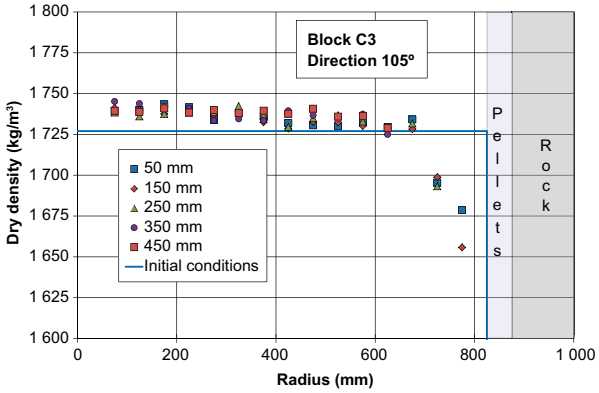
Block C3
Direction 105º
Dry density (kg/m³)
Radius (mm)
50 mm
150 mm
250 mm
350 mm
450 mm
Initial conditions
Pellets
Rock

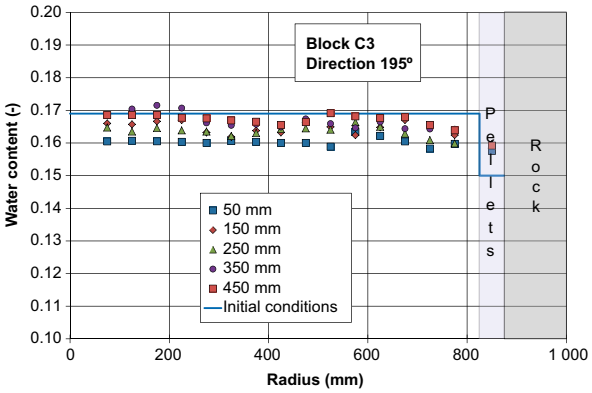
Block C3
Direction 195º
Water content (-)
Radius (mm)
50 mm
150 mm
250 mm
350 mm
450 mm
Initial conditions
Pellets
Rock

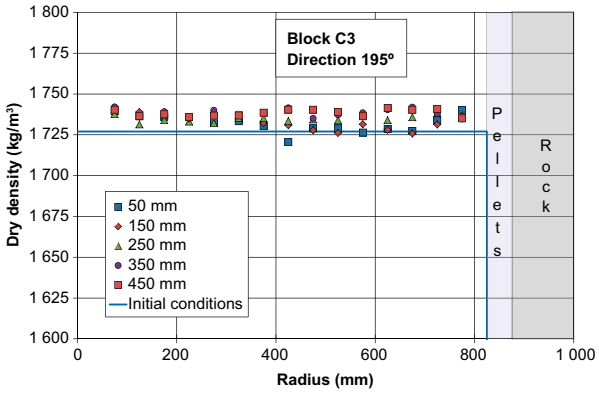
Block C3
Direction 195º
Dry density (kg/m³)
Radius (mm)
50 mm
150 mm
250 mm
350 mm
450 mm
Initial conditions
Pellets
Rock

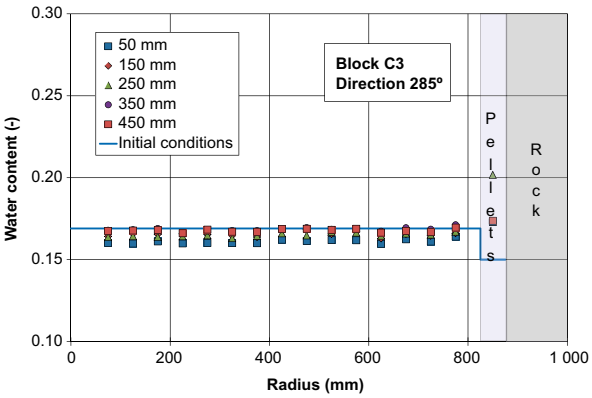
Block C3
Direction 285º
Water content (-)
Radius (mm)
50 mm
150 mm
250 mm
350 mm
450 mm
Initial conditions
Pellets
Rock

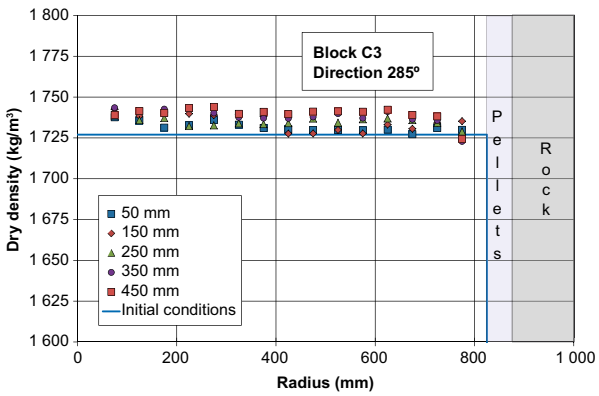
Block C3
Direction 285º
Dry density (kg/m³)
Radius (mm)
50 mm
150 mm
250 mm
350 mm
450 mm
Initial conditions
Pellets
Rock

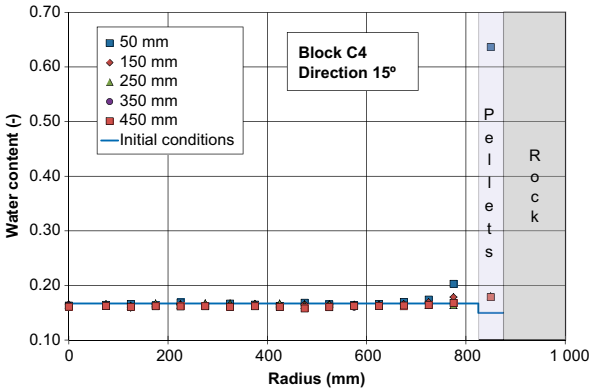
Block C4
Direction 15º
50 mm
150 mm
250 mm
350 mm
450 mm
Initial conditions
Water content (-)
Radius (mm)
Pellets
Rock

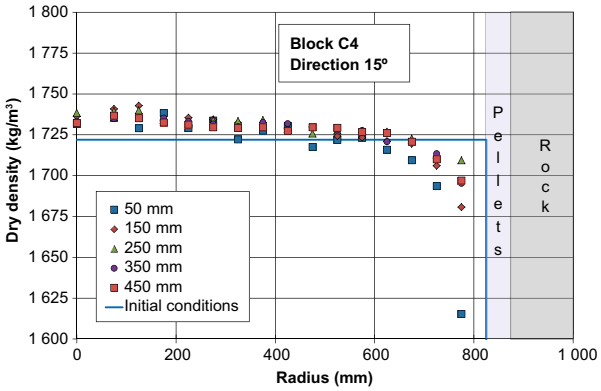
Block C4
Direction 15º
50 mm
150 mm
250 mm
350 mm
450 mm
Initial conditions
Dry density (kg/m³)
Radius (mm)
Pellets
Rock

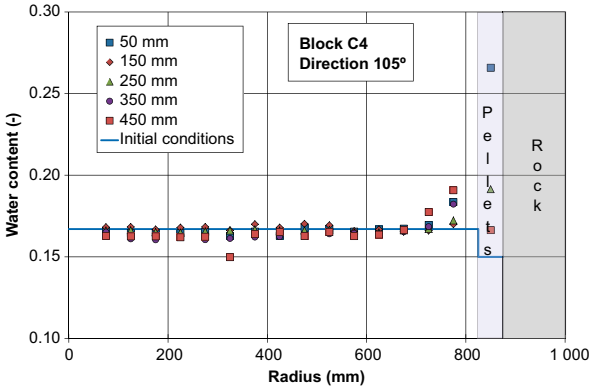
Block C4
Direction 105º
50 mm
150 mm
250 mm
350 mm
450 mm
Initial conditions
Water content (-)
Radius (mm)
Pellets
Rock

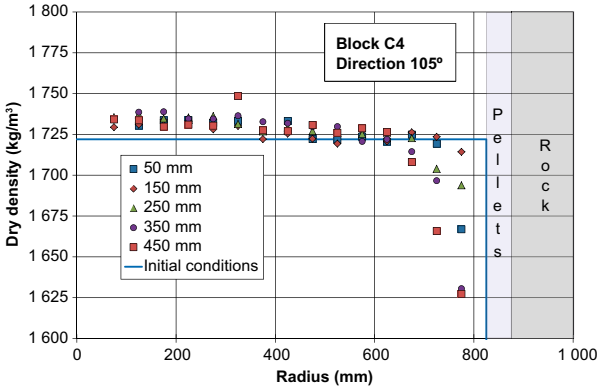
Block C4
Direction 105º
50 mm
150 mm
250 mm
350 mm
450 mm
Initial conditions
Dry density (kg/m³)
Radius (mm)
Pellets
Rock

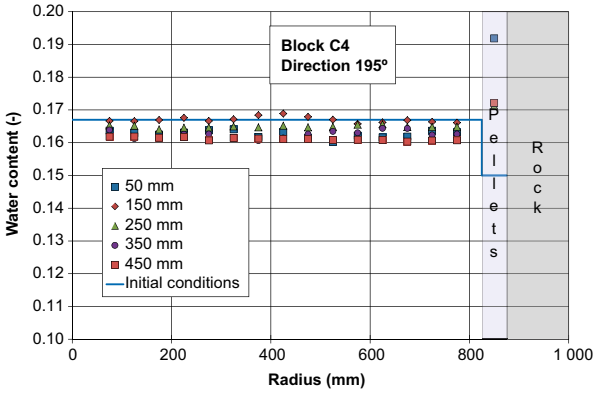
Block C4
Direction 195º
50 mm
150 mm
250 mm
350 mm
450 mm
Initial conditions
Water content (-)
Radius (mm)
Pellets
Rock

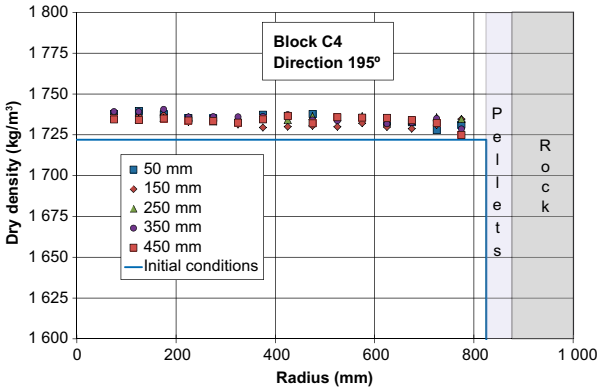
Block C4
Direction 195º
50 mm
150 mm
250 mm
350 mm
450 mm
Initial conditions
Dry density (kg/m³)
Radius (mm)
Pellets
Rock

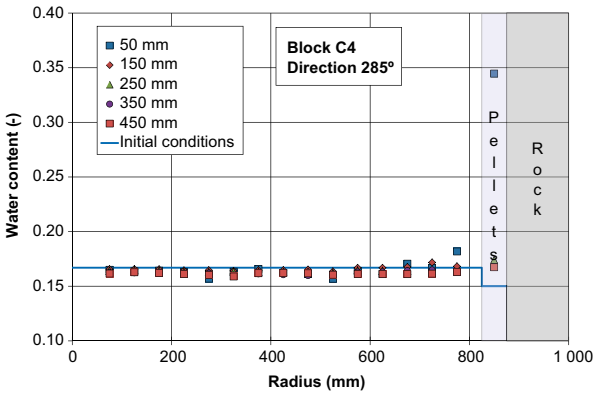
Block C4
Direction 285º
50 mm
150 mm
250 mm
350 mm
450 mm
Initial conditions
Water content (-)
Radius (mm)
Pellets
Rock

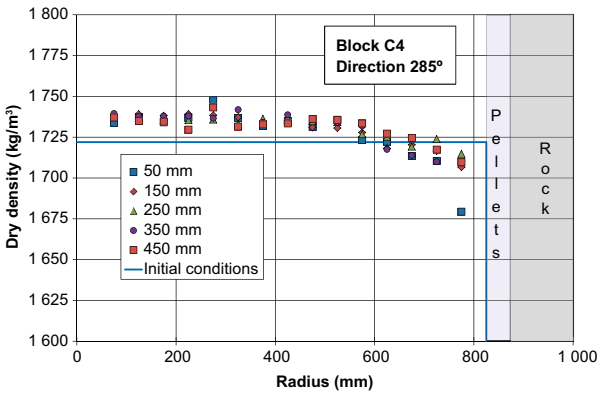
Block C4
Direction 285º
50 mm
150 mm
250 mm
350 mm
450 mm
Initial conditions
Dry density (kg/m³)
Radius (mm)
Pellets
Rock

Appendix 4

Temperature measurements made in Test 2

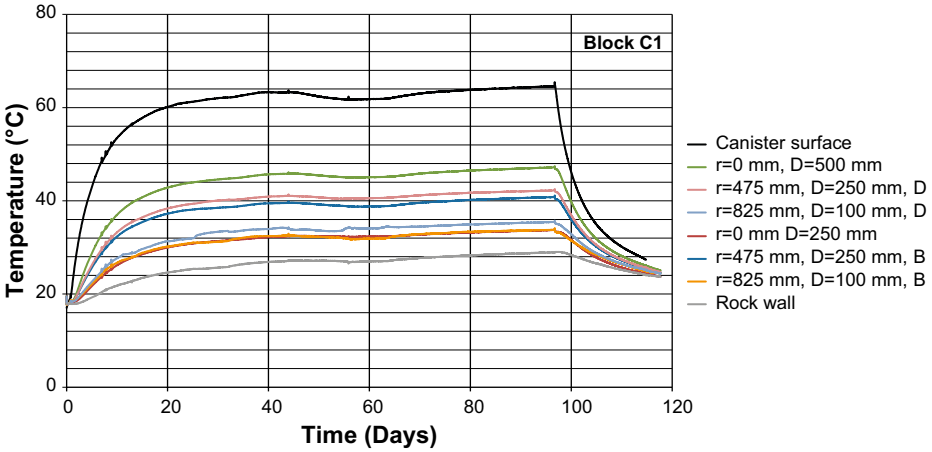

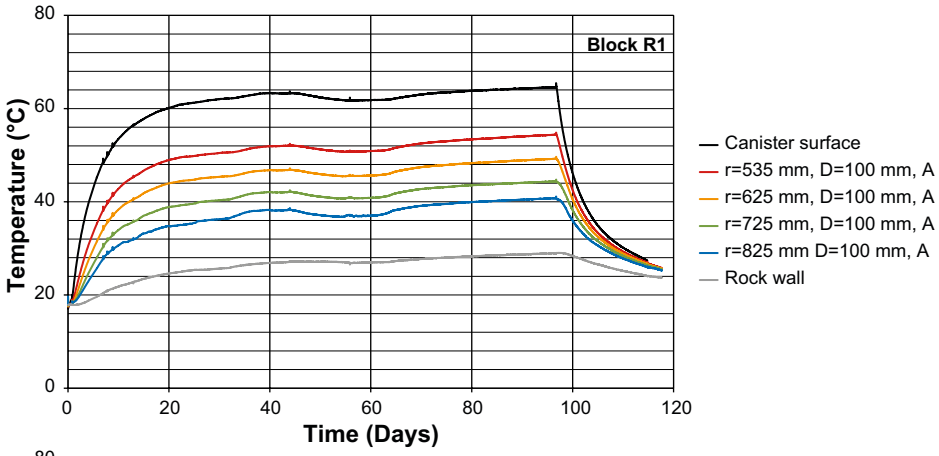
Block R1
Temperature (°C)
Time (Days)
0
20
40
60
80
100
120
Canister surface
r=535 mm, D=100 mm, A
r=625 mm, D=100 mm, A
r=725 mm, D=100 mm, A
r=825 mm D=100 mm, A
Rock wall

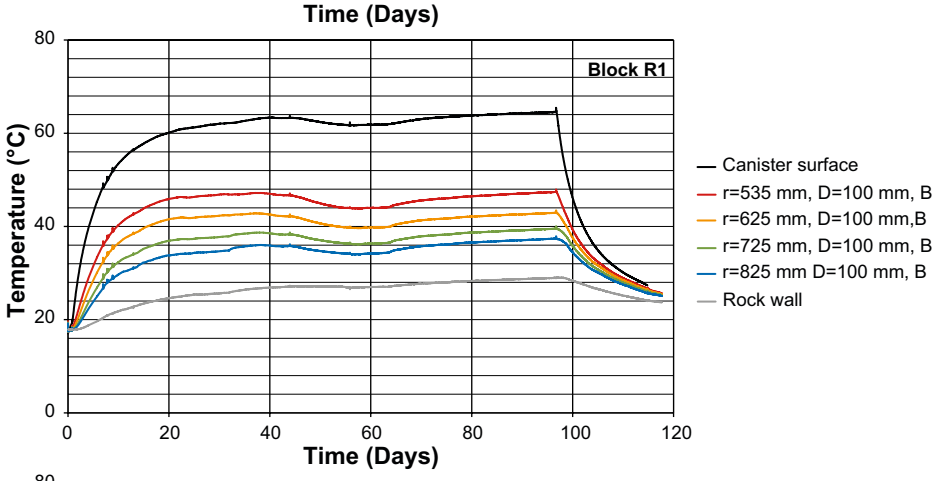
Block R1
Temperature (°C)
Time (Days)
0
20
40
60
80
100
120
Canister surface
r=535 mm, D=100 mm, B
r=625 mm, D=100 mm,B
r=725 mm, D=100 mm, B
r=825 mm D=100 mm, B
Rock wall

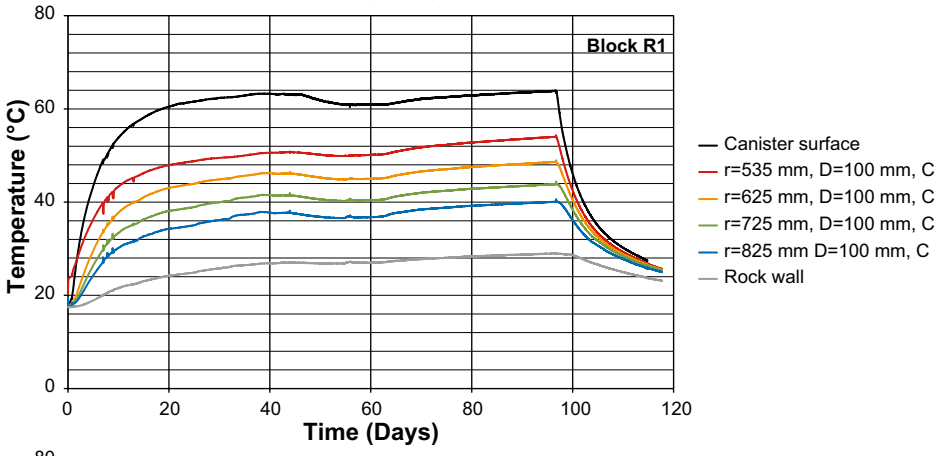
Block R1
Temperature (°C)
Time (Days)
0
20
40
60
80
100
120
Canister surface
r=535 mm, D=100 mm, C
r=625 mm, D=100 mm, C
r=725 mm, D=100 mm, C
r=825 mm D=100 mm, C
Rock wall

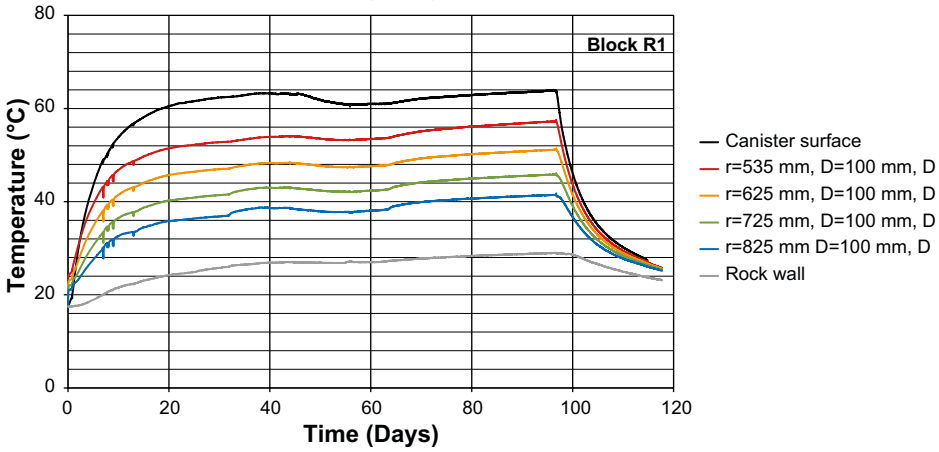
Block R1
Temperature (°C)
Time (Days)
0
20
40
60
80
100
120
Canister surface
r=535 mm, D=100 mm, D
r=625 mm, D=100 mm, D
r=725 mm, D=100 mm, D
r=825 mm D=100 mm, D
Rock wall

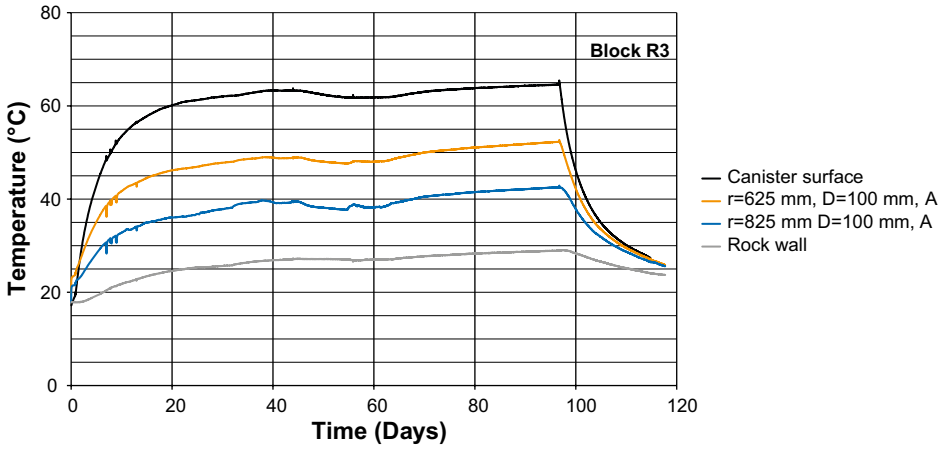
Block R3
Temperature (°C)
Time (Days)
0
20
40
60
80
100
120
Canister surface
r=625 mm, D=100 mm, A
r=825 mm D=100 mm, A
Rock wall

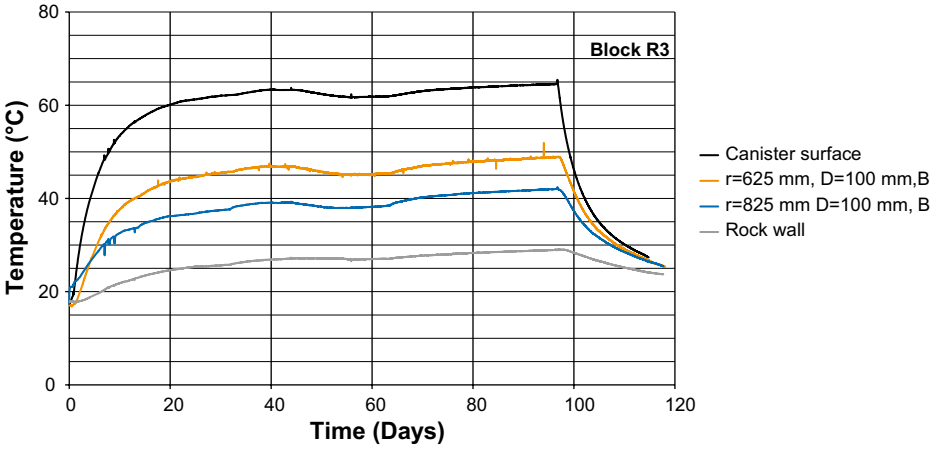
Block R3
Temperature (°C)
Time (Days)
0
20
40
60
80
100
120
Canister surface
r=625 mm, D=100 mm,B
r=825 mm D=100 mm, B
Rock wall

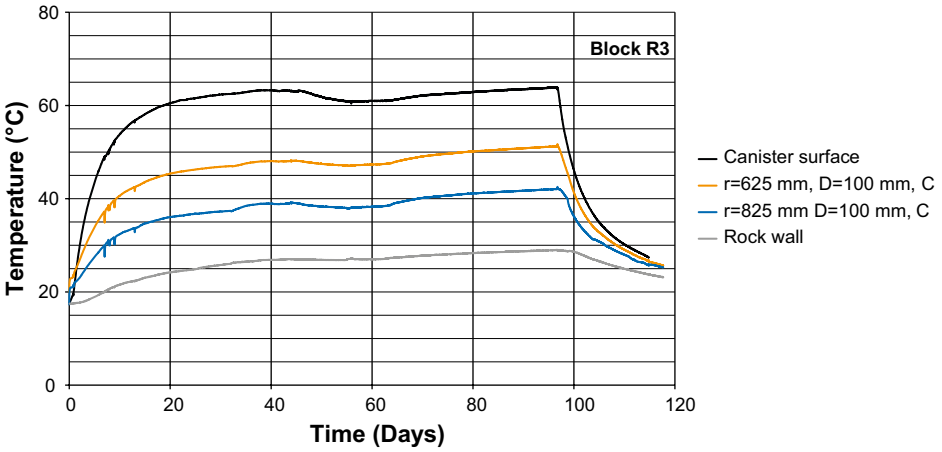
Block R3
Temperature (°C)
Time (Days)
0
20
40
60
80
100
120
Canister surface
r=625 mm, D=100 mm, C
r=825 mm D=100 mm, C
Rock wall

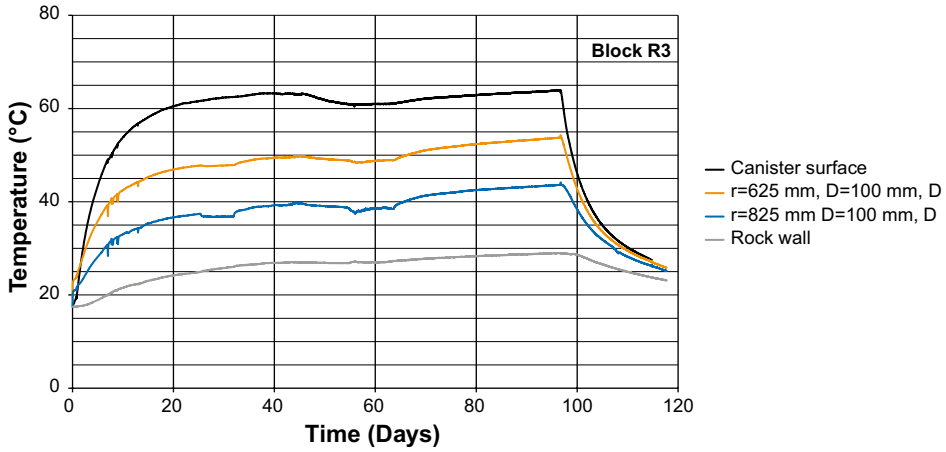
Block R3
Temperature (°C)
Time (Days)
0
20
40
60
80
100
120
Canister surface
r=625 mm, D=100 mm, D
r=825 mm D=100 mm, D
Rock wall

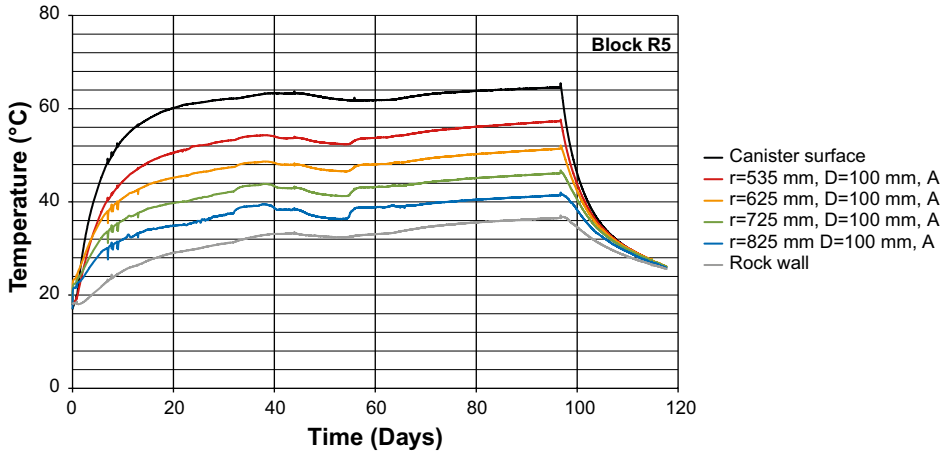
Block R5
Temperature (°C)
Time (Days)
0
20
40
60
80
100
120
Canister surface
r=535 mm, D=100 mm, A
r=625 mm, D=100 mm, A
r=725 mm, D=100 mm, A
r=825 mm D=100 mm, A
Rock wall

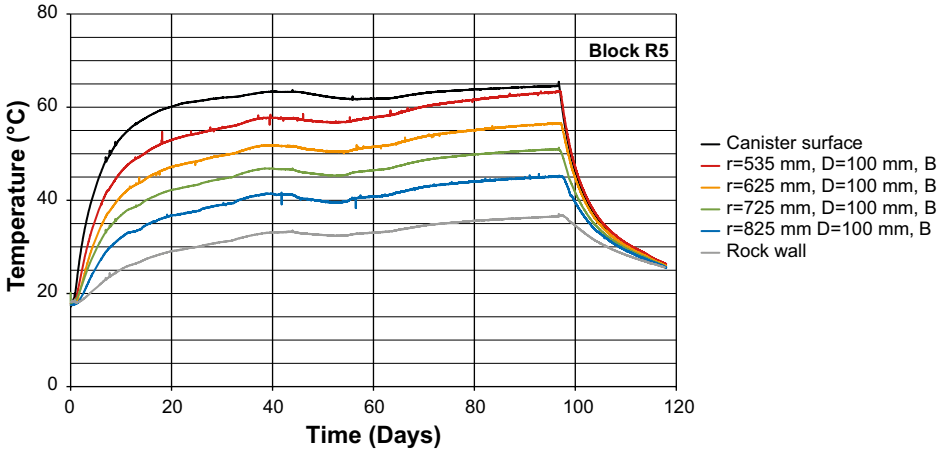
Block R5
Temperature (°C)
Time (Days)
0
20
40
60
80
100
120
Canister surface
r=535 mm, D=100 mm, B
r=625 mm, D=100 mm, B
r=725 mm, D=100 mm, B
r=825 mm D=100 mm, B
Rock wall

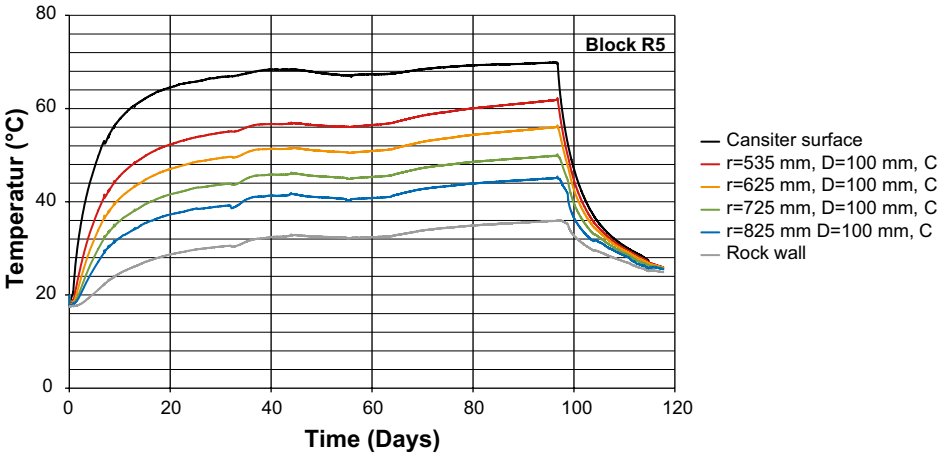
Block R5
Temperatur (°C)
Time (Days)
Cansiter surface
r=535 mm, D=100 mm, C
r=625 mm, D=100 mm, C
r=725 mm, D=100 mm, C
r=825 mm D=100 mm, C
Rock wall

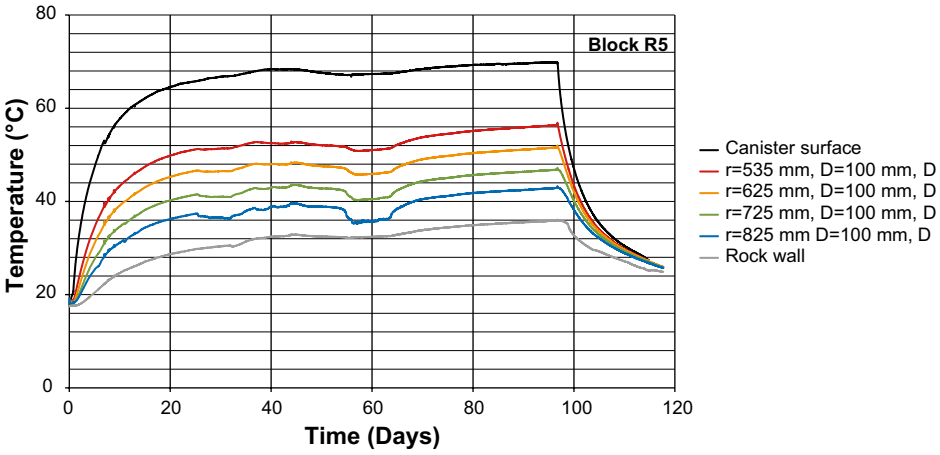
Block R5
Temperature (°C)
Time (Days)
Canister surface
r=535 mm, D=100 mm, D
r=625 mm, D=100 mm, D
r=725 mm, D=100 mm, D
r=825 mm D=100 mm, D
Rock wall

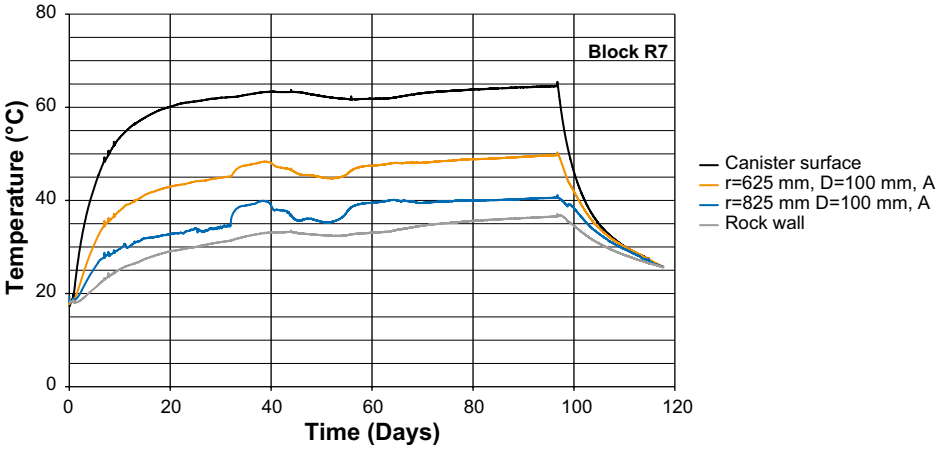
Block R7
Temperature (°C)
Time (Days)
Canister surface
r=625 mm, D=100 mm, A
r=825 mm D=100 mm, A
Rock wall

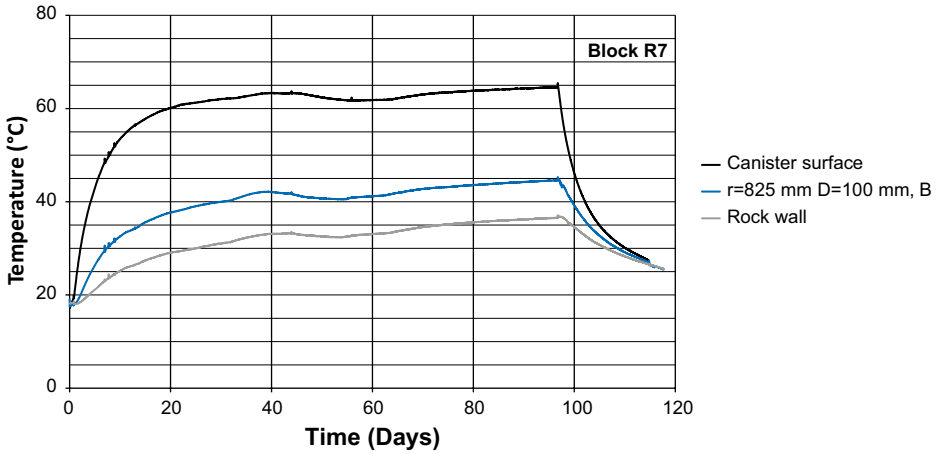
Block R7
Temperature (°C)
Time (Days)
0
20
40
60
80
100
120
Canister surface
r=825 mm D=100 mm, B
Rock wall

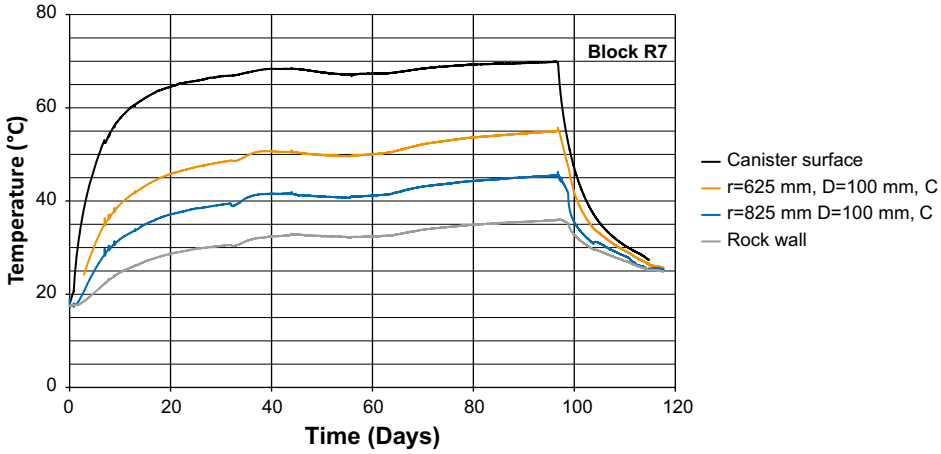
Block R7
Temperature (°C)
Time (Days)
0
20
40
60
80
100
120
Canister surface
r=625 mm, D=100 mm, C
r=825 mm D=100 mm, C
Rock wall

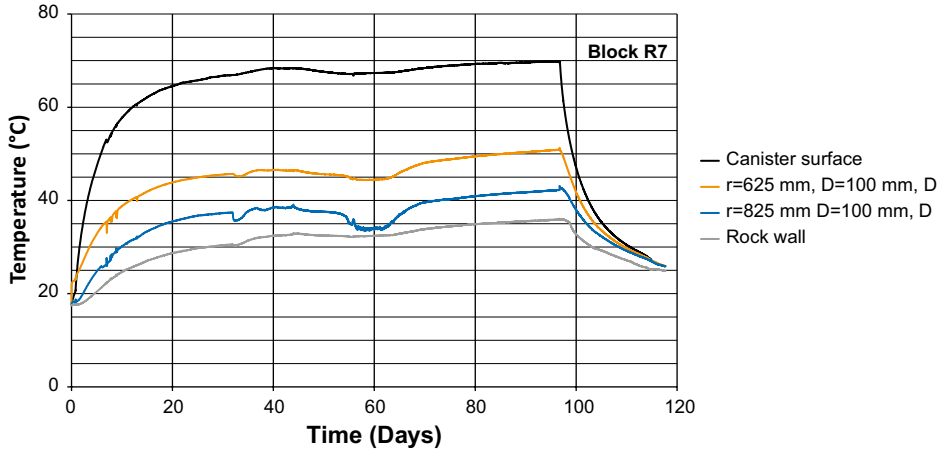
Block R7
Temperature (°C)
Time (Days)
0
20
40
60
80
100
120
Canister surface
r=625 mm, D=100 mm, D
r=825 mm D=100 mm, D
Rock wall

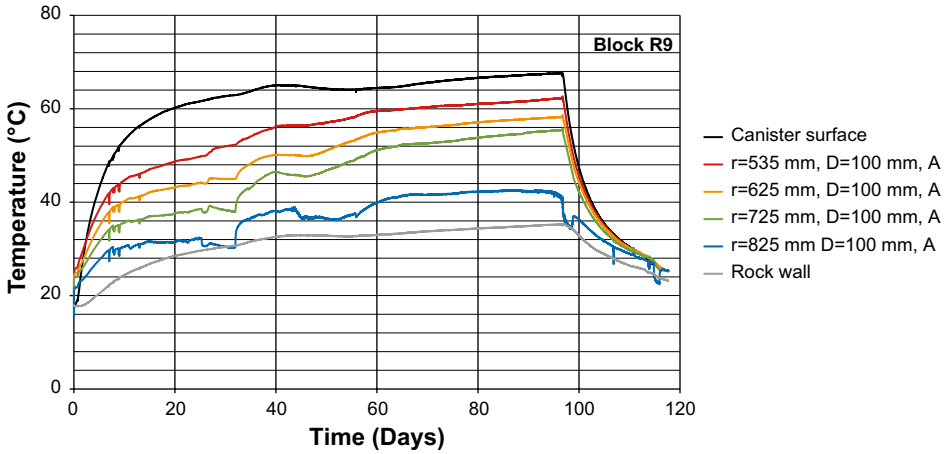
Block R9
Temperature (°C)
Time (Days)
Canister surface
r=535 mm, D=100 mm, A
r=625 mm, D=100 mm, A
r=725 mm, D=100 mm, A
r=825 mm D=100 mm, A
Rock wall

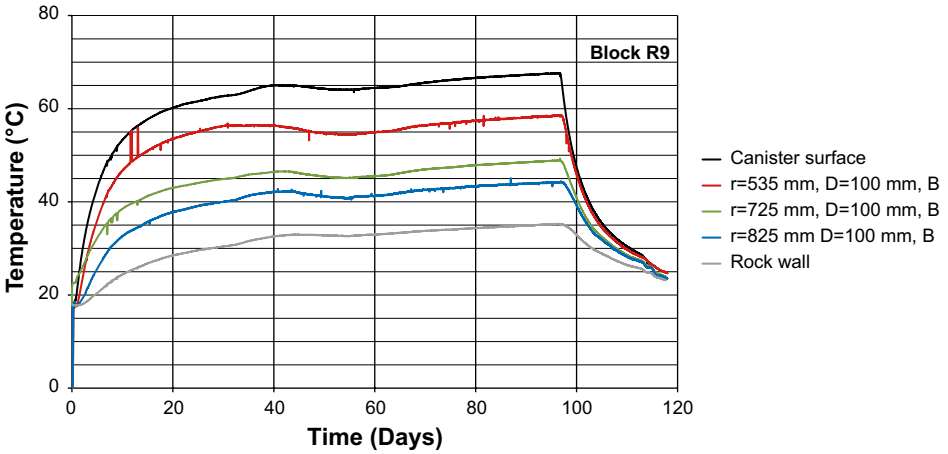
Block R9
Temperature (°C)
Time (Days)
Canister surface
r=535 mm, D=100 mm, B
r=725 mm, D=100 mm, B
r=825 mm D=100 mm, B
Rock wall

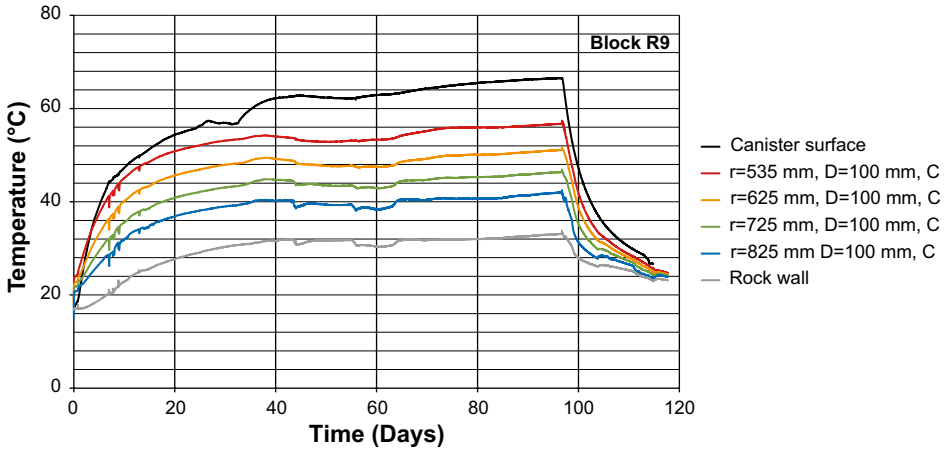
Block R9
Temperature (°C)
Time (Days)
Canister surface
r=535 mm, D=100 mm, C
r=625 mm, D=100 mm, C
r=725 mm, D=100 mm, C
r=825 mm D=100 mm, C
Rock wall

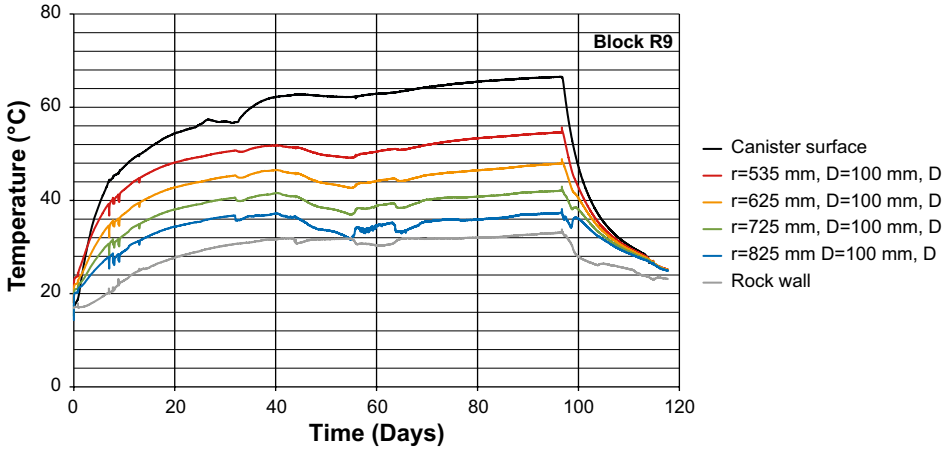
Block R9
Temperature (°C)
Time (Days)
Canister surface
r=535 mm, D=100 mm, D
r=625 mm, D=100 mm, D
r=725 mm, D=100 mm, D
r=825 mm D=100 mm, D
Rock wall

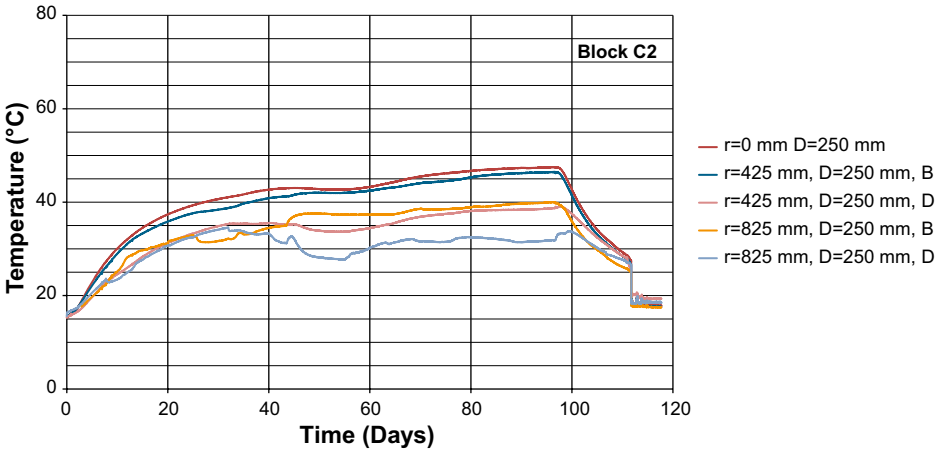
Block C2
Temperature (°C)
Time (Days)
0
20
40
60
80
100
120
r=0 mm D=250 mm
r=425 mm, D=250 mm, B
r=425 mm, D=250 mm, D
r=825 mm, D=250 mm, B
r=825 mm, D=250 mm, D

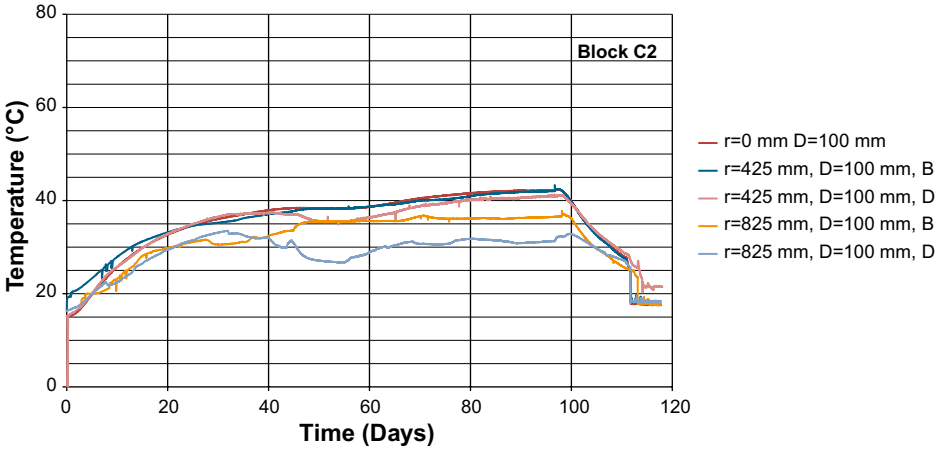
Block C2
Temperature (°C)
Time (Days)
0
20
40
60
80
100
120
r=0 mm D=100 mm
r=425 mm, D=100 mm, B
r=425 mm, D=100 mm, D
r=825 mm, D=100 mm, B
r=825 mm, D=100 mm, D

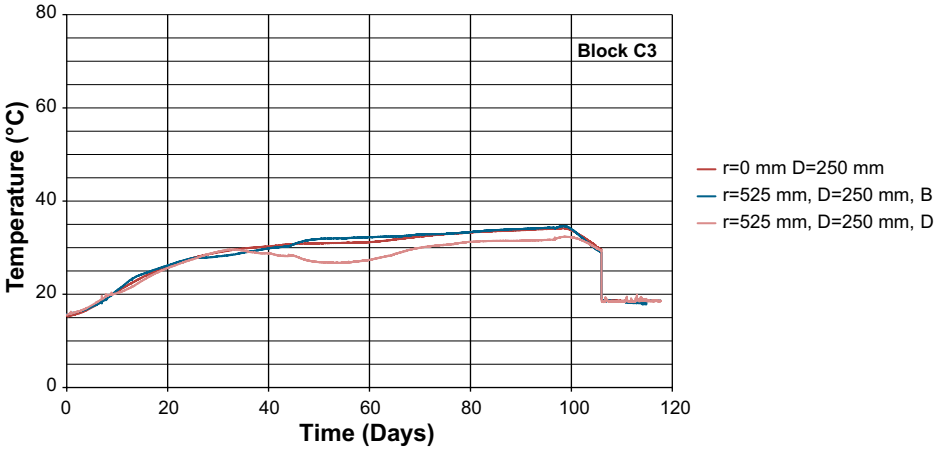
Block C3
Temperature (°C)
Time (Days)
0
20
40
60
80
100
120
r=0 mm D=250 mm
r=525 mm, D=250 mm, B
r=525 mm, D=250 mm, D

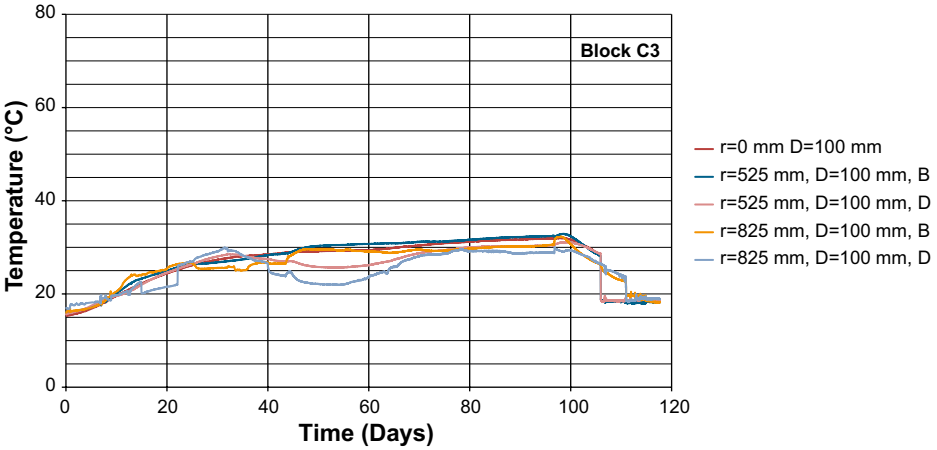
Block C3
Temperature (°C)
Time (Days)
0
20
40
60
80
100
120
r=0 mm D=100 mm
r=525 mm, D=100 mm, B
r=525 mm, D=100 mm, D
r=825 mm, D=100 mm, B
r=825 mm, D=100 mm, D

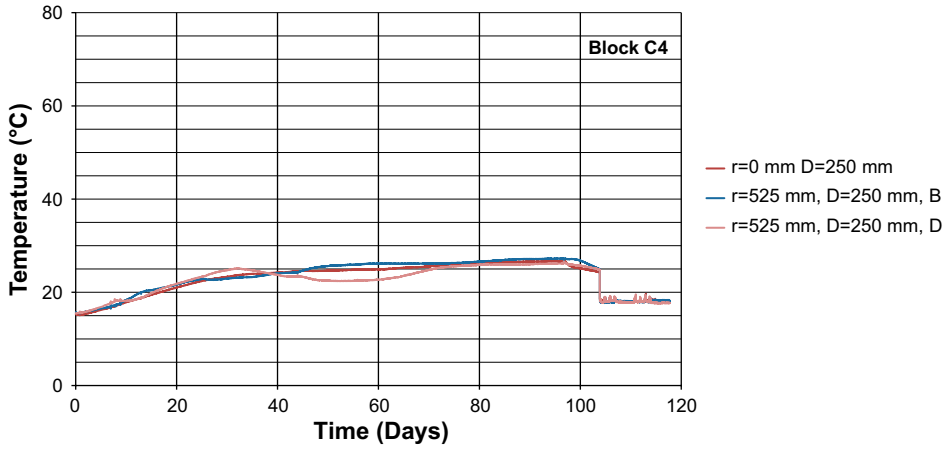
Block C4
Temperature (°C)
Time (Days)
0
20
40
60
80
100
120
r=0 mm D=250 mm
r=525 mm, D=250 mm, B
r=525 mm, D=250 mm, D

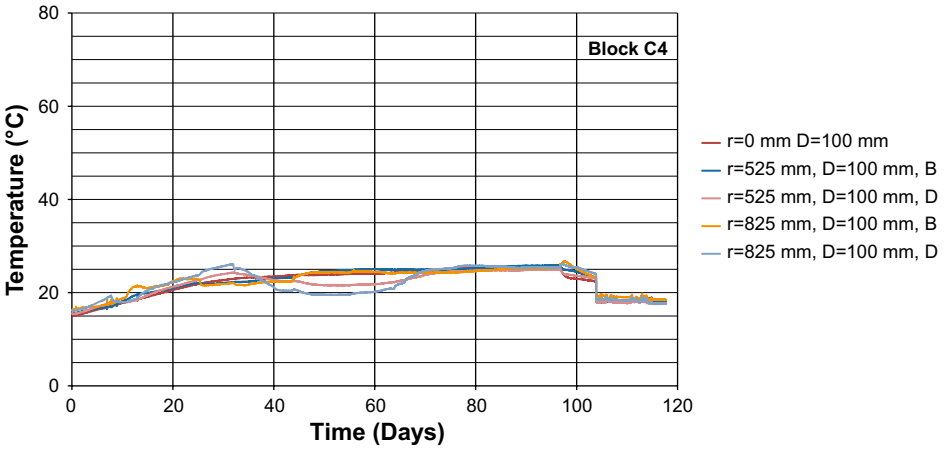
Block C4
Temperature (°C)
Time (Days)
0
20
40
60
80
100
120
r=0 mm D=100 mm
r=525 mm, D=100 mm, B
r=525 mm, D=100 mm, D
r=825 mm, D=100 mm, B
r=825 mm, D=100 mm, D

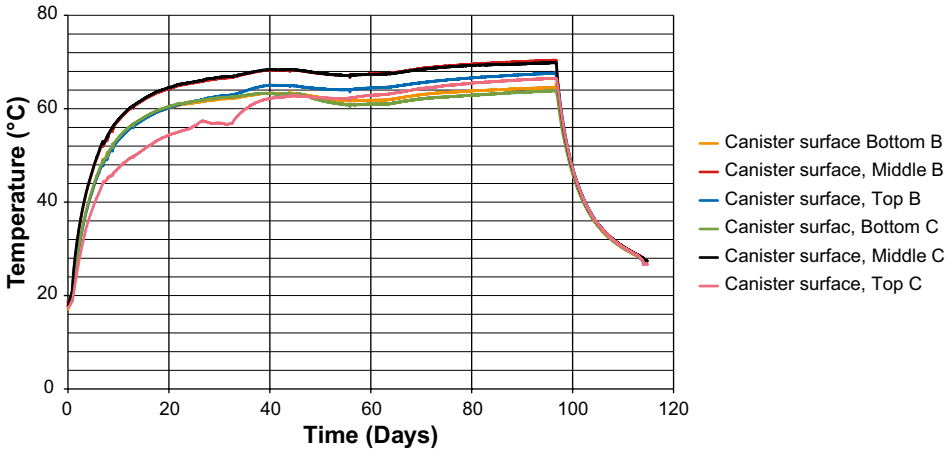
Temperature (°C)
Time (Days)
Canister surface Bottom B
Canister surface, Middle B
Canister surface, Top B
Canister surfac, Bottom C
Canister surface, Middle C
Canister surface, Top C

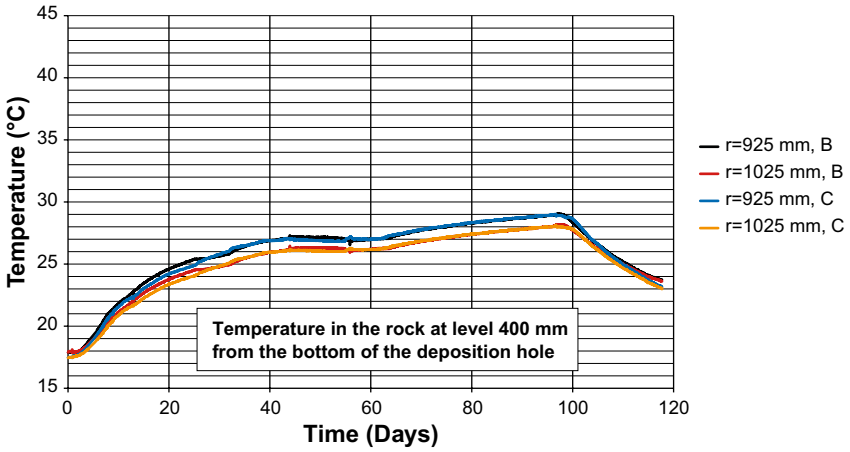
Temperature (°C)
Time (Days)
Temperature in the rock at level 400 mm from the bottom of the deposition hole
r=925 mm, B
r=1025 mm, B
r=925 mm, C
r=1025 mm, C

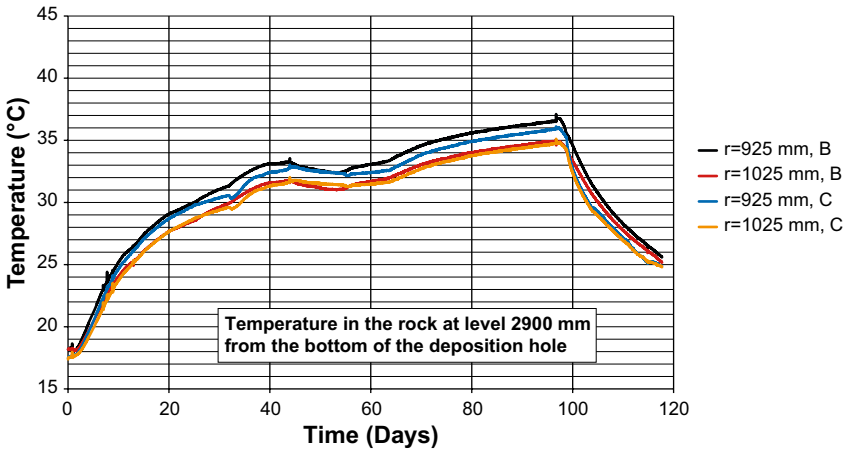
Temperature (°C)
Time (Days)
Temperature in the rock at level 2900 mm from the bottom of the deposition hole
r=925 mm, B
r=1025 mm, B
r=925 mm, C
r=1025 mm, C

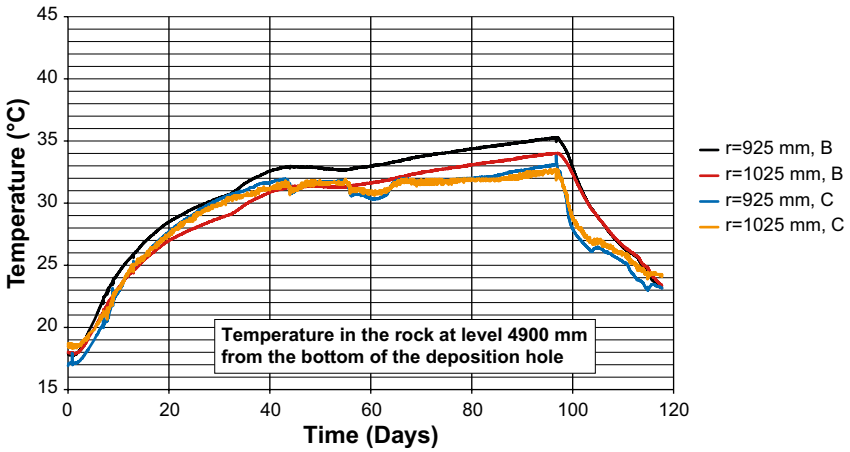
Temperature (°C)
Time (Days)
Temperature in the rock at level 4900 mm from the bottom of the deposition hole
r=925 mm, B
r=1025 mm, B
r=925 mm, C
r=1025 mm, C

Water content and dry density of the buffer Test 2

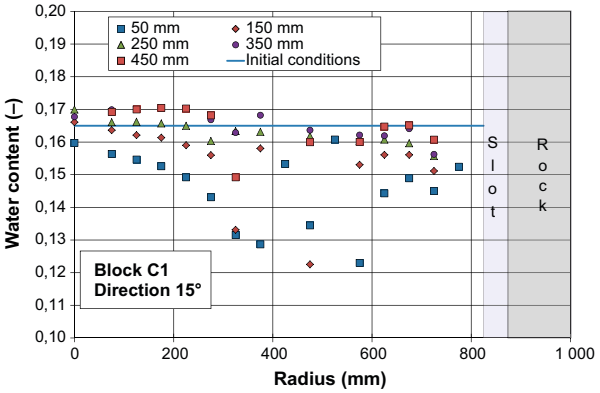

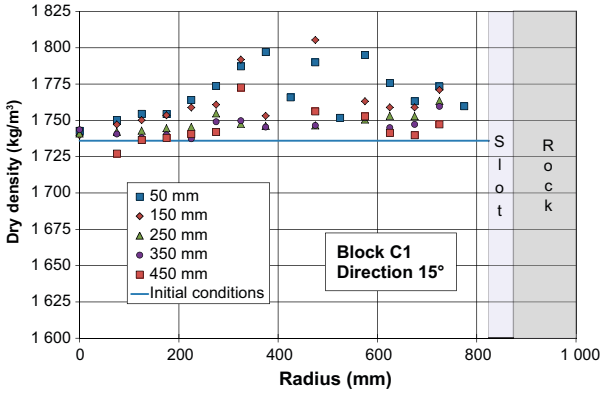

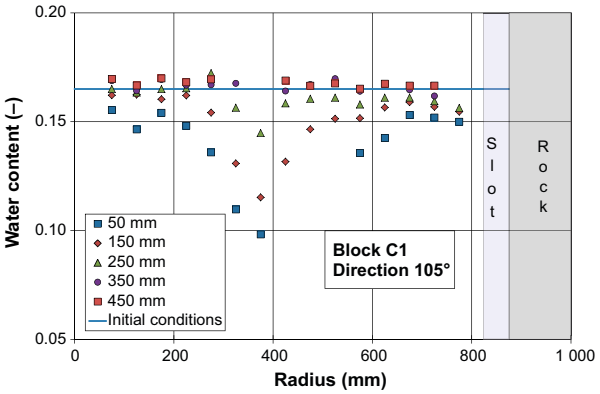

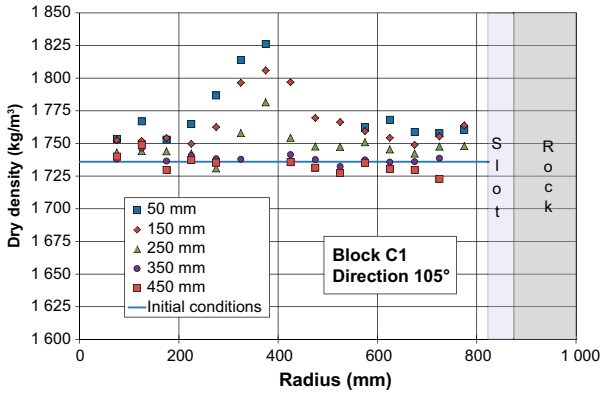

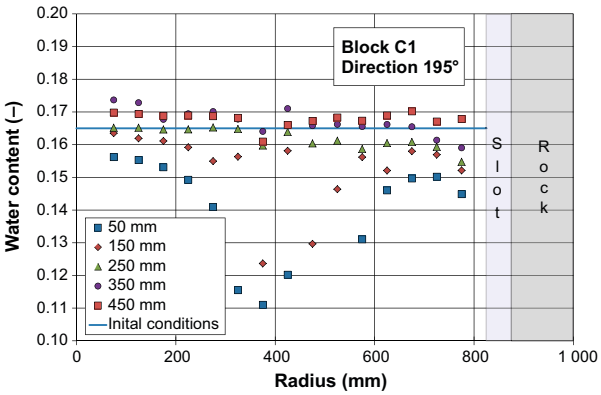

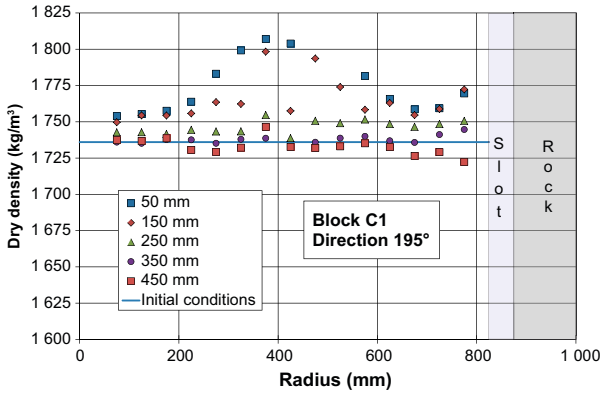

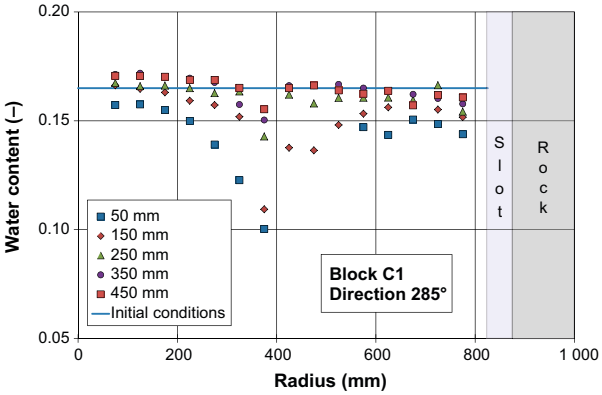

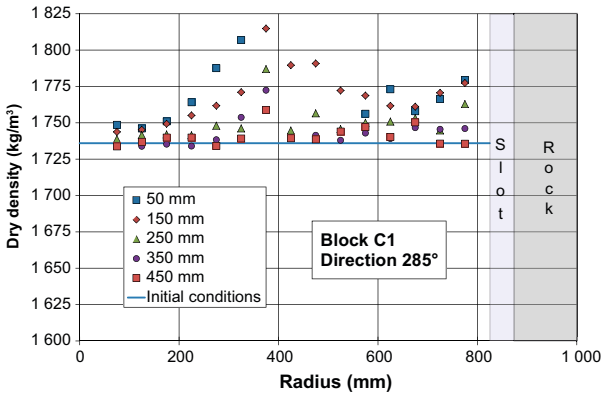

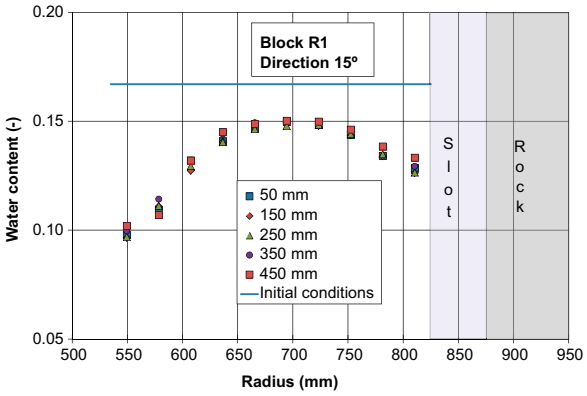
Block R1
Direction 15º
50 mm
150 mm
250 mm
350 mm
450 mm
Initial conditions
Water content (-)
Radius (mm)
Slot
Rock

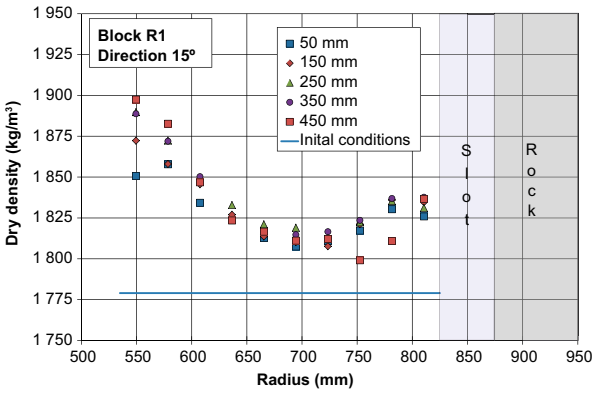
Block R1
Direction 15º
50 mm
150 mm
250 mm
350 mm
450 mm
Inital conditions
Dry density (kg/m³)
Radius (mm)
Slot
Rock

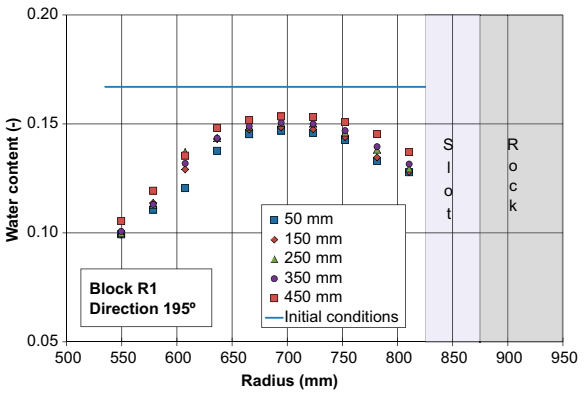
Block R1
Direction 195º
50 mm
150 mm
250 mm
350 mm
450 mm
Initial conditions
Water content (-)
Radius (mm)
Slot
Rock

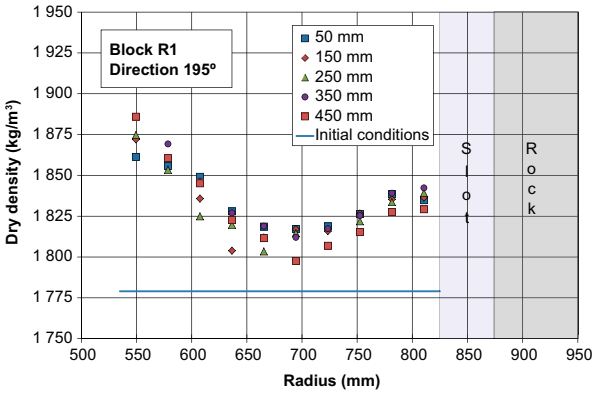
Block R1
Direction 195º
50 mm
150 mm
250 mm
350 mm
450 mm
Initial conditions
Dry density (kg/m³)
Radius (mm)
Slot
Rock

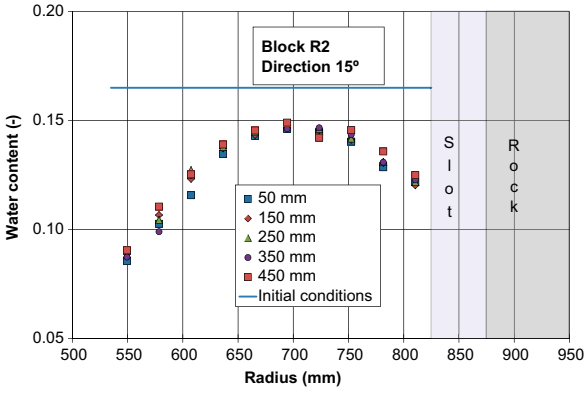
Block R2
Direction 15º
50 mm
150 mm
250 mm
350 mm
450 mm
Initial conditions
Water content (-)
Radius (mm)
Slot
Rock

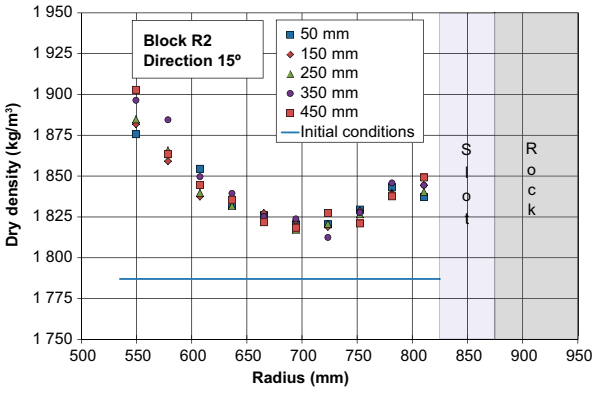
Block R2
Direction 15º
50 mm
150 mm
250 mm
350 mm
450 mm
Initial conditions
Dry density (kg/m³)
Radius (mm)
Slot
Rock

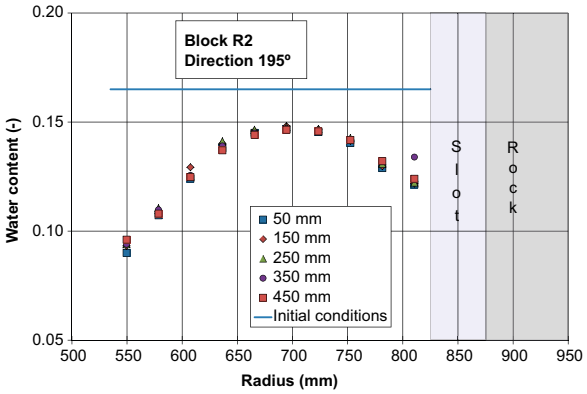
Block R2
Direction 195º
50 mm
150 mm
250 mm
350 mm
450 mm
Initial conditions
Water content (-)
Radius (mm)
Slot
Rock

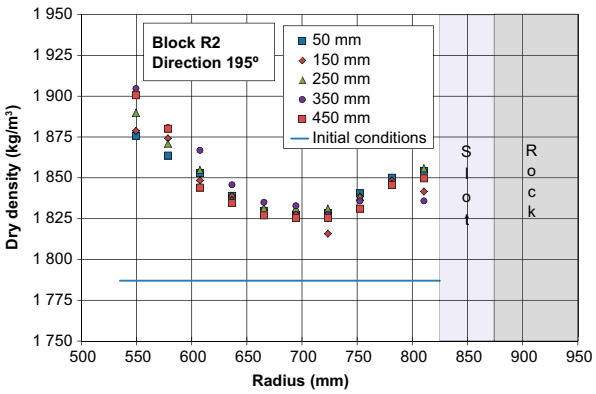
Block R2
Direction 195º
50 mm
150 mm
250 mm
350 mm
450 mm
Initial conditions
Dry density (kg/m³)
Radius (mm)
Slot
Rock

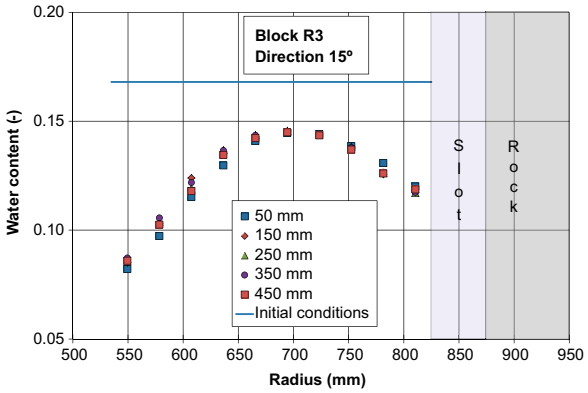
Block R3
Direction 15º
Water content (-)
Radius (mm)
50 mm
150 mm
250 mm
350 mm
450 mm
Initial conditions
Slot
Rock

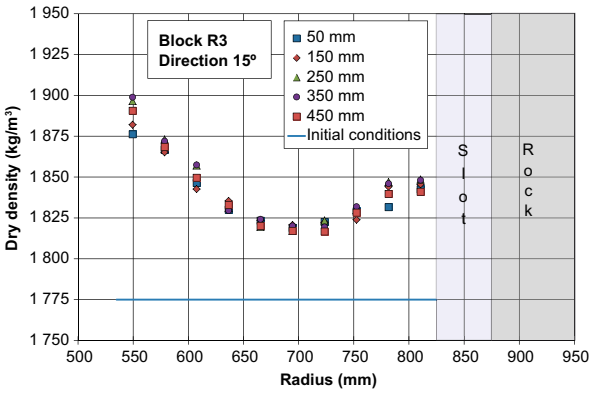
Block R3
Direction 15º
Dry density (kg/m³)
Radius (mm)
50 mm
150 mm
250 mm
350 mm
450 mm
Initial conditions
Slot
Rock

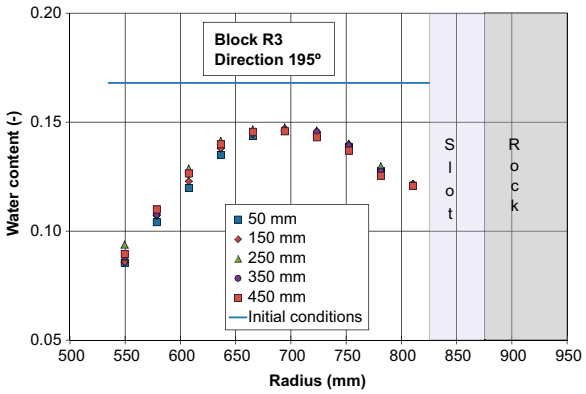
Block R3
Direction 195º
Water content (-)
Radius (mm)
50 mm
150 mm
250 mm
350 mm
450 mm
Initial conditions
Slot
Rock

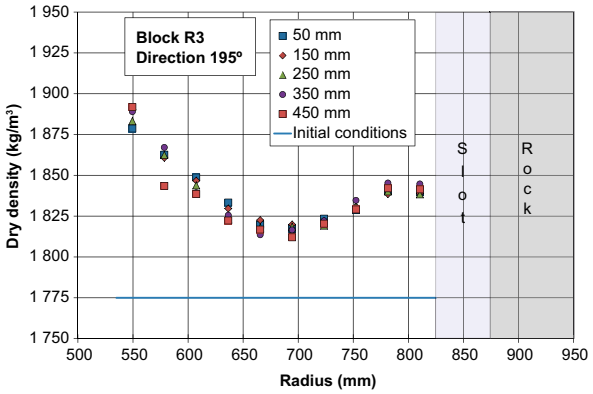
Block R3
Direction 195º
Dry density (kg/m³)
Radius (mm)
50 mm
150 mm
250 mm
350 mm
450 mm
Initial conditions
Slot
Rock

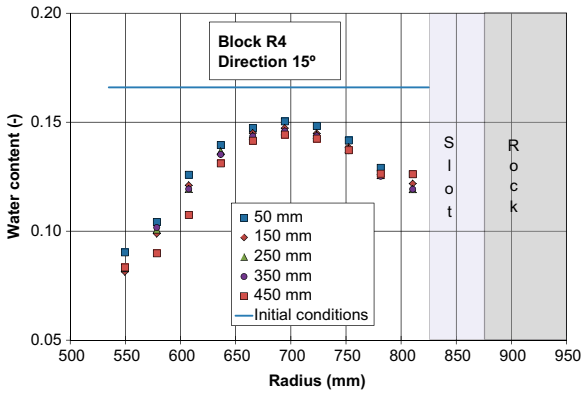
Block R4
Direction 15º
Water content (-)
Radius (mm)
50 mm
150 mm
250 mm
350 mm
450 mm
Initial conditions
Slot
Rock

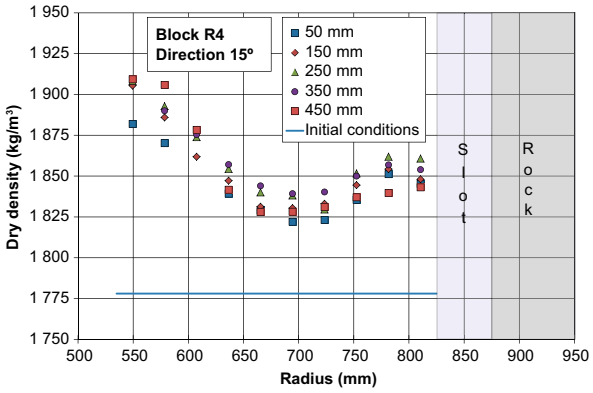
Block R4
Direction 15º
Dry density (kg/m³)
Radius (mm)
50 mm
150 mm
250 mm
350 mm
450 mm
Initial conditions
Slot
Rock

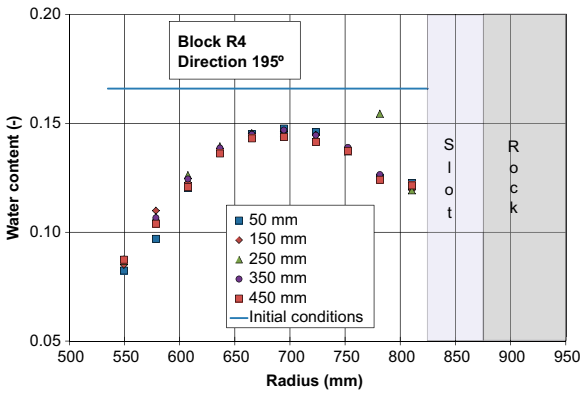
Block R4
Direction 195º
Water content (-)
Radius (mm)
50 mm
150 mm
250 mm
350 mm
450 mm
Initial conditions
Slot
Rock

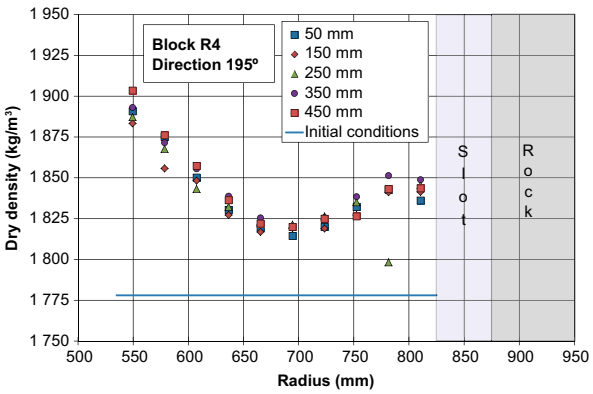
Block R4
Direction 195º
Dry density (kg/m³)
Radius (mm)
50 mm
150 mm
250 mm
350 mm
450 mm
Initial conditions
Slot
Rock

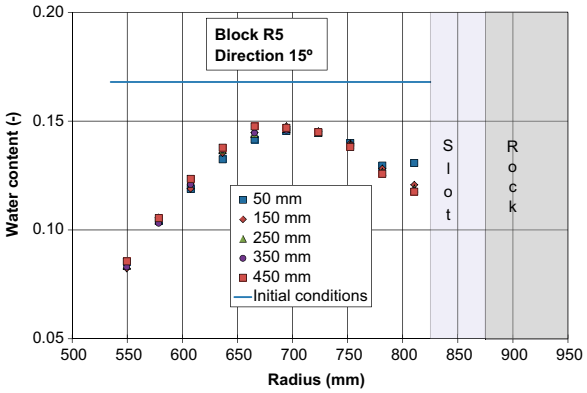
Block R5
Direction 15º
Water content (-)
Radius (mm)
50 mm
150 mm
250 mm
350 mm
450 mm
Initial conditions
Slot
Rock

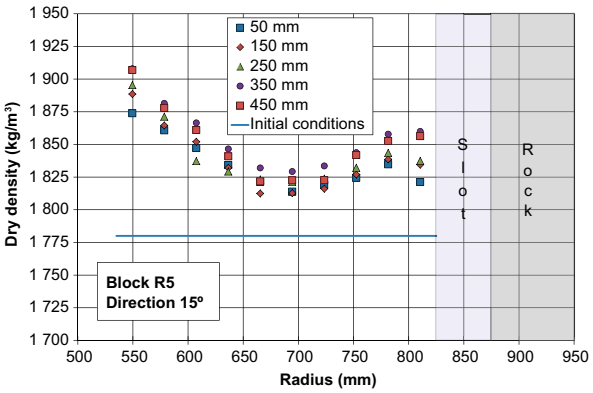
Block R5
Direction 15º
Dry density (kg/m³)
Radius (mm)
50 mm
150 mm
250 mm
350 mm
450 mm
Initial conditions
Slot
Rock

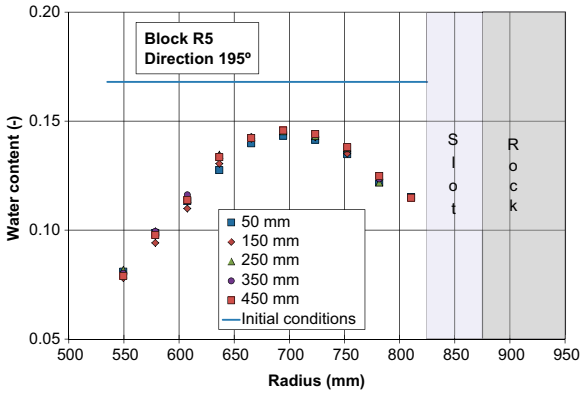
Block R5
Direction 195º
Water content (-)
Radius (mm)
50 mm
150 mm
250 mm
350 mm
450 mm
Initial conditions
Slot
Rock

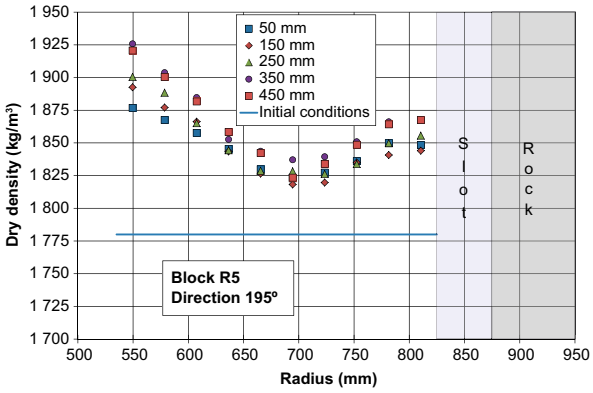
Block R5
Direction 195º
Dry density (kg/m³)
Radius (mm)
50 mm
150 mm
250 mm
350 mm
450 mm
Initial conditions
Slot
Rock

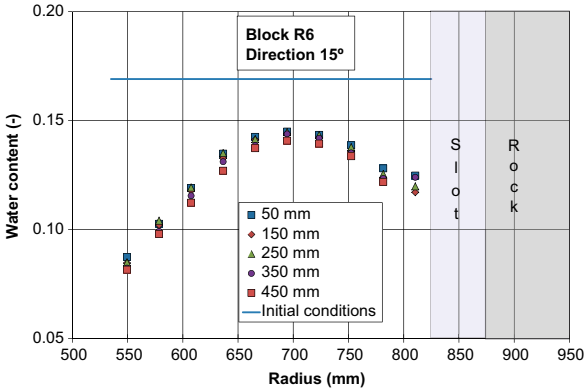
Block R6
Direction 15º
Water content (-)
Radius (mm)
50 mm
150 mm
250 mm
350 mm
450 mm
Initial conditions
Slot
Rock

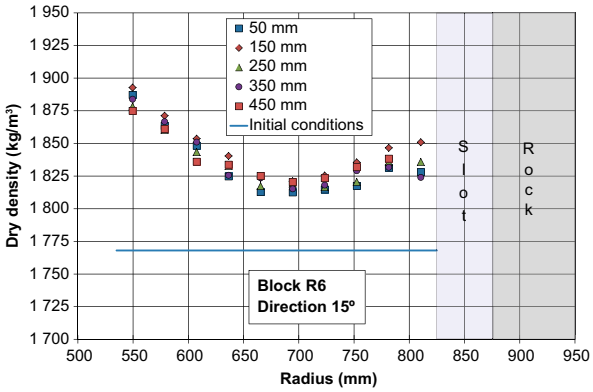
Block R6
Direction 15º
Dry density (kg/m³)
Radius (mm)
50 mm
150 mm
250 mm
350 mm
450 mm
Initial conditions
Slot
Rock

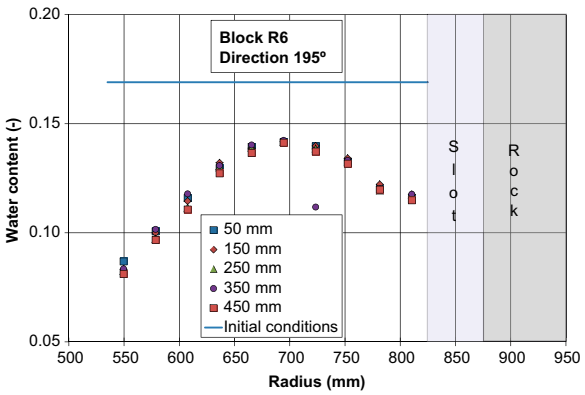
Block R6
Direction 195º
Water content (-)
Radius (mm)
50 mm
150 mm
250 mm
350 mm
450 mm
Initial conditions
Slot
Rock

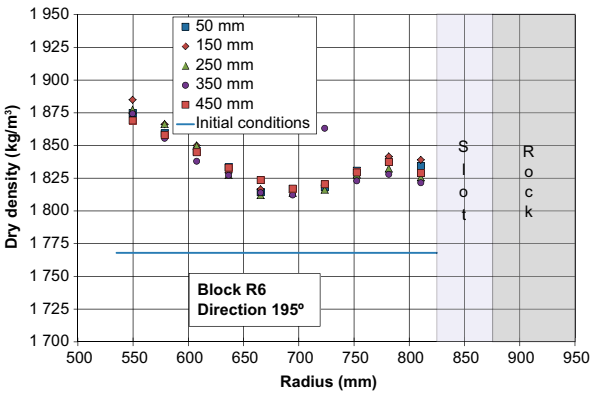
Block R6
Direction 195º
Dry density (kg/m³)
Radius (mm)
50 mm
150 mm
250 mm
350 mm
450 mm
Initial conditions
Slot
Rock

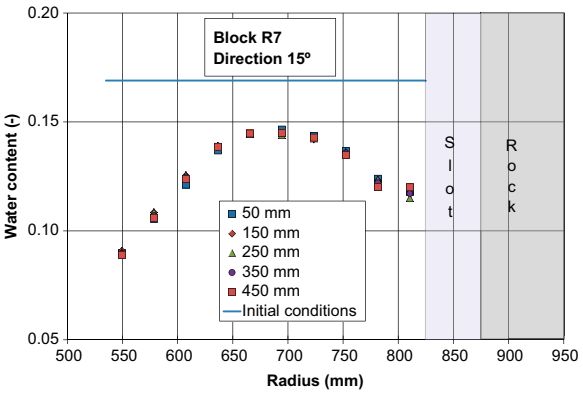
Block R7
Direction 15º
50 mm
150 mm
250 mm
350 mm
450 mm
Initial conditions
Water content (-)
Radius (mm)
Slot
Rock

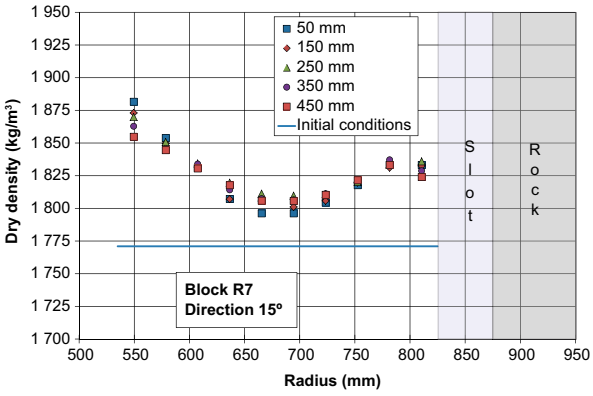
50 mm
150 mm
250 mm
350 mm
450 mm
Initial conditions
Block R7
Direction 15º
Dry density (kg/m³)
Radius (mm)
Slot
Rock

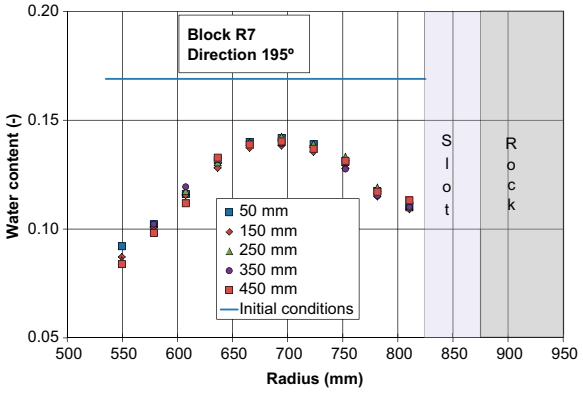
Block R7
Direction 195º
50 mm
150 mm
250 mm
350 mm
450 mm
Initial conditions
Water content (-)
Radius (mm)
Slot
Rock

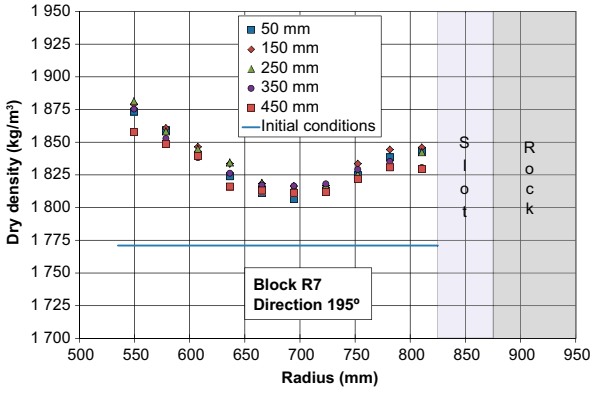
50 mm
150 mm
250 mm
350 mm
450 mm
Initial conditions
Block R7
Direction 195º
Dry density (kg/m³)
Radius (mm)
Slot
Rock

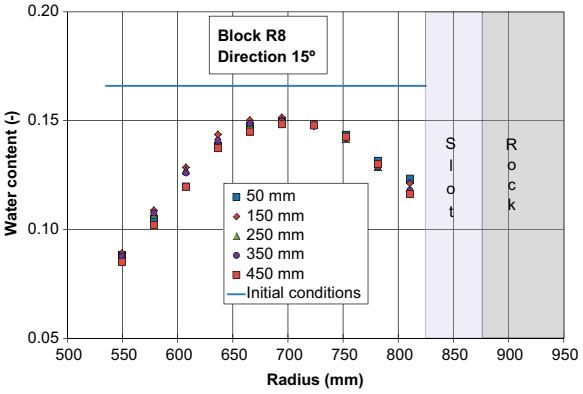
Block R8
Direction 15º
50 mm
150 mm
250 mm
350 mm
450 mm
Initial conditions
Water content (-)
Radius (mm)
Slot
Rock

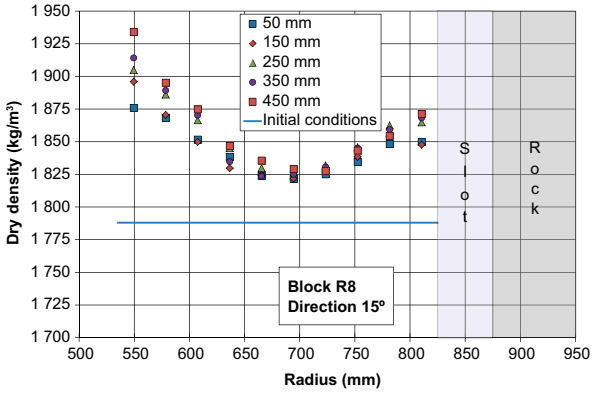
50 mm
150 mm
250 mm
350 mm
450 mm
Initial conditions
Block R8
Direction 15º
Dry density (kg/m³)
Radius (mm)
Slot
Rock

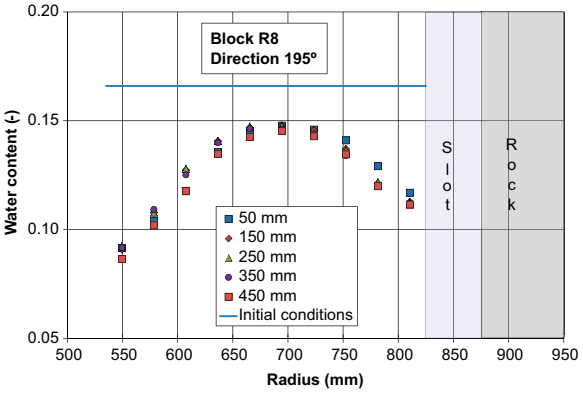
Block R8
Direction 195º
50 mm
150 mm
250 mm
350 mm
450 mm
Initial conditions
Water content (-)
Radius (mm)
Slot
Rock

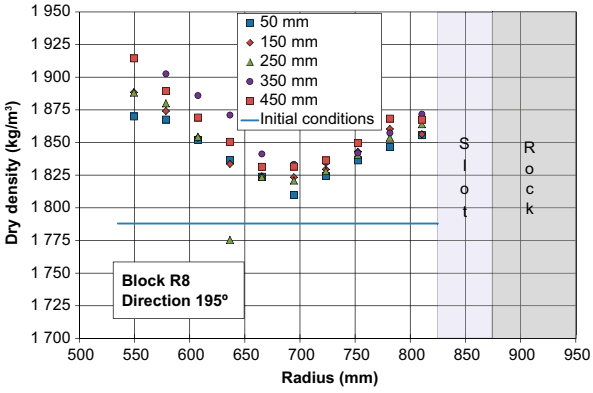
50 mm
150 mm
250 mm
350 mm
450 mm
Initial conditions
Block R8
Direction 195º
Dry density (kg/m³)
Radius (mm)
Slot
Rock

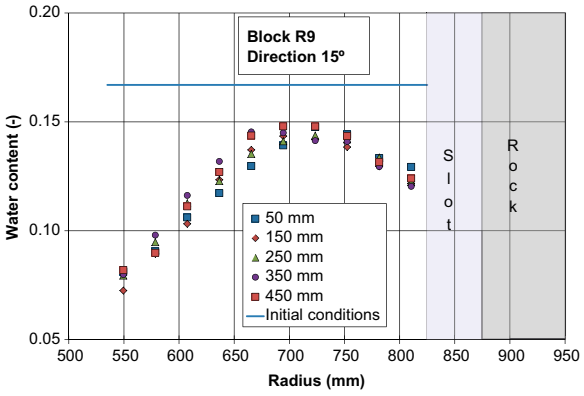
Block R9
Direction 15º
Water content (-)
Radius (mm)
50 mm
150 mm
250 mm
350 mm
450 mm
Initial conditions
Slot
Rock

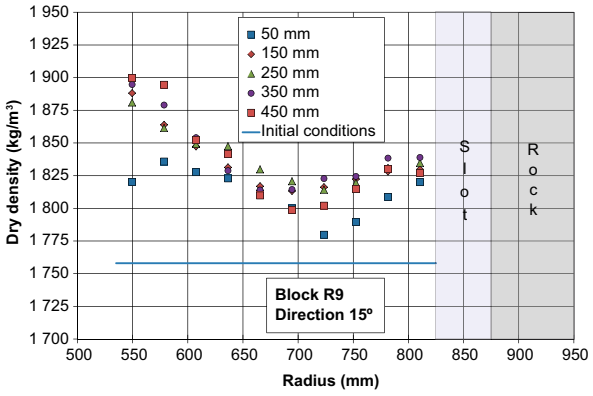
Block R9
Direction 15º
Dry density (kg/m³)
Radius (mm)
50 mm
150 mm
250 mm
350 mm
450 mm
Initial conditions
Slot
Rock

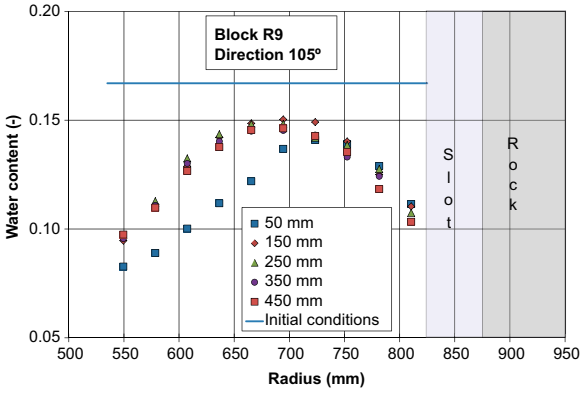
Block R9
Direction 105º
Water content (-)
Radius (mm)
50 mm
150 mm
250 mm
350 mm
450 mm
Initial conditions
Slot
Rock

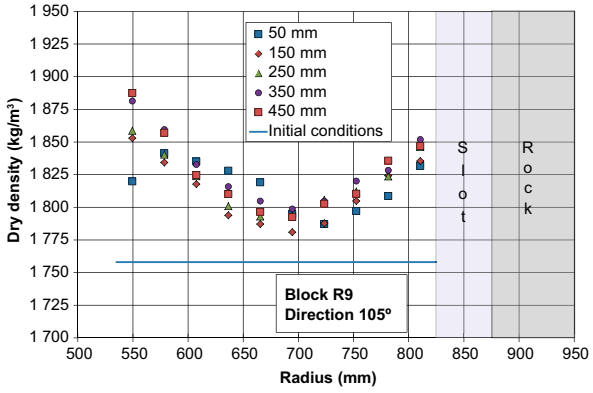
Block R9
Direction 105º
Dry density (kg/m³)
Radius (mm)
50 mm
150 mm
250 mm
350 mm
450 mm
Initial conditions
Slot
Rock

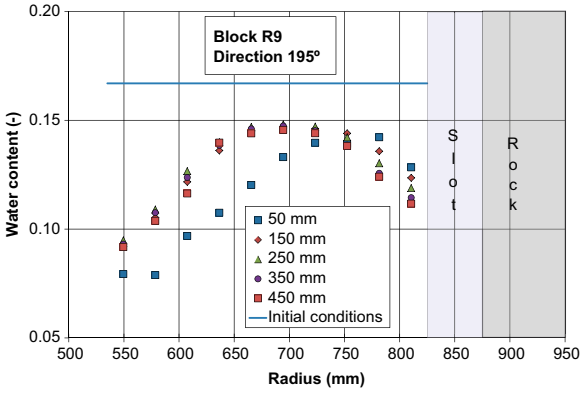
Block R9
Direction 195º
Water content (-)
Radius (mm)
50 mm
150 mm
250 mm
350 mm
450 mm
Initial conditions
Slot
Rock

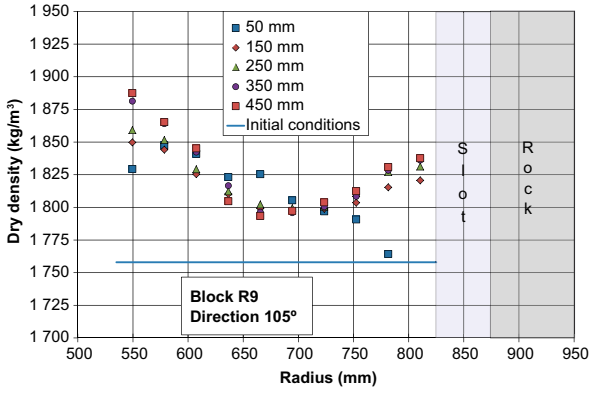
Block R9
Direction 105º
Dry density (kg/m³)
Radius (mm)
50 mm
150 mm
250 mm
350 mm
450 mm
Initial conditions
Slot
Rock

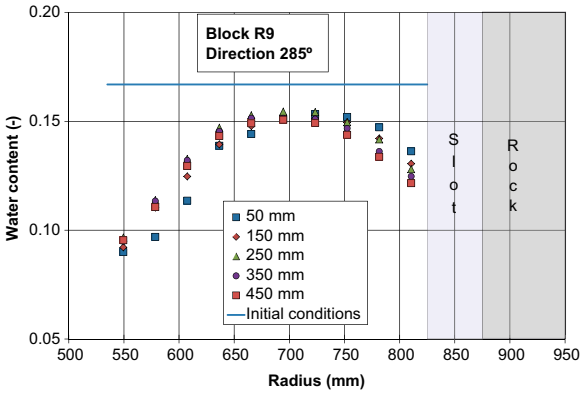
Block R9
Direction 285º
Water content (-)
Radius (mm)
50 mm
150 mm
250 mm
350 mm
450 mm
Initial conditions
Slot
Rock

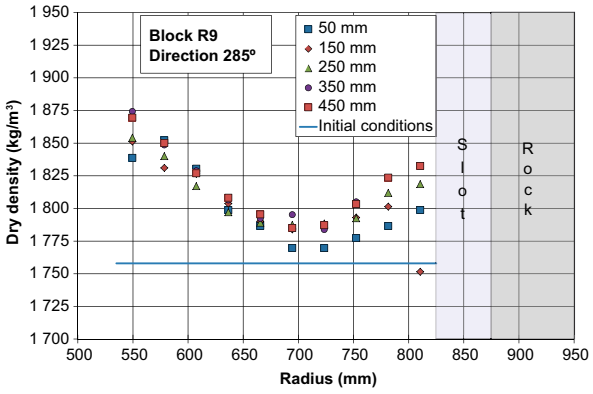
Block R9
Direction 285º
Dry density (kg/m³)
Radius (mm)
50 mm
150 mm
250 mm
350 mm
450 mm
Initial conditions
Slot
Rock

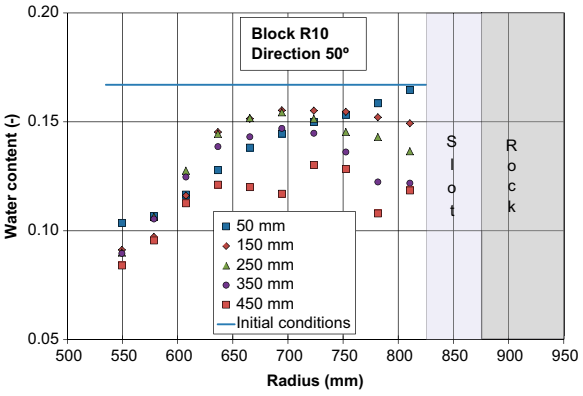
Block R10
Direction 50°
Water content (-)
Radius (mm)
50 mm
150 mm
250 mm
350 mm
450 mm
Initial conditions
Slot
Rock

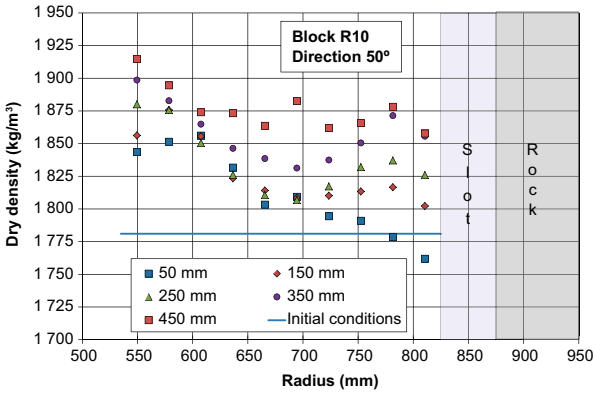
Block R10
Direction 50°
Dry density (kg/m³)
Radius (mm)
50 mm
150 mm
250 mm
350 mm
450 mm
Initial conditions
Slot
Rock

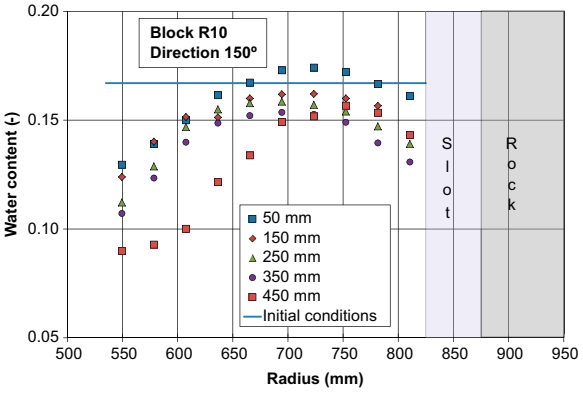
Block R10
Direction 150°
Water content (-)
Radius (mm)
50 mm
150 mm
250 mm
350 mm
450 mm
Initial conditions
Slot
Rock

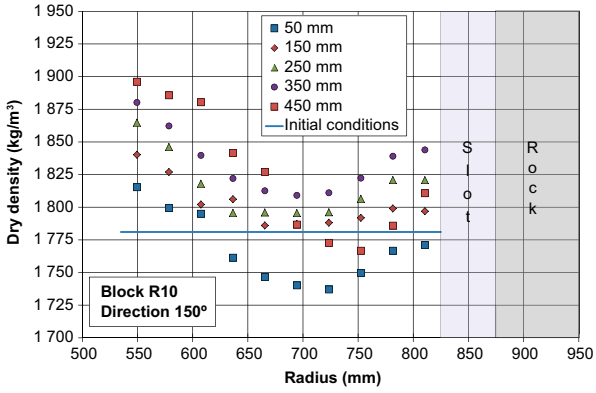
Block R10
Direction 150°
Dry density (kg/m³)
Radius (mm)
50 mm
150 mm
250 mm
350 mm
450 mm
Initial conditions
Slot
Rock

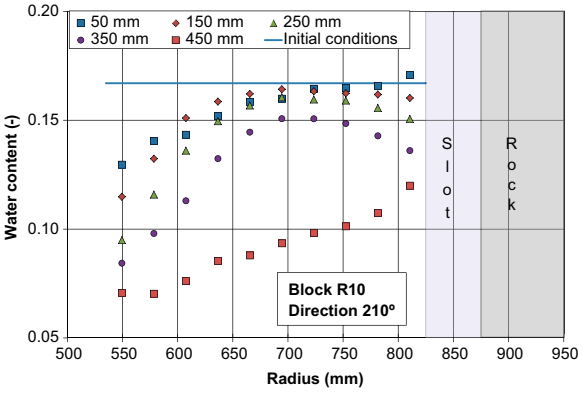
Block R10
Direction 210°
Water content (-)
Radius (mm)
50 mm
150 mm
250 mm
350 mm
450 mm
Initial conditions
Slot
Rock

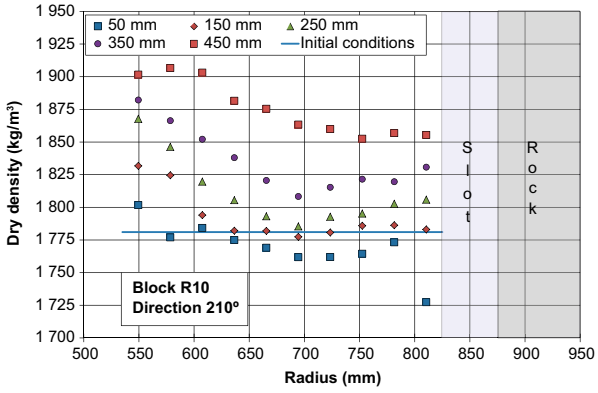
Block R10
Direction 210°
Dry density (kg/m³)
Radius (mm)
50 mm
150 mm
250 mm
350 mm
450 mm
Initial conditions
Slot
Rock

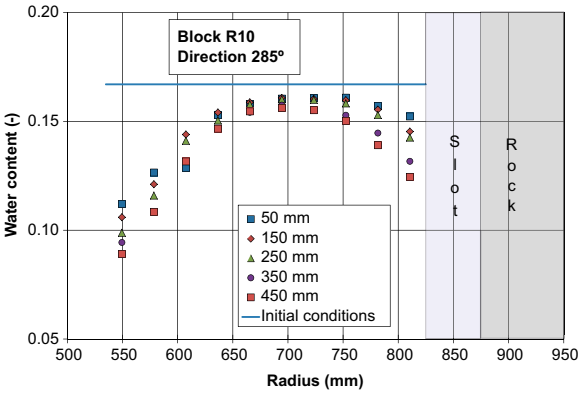
Block R10
Direction 285°
Water content (-)
Radius (mm)
50 mm
150 mm
250 mm
350 mm
450 mm
Initial conditions
Slot
Rock

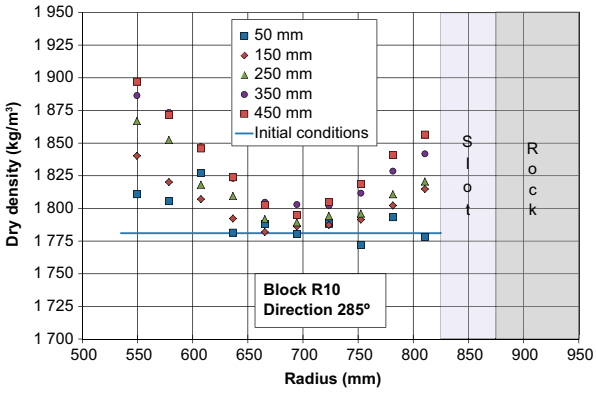
Block R10
Direction 285°
Dry density (kg/m³)
Radius (mm)
50 mm
150 mm
250 mm
350 mm
450 mm
Initial conditions
Slot
Rock

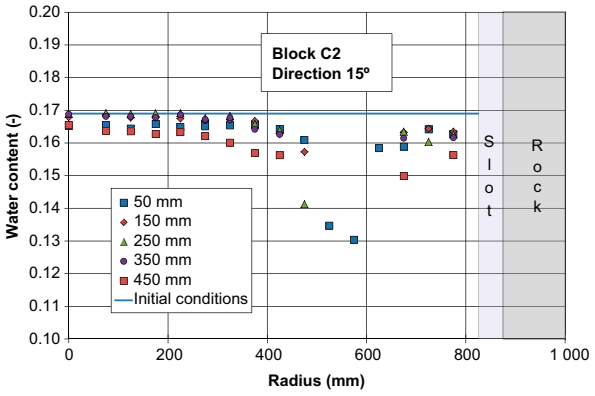
Block C2
Direction 15º
Water content (-)
Radius (mm)
50 mm
150 mm
250 mm
350 mm
450 mm
Initial conditions
Slot
Rock

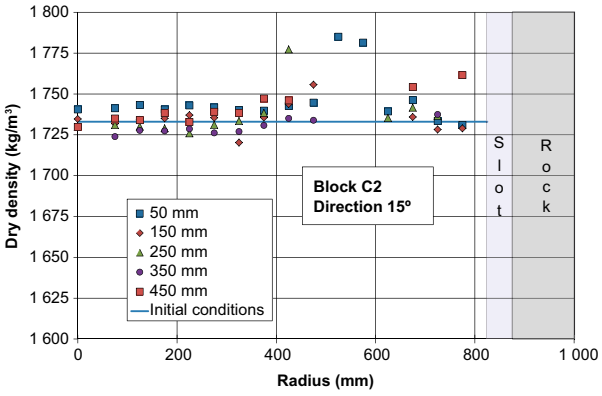
Block C2
Direction 15º
Dry density (kg/m³)
Radius (mm)
50 mm
150 mm
250 mm
350 mm
450 mm
Initial conditions
Slot
Rock

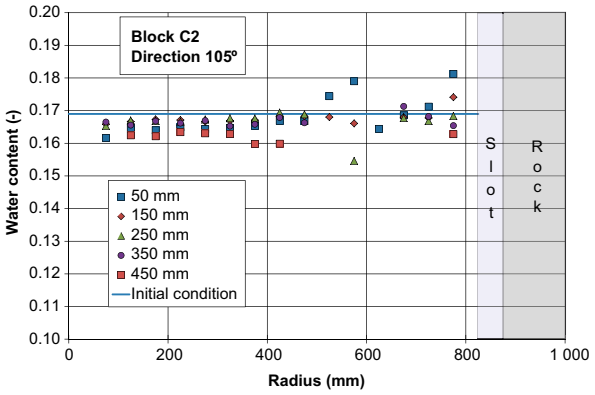
Block C2
Direction 105º
Water content (-)
Radius (mm)
50 mm
150 mm
250 mm
350 mm
450 mm
Initial condition
Slot
Rock

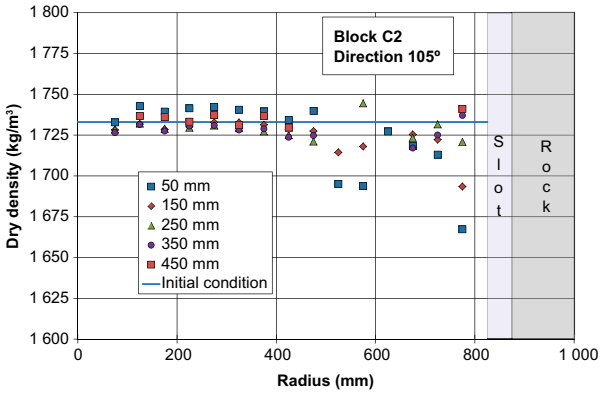
Block C2
Direction 105º
Dry density (kg/m³)
Radius (mm)
50 mm
150 mm
250 mm
350 mm
450 mm
Initial condition
Slot
Rock

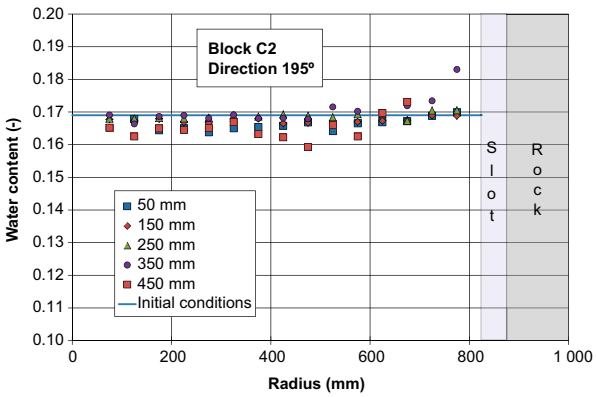
Block C2
Direction 195º
Water content (-)
Radius (mm)
50 mm
150 mm
250 mm
350 mm
450 mm
Initial conditions
Slot
Rock

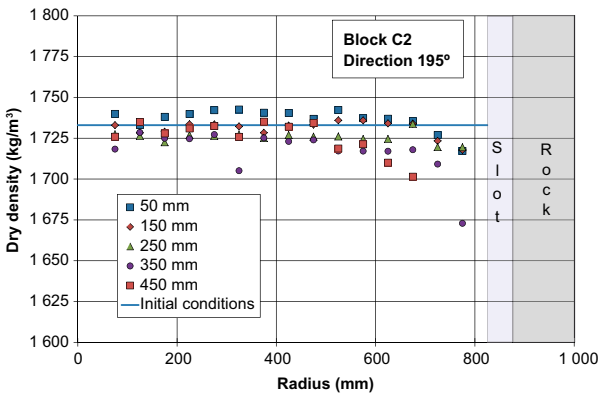
Block C2
Direction 195º
Dry density (kg/m³)
Radius (mm)
50 mm
150 mm
250 mm
350 mm
450 mm
Initial conditions
Slot
Rock

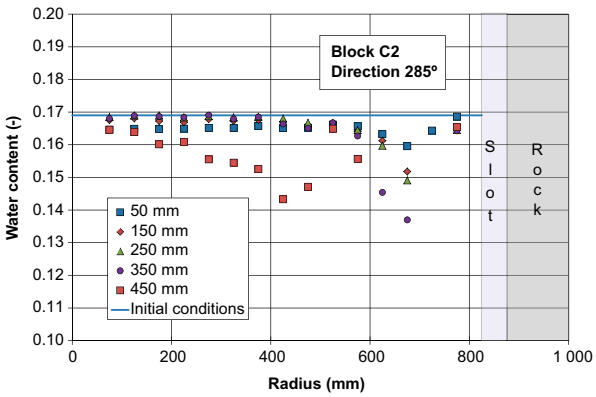
Block C2
Direction 285º
Water content (-)
Radius (mm)
50 mm
150 mm
250 mm
350 mm
450 mm
Initial conditions
Slot
Rock

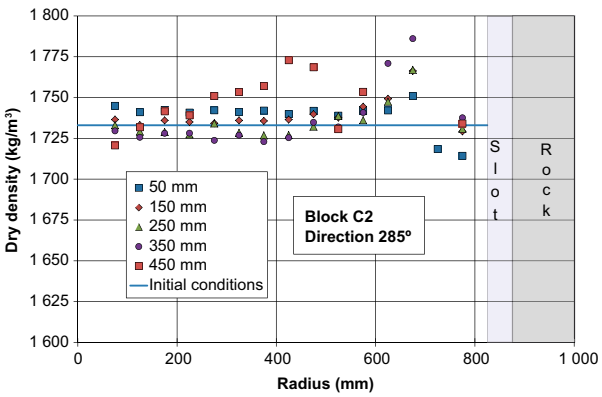
Block C2
Direction 285º
Dry density (kg/m³)
Radius (mm)
50 mm
150 mm
250 mm
350 mm
450 mm
Initial conditions
Slot
Rock

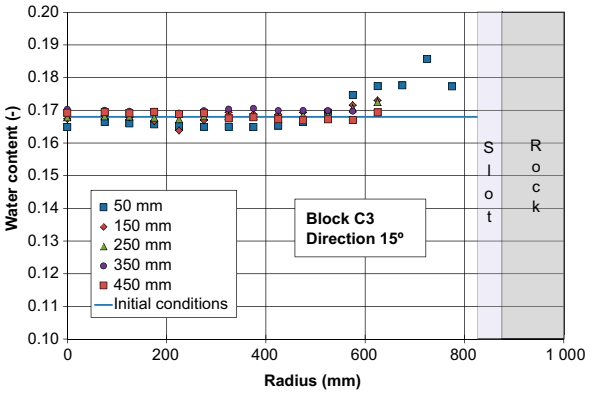
Water content (-)
Radius (mm)
Block C3
Direction 15º
50 mm
150 mm
250 mm
350 mm
450 mm
Initial conditions
Slot
Rock

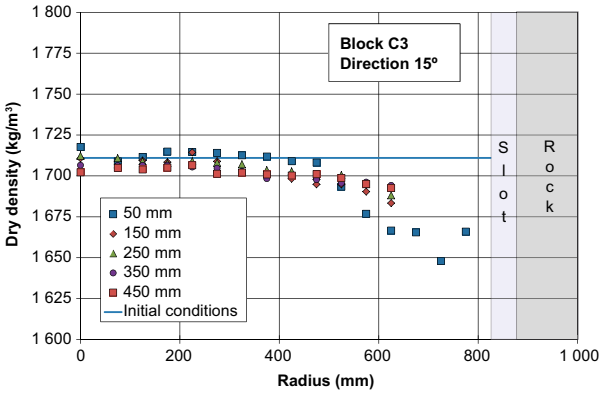
Dry density (kg/m³)
Radius (mm)
Block C3
Direction 15º
50 mm
150 mm
250 mm
350 mm
450 mm
Initial conditions
Slot
Rock

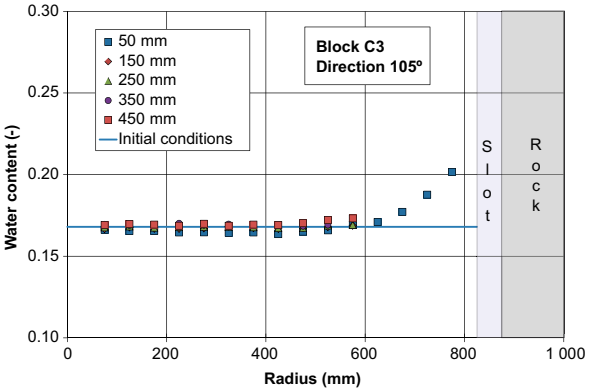
Water content (-)
Radius (mm)
Block C3
Direction 105º
50 mm
150 mm
250 mm
350 mm
450 mm
Initial conditions
Slot
Rock

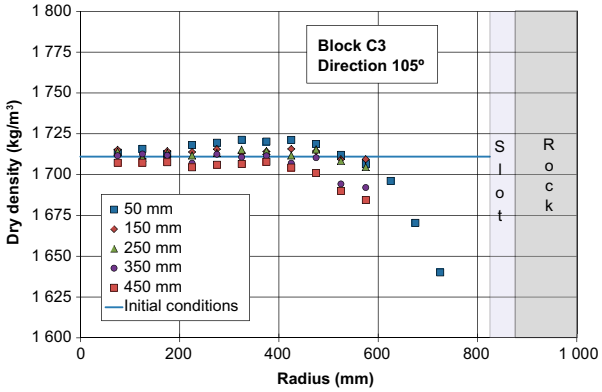
Dry density (kg/m³)
Radius (mm)
Block C3
Direction 105º
50 mm
150 mm
250 mm
350 mm
450 mm
Initial conditions
Slot
Rock

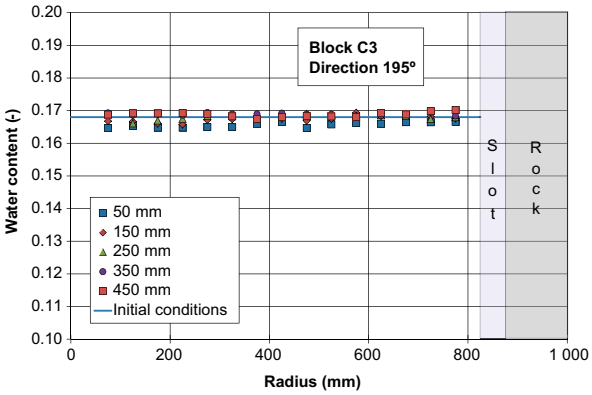
Water content (-)
Radius (mm)
Block C3
Direction 195º
50 mm
150 mm
250 mm
350 mm
450 mm
Initial conditions
Slot
Rock

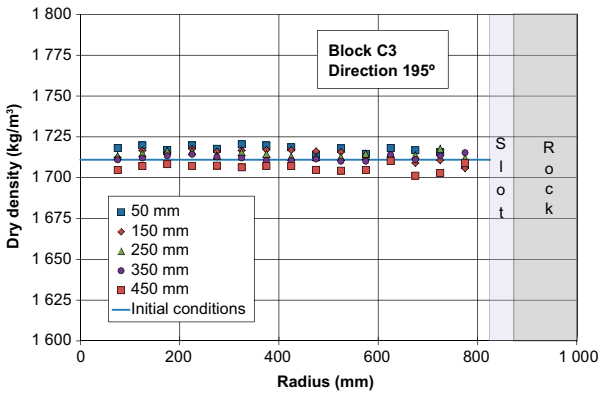
Dry density (kg/m³)
Radius (mm)
Block C3
Direction 195º
50 mm
150 mm
250 mm
350 mm
450 mm
Initial conditions
Slot
Rock

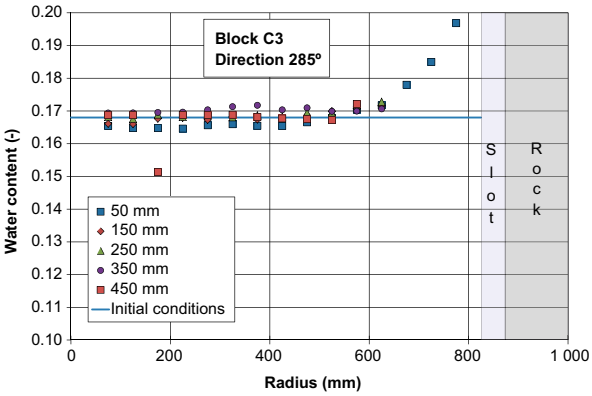
Water content (-)
Radius (mm)
Block C3
Direction 285º
50 mm
150 mm
250 mm
350 mm
450 mm
Initial conditions
Slot
Rock

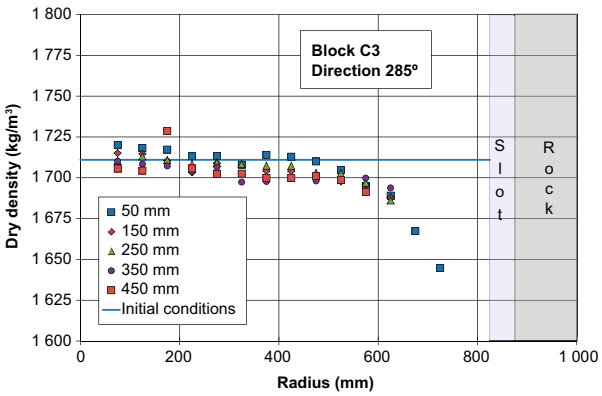
Dry density (kg/m³)
Radius (mm)
Block C3
Direction 285º
50 mm
150 mm
250 mm
350 mm
450 mm
Initial conditions
Slot
Rock

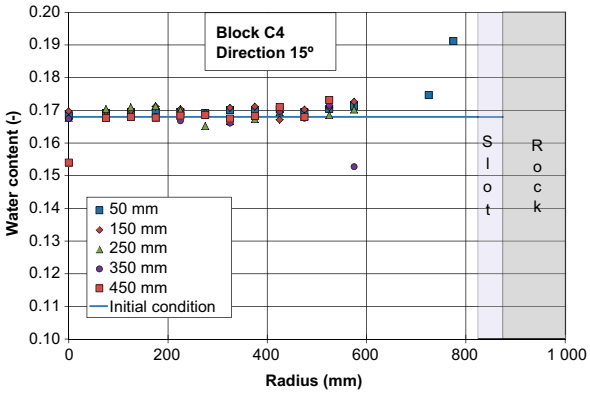
Block C4
Direction 15º
Water content (-)
Radius (mm)
50 mm
150 mm
250 mm
350 mm
450 mm
Initial condition
Slot
Rock

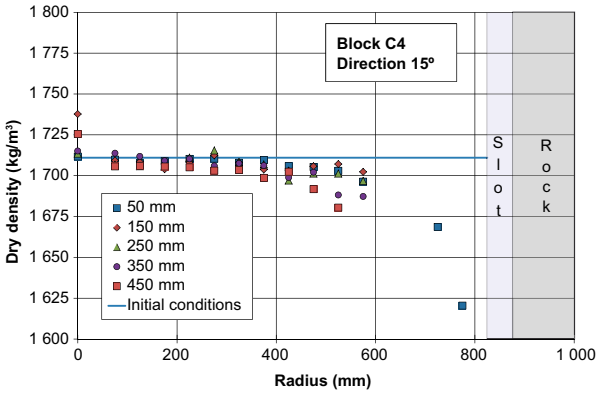
Block C4
Direction 15º
Dry density (kg/m³)
Radius (mm)
50 mm
150 mm
250 mm
350 mm
450 mm
Initial conditions
Slot
Rock

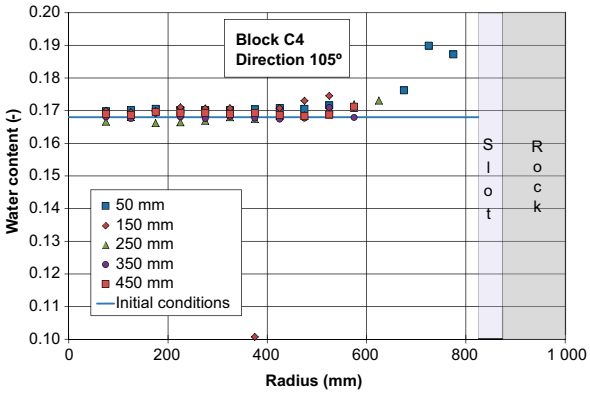
Block C4
Direction 105º
Water content (-)
Radius (mm)
50 mm
150 mm
250 mm
350 mm
450 mm
Initial conditions
Slot
Rock

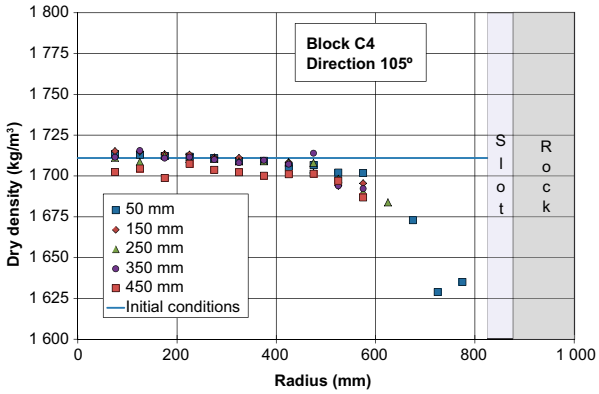
Block C4
Direction 105º
Dry density (kg/m³)
Radius (mm)
50 mm
150 mm
250 mm
350 mm
450 mm
Initial conditions
Slot
Rock

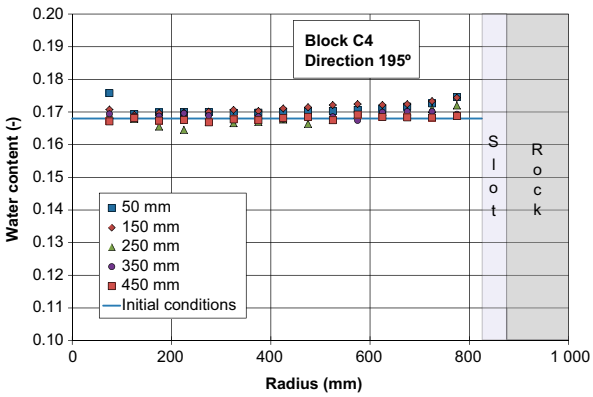
Block C4
Direction 195º
Water content (-)
Radius (mm)
50 mm
150 mm
250 mm
350 mm
450 mm
Initial conditions
Slot
Rock

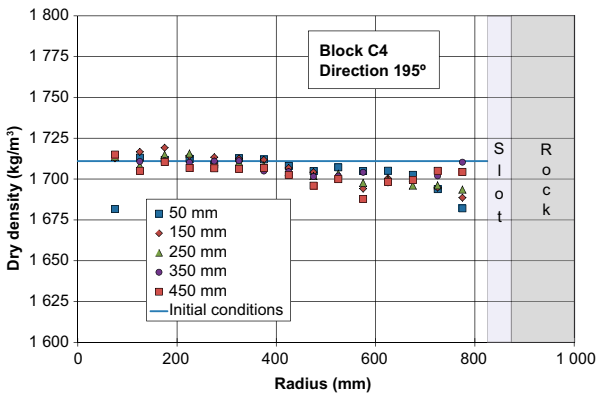
Block C4
Direction 195º
Dry density (kg/m³)
Radius (mm)
50 mm
150 mm
250 mm
350 mm
450 mm
Initial conditions
Slot
Rock

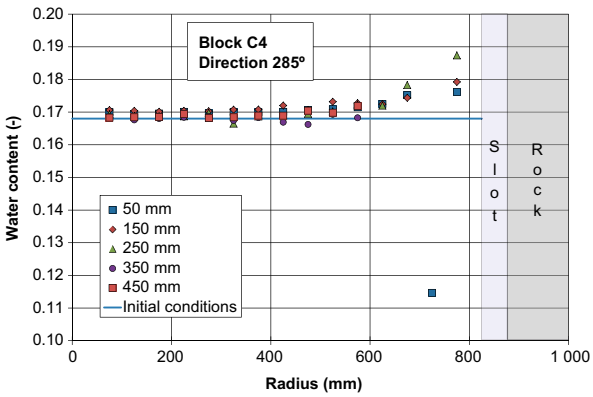
Block C4
Direction 285º
Water content (-)
Radius (mm)
50 mm
150 mm
250 mm
350 mm
450 mm
Initial conditions
Slot
Rock

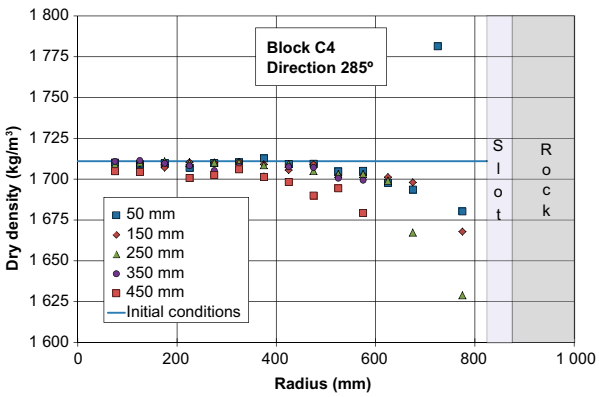
Block C4
Direction 285º
Dry density (kg/m³)
Radius (mm)
50 mm
150 mm
250 mm
350 mm
450 mm
Initial conditions
Slot
Rock

Arkitektkopia AB, Bromma, 2018

SKB is responsible for managing spent nuclear fuel and radioactive waste produced by the Swedish nuclear power plants such that man and the environment are protected in the near and distant future.

skb.se